UNIVERSIDADE DE LISBOA
INSTITUTO SUPERIOR TÉCNICO

CARNEGIE MELLON UNIVERSITY

Opportunities to Improve Deployment Prospects of Offshore Wind

Rudolph Caballero Santarromana

Supervisor:	**Doctor Joana Serra da Luz Mendonça**
Co-supervisors:	**Doctor M. Granger Morgan**
	Doctor Ahmed Abdulla

Thesis approved in public session to obtain the PhD Degree in Engineering and Public Policy

Jury final classification: Pass

2024

(This page is intentionally left blank)

UNIVERSIDADE DE LISBOA
INSTITUTO SUPERIOR TÉCNICO

CARNEGIE MELLON UNIVERSITY

Opportunities to Improve Deployment Prospects of Offshore Wind

Rudolph Caballero Santarromana

Supervisor: **Doctor Joana Serra da Luz Mendonça**
Co-supervisors: **Doctor M. Granger Morgan**
Doctor Ahmed Abdulla

Thesis approved in public session to obtain the PhD Degree in Engineering and Public Policy

Jury final classification: Pass

Jury

Doctor M. Granger Morgan, Heinz College, Carnegie Mellon University, USA
Doctor Joana Serra da Luz Mendonça, Instituto Superior Técnico, Universidade de Lisboa, Portugal
Doctor Ahmed Abdulla, Carleton University, Canada
Doctor Jay Apt, Tepper School of Business, Carnegie Mellon University, USA
Doctor James Corbett, School of Marine Science and Policy, University of Delaware, USA

Funding Institution:
FCT – Fundação para a Ciência e a Tecnologia (Carnegie Mellon Portugal Program)

2024

To Virginia

Because your example has and always will stay with me.

Acknowledgements

Although a Doctoral degree is a personal endeavor, it is not, by any means, something accomplished alone. There are many individuals I would like to thank for their support and guidance while navigating this journey.

First and foremost, I would like to thank my supervisors and committee members. I am extremely grateful to my committee co-chairs and advisors Granger Morgan, Ahmed Abdulla, and Joana Mendonça who have been with me from the very beginning, always encouraging me, and being more than just academic or research supervisors. Granger has been an excellent mentor and has always made time for the small things and the large things alike. He always knows how to tackle a problem, what resources are needed, and helped me identify the main questions of my research, and I am grateful to learn from and work with him. Ahmed has led me to think in new ways and frameworks, helping me identify *how* to execute my research when I only had an idea. He has given me guidance that I will take with me and implement throughout my career. Joana has been an asset to get me to take a step back and think about the implications of my work. She has helped me stay on track when I began to stray. This journey would not be remotely possible without their help, support, mentorship, and guidance throughout this process—with navigating the academic experience and with the administrative and geographic hurdles that included regular intercontinental moves throughout. Jim Corbett has been a great resource throughout this process. His questions and comments have helped me crystallize the work I did and see things from different perspectives. Jay Apt has been a source of insight as an instructor, as well as a committee member. I am extremely grateful to Jay for stepping-in as part of this committee after the loss of Jared Cohon, only weeks before my defense. Finally, I am grateful to the late Jared Cohon—an honorary member of this committee—who helped me refine my multi-criteria decision frameworks and gave me insights that were invaluable to my work. I am extremely fortunate to have both Jim and Jay on my committee, and to have had Jared's input and participation as well.

I would like to thank the institutions who have supported my research. Specifically, I would like to thank the Carnegie Mellon Portugal Program, the Fundação para a Ciência e Tecnologia (Portuguese Foundation for Science and Technology, Grant Number: SFRH/BD/150678/2020), Center for Climate and Energy Decision Making, and academic funds at Carnegie Mellon University, Carleton University, and Instituto Superior Técnico (University of Lisbon Technical Institute) for funding this work.

I would like to thank my friends in Pittsburgh, Lisbon, Chicago, and beyond who have kept me grounded and encouraged me throughout this process in their own ways.

None of this would have been possible without my family, especially Josie, Rodolfo, Rhoda Vi, and Rachel. I am who I am because of their support and love. Countless favors, rides, stays, crossing the country to be at my hospital bedside after getting injured, and never doubting me are among the innumerable ways that they have supported me. I would also like to thank Gigi and Tiziana for always making me feel at home, away from home.

Finally, thank you to my partner, Laura, who is everything to me and who was the first to believe that I could complete a doctoral degree and speak the idea into existence when it was only a thought in my head. Without your encouragement and support, this would not be possible. Thank you for always being by my side, regardless of our geographic distance.

Rudolph Santarromana, 2024

Resumo

Esta dissertação cobre um conjunto de trabalhos relacionados com a implantação de energia eólica offshore. A implantação de grandes quantidades de energia renovável é um aspecto fundamental na transição para uma economia de baixo carbono e na limitação dos efeitos negativos das alterações climáticas. Contudo, para além dos desafios técnicos e económicos, a implantação de energias renováveis deve satisfazer interesses ambientais, sociais e regulamentares. Dada a amplitude de interesses díspares que afetam as perspectivas de implantação, desenvolvo modelos e estruturas que ajudam a quantificar os custos e benefícios da implantação de energia eólica offshore, demonstram como vários interesses podem ser equilibrados no projeto da planta e operacionalizam fatores qualitativos para informar os tomadores de decisão sobre as compensações de estratégias de implantação. O âmbito tecnológico destes estudos incide sobre a energia renovável eólica offshore, que é uma fonte de energia nascente com um grande potencial técnico – ainda inexplorado – e potencial de descarbonização energética.

Em primeiro lugar, considero uma nova forma de implantar turbinas eólicas offshore flutuantes que reduza as obstruções físicas e permita a construção de turbinas em águas menos controversas. Quantifico um benefício ambiental e o custo desta estratégia. Considero que a estratégia acarreta uma penalização de custos de pelo menos 30 dólares americanos/megawatt-hora e elimina até 900 quilómetros de correntes de amarração para uma rede de 1 gigawatt. Embora este custo adicional seja substancial, existem outras oportunidades e cenários onde esta estratégia pode fazer sentido. Em seguida, investigo a tecnologia da planta e as alternativas locais usando uma estrutura de análise multicritério para comparar a adequação das alternativas com base na otimização da tecnoeconomia e na minimização dos impactos. Concluo que as fábricas maiores que a indústria está a impulsionar são frágeis em termos de localização, enquanto as fábricas mais pequenas são mais robustas em termos de localização e que existem grandes áreas onde as duas perspectivas se alinham e que a indústria deve perseguir. Isto sugere que apenas uma visão estreita da tecnoeconomia pode levar a resultados incertos dos projectos. Finalmente, proponho uma forma de operacionalizar os aspectos sociopolíticos e as obrigações regulatórias do ambiente de adoção, a fim de comparar estratégias de transmissão da energia eólica offshore que podem enfrentar obrigações diferenciadas. Considero que encurtar o processo de desenvolvimento em um ano equivale a um crédito fiscal ao investimento de 2,6% e pode valer mais de 65 milhões de euros para um único projecto. Considero também que existem muito poucos cenários em que uma estratégia de transmissão nova e dispendiosa seja mais vantajosa do que a tecnologia de base, mas é fundamental quantificar o impacto de estratégias mais dispendiosas que possam facilitar as obrigações regulamentares. Os resultados sugerem que são necessárias melhorias adicionais na nova tecnologia para competir diretamente com base nos custos. Em trabalhos futuros, pretendo explorar a implantação do hidrogénio verde que considere factores sócio-políticos e um elemento de evolução do mercado da tecnologia para compreender como diferentes ambientes de adopção ou atitudes sócio-políticas podem afectar os níveis de obtenção de capacidade de energia renovável ou redução global de carbono.

Palavras-chave: energia eólica offshore, implantação, partes interessadas, descarbonização, energia renovável

Abstract

This dissertation covers a body of work concerned with the deployment of offshore wind energy. Deploying large amounts of renewable energy is a key aspect in transitioning to a low-carbon economy and limiting the negative effects of climate change. However, in addition to technical and economic challenges, renewable energy deployment must satisfy environmental, social, and regulatory interests. Given the breadth of disparate interests affecting deployment prospects, I develop models and frameworks that help quantify the costs and benefits of offshore wind deployment, demonstrate how several interests can be balanced in plant design, and operationalize qualitative factors to inform decision makers on the tradeoffs of deployment strategies. The technological scope of these studies is on offshore wind renewable energy which is a nascent energy source with a large—still untapped—technical potential, and energy decarbonization potential.

First, I consider a novel way of deploying floating offshore wind turbines that reduces physical obstructions and allows turbines to be built in less-contentious waters. I quantify one environmental benefit and the cost of this strategy. I find that the strategy realizes a cost penalty of at least 30 US dollars/megawatt-hour and eliminates up to 900 kilometers of mooring chains for a 1-gigawatt array. While this added cost is substantial, there are further opportunities and scenarios where this strategy can make sense. I then investigate plant technology and site alternatives using a multi-criteria analysis framework to compare the suitability of alternatives based on optimizing techno-economics and minimizing impacts. I find that the larger plants the industry is pushing toward are fragile to locations, while smaller plants are more robust to locations and that there are large areas where the two perspectives align that the industry should pursue. This suggests that a narrow view on techno-economics only can lead to uncertain project outcomes. Finally, I propose a way to operationalize socio-political aspects and regulatory obligations of the adoption environment in order to compare transmission strategies from offshore wind which may face differential obligations. I find that shortening the development process by one year is equivalent to an investment tax credit of 2.6% and may be worth more than 65 million euros for a single project. I also find that there are very few scenarios where a novel and expensive transmission strategy is more advantageous than the baseline technology, but it is critical to quantify the impact of more expensive strategies that may ease regulatory obligations. The results suggest that further improvements of the novel technology are needed to directly compete on a cost basis. In future work, I plan to explore green hydrogen deployment that considers socio-political factors and a market evolution element of the technology to understand how different adoption environments or socio-political attitudes can affect levels of attainment of renewable energy capacity or overall carbon abatement.

Keywords: offshore wind, deployment, stakeholders, decarbonization, renewable energy

Table of Contents

List of Abbreviations

Abbreviation	Definition
ABS	American Bureau of Shipping
APU	Auxiliary Power Unit
ATB	Annual Technology Baseline
CAPEX	Capital Expenditure
CF	Capacity Factor
COP	Construction and Operations Plan
CFF	Construction Finance Factor
CRF	Capital Recovery Factor
DLC	Design Load Case
DMPA	De Facto Marine Protected Area
DP	Dynamic Positioning
EEZ	Exclusive Economic Zone
EU	European Union
EUR	Euro
FLORIS	Flow Redirection and Induction in Steady State
FOM	Fixed Operations and Maintenance
GW	Gigawatt
GWEC	Global Wind Energy Council
GWh	Gigawatt-hour
H_2	Hydrogen
HVAC	High Voltage Alternating Current
HVC	High Voltage Cable
HVDC	High Voltage Direct Current
Hz	Hertz
IA	Influence Area
IEA	International Energy Agency
IRENA	International Renewable Energy Agency
ITC	Investment Tax Credit
kg	Kilogram
km	Kilometer

Abbreviation	Definition
kN	Kilonewton
kV	Kilovolt
kW	Kilowatt
kWh	Kilowatt-hour
LCOE	Levelized Cost of Energy
LCOH	Levelized Cost of Hydrogen
m	Meter
MCDM	Multi Criteria Decision Model
MPA	Marine Protected Area
MVA	Megavolt-Amp
MW	Megawatt
MWh	Megawatt-hour
N	Newton
nm	Nautical Mile
netCF	Net Capacity Factor
netOCC	Net Overnight Capital Cost
NPV	Net Present Value
NREL	National Renewable Energy Laboratory
Ω	Ohm
OCC	Overnight Capital Cost
OPEX	Operational Expenditure
OSW	Offshore Wind
PFF	Production Finance Factor
PID	Proportional-Integral-Derivative
PPA	Power Purchase Agreement
PtH	Power to Hydrogen
s	Second
TCP	Thruster Consumption Percent
UK	United Kingdom
US	United States
USD	United States Dollar
WSC	Wind Speed Class

List of Tables

List of Figures

Chapter I
Introduction

Anthropogenic climate change significantly increases the likelihood of extreme weather that realizes economic damages, affects food security, human mobility, national development, and overall progress toward sustainable development [1]. Even since the adoption of the Kyoto Protocol more than 25 years ago which set targets for emissions reductions, emissions have increased—2023 set the record for annual global emissions [2]. There is a clear gap between the intention to decarbonize and execution of that goal, and this work is motivated by the need to decarbonize the global economy.

Part of this effort, and the focus of this work, is decarbonizing energy generation, which will require the deployment of low-carbon energy technologies. A range of viable technology options now exist which can reduce emissions, they just need to be deployed at record rates [2]. However, among 50 tracked technologies that are needed to decarbonize energy, only three are being deployed at a rate that is on track with achieving ‘net zero’ annual emissions by 2050 [3]. Offshore wind (OSW) is one of these technologies that needs to be deployed faster to achieve decarbonization targets. OSW technology describes wind turbines that are installed in marine environments in contrast to land-based, onshore wind. Due to the presence of fewer obstructions offshore, these turbines experience much stronger, and steadier winds, and allow for much larger turbines to be deployed, which is the trend that the market follows today [4], [5]. Pilot projects and studies estimate that capacity factors for OSW may reach greater than 60% in future installations, rivaling dispatchable fossil fuel technologies in some jurisdictions [4], and demonstrating that OSW presents an opportunity to displace some of those fossil fuel technologies which will be critical toward decarbonizing energy. However, whether OSW deployment targets will be met is still uncertain. In retrospect, none of the 2020 capacity targets or projections for regional OSW deployment set in the early 2010s [6], [7] have yet been met [8] (see Table A.1 of Appendix A.1 for details). Looking forward, Figure 1.1 depicts several simulated adoption pathways for global OSW capacity in a probabilistic feasibility space for its growth [9] (see Appendix A.2 for details on the methodology). Among 1,000 simulated adoption pathways depicted, only the most optimistic pathways (above the 90th percentile) can achieve a key decarbonization scenario and industry projections [10].

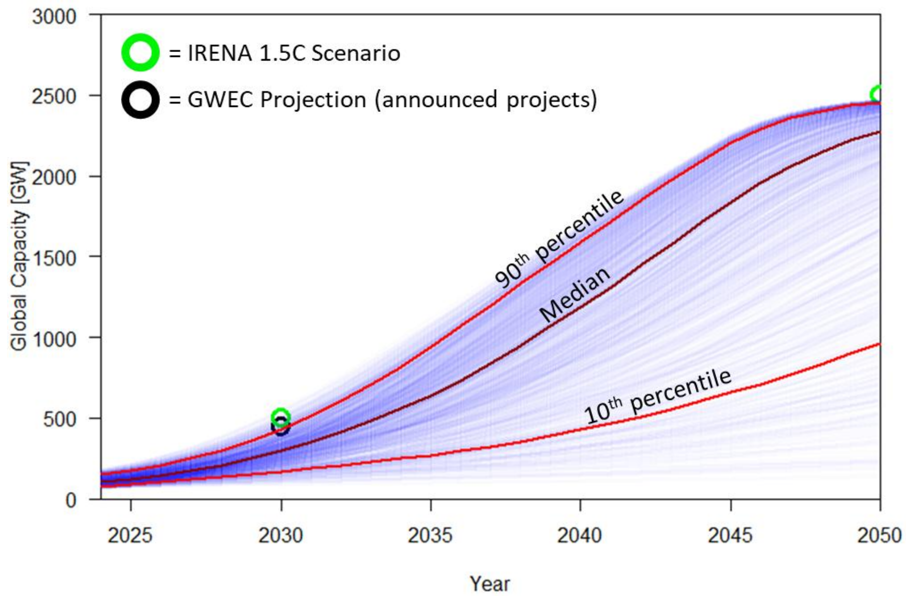

Figure 1.1: Diffusion feasibility space for OSW deployment. Depicted points include an International Renewable Energy Agency (IRENA) decarbonization scenario and a Global Wind Energy Council (GWEC) projection based on announced projects [10].

Putting the industry on a path to achieve decarbonization targets will require improving deployment prospects and hastening deployment. The cost of energy from OSW fell by 60% from 2010 to 2021 [11], but there are other factors that affect the rate of deployment beyond techno-economic performance that must be accounted for as techno-economics alone do not drive technology adoption [12], [13]. Institutional incentives and barriers play a role in adoption and deployment decisions. Deploying OSW—as with any large infrastructure—must satisfy a range of interests and regulations during the development process. Development timelines are several years long and have only gotten longer over the last two decades, even after the Paris Agreement in 2015 which established decarbonization targets for countries of the world [14]. A range of regulatory, social, stakeholder, and market factors—which I refer to generally as 'socio-political factors' in this dissertation [15]—affect project execution time, project cost, the overall prospects of the industry, and have been cited as a challenge and a potential risk to OSW deployment in government reports in the US [16] and UK [17]. External entities and interests have demonstrated some agency over deployment outcomes in the past. Socio-political factors play a role in all infrastructure deployment, but in these (relatively) early stages of the OSW industry, where commercial deployment has not yet been achieved in most of the world, it is key to identify opportunities to improve deployment prospects by assessing strategies and technologies on metrics that go beyond techno-economics and balance a range of concerns and interests.

The aim of this dissertation is to advance efforts on how to quantify and consider the impacts and tradeoffs of project choices in the OSW industry. I attempt to advance the discussion of balancing socio-political interests with techno-economic ones by juxtaposing the two perspectives and considering how to quantify and operationalize socio-political factors into modeling work. Effectively quantifying and managing such factors would also be informative for the deployment of other low-carbon energy technologies.

This dissertation is structured as follows. In Chapter 2, I consider a novel method for deploying OSW turbines—using dynamic positioning—that reduces obstructions in the open ocean—a potential risk to marine life—and allows turbines to be installed in deeper waters, far from shore, where fewer entities have interest, potentially easing deployment. The strategy comes at a higher cost, and therefore, I quantify the cost penalty above conventional methods. I also quantify a benefit that can be realized, and qualitatively discuss others that can be quantified in future studies with this strategy. I find that, while prior studies on the energy performance of DP were pessimistic, there are design and operation improvements that can lower its cost of energy. In future studies on this application, monetizing the benefits may also reveal a larger opportunity with this strategy.

In Chapter 3, I investigate OSW siting and plant alternatives in the US to identify how deployment prospects might be improved by choosing different plant sizes or locations. I consider two perspectives—a ‘techno-economic optimizer’ and a ‘stakeholder and environmental impact minimizer’—and construct a representative weight profile for each, apply them to a large set of plant alternatives, and quantify a ‘suitability’ for the alternatives under each perspective in a multi-criteria decision analysis framework. I find that, while the largest plants realize the best ‘suitability’ scores, they are also fragile to locations by attaining a high variance of scores; conversely smaller plants are robust and realize similar suitability across sites demonstrating that the latter have less uncertainty in the impacts they realize. I also find that there are large areas where the two perspectives align on the US East Coast, but very few on the US West Coast, and incentives for deployment methods that reduce physical and environmental impacts greatly increases these ‘consensus’ areas on the West Coast.

In Chapter 4, I demonstrate a modeling framework to operationalize socio-political and regulatory obligations on project deployment to quantify the ‘value’ of reducing these through policy. I operationalize these obligations as a temporal factor that impacts the cost of energy calculation. I demonstrate the framework on transmission topologies to bring energy to shore from OSW. I find that, on a purely cost of energy basis, there are very few scenarios where novel power-to-hydrogen (PtH) transmission topologies are cheaper than a baseline high voltage cable transmission method. There are several ways that the framework can be improved to reflect reality given expert insights which I discuss, and in future work, this framework can be applied to improve the cost calculations as comparison to other benefits technology options may realize.

Finally, in Chapter 5, I summarize the findings from this dissertation, discuss some of the contributions of this work, and discuss future directions for research.

Chapter II
Assessing the Costs and Benefits of Dynamically Positioned Floating Wind Turbines to Enable Expanded Deployment

The contents of this chapter are the abridged version of a published manuscript at *Energy Conversion and Management* with co-authors: Ahmed Abdulla, Joana Mendonça, M. Granger Morgan, Massimiliano Russo, and Rune Haakonsen:

> Santarromana, R., Abdulla, A., Mendonça, J., Granger Morgan, M., Russo, M., & Haakonsen, R. (2024). Assessing the costs and benefits of dynamically positioned floating wind turbines to enable expanded deployment. *Energy Conversion and Management, 306,* 118301. https://doi.org/10.1016/j.enconman.2024.118301.

2.1 Introduction

Decarbonizing the global energy system will require the development and deployment of innovative low-carbon energy technologies. OSW presents a great potential resource. A recent assessment found that as much as 15 times the current global energy production could be generated with OSW in waters within 300 kilometers (km) of the world's coastlines and up to depths of 2,000 meters (m). Approximately 70% of that capacity is in waters that are too deep for fixed foundations [18], necessitating floating deployment. In addition to the technical and economic challenges the OSW sector faces, it must also contend with environmental and socio-political challenges that can constrain development.

Today, floating OSW turbines are held in place with mooring chains and anchors embedded in the seabed and considered viable up to depths of about 1,000m [19] or 1,300m [20]. The gross resource potential for US OSW falls by 64% once waters deeper than 1,000m are excluded [21]. In fact, depth becomes a limiting factor for the entire US West Coast, parts of the US East Coast [21], and other parts of the world, including Portugal—an early adopter of floating OSW [22]. The design of mooring systems for floating wind turbines is an established theme in the literature with recent papers on OSW wind mooring designs for 15 megawatt (MW) turbines [23], methods for optimizing mooring system designs with a 10MW floating turbine [24], and physical dynamics and monitoring of mooring systems [25]. The environmental impact of mooring is less explored, but also a theme of study as this installation disrupts the seafloor and creates impediments in the open ocean as moorings can have a swept volume nearly 200 times the chain volume [26]. Such interactions pose a potential danger to marine flora and fauna by way of entanglement [27], harm to benthic environments [28] and various other marine media impacts [29]. Because plant arrays include numerous turbines, the impacts to these habitats are compounded in a concentrated area, and these risks require environmental studies and permits.

Reducing the environmental impacts and socio-political constraints of floating OSW is key to their sustainable expanded deployment, and siting arrays far offshore could potentially reduce project execution risks [17]. This could be accomplished by substituting a dynamic positioning (DP) station-keeping system for mooring chains and building in deeper waters. DP has been widely used for vessels and offshore drilling applications [30], it has capabilities for very high positional accuracy (much greater than needed for OSW turbines), and similar technology is proposed to be used with floating OSW turbines to offset wind, wave, and current forces and provide station-keeping. The DP system would be powered by the turbine's generation, reducing its net output. The system employs a control system like the proportional-integral-derivative (PID) type controller proposed in [31] with the goal of keeping the platform stationary. Alternatively, a control system may allow more drifting, and reduce the thrust demand as explored in [32]. Figure 2.1A illustrates the most widely used mooring design, with catenary mooring chains and drag embedment anchors [33]. Figure 2.1B illustrates a floating turbine that uses DP in lieu of mooring chains.

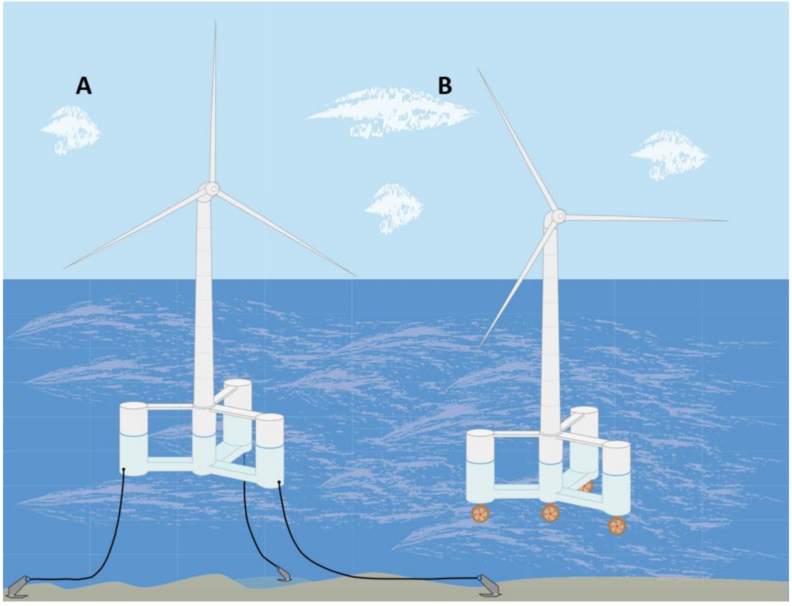

Figure 2.1: Two station-keeping options for floating turbines. A) Conventional bottom-anchored floating system with catenary mooring chains and drag embedment anchors. B) A dynamically positioned system proposed in this research that would instead use thrusters mounted on the substructure to station-keep. While only four thrusters are shown, in practice more or fewer thrusters could be employed depending on cost and operational efficiency, as analyzed here.

In this chapter, I consider DP as a potential solution to enable OSW deployment in deeper waters and eliminate mooring chain impacts. The use of this technology would expand the available resource area, reduce environmental interactions by avoiding anchors and mooring chains that pose a danger to marine flora and fauna, and allow for deployment in waters with fewer shared interests that tend to be in deeper waters farther from shore. For example, in the US, competing marine uses fall from 48% of area in near-shore sites to 8% of area in sites farther from shore (50 nautical miles, nm, to 200 nm—the edge of the exclusive economic zone, EEZ) [21]. Given this context and the potential deployment benefits that DP may realize as a substitute for mooring chains, the tradeoff with added cost of the system must be understood, and thus the main research question this chapter addresses is: what is the cost penalty for using DP in lieu of mooring chains to station-keep floating OSW turbines?

Although DP is a widely used technology in other maritime sectors, there is a paucity of work applying the technology to OSW turbines. Prior work on this application focused exclusively on technical performance. Xu and colleagues used simulations to analyze the energy performance of using DP to keep a stationary position on a single 5MW turbine finding that more than 50% of the energy generated near the rated wind speed is used to power the thrusters [31]. Alwan and colleagues do the same analysis on a 2MW turbine, getting a similar finding [34]. Connolly and Crawford allow for the turbine to move (and thus do not require a stationary position) and find an improvement in the amount of energy consumed by the thrusters, which can fall to around 20% for specific environmental conditions [32]. Recent work has also compared the energy performance of unmoored floating turbines with energy ships that "generate power via hydro-turbines mounted on the underside of the hull" as options for far-offshore energy generation [35]. Therefore, existing work on this application has demonstrated that there is a positive net energy output during operation of a floating wind turbine that uses DP to station-keep, although no studies directly compare moored and DP turbines, nor assess the levelized cost of energy (LCOE) of a DP system as a function of turbine size. Existing work also focuses on the operational domain of the turbine in energy analyses, implicitly assuming that the net energy output is zero when a turbine is arrested—this is not the case, however, as the DP must maintain some positional tolerance or heading and counteract small environmental forces even while the turbine is not generating. Although prior work demonstrates that the application can consume a great deal of power, by expanding the scope of the analysis to consider different turbine and thruster sizes, thruster configurations, and measuring the expected performance over a probabilistic distribution of environmental conditions (as opposed to only the performance at stationary conditions) it may be possible to identify strategies for improving the application, develop a more informed discussion on the viability of the application, and identify a decision space where this application may make techno-economic sense. A quantification of costs and benefits is necessary to understand this, and its previous absence is a gap in the literature which has thus far focused on the energy perspective. Therefore, the main contribution of this chapter to a nascent discussion on the application is an analysis of the LCOE of this application, which is done by considering the cost and performance data of a suite of commercially available thrusters from a global manufacturer across a range of conditions and configurations. I produce net power curves for this deployment paradigm which reveal key discontinuities that can inform design improvements and estimate the amount of energy needed to station-keep during periods of low winds—a key operational consideration for reliability of the system. Finally, I expand the discussion beyond techno-economics to potential environmental benefits realized by this application by estimating the length of mooring chains that would be eliminated by using DP—reducing seabed disruption and entanglement risks to marine life. The rest of this chapter is organized as follows: the analytical framework and methods is described including each module of the analysis; the main results are presented; and then a discussion is provided followed by a brief conclusion.

2.2 Data and Methods

The analysis consists of three parts: a physical model, a techno-economic model, and an environmental model. In the physical model, an analytical, steady-state model is developed to compute the overall turbine thrust forces at each condition—a super-position of the environmental forces gives the total turbine thrust force. The analytical model makes for straightforward computation at fixed environmental conditions, described in detail in this section. The results of the analytical model are validated with steady-state results from marine engineering simulations to confirm their agreement. Empirical analysis of historical data is used to estimate the worst case of energy storage needed to station-keep during periods when the turbine is not generating. The environmental model uses engineering design principles given the outputs of the physical model. The techno-economic performance is computed considering the probabilistic distribution of environmental conditions using expected values to account for uncertainty. Figure 2.2 comprises a flow chart that presents the analytical framework.

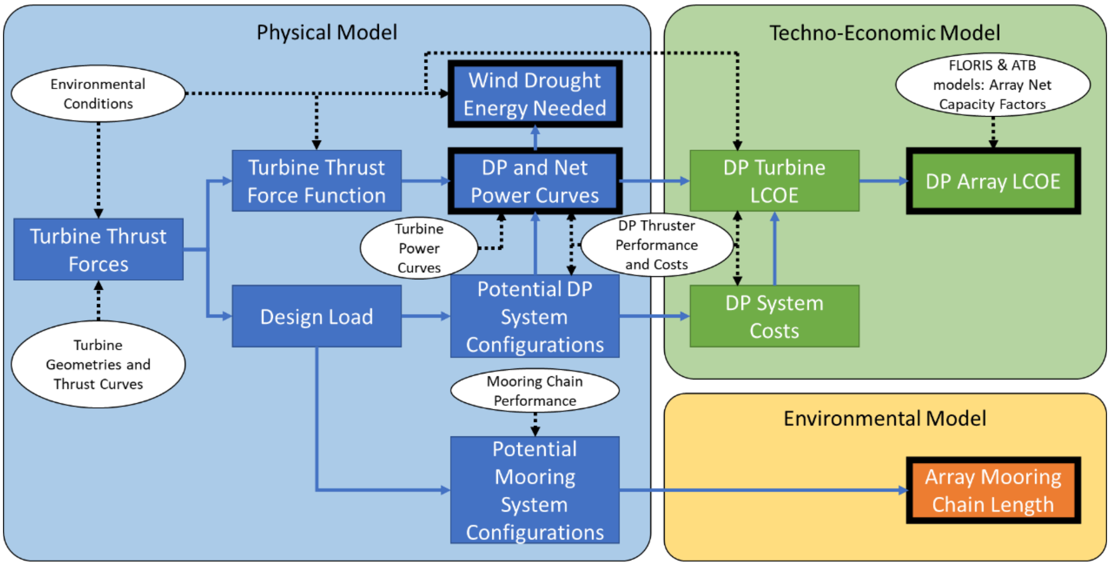

Figure 2.2: Analytical framework employed in this investigation. White ovals represent input models and data; boxes represent calculation modules in the analysis; bold boxes represent the main results. Dotted arrows denote where the input data are used, and solid arrows denote where module outputs are used.

The analysis uses reference turbine designs and specifications of commercial DP thrusters, neither of which are optimized for this application, and a super-position of forces is a simplification that assumes each part of the floating turbine is independent which may give rise to measurement inaccuracies compared to a real-world installation. To account for this, conservative simplifications to the physical model are made and validation of the results using marine engineering simulation software is carried out. As opposed to developing a detailed design, the goal of the physical model is to estimate the expected energy consumption of the thrusters to arrive at the main result: an estimate of the DP array LCOE in comparison to estimates of similar moored arrays across various turbine sizes, in a range of environmental conditions. R was used as the primary analysis software, and the codes used for this study are provided in a code repository given at the end of this chapter. Other software used for validation of the R analysis is described where it is used.

2.2.1 Environmental forces

A station-keeping system must counteract the combined environmental forces that displace the turbine (the turbine thrust force). Three environmental forces are considered: wind, current, and mean wave displacement forces. This analysis employs publicly available reference turbine data and the same semi-submersible floating platform for each [36]. This platform was designed for the International Energy Agency's (IEA) 15MW OSW turbine [37] (see Figure B.1 of Appendix B.1) and is therefore oversized for the smaller reference turbines considered. A summary of the specifications of the reference turbines used is given in Table 2.1.

Table 2.1: Technical specifications and dimensions of the reference turbines in this analysis. Data come from publicly available sources, provided in the table.

Turbine Rated Power (MW)	5	8	10	15
Tower Height (m)	90	110	119	150
Tower Base Diameter (m)	6	7.7	8.3	10
Blade Length (m)	61.5	82	97	117
Floater Diameter (m) [36]	12.5			
Floater Length (m) [36]	35			
Cut-in Wind Speed (m/s)	3	4	4	3
Rated Wind Speed (m/s)	11.4	12.5	10.5	10.6
Cut-out Wind Speed (m/s)	25	25	25	25
Source	[38]	[39]	[40]	[37]

The turbine thrust force is the vector sum of the wind, current, and wave force vectors. The overall turbine thrust force is computed by first computing the magnitude of each environmental force individually and then combining them considering different angular offsets between the environmental forces. The magnitude of each environmental force vector is the sum of all the components exposed to that force. When static components are exposed to a constant flow (for example, turbine floaters exposed to surface currents and wind of a constant velocity), the drag force on a solid body caused by a constant flow [41] is used:

$$F_{flow,component} = \frac{1}{2}\rho_f V_f^2 A_{eff} C_d \tag{2.1}$$

where ρ_f is the density of the flowing fluid, V_f is the speed of the flow, A_{eff} is the effective surface area subjected to the flow, and C_d is the drag coefficient, between 0 and 1.

The wind force acts on the tower, rotor, and the portions of the substructure above the water surface. When the floating turbine is not in operation and all components are static, equation (2.1) is used on all turbine components. During operation (when wind speeds are between the turbine cut-in and cut-out wind speeds and the turbine rotor is spinning), rotor thrust force functions (from the sources in Table 2.1) provide forces on the rotor for each turbine, and component drag forces for the remaining parts of the floating turbine exposed to wind (the tower and the substructure components above the water surface) are added to get the magnitude of the wind force vector. The wind speed varies as a function of height with a power law [42]:

$$V_{wind}(z) = V_{hub}\left(\frac{z}{z_{hub}}\right)^{\alpha}$$

where $V_{wind}(z)$ is the wind speed at height z measured in meters/second (m/s). z_{hub} and V_{hub} are the hub height (in m) and the wind speed at that hub height, respectively; wind speed measurements at 100m hub heights are used and rigid body motion, steady-state conditions, and α equal to 0.14 [42] are assumed. Thus, similar to the blade element method [43], an integration over each component of the floating turbine to account for changes in wind speed and component dimensions with height gives the component force from wind on static components,

$$F_{wind,component} = \int_{z} \frac{1}{2}\rho_{air}\, V_{wind}^{2}(z)\, D(z)\, C_d(z)\, dz$$

where ρ_{air} is the air density, $D(z)$ is the cross-section width of the component as a function of height z, and $C_d(z)$ is the cross-section drag coefficient as a function of height.

The water current force acts on the submerged portions of the substructure. Forces on these components are estimated as the drag force on the submerged bodies (equation (2.1)) assuming a constant current velocity for all portions of the submerged body. As the draft depth of the substructure is small compared to the water depth, an integration to account for changing current velocity—as done with wind—is not required.

The wave force also acts on the substructure. The nature of oscillating wave motion results in complex forces on submerged bodies requiring more complex methods to estimate the mean wave forces [44]. Wave drift force estimation for DP systems [45], and other estimations of the forces acting on a submerged cylinder using numerical methods and simulations [46] describe the complexities of computation. It is difficult to empirically calculate the wave drift force on a submerged floating substructure without dedicated modeling and testing. Previous studies on the energy consumption of DP on a floating turbine omit current or wave forces [31], [32]. In this study, a first order estimate of the wave drift force (as a component of the overall turbine thrust force) is used to size the station-keeping system and estimate the DP power consumption curve for the floating turbine. The mean wave drift force is a constant force arising from interactions of wave oscillations with the same frequency [47]. This force is estimated using Morison's equation over a range of wave parameters [48], which calculates the instantaneous wave force on a body using a drag-induced term and an inertia-induced term given its position in the wave field, the significant wave height, and the wave period. This is given by:

$$F_{wave,x} = \int_{-z_D}^{0} \frac{1}{2} C_D D \rho_{water} v|v| \, dz + \int_{-z_D}^{0} \frac{\pi}{4} C_M D^2 \rho_{water} \dot{v} \, dz \tag{2.2}$$

Each term in equation (2.2) is an integral from the substructure draft depth (z = z_D) to the still water level (z = 0), where C_D and C_M are the wave drag and inertia coefficients, respectively, which are assumed to be 1.0 and 2.0 for cylindrical bodies, respectively, based on [46]. D corresponds to the floater diameter. Assuming linear wave theory with deep waves, the horizontal particle velocity, v, and the acceleration, $\dot{v}$, are [49]:

$$v(x,z,t) = \frac{\pi H}{T} e^{kz} \cos(kx - \sigma t) \tag{2.3}$$

$$\dot{v}(x,z,t) = \frac{\partial v}{\partial t} = \frac{2\pi^2 H}{T^2} e^{kz} \sin(kx - \sigma t) \tag{2.4}$$

where x and z are cartesian coordinates that are described in Figure 2.3A, which illustrates wave motion and forces based on the position of a body in the wave field at a time, t, with H as the wave height (m), k as the wave number, which depends on the wavelength, L in (m), and σ as the wave frequency, which depends on the period, T in seconds (s) [49]. Figure 2.3B illustrates how the floater position in the wave field can subject the substructure to counteracting forces at the same instance (as seen in Figure 2.3, floater A is subject to a surface motion opposite the direction of propagation, while floaters B and C are both subject to surface motion in the direction of propagation based on their positions in the wave field). Further details on the method are given in Appendix B.5.

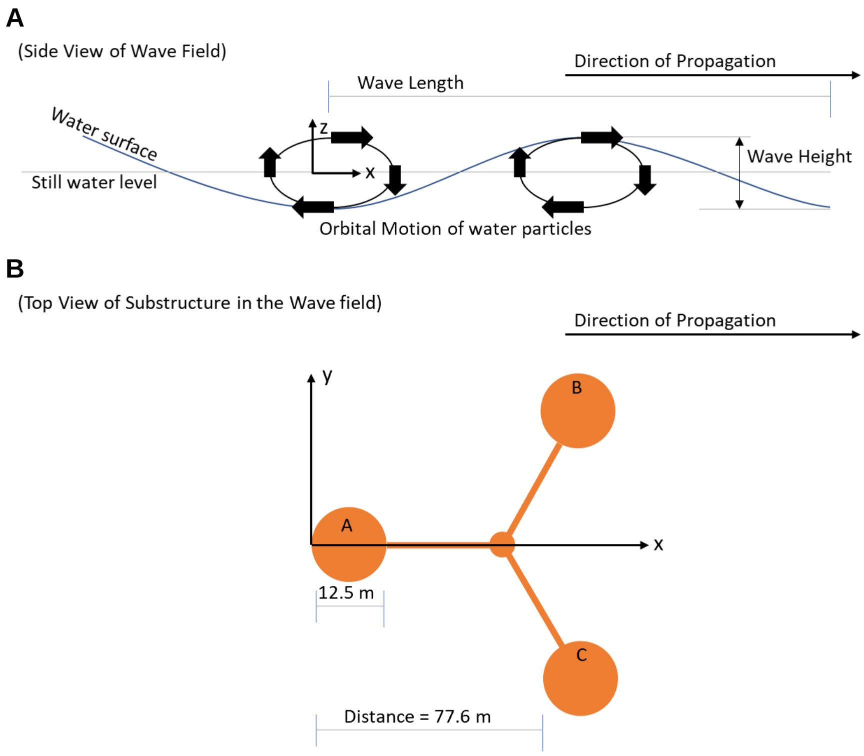

Figure 2.3: Illustration of instantaneous wave forces in relation to the floating substructure. A) A cross section of the wave field and force direction at various locations in the field adapted from [49]; the labeled axes correspond to the same used in equations (2.2) - (2.4). B) A top view illustration of the substructure in the same wave field showing how it can simultaneously be subjected to opposing forces.

Figure 2.4 presents the result of the computed wave forces over one period on the entire substructure, oriented in the direction with respect to the wave propagation shown in

Figure 2.3B and illustrates how the wave-induced drag and inertia forces combine on the floater. The wave conditions considered are shown in Table 2.2.

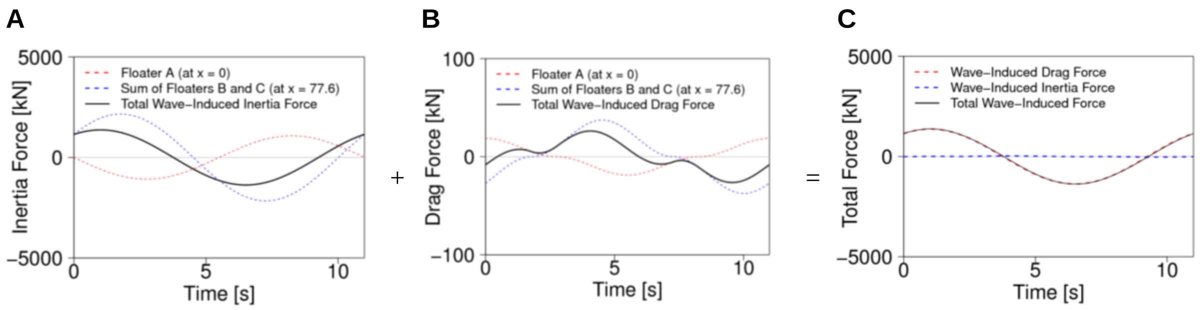

Figure 2.4: Wave induced forces over one period. Panels illustrate A) inertia force, B) drag force, and C) total combined forces calculated using Morison's equation considering a wave height of 1.8m and wave period of 11s. Note the difference in y-axis scale in panel B. Panels A and B illustrate the contribution of each floater (dotted lines), and the result for the whole substructure (solid line). Panel C illustrates the inertia and drag forces (dotted lines) and total force (solid line) on the entire substructure.

Table 2.2: Wave conditions considered in this analysis. Operational conditions come from [50] for Portugal and [51] for California. Extreme weather conditions come from [52] for Portugal and [53] for California.

	Operational Conditions		**Extreme Weather Conditions**	
	Wave Height [m]	**Wave Period [s]**	**Wave Height [m]**	**Wave Period [s]**
Potential Portugal Site	1.2	11	3.2	18.2
	1.2	14	3.5	18.3
	1.8	11	4.5	15.7
	1.8	14	4.1	18.4
Potential California Site	1.1	8.6	7	8.8
	1.1	10.9	9	12.18
	1.4	8.6	11.2	17.3
	1.4	10.9	9	21.1

The mean total wave force over one period is the mean wave drift force. As illustrated, the orientation of the substructure to the incoming wave will dictate its location in the wave field relative to the other floaters. Therefore, various substructure rotation angles are considered and the greatest result under each of the conditions described is taken as the resulting wave force.

Morison's equation can be applied only on slender bodies in which the ratio of the diameter to the wavelength is less than 0.2. Given that the diameter of the floaters of the substructure are 12.5m (see Appendix B.1), the wave period must be greater than 6.3 seconds to apply Morison's equation here—a condition satisfied in each of the wave conditions considered.

To cross-validate the wave forces attained through Morison's equation, Ashes simulation software [54] is also used to confirm that the results are of the same order of magnitude (see

Table B.3 of Appendix B.5). While the resulting wave force can differ greatly based on the wave parameters and method used, the magnitude of the force is small compared to the wind force on the structure, a result also obtained by Roald and colleagues [47]. It is thus the wind force—which can be empirically calculated with a high degree of reliability—that dominates the turbine thrust force. Hence, the simplification of the wave forces acting on the substructure does not bias the results. To be conservative, I apply the largest magnitude wave force from the conditions described in Table 2.2 uniformly across all the floating turbines.

2.2.2 Resultant turbine thrust forces

A vector combination of the wind, current, and wave forces considering their magnitudes and orientations gives the overall turbine thrust force. Design guidance from the American Bureau of Shipping (ABS) [42] is used to identify the parameters and orientations that must be considered for the environmental forces. Two design load cases (DLC) adapted to floating OSW turbines by the ABS are used: operational conditions (DLC 1.3) and extreme weather conditions (DLC 6.1). Details of the parameters in each case are given in Table 2.3 [42].

Table 2.3: Environmental loading conditions at the design level as defined by the ABS guide for designing station-keeping systems [42].

Parameter	Operational Conditions	Extreme Weather Conditions
ABS Design Load Case	DLC 1.3	DLC 6.1
Wind Speed (at hub height), V_{hub}	$V_{cut-in} < V_{hub} < V_{cut-out}$	V_{hub} = 50-year, 1-min maximum
Surface Current Speed, V_{curr}	The wind-generated currents based upon a 10-minute mean wind speed at hub height. $V_{curr} = \mathbb{E}[V_{curr} \| \mu(V_{hub})]$	V_{curr} = 50-year currents
Wave Height, H	Normal Sea State, $H = \mathbb{E}[H \| V_{hub}]$	$H =$ 50-year occurence
Wave Period, T	(Not defined)	(Not defined)
Wind and Wave Directionality	Unidirectional wind and wave directions	Misaligned wind and wave directions; the misalignment between wind and waves (ψ) is to be considered up to 90-degrees

Figure 2.5 presents the relative orientations of the forces considered in the two cases [42]. The maximum force under the conditions described in each DLC multiplied by a factor of safety gives the design load which the station-keeping system must be able to withstand.

Further details on the environmental parameters used to calculate the resulting design load are given in Appendix B.11.

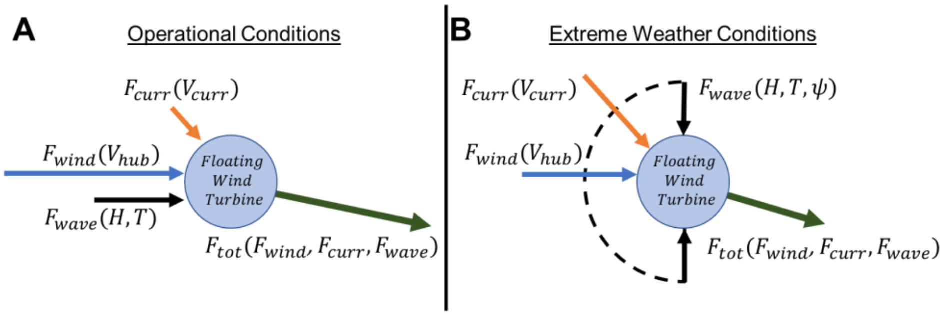

Figure 2.5: Orientations of the wind, current, and wave environmental forces. A) Operational conditions and B) extreme weather conditions were considered. The resultant vector F_{tot} is the vector combination of the three environmental force vectors for wind (F_{wind}), wave (F_{wave}), and current (F_{curr}) forces. The symbolic parameters that each force is dependent on correspond to the descriptions given in Table 2.3. Note: the magnitude and direction of the vectors are not to scale in this figure.

These two cases represent a range of potential DLCs. In a detailed design study, every DLC would be applied to a floating turbine configuration, and engineers would design their system to contend with the most unfavorable case. This would require detailed metocean data for a specific site, however this study considers broader regions (US and Portugal) described by a range of environmental conditions. Therefore, the design load under two DLCs is estimated and the case which results in a greater one is chosen. The following simplifying assumptions to the physical model are made, as the goal of the calculations is to estimate the energy consumption of the thrusters and the magnitude of the cost penalty as opposed to developing a detailed design:

- The orientation of the environmental forces is as defined by the DLCs as opposed to meteorological data from a specific site.
- The wind speed has a Weibull distribution.
- Following [55], the surface current speed is determined as a percent of wind speeds 10m above the water surface, with a 30° offset to the wind [40] since the angular offset was not specified by the DLCs.
- Although wave parameters may be determined in part by wind speed, in the absence of a generalizable relationship, wind speed and wave conditions are considered

independent. The parameters (height, period, angle offset to wind direction) in each DLC from Table 2.2 are used to compute a range of possible mean wave force magnitudes. The maximum wave force magnitude from the range of parameters is used, considered constant, and applied across the domain of wind speeds.

The total force vector can be formulated as a vector sum of each environmental force. The wave force is of uniform magnitude (as described), while the current and wave forces are functions of the wind speed measured at hub height, and thus the total overall thrust force vector is a function of the wind speed at hub height:

$$\vec{F}_{tot}(V_{hub}) = \vec{F}_{wind}(V_{hub}) + \vec{F}_{curr}(V_{curr}(V_{hub})) + \max_{H,T,\psi}\left(\vec{F}_{wave}(\hat{H},\hat{T},\hat{\psi})\right)$$

The magnitude of the force that must be applied by the thrusters to counteract environmental forces is the magnitude of the total force vector:

$$F_{appl}(V_{wind}) = \left\|\vec{F}_{tot}(V_{hub})\right\| \tag{2.5}$$

The forces calculated with this method are validated on a 5MW turbine using OrcaFlex simulation software furnished by Orcina [56]. Further details of the validation are provided in Appendix B.6.

2.2.3 Thruster system sizing

Cost and performance values for commercially available, pivoting, ducted thrusters from a global DP thruster supplier are employed [57]. Table 2.4 summarizes the technical specifications, and the cost of acquiring, transporting, and installing the various thruster options. For each of the nine thruster types, DP station-keeping configurations that include 1 to 30 replicates of the same thruster mounted on the underside of a turbine are considered—giving a total of 270 configurations assessed for each turbine size. Thruster types are described by input power in kilowatts (kW), delivered thrust in kilonewtons (kN), size (m), and unit price in US dollars (USD). Only those configurations which can supply the design load are considered.

Table 2.4: DP thruster specifications considered in the analysis [57]. Unit price includes the cost of acquiring, transporting, and commissioning the thruster. The computed delivered thrust is computed using equation (2.6) for comparison to the nominal value provided by the manufacturer.

Nominal Input Power (kW)	Propeller Size (m)	Nominal Delivered Thrust (kN)	Computed Delivered Thrust (kN)	Unit Price (USD)
3200	3.2	598	589	995,100
4000	3.5	737	726	1,070,000
4800	3.8	881	866	1,230,500
5500	4.1	1018	998	1,534,380
6500	4.5	1,214	1,187	2,210,620
3200	4.1	707	695	1,177,000
3800	4.5	853	830	1,444,500
4500	5.0	1,026	996	1,765,500
5500	5.5	1,254	1,214	2,461,000

ABS provides a generalized relationship between input power and applied force for the DP thrusters in equation (2.6) [58] which accurately represents technical data of DP thruster power versus delivered thrust (see Figure B.11 of Appendix B.8). Equation (2.7) gives the power as a function of applied force for a single thruster. An idealized situation is assumed in which the force is applied equally across all thrusters so that each consumes the same amount of power, and neglect interaction effects between thrusters in this analysis, given the size of the substructure relative to the dimensions of the DP thrusters. The power consumption of a system consisting of n thrusters is thus estimated with equation (2.8).

$$F_1 = K \times (P_1 \times D)^{\frac{2}{3}} \tag{2.6}$$

$$P_1 = \left(\frac{F_1}{K}\right)^{\frac{3}{2}} \times \frac{1}{D} \tag{2.7}$$

$$P_{DP}(F_{appl}, n) = \frac{n}{D} \times \left(\frac{F_{appl}}{n\,K}\right)^{\frac{3}{2}} \tag{2.8}$$

where F_1 is the bollard pull force in newtons (N) and P_1 is the power required (kW) for a single thruster, K is a constant equal to 1,250, and D is propeller diameter (m) [58]. F_{appl} is the needed station-keeping force as defined in equation (2.5) earlier, and P_{DP} is the DP system power requirement (kW). There is a direct relationship between thruster diameter and applied bollard pull force at a constant power level as seen by equations (2.6) - (2.8). In the future, thrusters might be designed to optimize the force delivered at a given power level for this application—however, existing specifications for a range of thruster options are used here.

The expected thruster energy consumption is calculated using probability density functions (see Figure B.12 of Appendix B.9) for one Portuguese site [59] and two characteristic US floating OSW sites defined by the National Renewable Energy Laboratory's (NREL)—referred to as Wind Speed Classes (WSC) [60]. The annual expected thruster energy consumption, $\mathbb{E}_{TC}$, and the expected gross energy production, $\mathbb{E}_{GEN}$, are calculated by taking the expectation of the DP consumption, $P_{DP,n}(F_{appl}, n)$, and gross turbine power curves, $P_{GEN}(V_{hub})$, respectively, given these probability density functions, $f(V_{hub})$.

$$\mathbb{E}_{TC} = 8760 \times \left[\int_{V_{hub}} f(V_{hub}) \times P_{DP,n}(F_{appl}, n)\, dV_{hub} \right]$$

$$\mathbb{E}_{GEN} = 8760 \times \left[\int_{V_{hub}} f(V_{hub}) \times P_{GEN}(V_{hub})\, dV_{hub} \right]$$

The thruster consumption percent (TCP) is the percent of annual expected turbine energy output that is consumed by the thrusters,

$$TCP = \frac{\mathbb{E}_{TC}}{\mathbb{E}_{GEN}}$$

The difference between the expected generation and the expected thruster consumption gives the annual expected net electricity generation,

$$\mathbb{E}_{NET} = \mathbb{E}_{GEN} - \mathbb{E}_{TC}$$

2.2.4 Turbine and array LCOE

To choose the DP configuration, the LCOE for each turbine in WSC 8 and 14 is calculated—the ends of the range of characteristic US floating OSW sites—across all configurations of DP thruster types and numbers [60]. The chosen configuration for each turbine is that which minimizes its LCOE, calculated using a method adopted from the NREL Annual Technology Baseline (ATB) [60]:

$$LCOE = ((CRF * PFF * CFF * netOCC) + FOM) * 1000/(netCF * 8760) \quad (2.9)$$

where CRF, PFF, and CFF are the capital recovery, production finance, and construction finance factors, respectively. The net capacity factor (CF) for the turbine is calculated as,

$$netCF_{turbine} = \frac{\mathbb{E}_{NET}}{8760 \times turbine\ size}$$

The fixed operations and maintenance cost, FOM, for the DP system includes annual monitoring per thruster, and one overhaul maintenance after 15 years. For mooring chains, estimates of the annual maintenance costs come from [61]. Details of both costs are included in Appendix B.3. These costs are added to the FOM estimates for turbine and substructure from the NREL ATB [60].

The net overnight capital cost, $netOCC$, for DP is adjusted from the NREL base overnight capital cost (OCC) by reducing it by the proportion estimated for mooring, and increasing it by the DP system cost (USD/kW),

$$netOCC = baseOCC \times (1 - mooring\%) + (DP\ Sys\ CAPEX/Turbine\ Size)$$

where the estimated proportion of the cost that is attributable to the mooring system, $mooring\%$, is equal to 11% according to [62]. the DP system capital expenditure, $DP\ Sys\ CAPEX$, is directly computed knowing the number and DP thruster type with data from the manufacturer [57]. Assumptions from the NREL ATB for financing factors (CRF, PFF, CFF) and baseline costs are used [60]. Note that in the NREL ATB, a grid connection cost is part of the LCOE [60]. To obtain the LCOE at the platform, this cost is set to zero for both moored and DP floating turbines.

Once the LCOE is computed for all configurations, the one that realizes the minimum LCOE is identified as the LCOE-minimizing DP configuration, and the LCOE for a 1,000MW array is then estimated. In an array, wake effects arising from disrupting wind flow reduce the array net CF. The array net CF is extrapolated using data obtained from two models: the NREL flow redirection and induction in steady state (FLORIS) and the NREL ATB for the 1,000MW arrays to estimate baseline array CFs, $baseCF$, for the turbine sizes considered in this study (see Appendix B.7). The baseline array CFs are used for the moored array. The DP array net CF is estimated by reducing the baseline array CF by the TCP as,

$$netCF_{DP\,array} = baseCF \times (1 - TCP)$$

The LCOE for the array is calculated using equation (2.9) above. One potential benefit of DP turbines not quantified in this analysis is the ability to reposition turbines to reduce wake effects. Rodrigues and colleagues [63] provide an example of optimizing layout and reconfigurations to reduce wake losses with moored turbines, and doing the same with DP arrays is recommended for future study.

2.2.5 Length of eliminated mooring chains

The length of mooring chains needed for a floating turbine is computed as in [64]:

$$L_s = h\sqrt{\left(2\frac{T_H}{\omega h} + 1\right)}$$

where h is water depth (m), T_H is the horizontal design load (tons), and ω is the unit weight of the mooring chain (ton/m). Chains weighing between 0.1-0.6 ton/m are assumed [65] which have breaking loads greater than the needed design loads across all turbines. Three catenary mooring chains are deployed at depths of either 160m and 635m, corresponding to WSC 8 and 14 in the NREL ATB, respectively [60]. With the length of chains needed for a single turbine, the length of chains for a 1,000MW array is computed by considering the number of turbines needed for an array of that capacity.

2.3 Results

Results of the validation of the overall thrust force calculations using OrcaFlex [56] are shown in Figure 2.6A demonstrating general agreement with the analytic R model in this study with only slight discrepancies. The slight discrepancies likely owe to model differences, such as different drag coefficients and dimensions of the floating turbine components, and the interactions between turbine components interrupting wind and current flow. While the model used in this study underestimates the OrcaFlex results beyond the turbine cut-out wind speed, these winds occur with little frequency. Taking the expectation of the turbine thrust force, the expectation from this analytic model is greater than that of the OrcaFlex simulation model results by less than 2%. Therefore, the simplifications used to analytically estimate the turbine thrust forces are close to the results that would be obtained through sophisticated marine engineering software.

Thrust forces on the OSW turbine are nonlinear with respect to increasing wind speeds, as shown in Figure 2.6. Below the turbine's cut-in wind speed and above the turbine's cut-out wind speed, the blades are feathered to reduce turbine thrust forces, giving rise to the discontinuities in Figure 2.6. At just above the cut-in wind speed, blades are positioned to convert as much wind as possible. At wind speeds above the rated wind speed, blades begin to feather to maintain a constant rate of rotation and level of power generation, consequently reducing the thrust forces on the rotor. A discussion of this behavior is provided in Appendix B.10. Figure 2.6A illustrates the results of the model used in this study versus steady-state results using OrcaFlex simulation software, demonstrating agreement between the two methods.

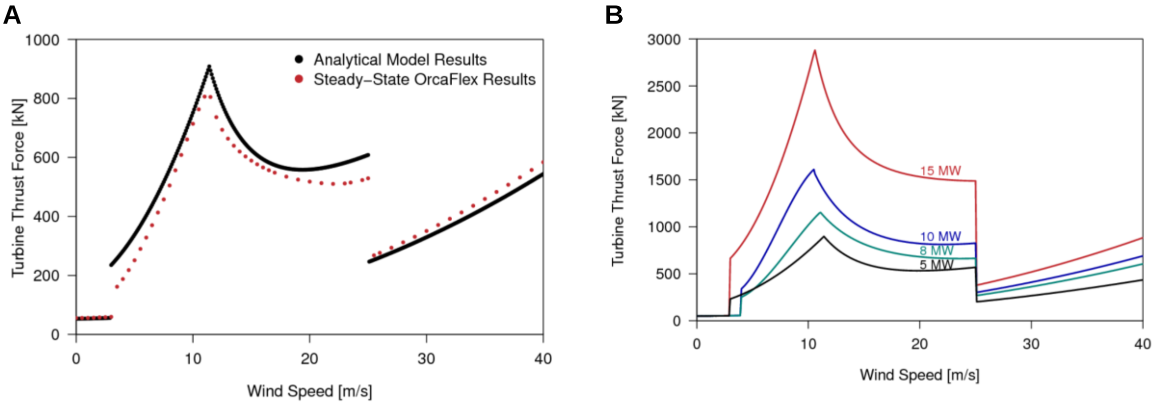

Figure 2.6: Overall turbine thrust force results. A) Verification results of the analytical R model (black) used to calculate the turbine thrust force compared with the results obtained at steady state using OrcaFlex software (red dots) on the 5MW turbine. B) Resultant turbine thrust forces on the 5, 8, 10, and 15MW OSW turbines.

Turbine thrust forces are much higher during operation than extreme wind speeds when blades are feathered. Therefore, the maximum force under operational conditions multiplied by a safety factor of 1.67 [58] gives the design load for the station-keeping system.

2.3.1 Net power curves illustrate potential for operational and design improvements

For each configuration of DP thruster sizes and numbers, the turbine thrust curves (Figure 2.6) are translated into power consumption curves. Figure 2.7 shows a subset of the results: the resulting power consumption and net power curves for two DP configurations for a 5MW turbine. The power ratio (the thruster power consumption divided by the generated power at a given wind speed) falls rapidly beyond the rated wind speed, which a prior study found to be greater than 50% for this turbine [31]; however, the discontinuity above the rated wind speed due to a feathering of the blades was not captured in prior studies.

Figure 2.7 provides the resulting net power curves for two configurations for one turbine. Due to the greater efficiency of DP thrusters at lower power levels, for a given thruster size, more thrusters consume less energy to deliver a fixed level of thrust (see equation (2.8))—albeit at a higher capital cost. Therefore, it follows that a DP configuration with four thrusters (Figure 2.7A), and one with ten thrusters (Figure 2.7B) illustrates that increasing numbers of thrusters can greatly reduce thruster power consumption, evidenced by the red curves in Figure 2.7. For the four-thruster configuration (the same configuration studied in [31]), about 50% of the turbine generation is needed to power the DP system at the rated wind speed echoing prior findings from Xu and colleagues [31]. This falls to nearly 30% for the ten-thruster configuration indicating the importance of the thruster system configuration to the energy analysis.

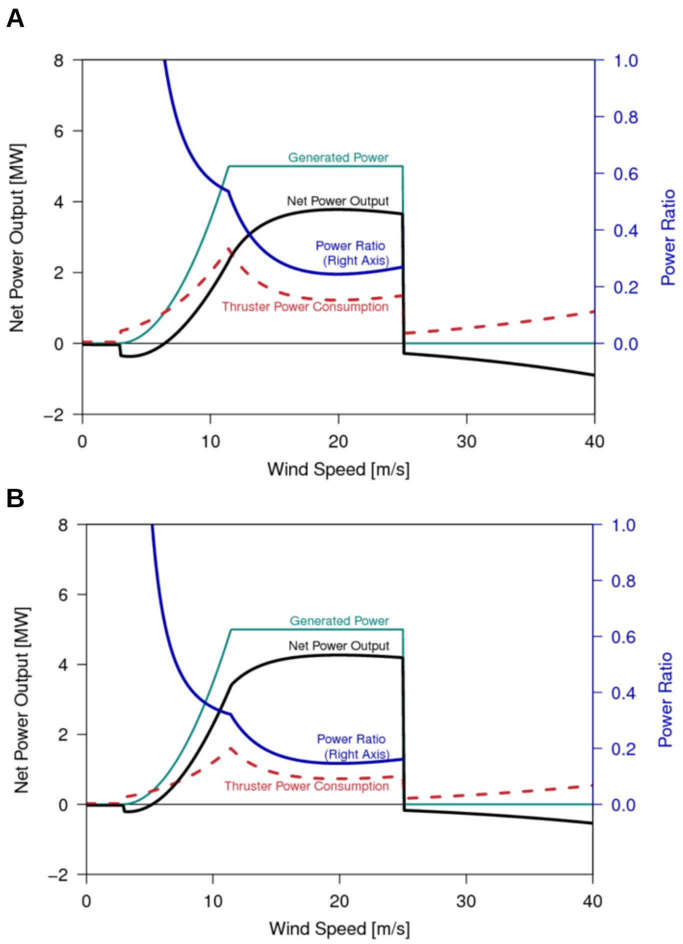

Figure 2.7: Net power curves and power ratios with a 5MW DP turbine. Detailed results on two configurations are shown: A) A configuration with 4, 3.8m diameter thrusters and B) a configuration with 10, 3.8m diameter thrusters.

The power curves illustrate the need for an auxiliary power unit (APU)—the size of which has not been estimated in prior studies to date. There are instances when the net power output is negative when the turbine is operating—just above the 3 m/s cut-in wind speed for this turbine. In practice, it would be advisable to not operate the turbine, keep the blades feathered, and incur the minimum thruster energy consumption at these low wind speeds. Another option would be to alter turbine design and operation such that the blades always remain feathered to some degree (as is done beyond the rated wind speed); for example, studies assess the impact of operational strategies for manipulating thrust forces on a floating turbine using yaw and pitch angles of the turbine to improve array efficiency, structural stability, and reduce structural fatigue as described in [66] in which fatigue loads are minimized through position control, that can be further enabled by DP. In this analysis, I do not address strategies to improve operations at these low wind speeds, which results in an overestimation how much the DP system consumes compared to how this novel turbine system would be operated in a real application. The net power output is also negative outside of operational wind speeds which would also require an APU. To estimate the size of the APU needed, wind speed data over a 10-year period from 2011-2020 at potential sites for near-term OSW development in the US and Portugal were analyzed. Up to 3 megawatt-hours (MWh) of stored energy is needed to station-keep during the longest continuous period of non-operating winds over that decade (see Table B.1 of Appendix B.4 and Table B.7 of Appendix B.12).

2.3.2 Intermediate turbines perform techno-economically better than the largest

The cost incurred by using DP is a fundamental consideration for the potential viability of this application to future wind farms. Figure 2.8 illustrates how additional thrusters monotonically decrease the TCP as previously mentioned. Figure 2.8 also illustrates the impact on LCOE that the added thrusters have, and that an optimal, LCOE-minimizing configuration is not found with the maximum (or minimum) number of thrusters. This behavior indicates that an analysis of only the energy performance is arbitrary because adding more thrusters monotonically reduces the TCP and improves the net energy output of a DP turbine. However, the added cost eventually outpaces the efficiency gains as LCOE initially falls and begins to rise with additional thrusters. The tradeoff of adding more thrusters with cost is thus an important point of analysis for this application. The TCP and LCOE for each wind turbine, DP configuration, and WSC are provided in the Appendix B.15, along with details of the LCOE-minimizing DP system configuration for each wind turbine size.

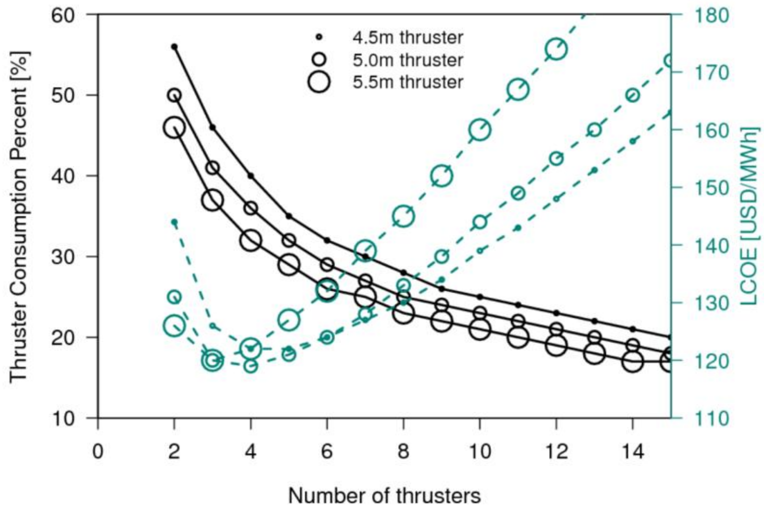

Figure 2.8: The TCP (black, left axis) and LCOE (green dashed, right axis) for the 5MW turbine considering different thruster diameters and numbers of thrusters. The behavior illustrates how the energy performance (measured by the TCP) continuously falls as more thrusters are added, while the added cost of each additional thruster increases the LCOE beyond a certain number of thrusters.

Figure 2.9 depicts the resulting LCOE of the LCOE-minimizing configuration for each turbine size for a 1,000MW array in comparison to an array that uses moored turbines. The distance between the horizontal bands and points of the same color in Figure 2.9A represents the increased LCOE (i.e., the cost penalty) incurred by deploying DP turbines in lieu of moored turbines of that size; this penalty is explicitly reported in Figure 2.9B. The LCOE penalty for DP systems under the conditions studied is between 30 and 200 USD/MWh. The LCOE for a DP turbine array does not decrease as turbines get larger as it does with a moored array; intermediate turbine sizes (8-10MW) realize the lowest LCOEs among the turbine sizes studied—this result also holds for all DP configurations when the same configuration is used for each turbine (see Figure B.15 of Appendix B.14). This is a notable result considering industry reports [18] and studies cite turbine upsizing as a means to reduce LCOE [67]. Because they experience greater turbine thrust forces, the energy requirement to dynamically position large turbines outpaces gains in energy generation. As this analysis considers reference turbine designs which vary in multiple design dimensions simultaneously (tower height, blade length, tower diameter) as seen in Table 2.1, the drivers of this behavior cannot be isolated, but presents an interesting avenue for future work where all feasible designs for each turbine capacity are analyzed with DP. As the turbine thrust forces have an impact on the power output in this paradigm, methods of minimizing the thrust forces while maintaining power production should be considered to further improve the output of turbines that use DP and reduce the LCOE penalty.

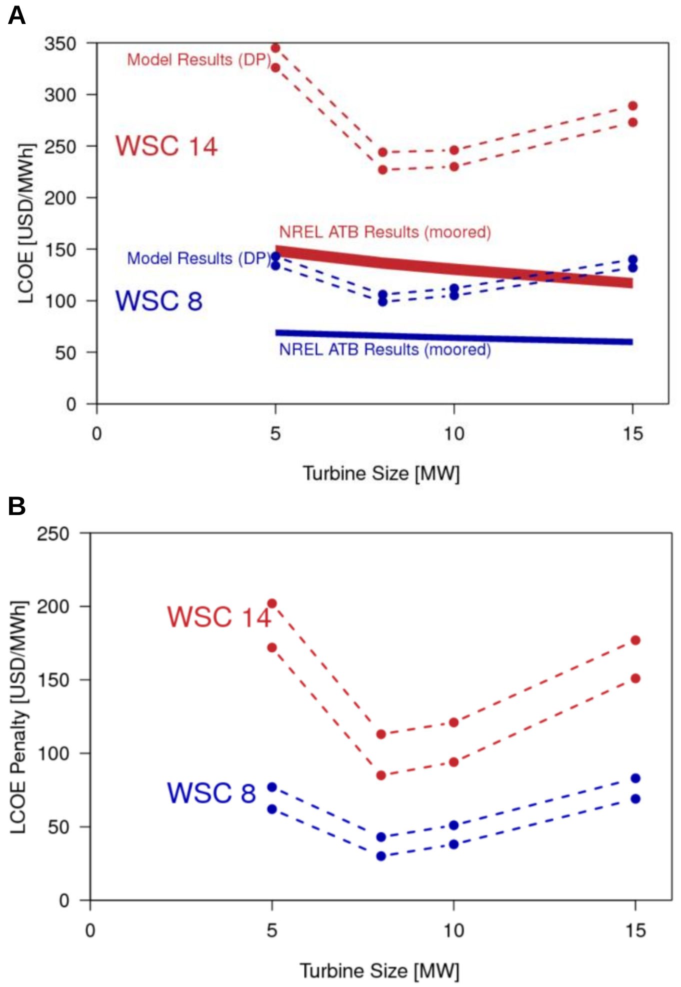

Figure 2.9: LCOE Results for DP arrays. A) LCOE ranges for DP system configurations for turbine arrays in WSC 14 (upper red, dashed) and WSC 8 (lower blue, dashed), compared with arrays of moored turbines in the same WSC using NREL ATB data [60] (bands of the corresponding colors). B) Range of LCOE penalties (difference between LCOE of DP arrays and moored arrays) for each turbine size.

If all other things are held equal, greater water depth increases mooring costs, while the cost of DP is unaffected by increased depths, resulting in a reduction in the LCOE penalty when water depths are great and increasing the viability of DP for use in deeper waters. Isolating the effect of increased depth on the viability of DP compared to the increased cost of mooring is another theme suggested for future study.

2.3.3 More than 900km of array mooring chains can be eliminated

Figure 2.10 illustrates the length of mooring chains needed for a 1,000MW OSW farm. A range of chain weights is shown to illustrate the effect that choosing stronger and heavier chains would have on the cumulative chain lengths, and the results are presented considering average water depths in the two WSCs. WSC 8 considers an average depth of 160m and WSC 14 considers an average depth of 635m. Between 110km (15MW turbine, 0.6 ton/m chain, 160m depth) and 910km (5MW turbine, 0.1 ton/m chain, 635m depth) of chains can be eliminated by using DP for a 1,000MW array.

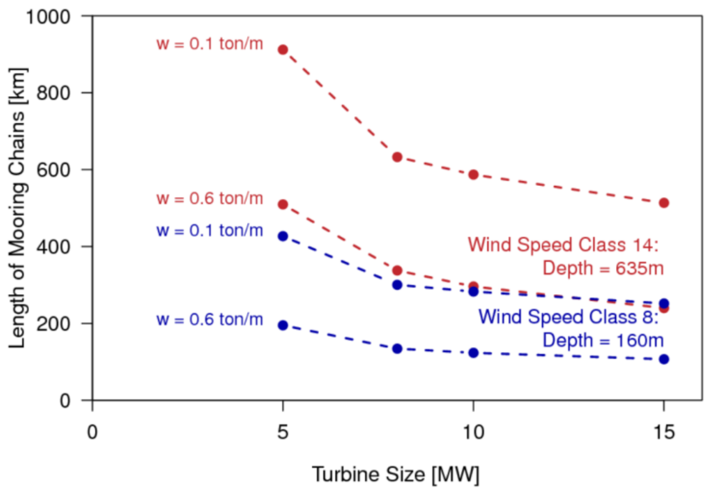

Figure 2.10: Length of mooring chains needed for a 1,000MW plant considering water depths of 160m (blue) and 635m (red) and considering three mooring chains per floating turbine.

Figure 2.10 shows several things. Of course, deeper waters require longer mooring chains—at least 130km more chains are needed for a 1,000MW array when depth increases from 160m to 635m (15MW turbine with 0.6 ton/m chains), and as much as 485km more chains may be needed (5MW turbine with 0.1 ton/m chains). Increasing turbine size reduces the length of needed mooring chains because fewer turbines are needed to achieve the 1,000MW array capacity falling by as much as 400km (the difference between the length needed for a 5MW turbine array and 15MW turbine array in 635m depths). Therefore—classifying eliminated mooring chains as an environmental benefit—the benefit of directly substituting DP with mooring chains is greater in deeper waters, and for arrays that deploy smaller turbines, behaving differently than the cost penalty as a function of turbine size. A more detailed quantification and weighting of the environmental benefit of eliminating mooring chains with respect to the cost penalty of using DP, and thus a more advanced benefit-cost analysis of the DP strategy, is an avenue for future work.

2.4 Discussion

The design of a DP station-keeping system has recently become an interesting avenue for research as evidenced by recent work on the energy performance of the application [31], [32], [34], [35]. The primary contribution of this chapter to the growing interest in the application is the reporting of the cost implications, which is necessary in any discussion on its viability. Furthermore, the finding that intermediate size turbines are more likely to be attractive than very large turbines is a novel one. As demonstrated, without considering costs, the energy performance continually improves by adding thrusters (Figure 2.8), and therefore a cost analysis is critical for advancing an adequate understanding of this application.

The prevailing trend in OSW power has been to pursue larger turbines, because they are able to generate more energy per unit of marine area and require fewer installations to achieve a given plant capacity [68]. In contrast, for floating DP systems, the largest turbines do not minimize the LCOE of this application. This finding adds support from a technical perspective for the growing literature which suggests that deploying smaller, modular technologies can benefit the diffusion of the technology through cost reduction [69] and realize a broad range of other deployment benefits [70], including the possibility of siting in waters that are too deep for conventional mooring.

It is important to note that there is still an LCOE penalty in all the conditions studied here. Despite the higher LCOE of a DP system compared to a moored one at the conditions studied, it can realize several benefits. A DP system would promote cost control and serial manufacturing by reducing installation work needed [62]; allow for turbines to be repositioned to reduce wake effects [63]—improving the CF; allow for repositioning to avoid extreme weather events; reduce regulatory risks since laws like the US Jones Act would be inapplicable to these structures [5]; and realize additional benefits [15]. The main benefit quantified here is the reduced interaction with the seabed and open ocean by eliminating as much as 900km of mooring chains. Mooring chains create structural impediments and pose a moderate entanglement risk to marine life [27]. Anchor and chain disturbance on the seafloor also pose a risk to benthic habitats [71]. Although there is a possibility that fixed-bottom foundations promote habitat growth through an 'artificial reef effect' [72], there are also concerns that such growth on mooring chains may cause 'biomass fouling' [17]. In contrast, ducted propellers eliminate interaction with the seafloor from embedded anchors and catenary chains that lay and drag along the seafloor, and a review of collision risk with sea life finds that ducted propellers reduce the risk by 75% compared to open propellers on moving ships [73]. The continuous operation of DP thrusters would also add to the noise already produced by the floating turbine [29], however there is low confidence that anthropogenic marine noise increases mortality of marine animals [74], and new thruster designs are being developed to reduce noise generation [75]. Nevertheless, noise impacts should be explored in future work with floating turbines that use DP. While the full environmental impacts of floating installations, mooring chains, and DP requires further study, public and stakeholder concerns regarding these effects have been raised in the past and resulted in the need for substantial environmental reviews of the potential local impacts in the US [72] and the UK [17]. While the agency that external stakeholders have over current and future deployments has not been sufficiently studied in the literature, some studies and reports cover stakeholder disputes with proposed OSW farms and the regulatory and political challenges these disputes give rise to. Collectively, experience reveals that, these interests have been able to slow or block deployment of plants in the past [76]. Therefore, reducing the environmental impact has multiple implications by reducing physical risk, regulatory risk, and execution risks of floating OSW projects.

Low-carbon energy systems should accommodate environmental concerns and stakeholder interests. Doing so should facilitate easier deployment under the existing socio-technical regime. Competing marine uses fall from 48% of near shore area to 8% beyond 50 nm from the US coast [21]. For context, only 10% of continental US waters are beyond 50nm from shore and within the 1,000m depth limit of mooring technology. DP turbines thus provide one example of how accommodating other interests might be accomplished as they can be built in deeper, more distant, and less-contentious waters, while also eliminating mooring chains.

While this chapter focused on using existing turbine and DP specifications, developers interested in adopting DP will need to optimize this configuration and develop operational procedures in the event of catastrophic failures in the positioning system. They should also perform an analysis of the environmental and economic benefits of a DP system like the possible lower development, installation, and decommissioning costs, in addition to a quantification of the benefits qualitatively discussed here.

2.5 Conclusions

This chapter assesses the techno-economic performance of dynamically positioned floating OSW turbines compared to moored systems which are the prevailing station-keeping method used for floating turbines today and finds that under several circumstances DP systems may be advantageous. While prior analysis on this application has focused on energy performance only, the implications on system cost is assessed here. The analysis of costs is an important contribution because energy performance can be continuously improved by adding DP thrusters to a turbine, but the added cost of additional thrusters eventually increases the cost of energy.

DP systems can realize several benefits. The system would avoid adverse environmental impacts of mooring chains and would open up an expanded ocean area where depths are too great for mooring. I develop a physical model to estimate the turbine thrust force experienced by 5-15MW reference turbines to size the station-keeping system, and thereafter estimate the expected DP system energy consumption when exposed to a range of environmental conditions. Turbines of intermediate size (8-10MW) achieve lower LCOEs than the largest 15MW turbine considered in this analysis—which is a novel finding as turbine upsizing is often cited as a means for reducing LCOE.

A DP system would consume electricity to power station keeping while the turbine is not generating—necessitating auxiliary power and energy storage. The estimated maximum stored energy needed to station-keep during an observed wind drought to be about 3MWh. While this system would be more expensive than a mooring system at depths of 630m, it eliminates up to 910km of mooring chains for a 1,000MW plant potentially reducing environmental impacts, easing stakeholder concerns, and easing the deployment process.

2.6 Code availability

The R codes used in this analysis are provided in the following repository: https://doi.org/10.5281/zenodo.7795777

Chapter III

Multi-Criteria Models Provide Enhanced Insight for Siting US Offshore Wind

3.1 Introduction

Large economies like China [77], the European Union [78], and the United States [79] view OSW energy as a key contributor to deep decarbonization. However, implementation in the US has been slow. While the US has a target of 30GW of OSW by 2030, not a single commercial OSW project is in operation in federal US waters [80]. The US has almost 40GW in the development pipeline, but past experience with development in the US raises doubts about how much OSW will ultimately be deployed.

Stakeholder and financial interests have played a strong role in early US project developments. The Cape Wind project was to be the first commercial OSW project in US federal waters, securing a lease in 2010 [81]. The leaseholder relinquished the rights to build the plant in 2017 after dozens of cases were brought on the plant with overwhelming concerns from coastal residents [77], [81], [82]. Bluewater Wind secured a lease off the coast of Delaware but faced financial setbacks and failed to have their cable landfall proposal (which was to be built under a public beach) approved by local and State authorities. The company eventually assigned their lease to another developer in 2016 [83], [84]. The Morro Bay wind energy area in California faced scrutiny during its early planning stages from the US Navy, which claimed that part of the site would interfere with their activities [85]. A case brought against Vineyard Wind alleged that the building of the plant should not take precedence over other marine interests and activities like fishing, navigation, and the ecological environment [86]. More recently, even projects with power purchase agreements (PPA) in place elected to pay penalties and withdraw from their contracts siting financial reasons [87], [88]. As this brief history makes clear, project developers must balance many concerns—internal and external—in their decision making. In the broader context of the challenges and tradeoffs with deploying technology at scale to achieve national decarbonization targets with satisfying a range of project-level concerns, a major challenge is how to decide who bears the monetary and non-monetary costs of developments. This chapter contributes to this discussion by developing a framework to balance project-level concerns.

Project design decisions like scale, location, and technologies carry many implications and impact techno-economic, environmental, ecological, and spatial concerns. Studies on project economics show that the largest plants and turbines tend to reduce costs [67], and the overall OSW market trend has been to move toward ever-larger plants and turbine sizes [80]. Conversely, experience also reveals that mega-scale projects can result in cost overruns and schedule slippage [89], and that smaller scale and modular deployments may accelerate adoption [69], [70]. Similarly, design choices dictate the physical assets needed, impact project space requirements, and environmental interactions. While planning and balancing the needs and uses of marine areas is key for sustainable energy development, in the US, no formal process for marine spatial planning is in place today [90]. Prior efforts at quantifying the tradeoffs of wind energy installations have considered visual, tourism/recreation, environmental/ecological, and industry impacts; and many studies use choice experiments or surveys of localized populations in their studies. Public concerns of visual disamenity as a cost has been studied as a tradeoff for OSW siting [91], [92], [93]. Choice experiments done in Scandanavia [94], [95] and in the US [96] find that there is a willingness to pay to reduce visual disamenity from wind plants. Further assessment on the economic implications of OSW plant siting has considered plant impacts on tourism [97], [98], [99] and coastal recreation [100], [101]. The value of reducing ecological and visual impacts of wind farms in the Irish Sea was estimated by Börger and colleagues [102]. With respect to impacts on existing shipping and fishing industries, Samoteskul and colleagues evaluate the impact of siting OSW farms closer to shore and find that the cost savings to OSW installations is greater than the increased costs to vessel navigation from re-routing [103]; and Hoagland and colleagues analyze OSW impacts in the US Northeast [104] finding that total economic welfare losses could amount to 14 million USD. Overall, a major theme in the literature on technology adoption is how social acceptance impacts technology diffusion of renewable energy [15]. The elements described above are elements of socio-political acceptance, and experience with resistance of wind energy in North America [105], [106] and a review of socio-political impacts from OSW in the US and Europe recommends that a clear, equitable, and transparent process for managing stakeholder interests is key for successful project implementation [107].

Given this context, selecting a site, and designing an OSW plant requires the consideration of multiple factors. This argues for the use of a multi-criteria decision model (MCDM) [108]. Here, I build such a model that makes three novel contributions. First, I explore the combination of site, technology, and plant size and the impact that they have on the criteria, developing the largest alternatives space for an energy siting study of this kind. Second, I contrast alternatives that have attractive techno-economics with those that address a broad range of plant impact concerns that may be raised by environmentalists, coastal residents, fishing interests, and others. For simplicity, I call these two perspectives “developer” and “stakeholder” paradigms, respectively. In the real-world, a developer may not only be a techno-economic optimizer, and a stakeholder may not only be a minimizer of environmental, ecological, industry, and aesthetic impacts. Therefore, I compare the best alternatives in each paradigm to identify where the two align and identify these as ‘consensus’ areas. Existing project proposals score high in the developer perspective but lower in the stakeholder perspective, suggesting that the record of failed implementation is unsurprising (see Figure C.1

of Appendix C.1). Third, I develop a detailed map of suitable deployment sites for all continental US federal waters, point investors and policy makers to sites that score highly under both perspectives and are therefore more likely to succeed, and suggest how government incentives could encourage successful implementation. The model uses publicly available datasets and representative weight profiles as used in a prior study [109].

Prior MCDM studies for OSW siting have assessed a limited and discrete set of alternative plants, ignored the impact of plant size, and failed to compare alternative technological paradigms to the status quo [110], [111], [112]. Only two studies have used MCDM methods to assess OSW site alternatives in a US domain [111], [113]. Technical criteria (wind speed, proximity to shore, water depth) are normally considered in the suitability of proposed alternatives [114]. Economic and social criteria (capital costs, revenues, proximity to shipping lanes, employment, and marine life impacts) are also accounted for in other studies, but on a limited set of alternatives [110], [111], [112]. When studies have used experts to identify weights on the metrics, they are either limited in number or comprise a set of experts that come from the OSW industry itself [108], [110], while external stakeholders and local communities have shown to have considerable agency over proposed projects. A few studies develop a fuller perspective over an entire jurisdiction's territorial waters; however, the resulting suitability maps are binary [115], or consider only energy performance metrics [114], and no such suitability maps are produced for the US. No studies consider how the choice of plant scale and technologies combine with its location to affect physical performance, and physical impacts that may result in concerns from external stakeholders. A literature review on MCDM applications for site selection for all renewable energy technology types can be found in [116]. In this study, I make several novel contributions to the literature. I assess all possible sites in a highly granular grid of continental US federal waters between 3 nautical miles (nm) and the 200 nm (370 km) EEZ. I consider a range of technology value chains that includes different plant and turbine sizes. The resulting suitability scores are compared to the status quo—a "No-Action" suitability score in which a plant is not built. The result is a large alternatives space (combining technology, scale, and site) which reveals insights on the U.S. OSW market, and strategies for improved deployment prospects. After exclusion criteria are applied (Table 3.6), 66 million alternatives (from an initial alternatives space of 146 million) are scored. The method of aggregating the impacts of neighboring grid cells allows for the comparison of plants of varying capacity, component size, and footprint which has not been done in the past. I also quantify an OSW farm's visual impacts from shore, considering different turbine and plant sizes; evaluate the extent of disrupted seabed that OSW deployment might cause; identify and integrate submerged obstructions, including cables; and integrate vessel traffic density, fishing effort, and the estimated biodiversity in each cell. Details of the technology value chains considered can be found in Appendix C.2.

Building on recent OSW market analysis [117], the "baseline" facility is a 1,000MW plant comprising 10MW turbines, with fixed foundations for depths up to 60m and moored floating foundations for depths between 60 and 1,300m. Plants transmit power to shore via high voltage cables (HVC). Results highlight when changes to this baseline case might lead to enhanced deployment prospects. Attributes considered (see Table 3.1) are: 1) total overnight capital cost; 2) unit overnight capital cost; 3) annual energy output; 4) levelized cost of energy; 5) visual impact; 6) impact on fishing; 7) impact on marine life; 8) impact on vessel traffic; 9) disrupted seabed; and 10) obstructions.

Table 3.1: Final plant metrics considering complete value chain, and location of the value chain.

Plant metric	Main Interested Party	Type	Description	Unit
OCC	Developer	Cost	Estimated Capital Cost of fabrication and acquisition of the plant	MUSD
Unit OCC	Developer	Cost		USD/MW
Annual Energy/H_2 Output	Developer, Public	Benefit	Expected annual energy output (electricity or hydrogen)	MWh/year or tH_2/year
LCOE/LCOH	Developer	Cost	Levelized cost of energy or levelized cost of hydrogen	USD/MWh or USD/kgH_2
Visual Impact	Coastal Residents	Cost	Expected number of visible turbines from shore	Turbines/plant
Impact on Fishing	Fisheries	Cost	Expected hours of fishing effort in the installed plant area (pre-plant existence)	Hours/year
Impact on Marine Life	Environmentalists, Conservationists	Cost	Expected number of observed species in the installed plant area (pre-plant existence)	Species/plant
Impact on Vessel Traffic	Vessel Operators	Cost	Expected number of vessel transits in the installed plant area (pre-plant existence)	Vessel transits/plant
Disrupted Seabed	Environmentalists, Conservationists	Cost	Expected area of seabed disrupted or unusable in the installed plant area	km2 of seabed/plant
Obstructions	Environmentalists, Conservationists, Fisheries	Cost	Expected volume of submerged obstructions in the installed plant area	m3 of obstructions/plant

These metrics represent a range of techno-economic outcomes and physical interactions with the plant. The latter quantifies the degree of potential plant exposure and interaction with various social, conservation, environmental, and industrial interests. The valuation of these impacts may go beyond the degree of exposure, however. For example, visual impact can further be classified based on the orientation of turbines [118], impacts on fishing activities and marine life can be classified based on the type of fish or species present in an area [72], and impacts on vessel traffic may depend on the type of vessel or shipping activity [103]. Furthermore, the perception and values of the groups of impacted stakeholders (or receptors) would alter the impact valuation, and these values may change from community to community as demonstrated with stated preference studies on visual disamenity [92], [94], [95]. I use the degree of potential physical exposure here because the metrics can be computed given the plant assets themselves and publicly available spatial datasets and do not require value functions from each group of receptors. Furthermore, I apply ‘representative weighting profiles’ constructed similar to a previous study [109] (see Section 3.2.4). The simplicity of the method therefore allows for the analysis to be carried out without surveying impacted stakeholders to elicit their values on the metrics and can be a tool used by developers in the early feasibility assessment stages of project design. I demonstrate the model's usefulness with observed data and provide insights on key decisions (size and sites) for project developers. To examine the impact of different representative weight profiles, I consider several others than the "developer" and "stakeholder" profiles I present in the main results (see Appendix C.8) and do a sensitivity analysis by considering several other weight profiles and their impact on the results (see Appendix C.9). The rest of this chapter is organized as follows: the metric calculation process and multi-criteria method is described in detail; the results are then presented; and then a discussion and brief conclusion follow.

3.2 Data and Methods

The suitability score is calculated with the following steps, depicted in Figure 3.1:

1. Analysis domain setup
2. Grid square metric calculations
3. Plant site metric calculations
4. Suitability score calculations

Figure 3.1: Suitability score methodology process.

The following section describes each step, and further details on parts of the methodology are provided in Appendix C.

3.2.1 Analysis domain setup

The geographic domain is the federal waters of the contiguous US: all waters from 3 nm from the shoreline (9 nm from the shoreline for Texas and the Gulf Coast of Florida as per the Submerged Lands Act [119]) to 200 nm from the shoreline—the extent of the EEZ—of the continental US. A 2km x 2km grid is established, and each grid square may contain one wind turbine, or one collector platform. QGIS is an open-source software used as the primary geographic software for this analysis. This grid spacing follows recommendations from a study by the US Coast Guard to allow for safe vessel navigation through an OSW plant, which it established as 1nm (1.85km) [120]. There are 868,064 2km x 2km grid squares in the continental US federal waters.

The technological domain describes the value chain options of turbine size, station-keeping type, plant size, and transmission method (Table 3.2). A detailed description of each technology is provided in Appendix C.2. These options were chosen based on data availability and to get a range of current and novel technologies which may be used to deploy OSW. Novel technologies considered—DP station-keeping and PtH transmission—offer a tradeoff in increased costs, at a reduced physical presence (fewer obstructions and disrupted seabed).

Table 3.2: Value chain options for the set of OSW plants considered in this study.

Turbine size	Station-keeping method	Transmission method	Plant size
• 5 MW • 8 MW • 10 MW • 15 MW	• 'Fixed': Fixed foundations using monopiles • 'Moored': Floating semisubmersible foundations with mooring chains • 'DP': Floating semisubmersible foundation with dynamic positioning (DP)	• 'HVC': High voltage export cable. Either alternating or direct current. • 'PtH': Power-to-hydrogen that is shipped to shore	• 200 MW • 400 MW • 600 MW • 800 MW • 1,000 MW • 1,200 MW • 1,400 MW
• 'No-Action': Alternative where no plant is built			

These value chains are upstream of the end-user and terminate upon delivery to shore, therefore, I do not assume anything about the market size or sectors in which the electricity or hydrogen will be used. Therefore, the difference in price of hydrogen or electricity and the markets that would use each is not considered and the metrics focus on cost, as opposed to profitability. Nonetheless, considering end-use markets presents an interesting avenue for future work. There are 168 value chains possible given the combinations of options listed in Table 3.2. I further consider one "No-Action" option in which a plant is not developed. Considering any of these value chains centered in any of the grid squares, there are 146,702,816 alternatives (combinations of value chain options and locations) in this analysis. As discussed later, exclusion criteria and infeasibility eliminate many of these alternatives.

The metrics in Table 3.3 are collected and parsed into a value for each grid square; the source for each metric is provided in the table.

Table 3.3: Data for each grid square.

Parameter	**Description**	**Units**	**Source**
Mean depth	Mean water depth in the grid square	m	[121]
Distance to shoreline	Distance from centroid of grid square to the nearest shore	km	*
Length of submerged cables	Length of submarine cables within the grid square	m	[122]
Marine protected area	Whether the grid square overlaps with an established marine protected area (MPA)	[1,0]	[123]
Shipping fairways	Whether the grid square overlaps with an established shipping fairway.	[1,0]	[124], [125], [126], [127]
De facto marine protected area	Whether the grid square overlaps with a de facto marine protected area (DMPA) which is a place restricted by law for reasons other than conservation or natural resource management (includes natural and cultural heritage sites)	[1,0]	[128]
Fishing effort hours	Mean of maximum fishing vessel effort from 2012-2021	hrs	[129]
Capacity factor	Capacity factor for a turbine installed in the grid square	%	[130]
Mean wind speed	Mean wind speed in the grid square	m/s	[130]
Land distance to transmission system	Distance from landfall point to point of interconnection	km	[130]
Vessel traffic	Mean of the maximum number of transits from 2015-2021	vessels/area	[131]
Marine life	Marine life species richness	species/area	[132]

* Calculated using GIS software

The fishing effort value came from a finer grid (1.1km x 1.1 km) than the one used here [129]. I take the maximum value among the observations within each grid square as the value for the year. The same process was used for the number of vessel transits in each grid square in which the original dataset used a 100m x 100m grid [131].

Capacity factor, wind speed, and landfall distance to transmission were all calculated using a NREL dataset [130] which was less granular than the grid spacing used (the spacing used was greater than 2km x 2km). The values of each metric in the nearest point in the NREL dataset to the centroid of each grid square was recorded as the value for each grid square.

The marine life value used data from the UNESCO Ocean Biodiversity Information System [132] and followed a data processing procedure from [133].

3.2.2 Grid square metric calculations

Additional metrics must consider the parameters of the value chain. The metrics in Table 3.4 are computed for each value chain—some pertain to only a few options. I compute the relevant metrics should either a turbine or collector platform be placed in the grid square. Upon calculating the plant metrics in the next step, only the metrics for the asset in the grid square are considered.

Table 3.4: Additional grid square metrics computed for each combination of turbine size, station-keeping type, and transmission.

Metric	Units	Specific to Value Chain Option
Turbine visibility	[0,1]	
Obstructions	m^3/turbine	
Disrupted seabed	m^2/turbine or m^2/collector	Fixed, Moored, HVC
Turbine annual energy	MWh/turbine-year	
Turbine asset costs	MUSD/turbine	
Export system costs	MUSD/plant	
Export system efficiency	%	

Turbine visibility: According to Maslov and colleagues, the minimum object size that is discernable with normal visual acuity is one arc minute [118]. Considering the tower width (which is the largest single body of the turbine), the distance at which the turbine tower is equal to one arc minute in an observer visual field (standing on the shore) is the sight distance used here. In other words, to be visible the tower diameter, D, must be greater than one arc minute of the circumference of a circle a distance r away:

$$D_{tower} \geq \frac{2\pi r}{360 \times 60}$$

For a given tower diameter, solving for r_{sight} gives the maximum distance at which a tower is discernible, this simplifies to,

$$r_{sight} \leq \frac{10{,}800 \times D_{tower}}{\pi}$$

Which becomes the necessary condition for which a single turbine is visible from shore. The results for the turbines in this study are reported in Table 3.5. If a grid square has a distance to shore less than r_{sight} for the chosen turbine, its visibility value is one, or else it is zero.

Table 3.5: Turbine sizes and sight distances.

Turbine Capacity (MW)	**Turbine Tower Diameter, D_{tower} (m)**	**Computed Turbine Sight Distance, r_{sight} (km)**
5	6 [38]	20.6
8	7.7 [39]	26.5
10	8.3 [40]	28.5
15	10 [37]	34.4

Obstructions: This metric is calculated as the volume of submerged substructure and submerged moorings. For monopiles, the volume of submerged substructure is estimated as the volume of a cylinder with a diameter equal to the base diameter of the turbine and a height equal to the mean water depth of the grid square. The volume of the submerged floating substructure is computed using the dimensions and specifications of the semisubmersible used [36].

For moored floating turbines, the length of submerged mooring chains is calculated as in Huang & Yang [134]:

$$L_s = h\sqrt{\left(2\frac{T_H}{\omega h} + 1\right)}$$

where h is water depth (m), T_H is the horizontal load (tons), and ω is the unit weight of the mooring chain (ton/m). I assume chains weigh between 0.1-0.6 ton/m [135] which have breaking loads greater than the design loads across all turbines. A submerged mooring chain is considered to have a swept volume of 1 m^3/m of submerged mooring chain [136].

Disrupted seabed: The disrupted seabed is computed for components that lie on the seafloor. These are: scour protection, mooring chains on the seafloor, and cables. For each fixed turbine, the area of scour protection needed considers a scour radius of 50m [72]. For a moored turbine, the area of disrupted seabed from mooring chains is computed following Qi Pan and colleagues [137] and considers three mooring chains. For the export cable, the minimum distance to shore from the collector is considered with a buffer on either side of 60m [138].

Turbine annual energy: The annual output of a given turbine in a grid square is computed using the capacity factor and turbine size as,

$$E_{turbine}\left[\frac{\text{MWh}}{\text{year}}\right] = Cap\_factor \ \times Turbine[MW] \times 8760 \left[\frac{hrs}{year}\right]$$

When considering a DP turbine, the expected energy output is reduced by the TCP (see Appendix C.4). The energy output of a DP turbine is thus reduced by the TCP as,

$$E_{DP\ turbine}\left[\frac{\text{MWh}}{\text{year}}\right] = E_{turbine} \ \times \left(1 - TCP(V_{wind}, T)\right)$$

where the TCP is a function of the mean wind speed, V_{wind}, and the turbine size, T.

Turbine asset costs: The sum of the total costs incurred by installing a turbine in a grid square is computed considering the cost of the following components:

- Turbine
- Monopile (fixed)
- Semisubmersible (moored, DP)
- Inter-array cable

Export system costs: The sum of the total costs incurred by installing the collector system in a grid square is computed considering the cost of the following components:

- Submarine export cable cost (HVC)
- Offshore substation costs (HVC)
- Electrolyzer cost (PtH)
- Hydrogen shipping vessel cost (PtH)
- Transformer cost

Note that cable routing is an optimization problem with the objectives of reducing impacts on stakeholders and cost—as has been described in [139] and applied in [140]. I assume the export cable length as the straight-line distance to the closest point to shore, which is a lower limit, as cable routes will likely not follow a straight path to shore, nor terminate at the closest land point (the location of substations, transmission systems, and land ownership will constrain landfall areas). Cable routing can thus be treated as its own optimization problem using multi-criteria frameworks or others, and while it is not treated in this analysis, I may explore this as an avenue for future research.

Export system efficiency: The efficiency of the export system is used to calculate the amount of energy delivered to shore annually. It is computed by considering the conversion efficiency of components at the collector site and the losses incurred in transit from the collector site to shore. For cable transmission, transformer efficiency, cable parameters, and functions to compute cable losses come from Xiang and colleagues [141]. Resulting simplified equations for the efficiency of high voltage alternating current (HVAC) and high voltage direct current (HVDC) cable transmission to shore are:

$$\eta_{AC,trans} = 1 - \frac{S_{TT} \times F \times \eta_{AC,offT}}{V_{cn}^2} \times \frac{r_c \times l_c}{nc_{AC}}$$

$$\eta_{DC,trans} = 1 - \frac{S_{TT} \times F \times \eta_{DC,offC}}{V_{cn}^2} \times \frac{r_c \times l_c}{2nc_{DC}}$$

where S_{TT} is the power rating of system (in megavolt-amps, MVA), F is the power factor for transmission (assumed to be 1.0 here), $\eta_{AC,offT}$ is the efficiency of the HVAC offshore transformer station (equal to 99.4%), $\eta_{DC,offC}$ is the efficiency of the HVDC offshore converter station (equal to 98.28%), V_{cn} is the nominal voltage of the cable (kV), r_c is the cable resistance per kilometer (Ω/km), l_c is the length of the cable (km), nc is the number of subsea cable circuits needed, computed as the active power transfer capability of one circuit over the needed active power transfer (size of the plant). This is computed using the functions in Xiang and colleagues [141], and considering several cable options provided in Table C.3 and Table C.4 of Appendix C.2. For installations close to shore (< 80km) the cable alternative considers an HVAC transmission system, while for far-shore installations (80km and beyond) HVDC is the cable technology used [103]. The resulting efficiency, cost, and cable space metrics are computed considering this cable transmission option. For PtH transmission, electrolyzer efficiency, liquefication efficiency, and losses from burn-off (storage) in transit come from various sources (see Table C.7 of Appendix C.5). The resulting export efficiency is expressed as a percent for each plant alternative which can then be used to calculate the amount of energy delivered to shore annually—the annual energy delivered to shore is the product of the energy produced by the OSW plant and the export system efficiency. Both export systems incur greater losses with greater distance from shore.

3.2.3 Plant site metric calculation

All the component metrics calculated thus far are for individual grid squares. A plant will require several turbines, occupy numerous grid squares, and may have different layouts. The final plant metrics should reflect the magnitude and footprint of the overall plant. As this is not a layout optimization study, I do not choose a single layout, but instead, combine the metrics of neighboring grid squares using the following process, carried out for each grid square, considering it as the collector site.

1. The number of grid squares needed for the plant is determined as the discrete number of turbines needed given the plant size and turbine size of the value chain with a ceiling function:

$$n_{turbine} = \left\lceil \frac{Plant\ [MW]}{Turbine\ [MW]} \right\rceil$$

2. An 'influence area' (IA) is defined which considers the grid squares that may be part of the plant. This is done by taking all the grid squares within a maximum distance, D, from the collector grid square, i, computed as,

$$D = \left\lceil \sqrt{n_{turbine}} \right\rceil$$

   this distance defines the side length (in number of turbines) of a square array given a number of turbines, $n_{turbine}$. A square array can be placed with the collector site at any corner, and fit within the IA. Furthermore, other plausible orientations of turbines may also fit within the IA as seen in the example in Figure 3.2 with 10 turbines. The IA therefore gives a good approximation of which grid squares would likely be part of a plant with the collector at its centroid without requiring that a layout is chosen.

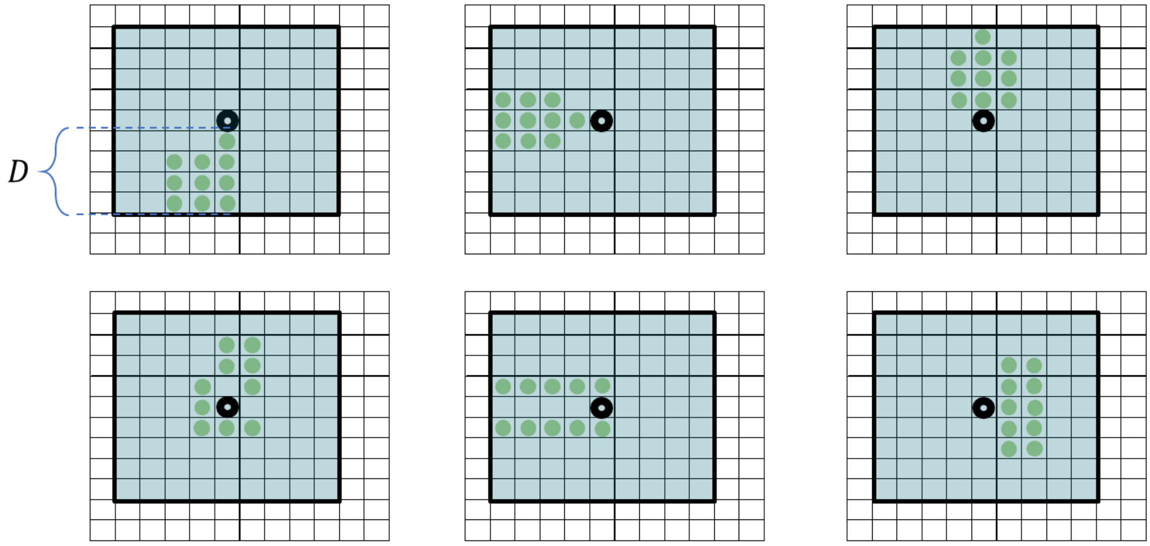

Figure 3.2: Illustration of the influence area given a collector site (black circle) for a 10-turbine plant. The influence area is the shaded area, and possible turbine locations are shown as green dots.

3. Within the IA, exclusion criteria may eliminate certain grid squares from development. I consider five exclusion criteria:
    a. Existing cables: grid squares that have any submarine cables running through them are eliminated from the IA when the value chain has fixed foundations or moored turbines.
    b. Depth limit: grid squares with depths greater than 60m for fixed foundation turbines [18], and depths greater than 1,300m for moored floating turbines [117] are eliminated from the IA.
    c. Marine protected area: any grid square that overlaps with an established marine protected area is eliminated from the IA regardless of the technology used.
    d. Shipping fairways: any grid square that overlaps with an established shipping fairway is eliminated from the IA regardless of the technology used.

   e. Cultural and heritage: any grid square that overlaps with a 'De Facto' MPA [128] with a designated restriction on energy extraction is eliminated from the IA regardless of the technology used.

   These exclusions are also applied to the collector grid square itself. If the collector grid square satisfies either of these three criteria, the grid square is removed from the alternatives space.

4. The remaining grid squares within the IA are used to compute the plant metrics in Table 3.1, described in further detail below. Each metric is defined as either a benefit (in which the metric should be maximized), or a cost (in which the metric should be minimized). If the number of remaining squares in the IA is less than the number of turbines needed for the plant, the grid square is removed from the alternative space. If the number of remaining grid squares in the IA is greater than the number of turbines, some of the metrics are scaled by the number of 'effective plants' remaining in the IA,

$$Effective\ Plants = \frac{Number\ grid\ squares\ in\ IA}{n_{turbine}} \tag{3.1}$$

OCC and Unit OCC: The capital costs of the components are summed to get a plant OCC, reported as the overall cost and cost per installed MW of plant capacity. This cost does not include certain project execution costs and assumes that the plant is built 'overnight', focusing on fabrication and acquisition costs. As shown in Table C.9 of Appendix C.5, this method captures the relative differences between plant proposals when compared to NREL model results.

Annual Energy/H_2 Output: The energy output to shore is estimated considering the losses in transmission to shore and conversion (in the case of hydrogen production) as described earlier.

$$\mathbb{E}[Annual\ Energy] = \frac{\sum_{IA} Annual\ turbine\ generation}{effective\ plants} \times transmission\ efficiency$$

$$\mathbb{E}[Annual\ H2] = \frac{\sum_{IA} Annual\ turbine\ generation}{effective\ plants} \times conversion\ and\ shipping\ efficiency$$

LCOE/LCOH: The LCOE and levelized cost of hydrogen (LCOH) are computed as the net present value (NPV) of costs divided by the NPV of energy flows using the following equations.

$$LCOE\left[\frac{USD}{MWh}\right] = \frac{NPV\ of\ costs}{NPV\ of\ energy\ flows} = \frac{\sum_t \left(\frac{CAPEX_t + OPEX_t}{(1+r)^t}\right)}{\sum_t \left(\frac{\mathbb{E}[Annual\ Energy]}{(1+r)^t}\right)}$$

$$LCOH2\left[\frac{USD}{MWh}\right] = \frac{NPV\ of\ costs}{NPV\ of\ H2\ flows} = \frac{\sum_t \left(\frac{CAPEX_t + OPEX_t}{(1+r)^t}\right)}{\sum_t \left(\frac{\mathbb{E}[Annual\ H2]}{(1+r)^t}\right)}$$

These calculations consider overnight capital expenditure (CAPEX) and annual operational expenditures (OPEX) which are estimated as a percentage of CAPEX incurred per year, (see Table C.7 of Appendix C.5). A discount rate, r, equal to 5.2% is used [142].

Visual Impact: The expected number of visible turbines from shore is divided by the number of effective plants (see equation (3.1)).

$$Visual\ Impact = \frac{Visible\ turbines\ in\ influence\ area}{effective\ plants}$$

Impact on Fishing: The expected hours of fishing effort that took place prior to building the plant in the IA are considered as the impact on fishing efforts. This is estimated using the hours of fishing effort in the IA divided by the number of effective plants.

$$Impact\ on\ Fishing = \frac{\sum_{IA} Hours\ of\ fishing}{effective\ plants}$$

Impact on Vessel Traffic: The expected vessel operations impact is estimated using the number of vessel transits in the IA before the plant is built divided by the number of effective plants. The measure used here is vessel transits in each grid square. Therefore, the same vessel transiting adjacent grid squares in the same IA is counted more than once. While this may seem like multiple counting of a single ship, in fact, it captures the intensity of the impact on traffic due to the development in the IA. For example, a vessel that transits only one grid square on the periphery of the IA would be less impacted (by the building of the plant) than a ship that transits through the middle of the IA, crossing many grid squares.

$$Impact\ on\ Vessel\ Traffic = \frac{\sum_{IA} Vessel\ transits}{effective\ plants}$$

Impact on Marine Life: The expected impact on marine life is quantified as the number of species observed in the IA divided by the number of effective plants. The same rationale to address potential ‘multiple counting’ for the impact on vessel traffic applies here.

$$Impact\ on\ Marine\ Life = \frac{\sum_{IA} Marine\ species\ richness}{effective\ plants}$$

Disrupted Seabed: The total area of disrupted seabed expected is estimated as the disrupted seabed caused by the turbines and cabled transmission systems.

$$Disrupted\ seabed = \frac{\sum_{IA} Disrupted\ seabed\ from\ turbines}{effective\ plants} + Disrupted\ seabed\ from\ export$$

Obstructions: The sum of the obstructions from the turbine installations is considered as the overall plant obstructions.

$$Obstructions = \frac{\sum_{IA} Obstructions}{effective\ plants}$$

<u>Cost exclusions</u>

There are limits to the costs (unit OCC, and cost of energy) that developers would pay to deploy a plant. Some of the alternatives may surpass observed energy deployment costs. The maximum unit capital cost to deploy a renewable energy plant observed in historical data is 11,000 USD/kW [11] and the maximum LCOE observed is 360 USD/MWh [143]. Alternatives that realize values greater than either of these are removed from the alternative space. While it is possible that developers may consider alternatives with higher costs if the benefits realized are immense, these exclusions are applied because it realizes a less-skewed distribution of normalized costs (described in the next section). For example, before cost exclusions, a maximum LCOE of 10,000 USD/MWh is found among the alternatives. Normalizing LCOE to this maximum would skew most of the plant alternatives to be tightly distributed close to one, although more than 90% of the plant alternatives realize an LCOE less than 360 USD/MWh. A summary of all the exclusions applied to the alternatives space is seen in Table 3.6.

Table 3.6: Summary of exclusion criteria and for which value chain the criterion applies.

Where the Exclusion Applies	Criterion	For Which Value Chain the Exclusion is applied
Eliminates grid squares from the IA	Submarine cable present = 1	Moored and Fixed
	Mean depth > 1,300m	Moored
	Mean depth > 60m	Fixed
	Marine protected areas = 1	All
	Shipping fairway present = 1	All
	De facto marine protected areas = 1	All
Eliminates plant alternatives from the alternatives space	LCOE > 360 USD/MWh	All
	Unit OCC > 11,000 USD/kW	All

3.2.4 Suitability score calculation

<u>Normalize metrics</u>

The purpose for normalization is to equalize the effect of all criteria (regardless of the weighting process) and obtain dimensionless criteria [144]. Normalization allows for compatibility of metrics which are measured on different scales by eliminating dimension and direction and linear normalization is commonly adopted among energy site selection studies [116]. I use a linear normalization of the metrics with the following equation that achieves these purposes:

$$Z_{ij} = \begin{cases} \dfrac{x_{ij}}{\max_i(x_j)}, if\ j\ is\ a\ benefit \\ 1 - \dfrac{x_{ij}}{\max_i(x_j)}, if\ j\ is\ a\ cost \end{cases} \tag{3.2}$$

The normalized score, Z, for alternative i in criterion j realizes a value of 0 to 1 where 1 is the most desirable normalized score for all the criterion. x_{ij} is the numeric value of alternative i in criterion j, and $\max_i(x_j)$ is the maximum value across the alternative space. This method is suitable for criteria in which an optimal direction (classifying criteria as either a cost or a benefit) is identified, in which there is no reference or optimal value assumed (that is between the minimum and maximum of criteria values in the alternatives space), and which only attain values greater than or equal to zero [144]—conditions satisfied by all the metrics in Table 3.1. The linear normalization method in equation (3.2) is widely used in MCDM studies [145] and is found to be one of the most robust and successful in dealing with unit differences; furthermore, it is the recommended method for use with a simple additive weighting method that I apply here [144]. Although a comparison of normalization methods has been explored in prior studies [144], [145], Shao and colleagues note that validating results in the metric normalization stage has not been done in prior studies focused on energy siting, and therefore is an avenue for future work [116]. Furthermore, the normalization method and exclusion criteria (Table 3.6) prevents any metric from realizing a negative value which, as noted by Wu and colleagues [146], would impact the other criteria, and has the potential to create bias among the alternatives.

Weight profiles

The weight profiles used are seen in Table 3.7. The weight profiles are developed considering different representative preference profiles—similar to Klein & Whalley [109]—that place uniform weight on the metrics that are of concern to developers and impacted external stakeholders. One benefit of generating weight profiles in this way is that with a national scope, eliciting weights from decision-makers or communities begs the question of ‘which community or set of individuals should evaluate the weights on criteria’? Different individuals and communities weigh decision criteria differently as noted in a National Academies report [147].

$$0 \leq w_k < maximum\ weight \tag{3.3}$$
$$w_p = \frac{maximum\ weight - w_k}{n_p} \tag{3.4}$$
$$w_o = 0 \tag{3.5}$$

A key metric, k, may be identified and assigned to a single key metric of concern. The preferred metrics, p, each have an equivalent portion of the maximum weight (equation (3.4)), and the remaining metrics, o, are given a value of zero.

A uniform weight profile assigns an equal value of one to each of the criteria; it was first proposed by Dawes & Corrigan [148], and has since been used in renewable energy site selection models [116]. A developer weight profile assigns equal weights to the primary metrics that a project developer is concerned with—costs and output. A stakeholder weight profile assigns equal weights to the metrics that various external stakeholders are concerned with—impacts and disamenities. The weight profiles have the same maximum score of 10.

Two additional weight profiles are also considered. I use annual energy output as a key metric in two profiles to analyze what would happen if the weight were more or less than other metrics—giving the “high concern” and “low concern” for clean energy deployment weight profiles in Table 3.7. Finally, to explore the impact of the results based on extreme weighting of the criteria, I conduct a sensitivity analysis on 10 additional weight profiles in which the majority of the weight is placed on each metric in turn (see Appendix C.9).

<u>Suitability scores using simple additive weighting</u>

A suitability score is computed using a simple additive weighting method:

$$Score_i = \sum w_j Z_{ij} \tag{3.6}$$

in which the normalized metrics are multiplied by their respective weights in the weight profile and summed to give the alternative suitability score—stated differently, it is the vector dot product between the weights of the chosen weight profile, w_j, with the vector of normalized metrics, Z_{ij}. The model is constructed such that a higher suitability score is expected to be the preferred action with a maximum possible score of 10. An ‘alternative’ is considered to be one of the 168 value chains centered in one of the 868,064 grid squares as detailed in Section 3.2.1; therefore, I do not preemptively choose which value chain is assigned to a location, but assess all possible combinations of value chains and locations to comprise the alternative space.

To compare the plant alternatives to maintaining the status quo and not developing a plant, I quantify the score of a “No-Action” decision which is the vector dot product between the vector of normalized No-Action metrics ($Z_{NA,j}$ in Table 3.7) and the vectors each weight profile (w_j in Table 3.7). The suitability scores of alternatives are compared with the No-Action score in that weight profile to identify whether the plant is “build-preferred” or “no-build-preferred”, in which the alternative suitability score is greater than or less than the No-Action score, respectively. Results of the additional weight profiles not in the main text are included as additional results in Appendix C.8 and Appendix C.9.

Table 3.7: No-Action decision suitability scores under different weighting paradigms. The maximum possible score under each set of weights is equal to 10. Symbolic representations of the variables are provided.

Metric	**Cost or Benefit**	**No-Action Metric Value**	**Normalized No-Action Metric** [a]	**Uniform Weight**	**Developer Weight**	**Stakeholder Weight**	**High Concern**	**Low Concern**
j	–	$x_{NA,j}$	$Z_{NA,j}$	w_j				
OCC	Cost	0	1	1	2.5	0	0	0
Unit OCC	Cost	0	1	1	2.5	0	0	0
Annual Energy/H_2 Output	Benefit	0	0	1	2.5	10/7	4	0.5
LCOE/ LCOH	Cost	– [b]	0	1	2.5	0	0	0
Visual Impact	Cost	0	1	1	0	10/7	1	9.5/6
Impact on Fishing	Cost	0	1	1	0	10/7	1	9.5/6
Impact on Marine Life	Cost	0	1	1	0	10/7	1	9.5/6
Impact on Vessel Traffic	Cost	0	1	1	0	10/7	1	9.5/6
Disrupted Seabed	Cost	0	1	1	0	10/7	1	9.5/6
Obstructions	Cost	0	1	1	0	10/7	1	9.5/6
No-Action Suitability Score (out of 10 possible): $\sum w_j Z_{NA,j}$				**8.0**	**5.0**	**8.6**	**6.0**	**9.5**

[a] The normalized metrics are computed as defined in equation (3.2) considering if the metric is a cost or benefit.
[b] Undefined.

3.2.5 Computational demands of the analysis

The analysis was carried out in R. During preliminary analyses the system used had 16GB of RAM with eight processors. To compute the plant metrics for the entire alternatives space (146 million alternatives) would have required nearly 2,900 hours of dedicated computing on the system described, or about 120 days. Therefore, optimizing the code once the initial functionality was established was a key step in this analysis. I undertook three key initiatives which reduced the computing time precipitously: changing the data-handling packages in R, upgrading my system hardware, and splitting the dataset to reduce filter time in each iteration of the code.

First, I changed the data structure from R ‘data frames’ to R ‘data tables’. The latter are optimized for only numerical data, which was the case in this analysis as no text data were part of the dataset. Data tables also improve computing time for new columns or metrics as well as the read time for each dataset, which was substantial in this case. Along with other small changes to the way the data were stored in each data table in R, this reduced the computing time by 29%, or 840 hours. The second and most effective change I made was to upgrade my system hardware from 16GB to 40GB of RAM and conduct the analysis in parallel using all eight of the system’s processors. This required re-writing the code so that each calculation could be executed independently, and therefore necessitated the use of ‘apply’ functions as opposed to ‘loops’ that iterated over each row in sequence. As a result, the computation time decreased by 41% or nearly 1,200 hours. The third most effective change came about after assessing each component of the code and realizing that to execute the plant aggregation method described in Section 3.2.3, the code used a ‘filter’ function that had to read every row of the data table of grid squares (of which there were 868,000 rows in each) to collect the ones that would be in the IA based on longitude and latitude values. After realizing that each loop would run faster if the filter had fewer rows to read, I split the dataset by east and west coasts in this step (since no IA would span both coasts) so that for each collection of the IA grid squares, the function would have to read fewer rows in the data table. I then put the data table back together after the metrics were computed. This change reduced the overall computing time by nearly 22% or 620 hours. After a few other smaller, less impactful, changes, the final computation time for this analysis was 38 hours or about 1.5 days, representing an improvement of more than 98% from the initial computation time, as summarized in Figure 3.3.

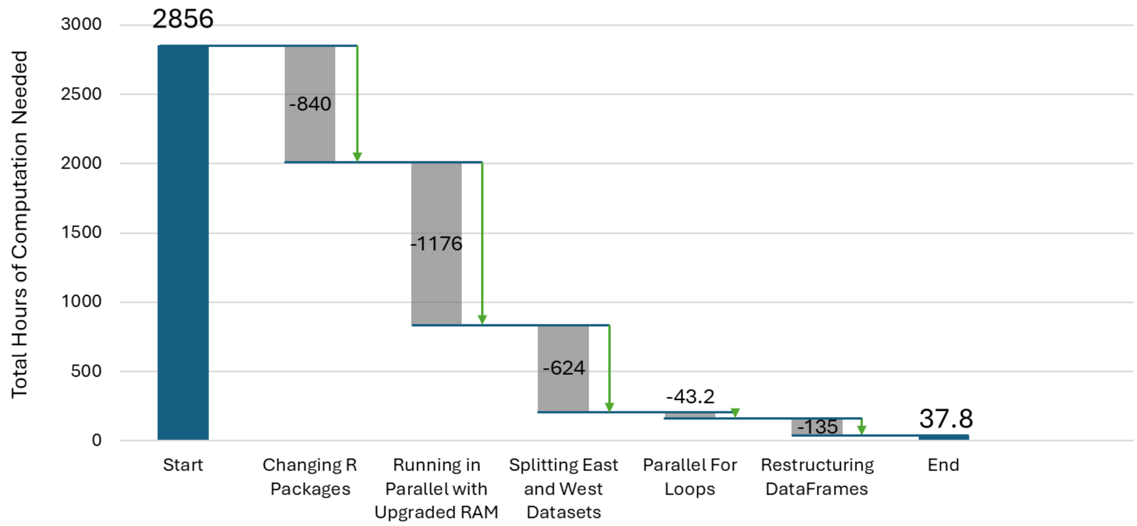

Figure 3.3: Summary of the computation improvements implemented to execute this analysis.

3.3 Results

The difference between an alternative's suitability score and the "No-Action" score is referred to as the "suitability score difference", with a positive value defining "build-preferred" and a negative value defining "no-build-preferred". From a developer perspective, 58% percent of the 66 million alternatives (after exclusions are applied) are "build-preferred" while 42% are "no-build-preferred." In contrast, under the stakeholder paradigm, 19% of alternatives are "build-preferred", whereas 81% are "no-build-preferred". Figure 3.4 shows distributions of alternatives' suitability score difference under both paradigms. Figure 3.5 presents suitability maps of the East and West Coasts for the baseline facility under both paradigms. The distribution of the normalized scores for each metric across the entire alternatives space is given in Figure C.3 of Appendix C.3.

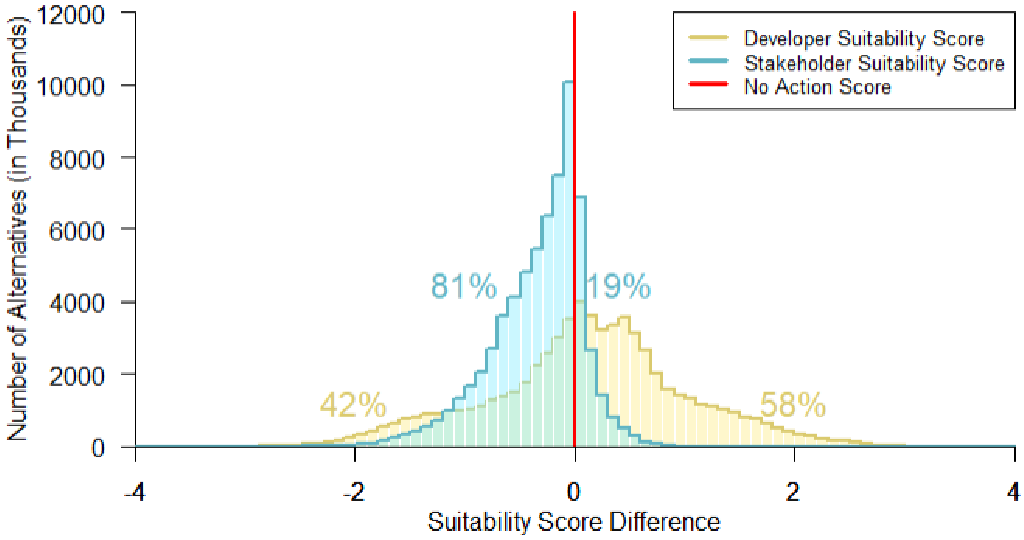

Figure 3.4: Histograms of the full alternatives space under both developer (yellow) and stakeholder (blue) paradigms illustrate how the attractiveness of OSW project alternatives changes from one to the other.

These results suggest that developers would seek to invest in more alternatives than are likely acceptable to a broad coalition of stakeholders, yielding potential delays or failure. This echoes findings from other studies [149] but helps to explain why poorly chosen sites may fail in implementation, regardless of how promising they appear to developers. Suitability maps based on the developer paradigm (Figure 3.5A and Figure 3.5B) closely approximate maps of ‘economic potential’ from a detailed assessment of US OSW sites [150]. Sites closer to shore tend to score higher, with scores decreasing as one moves farther from shore. However, maps based on the stakeholder paradigm (Figure 3.5C and Figure 3.5D) tell a richer story in which attributes like visual impact, impact on fishing, impact on marine life, and impact on vessel traffic depress attractiveness in some near-shore locations with promising economics as high scoring sites do not abut the shoreline as with the developer paradigm. While near-shore sites tend to score lower in the stakeholder paradigm, it does not merely push sites as far offshore as possible. Some offshore locations are disfavored due to seabed disruptions, obstructions, or transmission losses that increase as plants move away from shore. The stakeholder paradigm comprises an analytical framework that enables these tradeoffs to be expressed, discussed, and resolved by developers, analysts, and policy makers. For additional results, see Appendix C.7 and Appendix C.8.

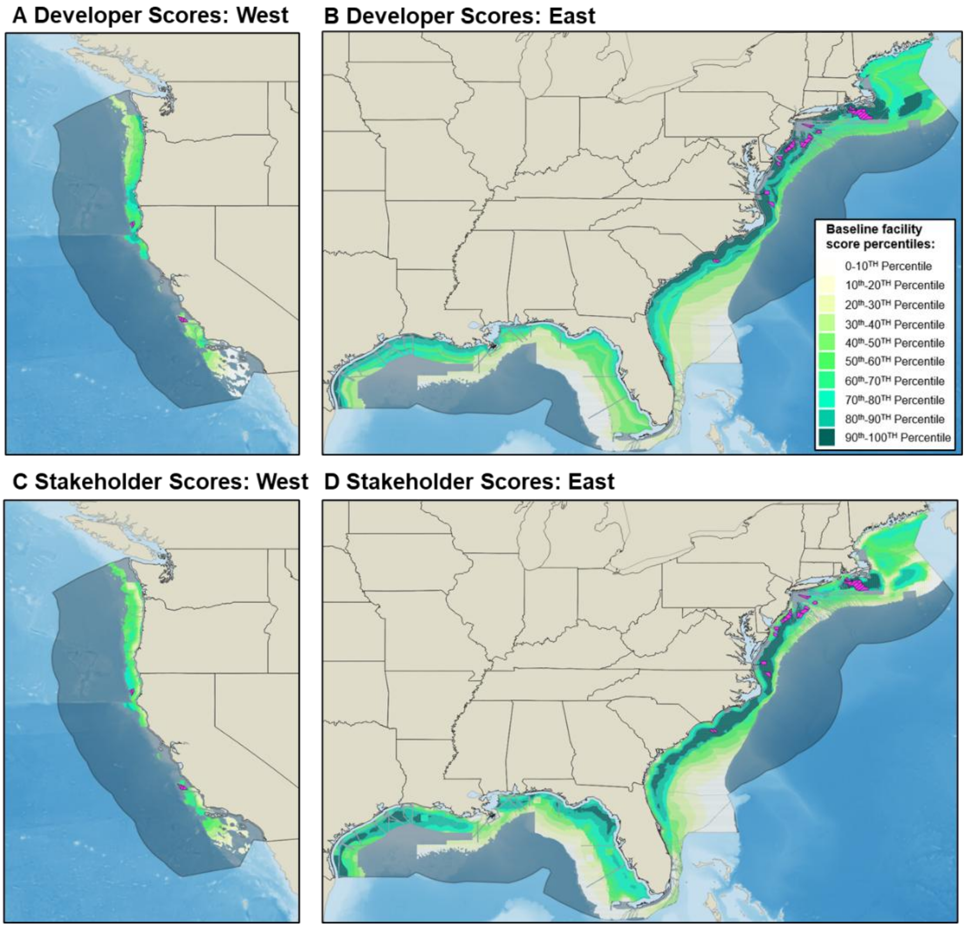

Figure 3.5: Suitability maps show the spatial distribution of site score quantiles for only the baseline facility (1,000MW plant with 10MW turbines and HVDC transmission). Fixed foundations considered for depths up to 60m, and moored foundations considered for depths from 60-1,300m. Uncolored areas are eliminated due to exclusion criteria (see Table 3.6 in the methods section). Existing wind development sites are also shown (pink).

3.3.1 Plant proposals align with the developer paradigm and capacity may be at risk

I calculate suitability scores under both developer and stakeholder paradigms for several existing and past OSW project proposals in the US, listed in Table 3.8. The projects included in the table are those that have a construction and operations plan (COP) submitted to the US Department of the Interior, signifying their advanced stage in the development process, and with project parameters defined (range of plant size and turbine size considered)—projects with a lease area, but no COP submitted (as of January 2024) are not included. The projects are listed in order of increasing distance to shore. The project envelope is typically described in the COP, which is why I include only projects that have submitted one, as the project boundaries are well-defined at the point of COP submission. I use the term ‘project’ to describe an entity that seeks a contract with a utility. Therefore, under this definition, different project phases (often denoted by sequential numbers) are considered as ‘projects’, and several projects may occupy the same lease area. Expectedly, all projects score highly under the developer paradigm, illustrating its usefulness at approximating developer decision-making. However, under the stakeholder paradigm, the scores are depressed, though several remain positive, if only marginally. The cancelled Cape Wind project experienced stakeholder challenges, and scores negatively under the stakeholder paradigm. Vineyard Wind, another project to face litigation and scrutiny from external stakeholders, scores marginally positive under the stakeholder paradigm [151]. Of 18GW of projects listed in the table, nearly 2GW—not including two cancelled projects, Cape Wind and Ocean Wind 1—have low stakeholder suitability scores of +0.1 or less (setting the Vineyard Wind score as the threshold given its experience with stakeholder resistance), indicating they may face stakeholder risk. Interestingly, while the cancelled Ocean Wind 1 cites macroeconomic factors as the reason for its cancellation (high inflation, interest rates, and supply chain bottlenecks) and not stakeholder challenges, it still realizes a low stakeholder suitability score.

Table 3.8: Existing and past US project proposals in advanced development. Note: all proposals consider high voltage export cables and fixed foundations with monopiles in their proposals. A negative score indicates that the No-Action suitability score is greater than the alternative's suitability score. Distances reported are the straight-line distance to the nearest point to shore; actual cable distances may be longer depending on the chosen cable landfall site.

Proposed OSW project	Lease Area	Distance to shore (km)	Plant size (MW)	Turbine Size (MW)	Stakeholder score [a]	Developer score [a]
Cape Wind[x] [81]	Not Specified	14	468	5	– 1.0 to – 0.7 [g]	+ 2.0 to + 2.2 [g]
Maryland Offshore Wind [152]	OCS-A 0490	26	2,000 [b]	≤18 [b]	+ 0.3	+ 3.0
Ocean Wind 1[d x] [153]	OCS-A 0498	30	1,100	12	+ 0.1 to + 0.3	+2.5 to + 2.7
Atlantic Shores 1 [154]	OCS-A 0499	30	1,510	12-20 [c]	+ 0.3	+ 3.0
Revolution Wind [155]	OCS-A 0486	36	704-880	8-12	0.0 to + 0.2	+ 2.1 to + 2.4
Empire Wind [156]	OCS-A 0512	39	2,200 [b]	15 [c]	+ 0.3	+ 2.8
South Fork Wind [157]	OCS-A 0517	42	90-180 [b c]	6-12	0.0	+ 1.5 to + 1.6
Vineyard Wind [158]	OCS-A 0501	55	800	12	+ 0.1 to + 0.3	+ 2.2 to + 2.3
Sunrise Wind [159]	OCS-A 0487	55	924-1,034	11	+ 0.3	+ 2.2 to + 2.3
Coastal Virginia Offshore Wind [160]	OCS-A 0483	57	2,800 [b]	14-16	+ 0.6	+ 2.6
Kitty Hawk Wind [161]	OCS-A 0508	59	1,000	>15 [c]	+ 0.4	+ 2.3
New England Wind[e y] [162]	OCS-A 0534	69	2,036 [b]	≥16	+ 0.3	+ 2.2
Beacon Wind (1 and 2) [163]	OCS-A 0520	79	1,230	8-20 [c]	+ 0.3 to + 0.6	+ 2.4 to + 2.8
SouthCoast Wind[f y] [164]	OCS-A 0521	88	804	12+ [c]	+ 0.2 to + 0.3	+ 2.2 to + 2.4

[a] Scores are shown as the suitability score difference described earlier.
[b] Outside the range of this analysis. I used the closest option.
[c] Not specified in project description but interpreted based on reported data.
[d] A second project (Ocean Wind 2) in the same lease area was also cancelled but had not submitted a COP yet [165].
[e] Formerly known as Vineyard Wind South. Consists of two phases: Park City Wind and Commonwealth Wind.
[f] Formerly known as Mayflower Wind.
[g] Site now falls in a De Facto Marine Protected Area. Provided score is the result before excluding from the analysis.
[x] Cancelled project in which development efforts by the project sponsors have ceased.
[y] Project withdrew from PPA and paid penalty to do so. There is no indication that the project will cease yet.

The result depicted in Figure 3.5 with the baseline facility—that near shore sites score lower under the developer paradigm than sites farther from shore—is also found here with various facilities. Low stakeholder scores are found only within 60km of the shore, while developer scores do not exhibit such a relationship. This behavior with stakeholder scores is unsurprising as, generally, proximate sites are more likely to interact with the public and other stakeholders (falling as much as 40% from near-shore to far-from shore sites) [166], and because marine biodiversity declines with depth [167]—both of which are metrics that inform the stakeholder weighting and scores.

3.3.2 Larger plants are more fragile from a stakeholder perspective

Smaller plants typically impinge on fewer stakeholder interests than larger plants due to their smaller footprint. A tighter distribution of energy output is also found for smaller plants, while the opposite is true for large plants (see Figure C.5 of Appendix C.7). This phenomenon of high variance of impacts and energy output was also found with utility-scale solar in the US

[168]. The accumulation of more assets in a larger plant and its interaction with a greater spatial extent leads to increased variance across all criteria compared to smaller facilities. As a result, impacts assume a wider range of values for large plants compared to small plants. Figure 3.6A demonstrates how variance in the suitability scores increases with plant size under both developer and stakeholder paradigms, with a more pronounced effect under a stakeholder paradigm. A similar effect of small variance for small plants is also found for other weight profiles assessed (see Figure C.7 of Appendix C.8 and Figure C.8 of Appendix C.9).

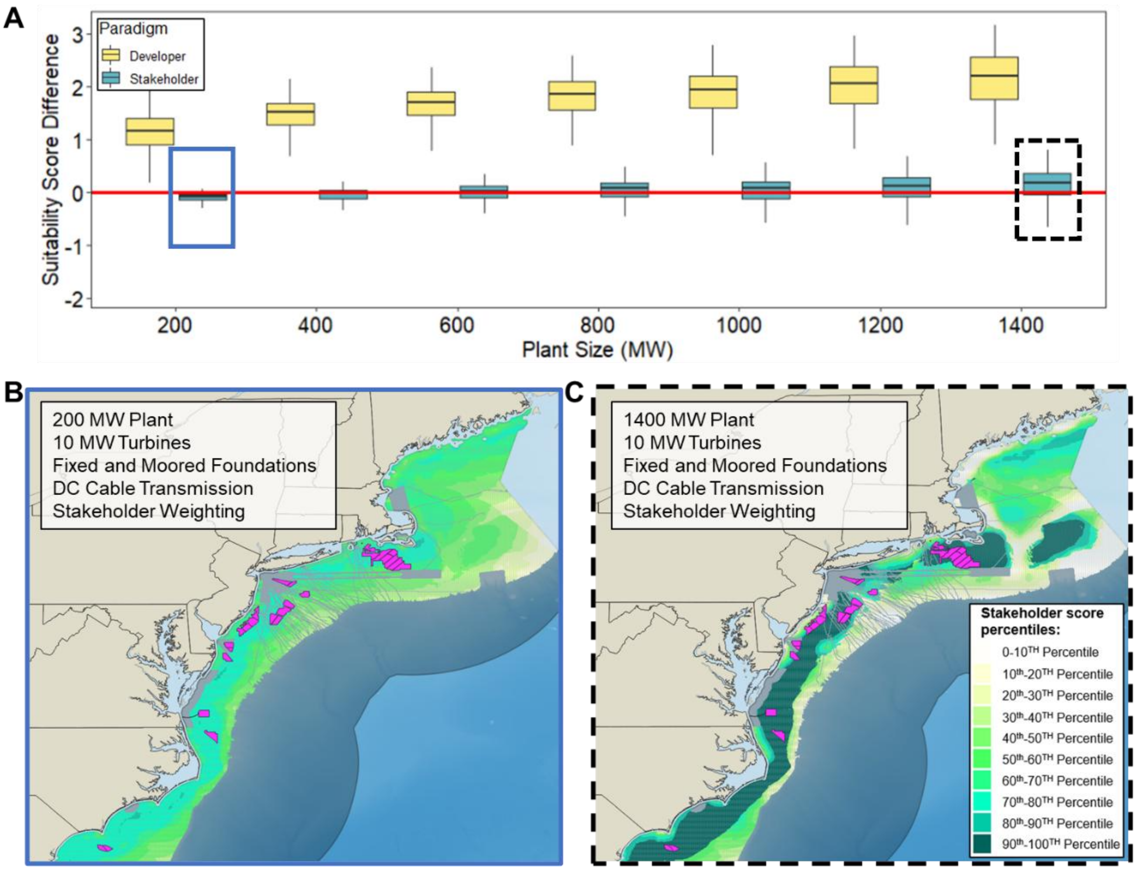

Figure 3.6: Plant size affects the distribution of scores under both developer and stakeholder paradigms. A) Suitability score differences for various plant sizes under both paradigms shows variance increases with plant size. All plant sizes assume 10 MW turbine with fixed-foundations and HVDC transmission. The maps illustrate the spatial distribution of quantiles across all plant scales for a B) 200MW plant and a C) 1,400MW plant. Existing wind development sites are also shown (pink).

This tighter distribution of scores for smaller plants under the stakeholder paradigm carries two implications. First, while it may be more difficult to identify sites that are unambiguously better than others, suitability scores for smaller plants are also more robust regardless of location, giving developers a certain amount of flexibility in choosing a location for their project—depicted graphically by the more monotone distribution of scores in Figure 3.6B.

Small plant sizes could therefore help developers reduce the uncertainty arising from various types of stakeholder concerns. Second, larger plants are more fragile; they exhibit greater variance in scores, meaning that location matters greatly. Because only certain locations are very suitable for deploying large plants, developers should accommodate those locations, ceding some of the flexibility that smaller plants afford.

3.3.3 There are areas where developer and stakeholder paradigms align

Finding locations where both developer and stakeholder paradigms yield the highest suitability scores could be key for rapid, successful implementation of OSW projects. Figure 3.7 presents these ‘consensus’ locations on the East Coast.

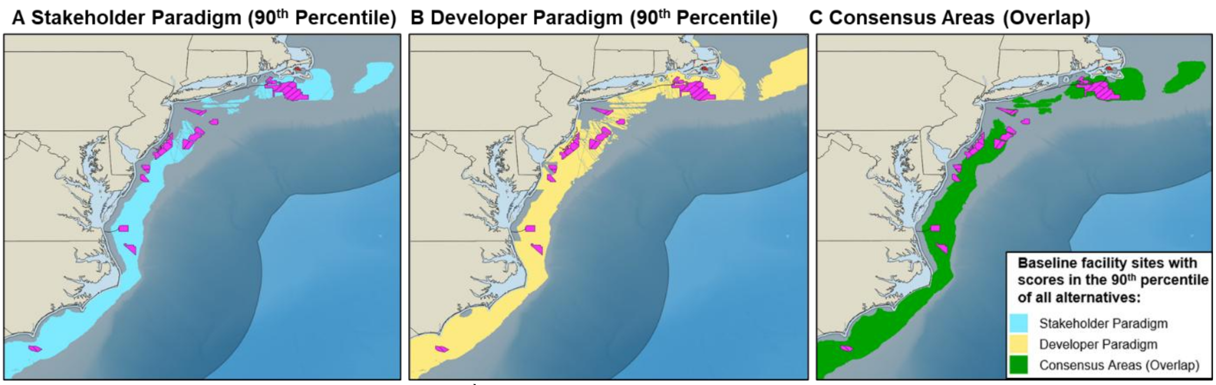

Figure 3.7: Baseline facility site scores in 90th percentile of all alternatives under the A) stakeholder and B) developer paradigms. C) Consensus areas (green) where stakeholder and developer paradigms align show there is considerable overlap on the East Coast. Existing wind development sites are also shown (pink).

Considering deployment only within the depth limits of fixed and moored technology [18], [117], there are enough consensus locations on the East Coast to deploy 600GW of OSW (Figure 3.7C). Some existing development areas on the East Coast fall within these consensus locations, though notably, many are farther from shore. On the West Coast, there is enough consensus locations for only 5GW of OSW within existing depth constraints.

3.3.4 Novel technologies are more expensive but could yield attractive West Coast sites

I find few consensus areas on the West Coast because of a lack of high-scoring sites under the stakeholder paradigm. This suggests that increasing a site’s attractiveness under the stakeholder paradigm is necessary to unlock consensus areas along that coast. I investigate a novel technological paradigm—dynamically positioned floating OSW turbines [31], [32], [34], [35], [169] (see Chapter 2 and Appendix C.4) with a PtH transmission pathway—in which the OSW plant produces hydrogen through water electrolysis [170] that is delivered to shore via hydrogen ships instead of cables. These technologies eliminate seabed disruption from mooring chains, anchors, and cables, and largely remove plant depth limits—making deployment farther offshore possible and resulting in more high-scoring sites under the stakeholder paradigm on the West Coast. However, these technologies incur greater cost than traditional moored systems and involve lower end-to-end efficiency due to energy consumption by the DP thrusters and low electrolyzer efficiency (see Table C.7 of Appendix C.5)—depressing suitability scores under the developer paradigm. I find that this novel technology, combined with existing fiscal incentives, could help stimulate OSW deployment on the West Coast by realizing more consensus areas. Figure 3.8 shows the impact on deployment of investment tax credits (ITC) of varying amounts—up to 30%, which is in place thanks to the 2022 Inflation Reduction Act [171]. This ITC would improve the cost-effectiveness of novel technologies, increasing their suitability scores under a developer paradigm and stimulating increased deployment in consensus areas.

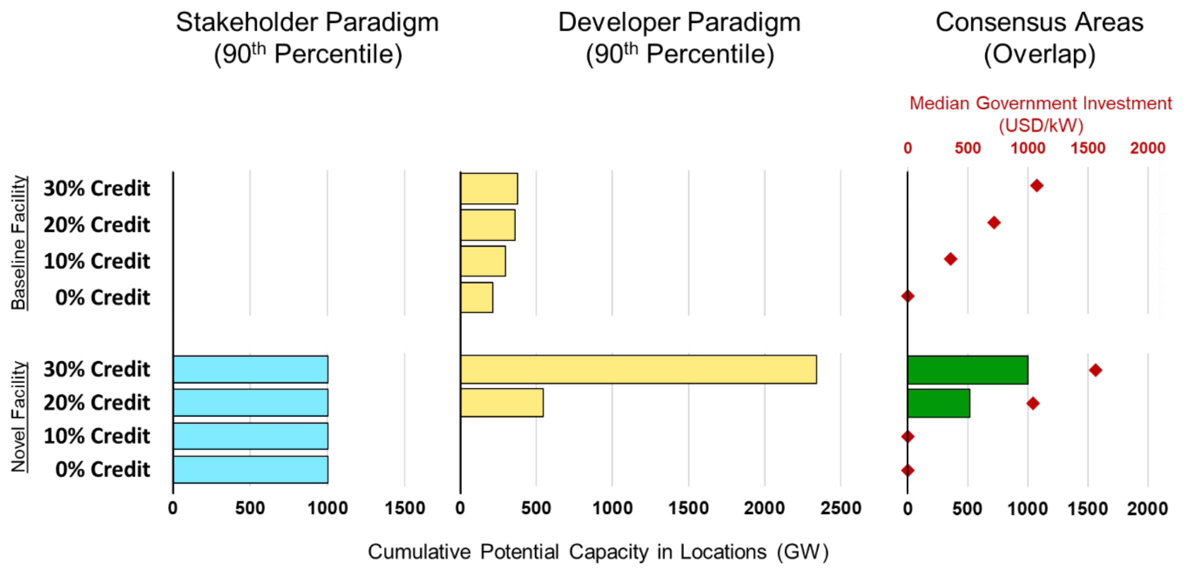

Figure 3.8: A comparison of the potential deployment capacity on the US West Coast of high-scoring (90th percentile of all alternatives) areas under the stakeholder paradigm (blue, left), developer paradigm (yellow, middle) and consensus areas (green, right). Both the baseline facility (top half) and the novel DP + PtH facility (bottom half) are considered at different ITC amounts. The amount of government investment needed per kW is reported as red points for the resulting consensus areas. A combination of novel technologies plus existing government incentives could radically boost deployment capacity on the West Coast.

Other forms of incentive may accomplish the same result, including a production tax credit or other subsidies that reduce the cost obligation on developers, implying that a fiscal incentive could increase consensus areas for development by compensating for the reduced economic potential of stakeholder-preferred sites, or by enhancing the economic prospects of deploying novel technologies. On the West Coast, developing the novel DP + PtH systems in the resulting consensus areas would require a government investment of up to 1,600 USD/kW.

3.4 Discussion

Here, I have presented the results using a binary framework that compares representative developer and stakeholder paradigms constructed in a limiting way that assumes developers are only techno-economic optimizers, and stakeholders are only impact minimizers. Deployment prospects are likely to sit somewhere between these two extremes. To explore this, I evaluated multiple weighting schemes beyond the developer and stakeholder paradigms, including the application of uniform weighting to all project attributes. Uniform weights generate an "improper linear model," which not only requires fewer assumptions, but has been shown to generate better results than complex weighting schemes, including those derived through expert judgement [148], [172]. Uniform weighting generates results that closely agree with the stakeholder paradigm presented here (see Figure C.6 of Appendix C.8). I also find that increasing the weight placed on energy output increases the suitability scores of alternatives at all scales (see Figure C.7C of Appendix C.8), implying that policies that increase the importance of deploying clean energy, such as those recommended by the European Commission [173], should be pursued.

Certain limits to this model must be noted. First, there are other potentially interesting metrics not included in this study [108]. In Table C.11 of Appendix C.9 I provide a qualitative analysis of potential metrics that could be included. Additional cost metrics (construction impacts, habitat loss, local noise effects, military operations, for example) would depress both developer and stakeholder scores, decrease the amount of consensus areas, and increase my estimate of “at-risk” plant proposals, while additional benefit metrics (job creation and pollution reduction, for example) would elevate stakeholder scores, and decrease my estimate of “at-risk” plant proposals. Moreover, the additional metrics I mention here may be tied to those I have already included, and therefore, including them may amplify the effects discussed. For example, habitat loss is likely closely tied to the marine life dataset, military operations are likely related to the vessel presence dataset, job creation is likely related to plant size, and pollution reduction is likely related to annual energy output. Furthermore, I do not expect that any missing metrics would counteract the effect with plant scale—added metrics are not expected to vary more with small plants than with larger ones—nor do I expect that missing metrics would counteract the effect with distance to shore—that is, no additional stakeholder benefits are expected to elevate nearshore sites more than far-from shore sites, and counteract the results that stakeholder scores tend to be lower close to shore than farther from shore. Therefore, the main effects with plant size and distance to shore discussed should be robust to the inclusion of other metrics. Second, with regard to weighting, further disaggregation and weighting of sub-metrics is possible (for example, different vessel types and sizes may receive their own weights and different marine species may receive their own weights). As mentioned, using uniform weights on metrics of concern in 'representative weight profiles' serves to simplify the analysis and has been used in the past [109]. Furthermore, the use of uniform weights on a range of stakeholder impacts has the added value of perceived fairness in policymaking, which is a key element of social acceptance of technology deployment and adoption [15]. In Figure C.8 of Appendix C.9 I do some additional sensitivity analysis by considering 10 additional weight profiles in which each of the ten metrics is heavily weighted relative to the others and find that in most of the scenarios, the smaller plants exhibit a tighter suitability score than the larger ones, demonstrating this result is robust to many other weighting scenarios.

While the focus has been on the US, the modelling framework could be applied elsewhere provided the spatial datasets used here are available. Future work should elicit weighting schemes from real-world developers and stakeholders and compare those preference elicitations to the results of this chapter. Future efforts could also incorporate a temporal element to the study because cost will change over time, and thus, *when* a plant is built may be a key factor for future analysis. Here I considered overnight costs, but financing plays a large role and could be included in future assessments. Financing costs can contribute a substantial proportion of an OSW project's levelized costs [18] reflecting their capital intensity; smaller plants are less capital intense, and would require less financing, and future studies could consider this as well.

Recent work suggests that smaller, granular deployments and technologies which do not rely on intensive customization are more conducive to faster growth and can thus be deployed more quickly in pursuit of urgent decarbonization [69], [70], [174]. Indeed, smaller plant sizes have better cost control as evidenced by a tighter distribution of capital costs (see Figure C.5H of Appendix C.7). And the results show that smaller plants exhibit a tight distribution of cumulative stakeholder impacts, demonstrating robustness to plant location. Preference has also been exhibited for smaller generation plants among local communities in southern Italy [175] and Germany [176] through choice experiments for terrestrial wind, mainly due to aesthetic reasons. Furthermore, I considered overnight capital costs in the model, while plant installation may take several years to construct and commission as installation is constrained to a few months of the year [14]—longer installation times and delaying operation contribute to an increased cost of energy. While I considered plant alternatives to have a single collector site, real-world plants may have two or more when plant capacities are larger. Therefore, limiting plant size (or increasing turbine size) may have an added economic value by reducing the number of assets that need to be installed, and thus, the overall installation time.

Project development typically occurs in stages: sites are identified based on a set of criteria; design and development then begin, and so does stakeholder engagement. However, decisions regarding siting, scale, and technology should not be made independently. As Figure 3.6 illustrates, I find that areas that are suitable for some plant scales are not suitable for others. Project developers looking to deploy plants of a certain scale should be mindful of this when planning their project. This study is the first to incorporate the impact on suitability of different OSW plant sizes, owing to the turbine site aggregation method. Furthermore, an analysis of a granular set of alternatives and sites as done here should be preferred to project-by-project stakeholder impact assessments. The former gives a fuller view of where cumulative impacts are the greatest, while the latter may result in developments being placed where the ability for stakeholders to petition decision-makers is weaker, regardless of how the cumulative impacts compare to other areas.

These results suggest that the poor track record of deploying US OSW projects is unsurprising. Prior (and some current) site and design decisions align with the developer paradigm but not with the stakeholder one, offering an explanation for failed deployments. While all early projects have been sited close to shore (Table 3.8) tending to optimize techno-economic criteria, I demonstrate that projects can move, even marginally, further from shore and remain within consensus areas (Figure 3.7) balancing techno-economic and plant impact criteria. By giving some weight to stakeholder impacts, plants can be sited in consensus areas. The implications for developers and policy makers are threefold. First, developers that have a strong preference for large projects should limit their attention to locations with higher scores under the stakeholder paradigm. To avoid failed deployment, policy makers should develop strategies that incentivize such choices. Second, while smaller plants yield higher unit and levelized costs, they might prove appropriate in more locations and institutional contexts than larger plants. Third, to facilitate development along the US West Coast and other coasts where depths increase rapidly, policy makers should provide research support and financial incentives to increase the viability of novel technologies that are deployed far offshore and score highly under the stakeholder paradigm.

OSW holds the potential to make a major contribution to decarbonizing the energy system, but unless developers and policymakers become more cognizant of stakeholder concerns and adopt strategies that mitigate them, the potential for radically expanded deployment could be depressed.

3.5 Code availability

The R code and raw data used in this analysis is provided in the following DOI: https://zenodo.org/doi/10.5281/zenodo.10037207.

Chapter IV

A Modeling Framework to Operationalize Regulatory Obligations on Offshore Wind Development

4.1 Introduction

An OSW project takes several years to develop, similar to other infrastructure developments. While OSW turbine installation itself can take from two to four years [177], [178], the permitting and development process may require two or three times as long depending on the jurisdiction. This can bring the whole project execution time, including all phases from inception to the start of operations, to 7 to 11 years on average [178], [179]. The typical permits required for projects to proceed are included in Table 4.1 below along with an estimate of the time it can take to receive the permit. These permits are typically required for energy generation and transmission infrastructure [17], [178], [180], [181], [182].

Table 4.1: Summary of typical permits for OSW projects [178], [181], [183]. Some of the permitting items can be pursued in parallel.

Permit Type (level)	Description	Typical Timeline
Wildlife protection (Federal)	Projects that may affect endangered species, fisheries, any natural body of water, marine mammals, migratory birds, or bald or golden eagles, require a consultation and/or permit.	2-year surveys for each wildlife group
Air and water protection (Federal, Regional)	Projects that may pollute the air or water require special permits.	3 years
Protected land usage (Federal, Regional, Local)	If a project proposes the land use of any federally owned or protected land, a permit is required from the relevant land administering agency.	Varies by location and level
Public and local inquiries (Local)	Projects typically allow periods of public comment where concerns on the development may be raised and may require the developers to address them.	Varies by location
Interconnection (Federal, Regional)	If a renewable energy project must connect to the electric grid, approval from the transmission network is required.	2-4 years

A report on the risks and opportunities for floating OSW development in the UK finds that a lack of suitable grid infrastructure in coastal areas, the complexity of permitting procedures, and the duration of the decision-making process to be among risks for deploying OSW [17]. Reducing plant interactions with surrounding environment by reducing spatial requirements and the amount of physical infrastructure needed for a project is one path to simplifying the permitting and consenting process. Deploying transmission infrastructure quickly is a key challenge for decarbonizing the energy system. A study done in the US finds that much as 80% of the decarbonization promised under the 2022 Inflation Reduction Act may be lost if future transmission deployment does not exceed past rates [184].

In Chapter 2 I examined the cost-effectiveness of reducing environmental interactions from OSW plants to allow permitting and deployment ease, which can also be further facilitated by building in deeper waters. However, bringing power to shore with transmission lines cannot avoid traversing near-shore waters and coastal lands—and the accompanying permits required for that. A former US project, Bluewater Wind, cited financial difficulties and a setback with their cable landfall site approval (which was set to pass beneath a public beach) as reasons for that project's cancellation [83], [84]. Deploying transmission systems is a long process and entails several other obligations—for example, with gaining public acceptance [185], permitting and rights of way [186], and interconnection studies and queues [183]. Furthermore, when project deployment timelines are long, project finances become more uncertain, as market conditions and material costs may change, and has been cited as a reason for recent OSW project cancellations [187].

Often, in research-based modeling, the development stage of a project is not considered in estimating cost metrics. The project is typically assumed to be deployed 'overnight' and therefore the 'lag' between inception and the beginning of operations is not considered. As noted, this lag can span several years, and can have significant implications for the cost of energy. This issue is growing in importance since a recent study has found that plant commissioning time has *increased* over the last two decades globally, for all renewable energy technologies. This is true even after 2015 when the Paris Agreement was adopted, marking a global recognition that quicker clean energy deployment was needed [14]. Mignon & Bergek have summarized the importance of temporal delays to developers in surveys they have done on various renewable energy adopters stating, "project development length was a challenge for most adopters, since they had to carry costs without getting any returns for considerable time periods without any guarantee that the project would eventually get a permit and give any return on investment at all" [12].

In this chapter I demonstrate ways to operationalize the temporal aspects of project development by comparing three transmission topologies from an OSW plant: a) high voltage cable transmission; b) hydrogen electrolysis offshore, with the hydrogen brought to shore via pipelines; and c) hydrogen electrolysis offshore, with the hydrogen brought to shore via ships [188]. I operationalize the regulatory and permitting obligation as a temporal delay to project operation and quantify the 'value' of reducing regulatory obligations by one year. This metric can be useful to quantify the value of a more accommodating deployment environment[1] and

[1] As one example, Sherman and colleagues qualitatively discuss the differences in institutional context between the US and China that can help explain wider adoption of OSW in the latter over the last decade [279].

thus quantify the comparative permitting or regulatory benefits needed for a (novel) technology to overcome its cost disadvantage with respect to established incumbents, and to compare the cost of policy efforts. This investigation is relevant to the policy analysis literature today as several policy and regulatory initiatives are aiming to give special consideration to renewable energy deployment against existing stakeholder uses [173], reduce permitting time [189], and reduce interconnection processing time [190] to ease regulatory requirements and expedite the renewable energy deployment process. A quantitative assessment of the impact of barriers can inform policymakers about the potential value of reducing those barriers. The balance of this chapter is organized as follows: a literature review that provides additional context for this analysis; the methodology and framework used; and then the main results and sensitivity analysis are provided followed by a brief conclusion.

4.1.1 Literature review

The time to execute a project and the potential for delays can be attributed to regulatory requirements, social acceptance[2], stakeholder acceptance, market acceptance, supply chain issues, and other institutional factors. Henceforth, I refer to these as "socio-political factors"[3]. Socio-political acceptance and its impacts on deployment prospects of renewable energy has been qualitatively discussed in the literature [15], [175], [191], [192], [193]. Surveys have been used to examine public opinions about renewable energy developments [194], [195], [196]. Empirical data on wind energy projects that faced public scrutiny in North America reveals that project resistance is closely tied to underlying demographic factors [105]. Project structure and participation has been identified as key for achieving acceptance [197], [198]. Research has identified shortening long project lead times as an important policy lever for renewable energy diffusion [199]. A long deployment lead time can be classified as a factor that impacts

[2] A National Academies report chapter highlights "The Social Acceptance Challenge" for nuclear energy [147, Ch. 8].
[3] Wüstenhagen and colleagues provide a good framework for the factors relating to socio-political acceptance [15].

the rate of diffusion [200]. Taken together, there are a range of social, regulatory, and institutional considerations to project development that are difficult to quantify but impact project development cost and execution times.

While there are empirical studies of socio-political barriers to deployment [15], [105], [186], [196], [201], [202], studies that operationalize these in models are largely missing from the literature. Geels and colleagues acknowledge this importance and state that “research on deep decarbonization requires complementing model-based analysis with sociotechnical research” [203], and Peng and colleagues suggest that political economy insights be incorporated as part of integrated assessment models [204]. Moore and colleagues identify ‘socio-politico-technical’ feedbacks in climate-social systems [205], and Noll and colleagues include a ‘switching cost’ to represent institutional barriers [206]. However, further efforts are needed to quantify the impacts of long project development timelines that stem from socio-political factors.

The technological focus of the present analysis is transmission systems from OSW plants. Specifically, I consider a novel PtH transmission pathway as a substitute for cable transmission. Some reasons for exploring this include:

- Transmission systems with lower space requirements interact with fewer environmental media, may reduce the extent of the needed environmental studies, and consequently may reduce deployment timelines.
- Transmission systems that do not directly interconnect with the grid may forgo interconnection studies, reducing deployment time.
- Hydrogen is seen by some as a key energy vector that can be used to decarbonize hard-to-abate sectors like steel production, the chemical industry, and perhaps some aviation.

Thus, substituting cable transmission for PtH pathways is a potential opportunity for green hydrogen deployment that may simultaneously address challenges with renewable energy deployment, transmission deployment, and grid modernization.

Considering PtH systems primarily for the benefits of transporting energy has been only sparsely explored. Hunt and colleagues [207] show that a 1.5GW solar plant in China can deliver its annual produced energy as hydrogen using airships. Li & Li [208] study how mobile hydrogen trucks may improve system resilience. And Ban and colleagues [209] model hydrogen fueling stations that also deliver excess hydrogen to local consumers. Comparative analyses of PtH systems with incumbent high voltage cable transmission systems have not been well-studied

Comparing hydrogen delivery topologies has been explored by Van Wingerden and colleagues [210]. Nunez-Jimenez and DeBlasio investigate the geopolitical implications of hydrogen trade through pipeline and shipping of hydrogen (in both liquid and ammonia forms) to identify opportunities to develop hydrogen trade within the EU and with international neighbors [211]. Neither of these studies consider a cable transmission topology to compare with the hydrogen ones.

4.2 Data and Methods

This analysis is carried out in three parts. In part 1, I provide a demonstration of how to value shorter deployment times considering a baseline transmission system that uses high voltage cables. In part 2, I calculate the level of regulatory difference that is needed to make the novel transmission system worth consideration considering various differential regulatory obligations and scenarios. In part 3, I perform a sensitivity analysis on the key parameters. The methods used to calculate the cost of energy from each topology is provided in this section.

4.2.1 Transmission system topologies

We consider three topologies, described in Figure 4.1. Topology A is the baseline transmission system in which electricity from OSW generation is brought to shore using HVDC cables. Topology B uses hydrogen pipelines to deliver green hydrogen from OSW to shore as done in [210]. Topology C is a 'decentralized' approach in which green hydrogen from OSW is brought to shore as liquified hydrogen using ships. The feasibility of this approach was explored in [211]. Alkhaledi and colleagues [188] produce feasibility studies on the performance of liquid hydrogen tankers.

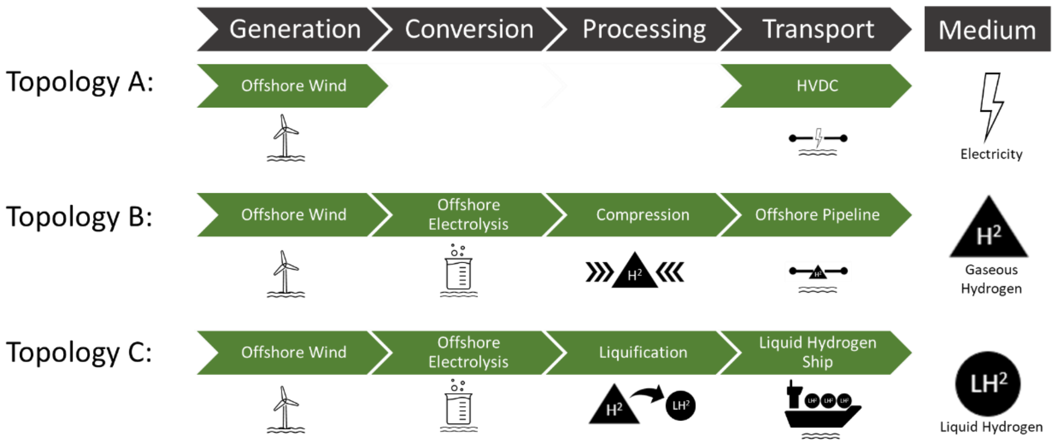

Figure 4.1: Summary of the three topologies considered in this study in which energy comes to shore via three different mediums: as electricity is gaseous hydrogen and as liquid hydrogen.

4.2.2 Cost and performance data

The main assumptions on cost and performance of the relevant components are given in Table 4.2 below.

Table 4.2: Main cost and performance assumptions for components for the different topologies.

	Capital Cost (EUR/MW)			**Operating Cost [a]**			**Efficiency**			**Source**
	Low	**Mid**	**High**	**Low**	**Mid**	**High**	**Low**	**Mid**	**High**	
Electricity Cost (EUR/MWh)	29	33	35	N/A	N/A	N/A	N/A	N/A	N/A	[18]
Offshore Platform (EUR per platform)	5,840,000	5,840,000	5,840,000	0.5%	0.5%	0.5%	N/A	N/A	N/A	[210]
Offshore Substation	685,000	685,000	685,000	2.3%	2.3%	2.3%	98%	98%	98%	[210]
High Voltage Cable	Various types			3.0%	3.0%	3.0%	Various types			[141]
Onshore Substation	200,000	200,000	200,000	1.5%	1.5%	1.5%	98%	98%	98%	[210]
PEM Electrolyzer	1,198,000	1,519,000	1,926,000	1.5%	1.5%	1.5%	64.1%	64.2%	64.3%	[210]
Compressor	15,000	15,000	15,000	4.0%	4.0%	4.0%	98.5%	98.5%	98.5%	[212]
Desalination (EUR/kgH_2)	0.04	0.04	0.04	—	—	—	—	—	—	[213]
Pipeline	615	615	615	1.0%	1.0%	1.0%	100%	100%	100%	[210]
Liquification	1,300	1,300	1,300	3.0%	3.0%	3.0%	70%	70%	70%	[212]
Ship (cost per ship)	43,000,000	43,000,000	43,000,000	2.5%	2.5%	2.5%	99.7%	99.7%	99.7%	[188]
Ship Capacity (m^3)	280,000	280,000	280,000							
LH_2 Storage (EUR/kg)	24	24	24	1.0%	1.0%	1.0%	99.7%	99.7%	99.7%	[212]

[a] Given as a percentage of the capital cost of the component incurred annually.

The cost and annual energy output can be computed by combining the components required for each topology considering plant size, capacity factor (assuming a 50% capacity factor throughout), and a distance to shore. For Topology A, several cable types are considered (Table C.4 of Appendix C.2) and formulas from Xiang and colleagues [141] are used to compute the number of required cables and the resulting efficiency from each cable type. The lowest-cost system is applied to compute the cost of energy from Topology A.

4.2.3 Levelized cost of energy for each topology

The LCOE for each topology is computed considering distance to shore as a parameter as plant distance to shore impacts the length of cable needed, length of pipeline needed, and the length of trip to ship liquid hydrogen to shore (increasing hydrogen burn off losses). I compute the LCOE for a baseline plant of 1,000MW as the sum of discounted cashflows over the sum of discounted energy flows:

$$LCOE = \frac{\sum_{t=0}^{T} \frac{CAPEX_t + OPEX_t}{(1+r)^t}}{\sum_{t=0}^{T} \frac{E_t}{(1+r)^t}} \tag{4.1}$$

Where the sum of discounted (by rate r) annual cash flows of CAPEX and OPEX are divided by the sum of discounted energy flows, E.

4.2.4 Operationalizing regulatory obligations as a time lag

In analyses that use overnight capital costs, the duration of project development, permitting, and commissioning is not considered, and the capital cost of the plant is incurred "overnight". The cash-flow structure and energy flows for in such a case are represented visually in Figure 4.2A. However, given the development and consenting process, energy generation does not begin until the plant begins operation, which can be several years after the decision to install a plant (which occurs in year 0 in this simple timeline). Assuming that the capital cost can be incurred in levelized increments the cash flow and energy flow diagram can be depicted as in Figure 4.2B which operationalizes the deployment process as a 'lag'—in this case I illustrate a lag of four years.

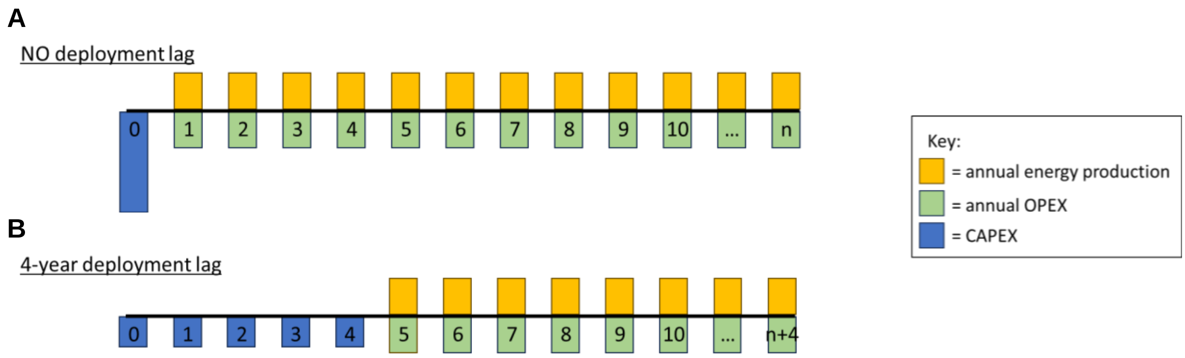

Figure 4.2: Depiction of cash and energy flows for a simplified project that considers A) overnight capital costs for a project with a lifetime of n years and B) a project with a development timeline ('lag') of 4 years. In the lower diagram, for simplicity, the sum of costs incurred in years 0 through 4 is the same as the cost in year zero in the upper diagram.

In this analysis I assume a uniform discount rate for all years equal to 5.2% which is the weighted average cost of capital for OSW plants according to the NREL ATB for OSW [142], and do not consider financing costs. To assess the impact of this discount rate, I conduct a sensitivity analysis on its impact as well. I assume that the absolute amount of CAPEX for the plant is the same, however it may be spread across years, and regardless of how long the lag is. Another implicit assumption in this is that supplier prices do not change over the course of the development and deployment process. In future analyses, differential cost of capital based on the maturity of the project and the project location may be considered [214], [215]. I also assess several types of cash flow distributions over the development years to assess the impact of this modeling choice.

4.3 Results and Discussion

We present the results considering a baseline plant of 1,000MW with a distance to shore of 20km, reflecting the global average distance of operating wind farms [216]. Throughout I assume HVDC cables are used as these would be the preferred option to 50/60 Hz HVAC cables, and probably even lower frequency AC over long distances [141].

4.3.1 Demonstration of how to value shorter deployment timelines

Figure 4.3 demonstrates how LCOE for an OSW plant that uses the baseline transmission topology (Topology A in Figure 4.1) changes with different lag periods between the time a project is started and when it becomes operational. Table 4.3 provides selected results for a 1,000MW array at 20km from the shore under different years of lag.

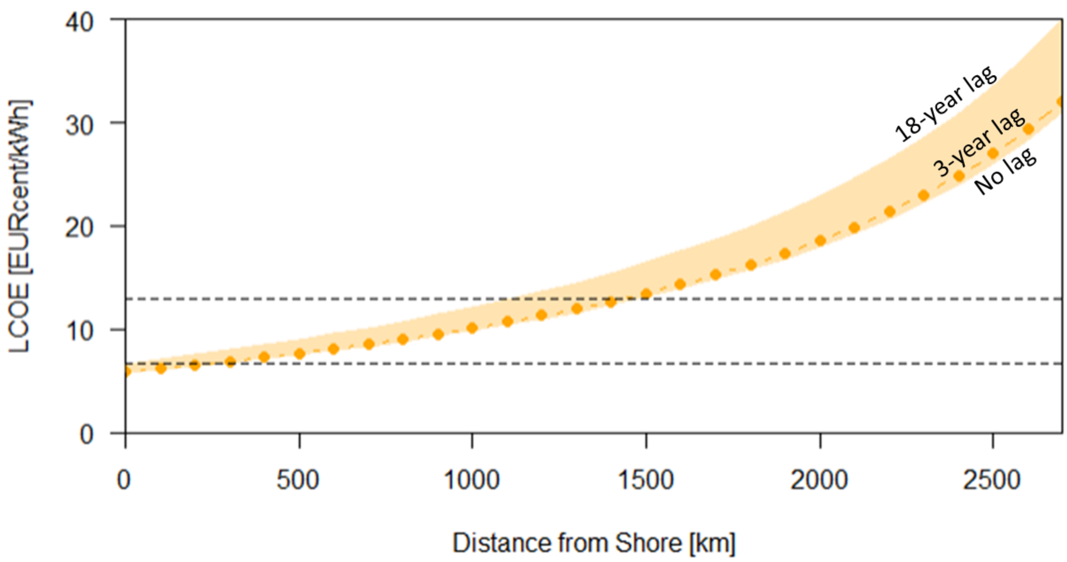

Figure 4.3: Resulting LCOE for OSW plants for different time lags between when a project is initiated and when it becomes operational using the baseline transmission topology. Horizontal dotted lines illustrate the range of OSW LCOEs for comparison [143].

Table 4.3: LCOE for a facility with different years of lag between the time when a project is initialized and when it becomes operational. This demonstrates how much the deployment time can impact the cost of a plant's energy.

Years of Lag	LCOE [EUR/MWh]
0	59.83
3	61.15
6	62.63
9	64.26
12	66.08
15	68.10
18	70.35

The average increase is 0.60 EUR/MWh per additional year of lag. Considering this size of plant and a capacity factor of 50%, this equates to 65.7 million EUR over this plant's 25-year lifetime.

4.3.2 Differential regulatory obligations show few scenarios where the baseline is inferior

Considering all three topologies based only on the range of component costs and performances (Table 4.2), the resulting comparative LCOE (expressed in eurocents per megajoule, MJ, to account for the difference in delivered energy medium—electricity and hydrogen) is shown in Figure 4.4. First, note that the PtH topologies are less sensitive to distance to shore than the cable topology, and Topology C—which does not have any longitudinal infrastructure in cables or pipelines—is the least sensitive to distance from shore since the main cost as plants move further from shore is the increased ship travel distance which results in more lost hydrogen (as burn-off in storage) and requires more fuel. As demonstrated in the figure, novel transmission topologies that use PtH do not achieve a lower cost of energy within the EEZ where projects are likely to be deployed, and only at very great distances from shore do these topologies begin to be cheaper than the baseline topology when there is no difference in lag between the technologies.

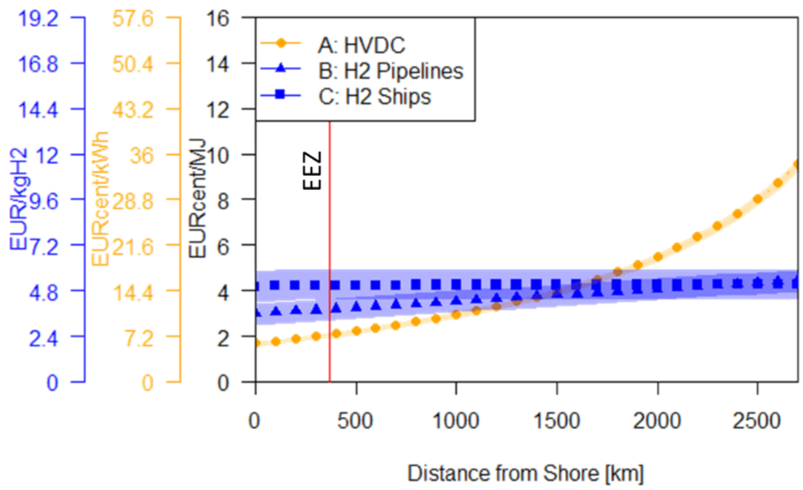

Figure 4.4: A comparison of the LCOE from the three transmission topologies without differential lag. In the absence of any differential lag periods (all scenarios consider 3 years of lag), novel transmission topologies (B and C, blue points and uncertainty ranges) are not cost effective within the EEZ (red line).

When three scenarios of lag are considered for each topology (0 years, 3 years, and 20 years) the result changes slightly as demonstrated in Figure 4.5. Given a high lag scenario for the baseline topology (A), the novel topologies (B and C) begin to be cheaper at a closer distance to shore than found in Figure 4.4, however, these novel topologies still do not become competitive with the baseline topology from a cost of energy standpoint within the EEZ, even when the worst case scenario of the baseline topology competes against the best case scenario of the novel topologies. Furthermore, it is questionable whether the difference in deployment time would ever be as great as the difference assumed between the high and low lag scenarios depicted in **Figure 4.5** casting further doubt as to whether novel transmission topologies can ever compete with the baseline topology within the EEZ even when operationalizing regulatory obligations as a lag between the two topologies.

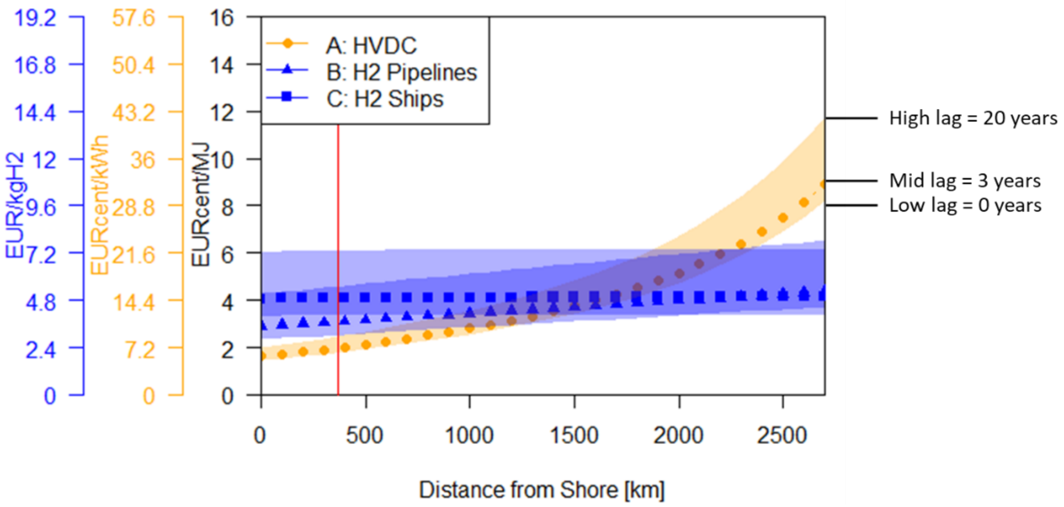

Figure 4.5: A comparison of the LCOE from the three transmission topologies with different amounts of lag between the time a project is initiated, and it becomes operational.

Because, as discussed earlier, there are other reasons aside from regulatory deployment obligations or delays that might force a developer to consider a PtH transmission topology instead of cable transmission, I explore one additional scenario—OSW 'overplanting'. Overplanting is the situation that occurs when the size of the array of turbines (or generators) deployed is greater than the capacity of the transmission system [217]. As a result, the generator can provide a more consistent power level, even when a variable energy source is used like wind or solar energy. This implies that a great deal of power is curtailed[4] by the generator. Some estimates for overplanted generators imply that levels of curtailment up to 35% [217] can be used, and a study for the State of Minnesota on the cost of curtailment versus installing energy storage shows that the cost of a system dominated by variable renewable sources is minimized at curtailment levels of 50%, or even higher [218]. This indicates that strategies that include high levels of curtailment may be feasible in the future. For the novel PtH topologies, the hydrogen generated can be stored, meaning that the plant would not have to curtail OSW production to accommodate the transmission system or demand constraints. Therefore, I consider an overplanted scenario (with up to 35% annual curtailment) in addition to the lag

[4] The term 'curtailment' broadly describes the situation when less energy potential (wind or solar) than is available at a given time is used or provided to the grid by arresting turbines, or 'disconnecting' generators. This may arise due to demand or transmission constraints and the unavailability of energy storage media [280].

differential in defining the low middle and high scenarios of the cost of energy from the different topologies. The results are depicted in Figure 4.6.

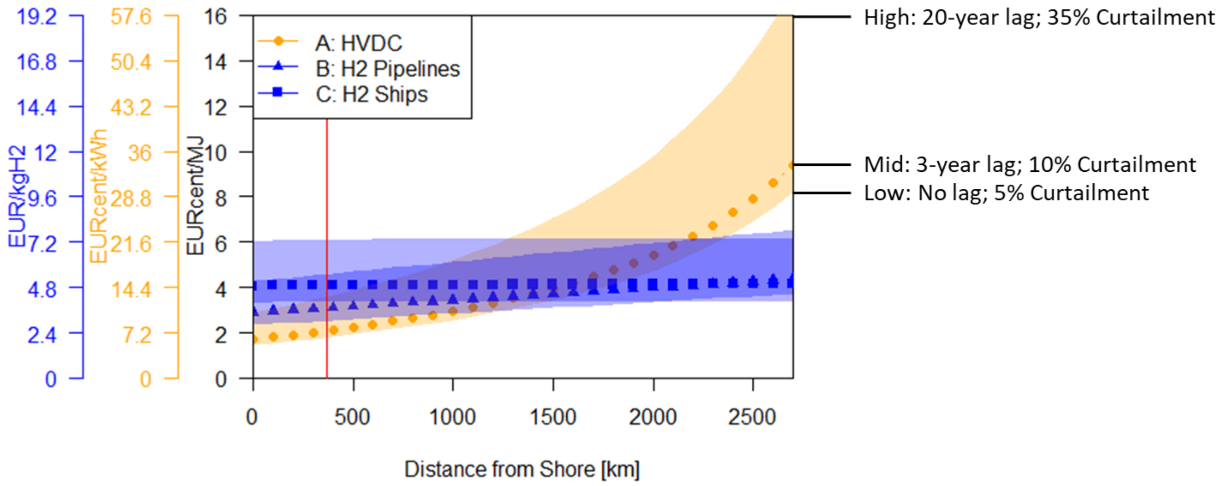

Figure 4.6: A comparison of the LCOE from the three transmission topologies with different levels of lag for all topologies and scenarios of curtailment for Topology A.

When adding curtailment scenarios, I find that the novel PtH transmission pathways realize comparable (possibly lower) costs of energy than the baseline transmission topology within the EEZ and very close to shore.

In summary, in the absence of any differential deployment times between baseline and novel transmission topologies, the latter do not have any cost advantages. Scenarios with differential deployment lag may favor the novel topologies, but the difference in deployment lag must be greater than what is likely in the real world (and of course experience suggest that developers might cancel projects in the face of long delays). It is only in situations of overplanting, or excessive curtailment faced by the baseline transmission topology that the novel PtH pathways realize cost advantages. In future work, other deployment costs and benefits should be included in the model to properly compare the novel methods with existing ones, and the evolution of costs with increased deployment should also be included in order to identify *when* the novel technologies may be more cost-advantageous than the incumbent technologies.

4.3.3 Sensitivity analyses

I conduct a sensitivity analysis on discount rate, years of lag, distance to shore, electricity cost, and project size, to examine which of these variables most greatly affect the cost of energy in the baseline topology. The results are depicted in Figure 4.7 with detailed results on the input and outcome parameters for each given in Table 4.4.

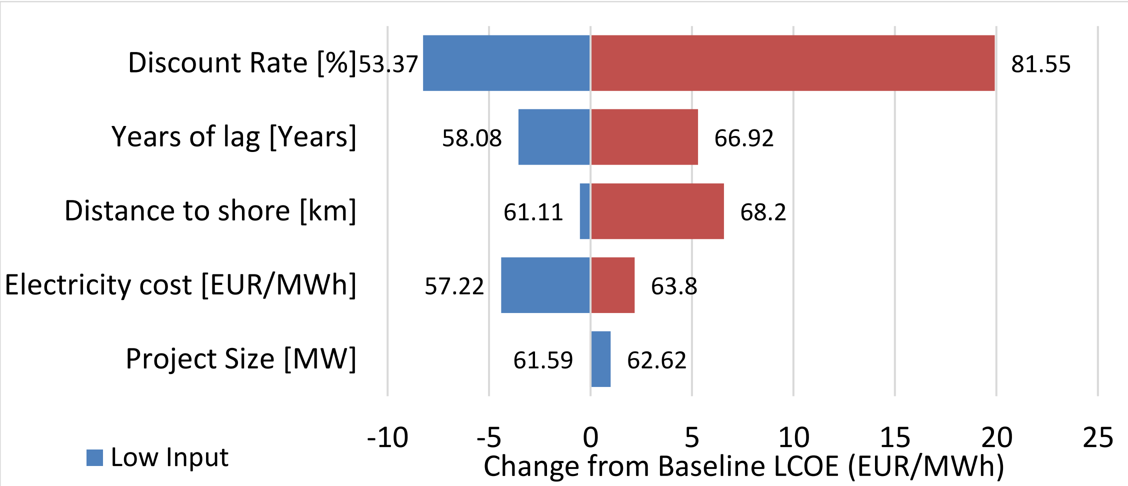

Figure 4.7: Sensitivity analysis of parameters. Values on bars provide the resulting LCOE of the scenario.

Table 4.4 shows that four of the five parameters have a direct influence on LCOE as expected—as the parameter increases, so does the LCOE. Only project size has an inverse relationship which illustrates economies of scale, also reflecting a real-world expectation in which project upsizing decreases the resulting cost of energy [67].

Table 4.4: Sensitivity analysis table

Parameter	Baseline Value of Input	Low input value (% change from baseline)	Low outcome (% change from baseline)	High input value (% change from baseline)	High outcome (% change from baseline)
Discount Rate [%]	**5.2%**	2.0% (-61.5%)	53.37 (-13%)	10% (+92%)	81.55 (+32%)
Years of lag [Years]	**10**	3 (-70%)	58.08 (-6%)	18 (+80%)	66.92 (+9%)
Distance to shore [km]	**20**	5 (-75%)	61.11 (-1%)	200 (+900%)	68.20 (+11%)
Electricity cost [EUR/MWh]	**33**	29 (-12%)	57.22 (-7%)	35 (+6%)	63.80 (+3%)
Project Size [MW]	**1,000**	100 (-90%)	62.62 (1.61%)	2000 (+100%)	61.59 (-0.06%)

As indicated, the discount rate has the largest impact on the cost of energy of the baseline topology. An IEA report [18] also finds that the cost of capital assumed has a significant impact on the LCOE of OSW plants. Years of lag, distance to shore, and electricity cost ranges all realize a similar impact on the resulting cost of energy. Finally, the cost of energy is least sensitive to the project size.

To understand how some of the relevant component costs and performance parameters impact the cost difference between the two PtH topologies and the baseline topology, I also conduct a sensitivity analysis on these and report how a percent change in the inputs impact the difference in the resulting LCOE as a difference to the baseline topology LCOE (expressed as a percentage change to the baseline situation). The results are presented in Figure 4.8 below.

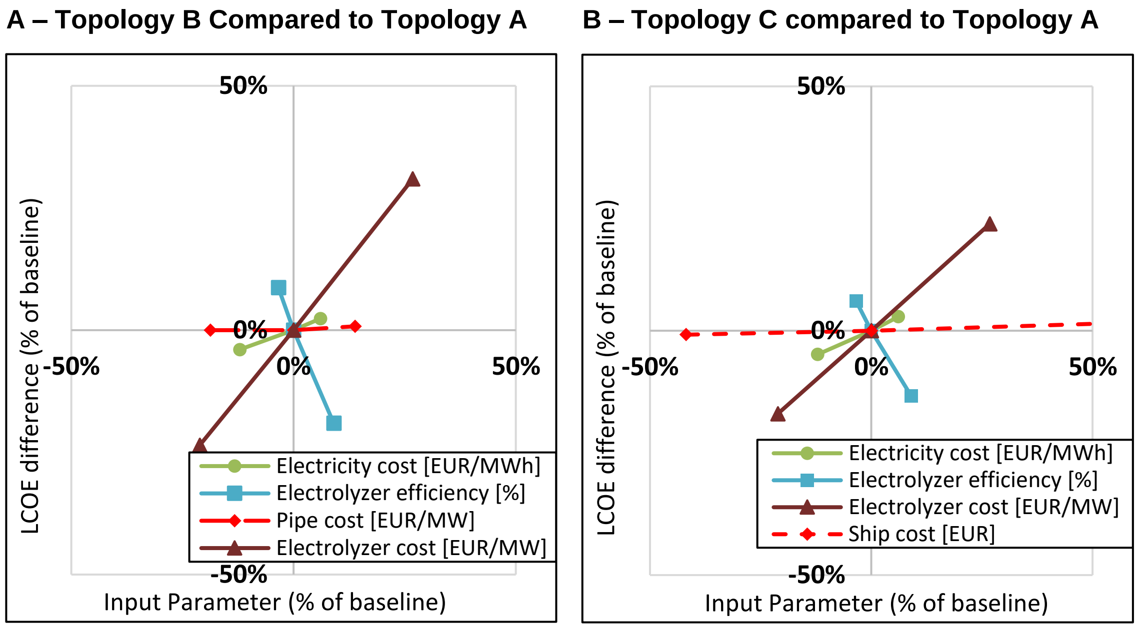

Figure 4.8: Spider plot illustrating the sensitivity of key input parameters to the cost differences. In A) the cost difference between Topology B and A is compared (presented as a percent change from the baseline case); in B) the cost difference between Topology C and A is compared. In the panels, if the novel topology (B or C) were to become cheaper than Topology A, the y value would be -100% or less.

In Figure 4.8, the more vertical the line, the more sensitive the cost difference is to the input value, that is, a more vertical line indicates that a small change of that input parameter (x-axis) has a large impact on the LCOE difference between a PtH transmission topology and the baseline topology (y-axis). Conversely, a more horizontal line indicates that the opposite is true. The vessel to bring hydrogen from the plant to shore for Topology C is a component that has not yet been commercially deployed and has mostly been explored theoretically [188], [219]. Its cost is thus very uncertain and represents a large investment to deploy the topology. The cost of energy difference from Topology C does not change much as the cost of the ship changes. This is because the range of the cost of one ship is still small relative to the overall cost of a 1GW plant. The cost of energy difference from Topology B is also relatively insensitive to the cost of the pipeline for the same reason. Both PtH topologies' cost differences are also insensitive to the cost of electricity assumed from the OSW array. This is unsurprising since the cost of energy from the OSW array should also impact the cost of energy from Topology A, therefore reducing the impact it has on the cost difference between Topology A and the PtH topologies. The cost difference for both topologies is more sensitive to the electrolyzer cost and the electrolyzer efficiency. A decrease in the electrolyzer cost by 21% makes the cost of energy 17 to 24% more competitive for both PtH topologies (it reduces the difference between Topology A and the PtH topologies by 17-24%). By improving electrolyzer efficiency to 70% (which is a 9% increase over the assumed baseline efficiency of 64.2%), the cost of energy for the PtH topologies improves by 13 to 19%. This shows that small improvements in electrolyzer technology—which is a topic of active research and development—enable the PtH topologies to become more competitive with the baseline case. The full sensitivity analysis is provided in Appendix D.1.

This sensitivity analysis of the cost of electrolyzers begs the question of what the needed electrolyzer cost is for the PtH topologies to be cheaper in the absence of regulatory differences between them. At the US Department of Energy target electrolyzer efficiency level of 77% [220] and all other factors held equal, at a distance of 370 km (the edge of the EEZ), the LCOE from Topology C becomes cheaper than that of Topology A when the electrolyzer cost falls to 450 EUR/kW. A negative electrolyzer cost is needed for Topology B to be cheaper than Topology A at this distance. At a distance of 20 km, a negative cost is needed for either PtH topology to be cheaper than Topology A. This indicates that it is unlikely for PtH topologies to compete on cost solely through electrolyzer techno-economic improvements. Pursuing novel PtH topologies must realize other benefits.

Finally, the framework operationalizes the lag by assuming that the overall capital cost is evenly distributed over the lag years. To illustrate the sensitivity that the resulting LCOE has based on the assumed distribution of cash flows over the years of development, I consider four cash flow types as depicted in Figure 4.9.

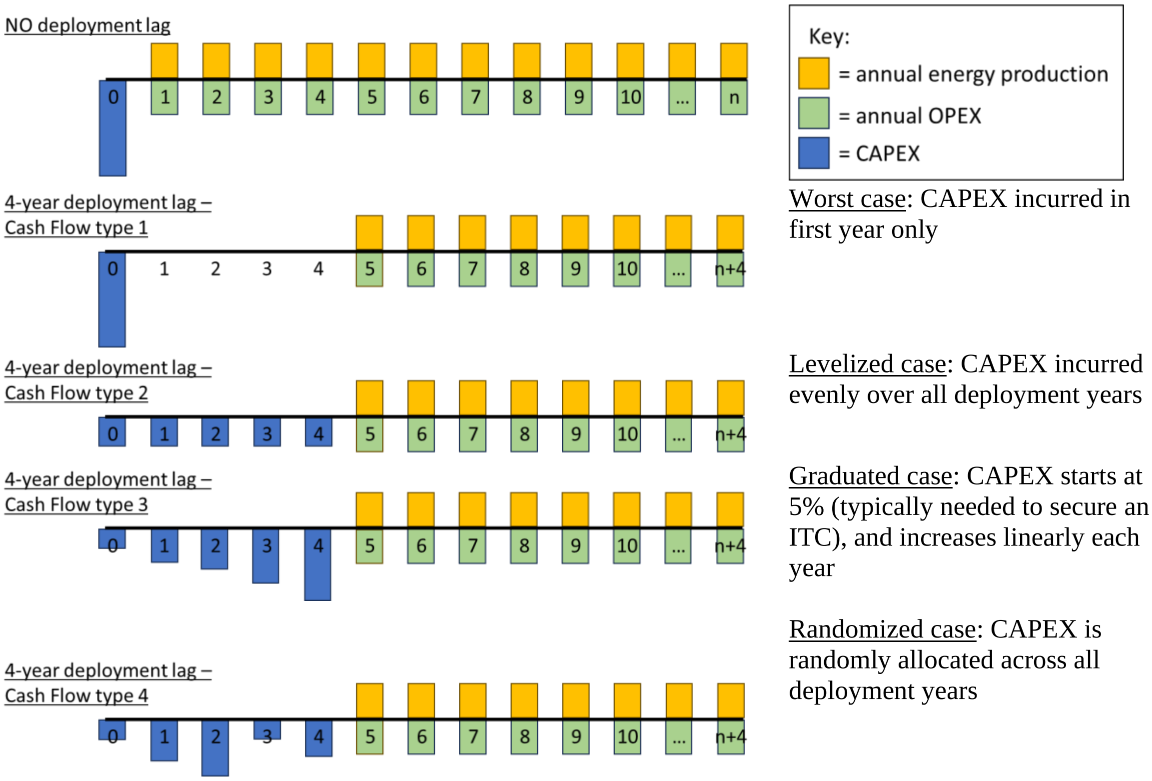

Figure 4.9: Possible cash flow types.

A 'worst-case' cash flow type assumes that all the CAPEX is incurred in the first year of a project, with no CAPEX henceforth committed as the project is developed and commissioned (during the lag years). This provides a 'backstop', or a maximum cost of energy given the project cost parameters and years of lag. A 'levelized case' cash flow type is that which has been used thus far in which the CAPEX is instead committed or spent evenly across the lag years. A 'graduated case' cash flow type assumes that 5% of the overall CAPEX is committed in the first year—this is usually the amount needed to secure an ITC—and the amount of CAPEX committed in the remaining years of lag linearly increases until all the CAPEX is spent. Finally, in a 'randomized case' the CAPEX is randomly committed across the deployment years. In estimating the randomized case, I run 1,000 instances of the randomized case and estimate the LCOE for each (at each number of lag years) and record the mean of the runs. The result of the LCOE for each of the cash flow types is depicted in Figure 4.10.

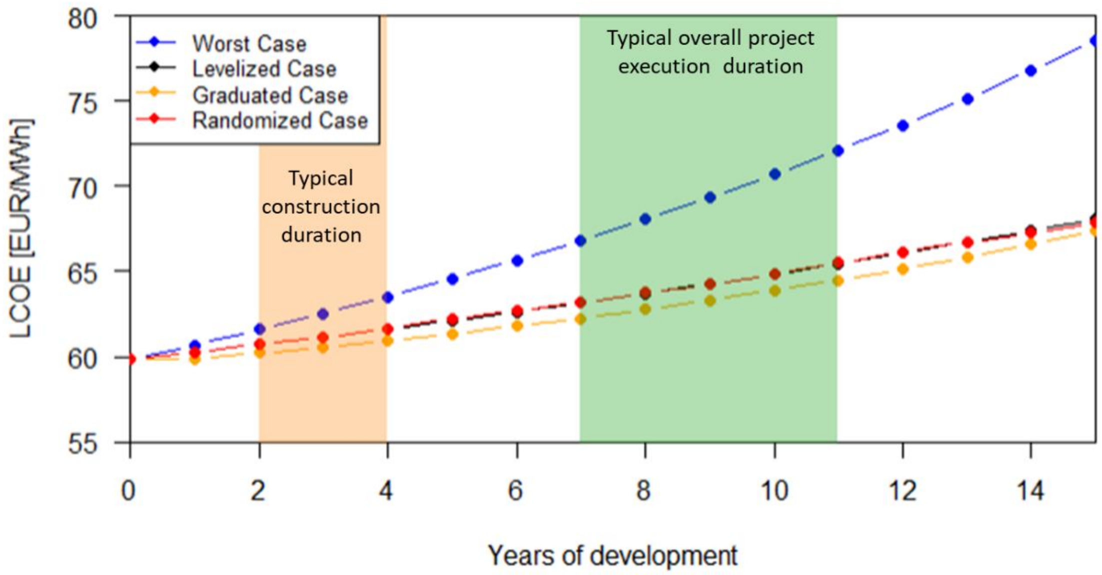

Figure 4.10: Sensitivity of Cash Flow Type over development years. Orange band illustrates typical plant installation and commissioning times, and green band illustrates typical overall deployment time.

As demonstrated in Figure 4.10, the way the CAPEX is committed over the development years has a significant impact on the resulting estimate of the cost of energy. With no years of lag, this is the equivalent of using overnight CAPEX to estimate the LCOE, and all cash flow types would report the same value. The worst-case cash flow increases rapidly as the extent of the lag increase, and the randomized case tracks closely with the levelized case indicating that in the absence of data on the cost schedule for a project over its development years, assuming the overall CAPEX is committed equivalently is just as good as assigning the CAPEX randomly. The ideal case to keep the cost of energy at a minimum is the graduated case which realizes the lowest LCOE across all lengths of development years.

4.3.4 Future extensions

The analysis framework presented here can be extended in several directions which I reserve for future work. A brief description of these is included in this section.

The first extension of this model would be to include cost escalation factors for the development years. The current model assumes equivalent total costs whether they are incurred in one year (overnight costs) or incurred over several years. This is a simplifying assumption, and indeed, when development is spread over several years, there is a cost penalty to doing so. Financing, inflation, and differential risk profiles of the project over the development years contribute to the cost escalation. In addition to cost escalation factors, the different risk profiles would result in a cost of capital that may be different in each year, although I assumed a uniform discount rate in the study. As the sensitivity analysis shows, the LCOE is very sensitive to discount rate, and therefore, refining how the cost of capital or discount rate is considered in these estimations is imperative, including how it might differ from country to country [214]. In a subsequent iteration of this model, I would interview developers to understand how cost escalation factors and differential costs of capital are distributed among project development years, and how they can better be represented when development timelines are long.

Another potential extension of this model is to include the probability of project abandonment. The current model assumes that projects are seen to completion, regardless of the duration of development. In reality, a long development timeline is a developer risk, and may be viewed adversely, and considered in deciding whether or not to proceed with the project. As development timelines grow, so does the risk that a project sponsor may grow impatient and abandon the project[5]. In a subsequent iteration of this model, I would conduct some type of elicitation survey or analyze empirical project data to operationalize the probability of project abandonment which should be proportional to the length of the deployment timeline—I hypothesize that more projects are abandoned when development timelines are long, than when they are short.

Finally, stochastic shocks, macroeconomic factors, and other market factors could be incorporated into the model. The current model assumes static discount rates and project component costs. These component parameters (cost and performance) have some probabilistic

[5] This is the case for OSW projects in the US which have recently abandoned power purchase agreements with utilities, incurring a penalty for doing so [87], [88].

distribution, however, which can be incorporated into the analysis using scenario analysis or some stochastic modeling. Macroeconomic shocks are a concern for projects with long development timelines, as they are subject to quick changes in the supply chain or financing terms. When development timelines are long, the likelihood of exposure to such an event also increases. These events occur with some likelihood that can be estimated from historical experience, and therefore potentially included into the model as a probability that macroeconomic fluctuations occur in each year. Running the analysis several times given the distribution of these parameters and probabilities of shocks may also provide insight into the further risks and uncertainties with long deployment times.

4.4 Conclusions and Policy Implications

Project execution in the real world—whether for OSW projects or other technologies—can take years owing to regulatory requirements and other factors that differ from adoption environment to adoption environment. Project planning and permitting are two activities in the development process that contribute to the timeline. For OSW, although project construction may last two to four years, the overall timeline may require 11 years or more depending on the jurisdiction, their regulatory requirements, and potential stakeholder resistance which has delayed OSW projects in the US in the past [151], [221]. In the face of the need to deploy vast amounts of renewable energy and transmission infrastructure to decarbonize the energy system, deployment timelines have gotten longer—not shorter—over the last two decades [14], as have interconnection queue waiting times [183]. The implications of this trend should be quantified in monetary terms. The present study has demonstrated and applied a framework for doing that.

Using straightforward project economic calculations for a typical OSW plant, I demonstrate that shortening the project execution timeline by one year can reduce the cost of energy for that plant by 0.6 EUR/MWh, or more than 65.7 million EUR over a 25-year operational life. To put that reduction in perspective, achieving a similar reduction in cost of energy for the same plant with an ITC would require a 2.6% ITC which would require a 23 million EUR government investment for one plant. Any policy initiative that aims to give special consideration or expedite project development can consider the computed value of shorter deployment time estimated here with the cost of the needed efforts from the policy.

I demonstrate this framework to compare the cost of energy between three specific transmission deployment topologies and find that there are very few scenarios that favor novel PtH transmission as a substitute for high voltage cables. The former only become competitive when high levels of curtailment are considered and an extremely high difference in deployment timeline, both of which may only occur in unique situations. However, I find that the level of competitiveness of the novel topologies is extremely sensitive to the cost and performance of electrolyzers, indicating that in the future, once the technology becomes more mature, PtH transmission may make more economic sense.

One limit of this study is that the cost of energy is the only parameter compared. However, the price for hydrogen and the price for electricity can also vary, and therefore the profitability gap is not reflected in this study. The price for hydrogen and electricity varies greatly depending on region, and who the end user is, and therefore should be examined in future study. Future research should also aim to understand how the cost of capital changes in each year of development, how costs may escalate with longer deployment times, and how the probability of project abandonment or macroeconomic shocks may impact project execution. For example, in early development years, the risk and uncertainty would be higher before a sponsor has secured any contracts, and thus, the cost of capital may be higher impacting project economics, and potentially increasing the value of reducing development timelines by one year than what I have calculated here.

This chapter demonstrates one way to operationalize the regulatory obligations to deployment and enables comparisons among different adoption environments or technologies should they face differential obligations. The temporal effects on project deployment should not be overlooked in modeling efforts.

4.5 Code availability

The analysis code to execute this analysis is saved in the following repository: https://doi.org/10.5281/zenodo.10730746.

Chapter V
Conclusions and Future Work

5.1 Summary of Findings and Implications

In this dissertation, I have investigated socio-political factors and considerations with OSW deployment and how they compare with techno-economic factors to identify opportunities for expanded deployment of the technology. The dissertation began as explorations in the potential for the OSW market to grow and its potential role in decarbonizing energy generation. The overall cost and cost of energy from OSW have steadily fallen globally over this period [11], and, in the period since I began the work in 2019, the industry has changed drastically and heterogeneously—global capacity grew 220% from 2019 to 2022, Chinese capacity grew more than 500% to over 30GW, taking over the UK as the global leader, the US grew 140%, the Netherlands grew 340%, Belgium grew 140%, and several countries had negative or zero growth (Spain, Finland, and Japan) [8]. Studies show that techno-economics alone do not predict deployment decisions [12], [13], and so this work was aimed at understanding and considering a range non-techno-economic factors of OSW deployment options which can aid in project or technology decision-making and help manage aspects of the adoption environment to pave the way for improved deployment prospects.

In Chapter 2 I assessed the techno-economic performance of dynamically positioned floating OSW turbines compared to moored systems, which are the prevailing station-keeping method used for floating turbines today, and find that under several circumstances DP systems may be advantageous. Turbines of intermediate size (8-10MW) achieve lower LCOEs than the largest 15MW turbine considered in the analysis—which is a novel finding as turbine upsizing is often cited as a means for reducing LCOE. While this system would be more expensive than a mooring system at depths of 630m, its use would eliminate up to 910km of mooring chains for a 1,000MW plant potentially reducing environmental impacts, easing stakeholder concerns, and easing the deployment process for developers.

In Chapter 3 I applied a multi-criteria analysis framework to assess the suitability of over 140 million OSW plant alternatives to a techno-economic optimizing decision-maker ("developer paradigm") and an environmental and stakeholder impact minimizing one ("stakeholder paradigm"). The results suggest that the poor track record of deploying US OSW projects is unsurprising (see Figure C.1. of Appendix C.1). Prior (and some current) site and design decisions align with the developer paradigm but not with the stakeholder one, offering an explanation for failed deployments. While all early projects have been sited close to shore tending to optimize techno-economic criteria, I demonstrate that if projects can move, even marginally, further from shore, they can remain within consensus areas that balance techno-economic and plant impact criteria. I also find that increasing the weight placed on energy output increases the suitability scores of alternatives at all scales (see Figure C.7C of Appendix C.8), implying that policies that increase the importance of deploying clean energy, such as those recommended by the European Commission [173], should be pursued. Furthermore, while the industry pursues larger plant capacities, I demonstrate that smaller capacities reduce the uncertainty of the impacts the plant may realize in the stakeholder paradigm—a potential value to developers.

In Chapter 4, I demonstrate a modeling framework to operationalize regulatory obligations and compare three OSW transmission topologies using the framework. I demonstrate that shortening the project execution timeline by one year can reduce the cost of energy for that plant by 0.6 EUR/MWh, or more than 65 million EUR over a 25-year operational life. To put that reduction in perspective, achieving a similar reduction in cost of energy for the same plant with an ITC would require a 2.6% ITC which would require a 23 million EUR government investment for one plant. This outcome is relevant to the policy analysis literature today as several policy and regulatory initiatives are aiming to give special consideration to renewable energy deployment against existing stakeholder uses [173], reduce permitting time [189], and reduce interconnection processing time [190] to ease regulatory requirements and expedite the renewable energy deployment process. Any policy initiative that aims to give special consideration or expedite project development can consider the computed value of shorter deployment time estimated here with the cost of the needed efforts to deploy the policy.

While OSW technology was the technology focus of this dissertation, the work also provides insights to the energy transition research literature as a whole. The size of a deployment of a technology has been considered in growing literature that investigates the benefits of granular or modular deployments to increase technology spillovers, learning, growth rates, other social indicators, and overall decarbonization [69], [70], [174], [222]. Conversely, in a purely cost of energy perspective, studies show that reducing the LCOE for OSW is achieved by upsizing plant and turbine sizes [67]. In Chapter 2 I find that intermediate-sized turbines (not the largest considered in the analysis) reduce LCOE when turbines are deployed with DP, and in Chapter 3, I demonstrate that smaller plants have a tighter distribution of suitability scores, reducing uncertainty of the potential impacts they realize when compared to large plants. These two findings provide evidence that smaller deployments can have their advantages. Another theme of growing research interest is socio-political barriers to energy deployment, and how to quantify and include them into modeling-based research. In Chapter 2 I quantify one environmental benefit; in Chapter 3 I quantify several environmental impacts of plant alternatives; and in Chapter 4 I develop a modeling framework to operationalize development obligations that come from socio-political or regulatory considerations as a temporal element in estimating the cost of energy.

Looking beyond the scope of OSW, among 50 tracked technologies that are needed to decarbonize energy, only three are being deployed at a rate that is on track with achieving ‘net zero' annual emissions by 2050 [3]. Many of these technologies have demonstrated market readiness and—in some cases—techno-economic advantages over existing options. It is apparent that it is important to consider, quantify, and operationalize non-monetary aspects in order to balance them with techno-economic metrics to evaluate deployment and policy options. Adequately incorporating these metrics in decision-making may improve deployment prospects and facilitate the shift toward a decarbonized energy system.

5.2 Future Research Directions

Bridging socio-political and techno-economic perspectives has been recognized as a key research frontier in energy transition research and modeling. Geels and colleagues acknowledge this importance and state that "research on deep decarbonization requires complementing model-based analysis with sociotechnical research" [203], and political economy insights are recommended to be part of integrated assessment models [204]. Moore and colleagues identify 'socio-politico-technical' feedbacks in climate-social systems [205], and Noll and colleagues include a 'switching cost' to represent institutional barriers [206], but further efforts are needed to bridge techno-economics and socio-political feasibility. The analyses in this dissertation were carried out without a temporal or market evolutionary element, however, the impact of one adoption decision today has impacts on the evolution of the industry, market, and levels of attainment of energy supply and decarbonization. Thus, it follows that adding a temporal element to investigate technology competition among low-carbon energy options should be part of future analyses.

Low-carbon energy use and supply technology options compete with established incumbent technologies. For example, fuel combustion cars, trucks, ships, and airplanes have been around for decades although electric vehicles and biofuel options now exist which both realize fewer overall emissions. The competition dynamics for energy services and end uses has been a theme of study for competing energy storage systems [223], [224], [225], road freight options [206], and solar energy technologies [226]. Often, such models focus on a techno-economic perspective, but there are socio-political elements which warrant inclusion in competition modeling efforts that may provide key insights into how technologies are chosen in the real world. Therefore, non-monetary, socio-political metrics should be part of models to weigh against techno-economic ones.

I therefore aim to extend the work in this dissertation by bridging socio-political and techno-economic perspectives on a key component for decarbonization—green hydrogen[6]. Green hydrogen can be used in many end-uses and decarbonize several sectors—this may be a benefit but raises uncertainty in the potential market share that it can take as it competes against other low-carbon and incumbent technology options. Hydrogen's potential to compete against existing options is of growing interest, and several applications have been characterized in a qualitative 'hydrogen ladder' [227]. Several of these applications have an unclear future market and compete against incumbent and other low-carbon options such as shipping, aviation, and bulk energy transport. I aim to investigate several over-arching questions with this work including: which green hydrogen applications hold the most promise; how important are socio-political metrics in investment decisions; and how will socio-political metrics impact system dynamic competition models. I aim to report the carbon abatement impacts realized by varying importance of socio-political metrics.

From a model-architecture perspective, I will model investment decisions as a multi-criteria decision problem in the simulations. Weights on each metric will be elicited from decision-makers, and a sensitivity analysis on the model weights will also be carried out. By giving socio-political metrics different weights in each run, the outcomes of the model (market shares and carbon abatement) can be assessed, and I can quantify the difference in levels of attainment under different institutional contexts (combination of model weights).

[6] Hydrogen that is generated from renewable energy through water electrolysis. Today, most hydrogen demand is supplied by 'gray' hydrogen, which is created using methane [230].

Conceptually, my past and future work relates to several research themes. At the broadest level, it adds to the literature on the energy transition [200], [228], and more specifically, work on socio-technical aspects of the energy transition [203], [228]; it contributes to market understanding of the potential of hydrogen applications [213], [227], [229], [230], [231]; it advances society's understanding of socio-political barriers and mechanisms that impact technology adoption [15], [204], [205], [232] moving from qualitative to more quantitative studies on the topic; and furthermore, it potentially relates to recent work on how technology characteristics (namely size and need for customizability) can impact the speed of adoption [69], [70], [174].

Appendix A

Supplementary Materials for Chapter I

A.1 Targets and Actual Capacity

Table A.1: Capacity projections or targets for OSW in the early 2010s and actual capacity for the projection year.

Country/Region	2020 Target or Projection (set in early 2010s) [6]	Actual 2020 Capacity (% of target) [8]	Actual 2022 Capacity (% of target) [8]
South Korea	2.5 GW	136 MW (5%)	136 MW (5%)
France	6 GW	2 MW (0.03%)	482 MW (8%)
EU (including the UK)	43 GW	24.9 GW (58%)	30.5 GW (70%)
Germany	10 GW	7.8 GW (78%)	8.1 GW (81%)
Portugal	500 MW	25 MW (5%)	25 MW (5%)
Spain	3 GW	5 MW (0.2%)	5 MW (0.2%)
United States	> 3 GW by 2018 [7]	29 MW (1%)	41 MW (1.4%)

A.2 Probabilistic Feasibility Space Methodology

Following Odenweller and colleagues who develop a probabilistic feasibility space of scaling up green hydrogen supply [9], a probabilistic feasibility space for OSW (OSW) scale up is developed using a similar methodology. Truncated triangular distributions are used to represent two key parameters that identify the adoption pathway: initial capacity (in 2024) and growth rates as seen in Figure A.1 below.

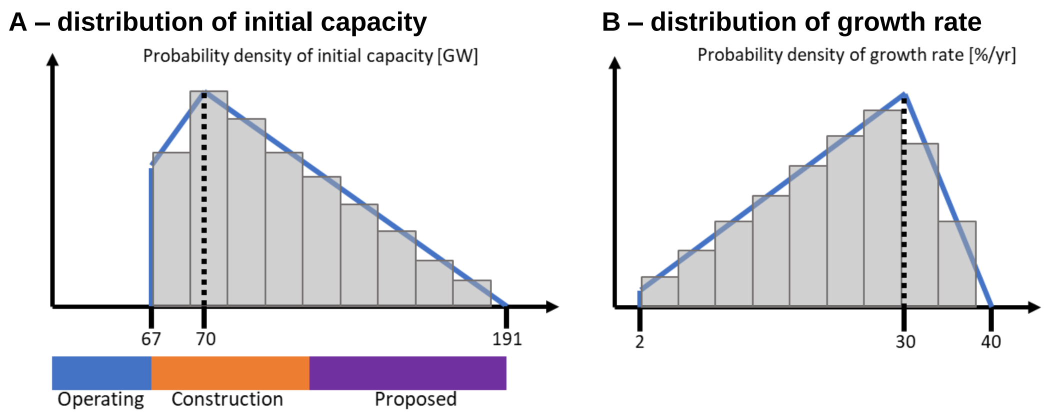

Figure A.1: Distributions of A) initial capacity and B) growth rate to develop a feasibility space for OSW growth. Figures are not to scale.

I use truncated triangular distributions for both parameters with lower truncation based on the lower thresholds that these two parameters will likely realize. The minimum value for both parameters is zero (defining the minimum for the entire triangular distribution), but a lower threshold is set for which I do not expect to see values. For initial capacity, the lower threshold (truncation) is set to the operating capacity for OSW in 2023 [10]—no plants are not expected to be decommissioned sooner than new plants are built by the end of 2024 to result in a starting capacity less than the operating capacity in 2023. For growth rate, I set the lower threshold at 2% growth per year as this was the smallest annual growth rate for onshore wind observed across several countries over the period from 1980 to 2009 [233]. The maximum and mode values (the remaining values that define a triangular distribution) are defined as follows.

For initial capacity:

- Maximum = sum of global OSW capacity in operation, under construction, and proposed [10].
- Mode = 20% of the global OSW capacity under construction plus the operating capacity in 2023.

For growth rate:

- Maximum = global compound annual growth rate (CAGR) of onshore wind during the emergence period (1980-2009) [233].
- Mode = projected growth of global OSW according to the Global Wind Energy Council (GWEC) [10].

In addition to these parameters, a "demand pull" parameter is defined each year. It is meant to represent some commitment that can spur growth in the industry. In this first-order analysis, I apply a linear interpolation of the OSW capacity objectives in 2030 (500GW) and 2050 (2500GW) for the International Renewable Energy Agency (IRENA) 1.5C pathway [10] with a 5-year anticipation (the same anticipation used by Odenweller and colleagues). This "demand pull" is shown as the dotted line in Figure A.2 below.

In each run (adoption pathway) a draw from the two parameters in Figure A.1 is taken, and applied into a logistic growth model to compute the cumulative growth capacity each year:

$$C_t = C_t + bC_{t-1}\left(1 - \frac{C_{t-1}}{C_{max,t}}\right) \quad \text{(A.1)}$$

where b is the growth rate, C_0 is the initial capacity, and $C_{max,t}$ is the annual demand-pull value. The results are presented in Figure A.2 below.

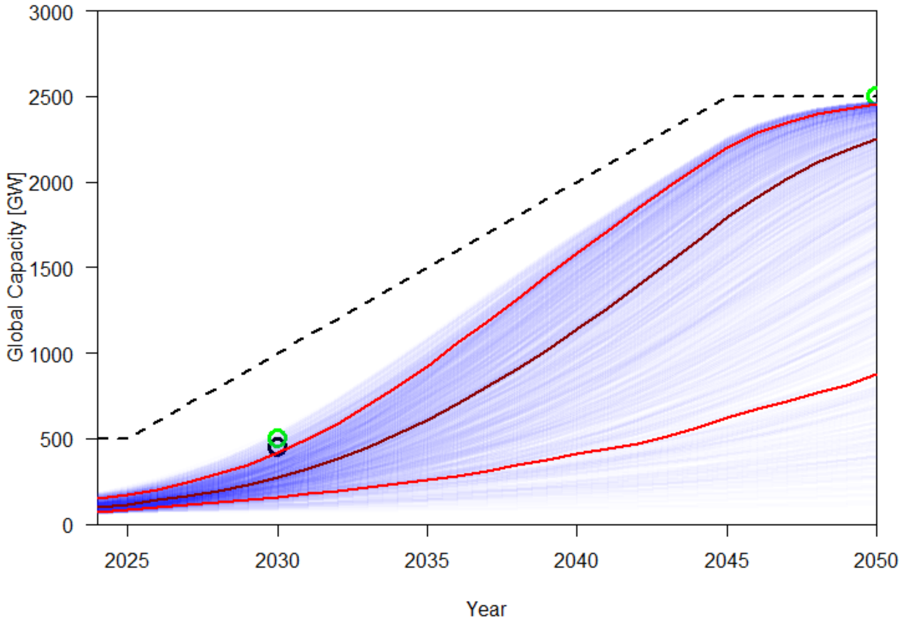

Figure A.2: Result of 1,000 runs of the model. The light red lines represent the 90th and 10th percentile values in each year, the dark red line represents the median of the runs, and the light blue lines illustrate each run. The dotted line illustrates the demand-pull function. The green circles illustrate the cumulative installed values under the IRENA 1.5C scenario, and the dark black circle is a projection for the installed capacity by GWEC [10].

The codes used to develop this figure are include in the following R code repository: https://doi.org/10.5281/zenodo.10792705.

Appendix B

Supplementary Material for Chapter II

B.1 Floating Semisubmersible Dimensions

Figure B.1 describes the floating substructure used in the analysis for all the turbine sizes. It was designed for the 15MW National Renewable Energy Laboratory (NREL) reference OSW turbine and is therefore oversized for the smaller turbines used in this analysis. The following image is adapted from [234, Fig. 3]:

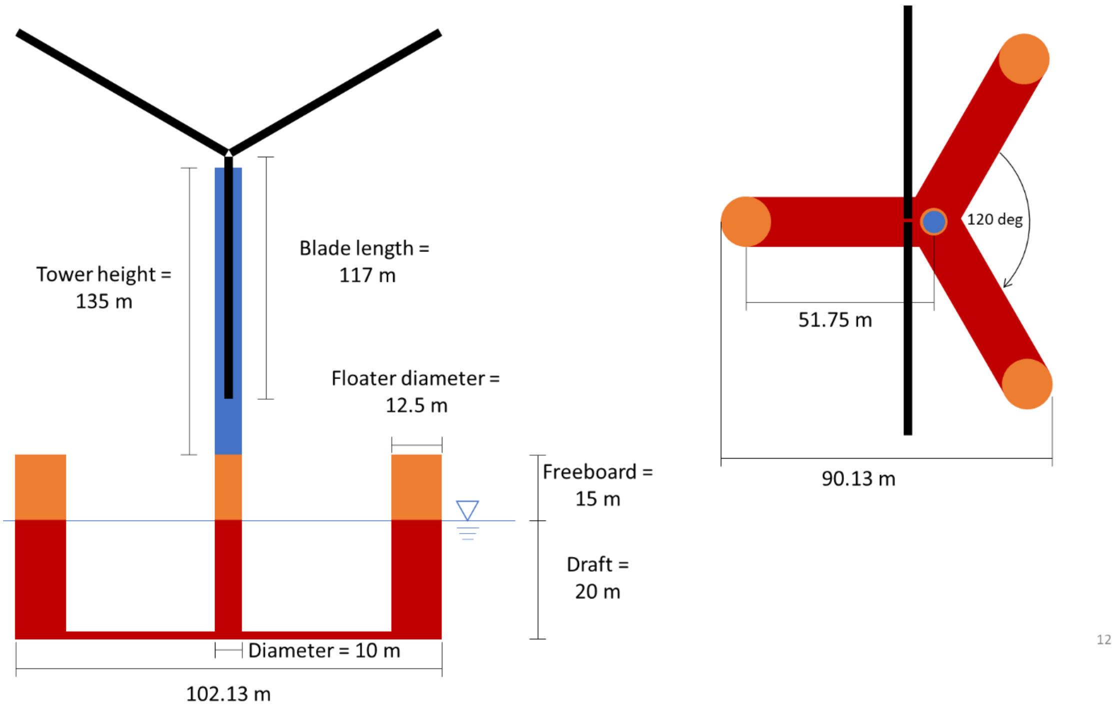

Figure B.1: Dimensions of floating substructure used. These are adapted from [234, Fig. 3]. Turbine dimensions shown are for the 15MW turbine, while the smaller turbines are also used with this substructure.

B.2 Wind, Current, and Wave Force Calculations

For forces from the wind, I consider each component of the floating turbine separately and sum the forces on each body. For the static components (tower, substructure above the water surface, and blades when they are not operating), I represent the wind speed as a function of height with a power law [42]:

$$V_{wind}(z) = V_{hub}\left(\frac{z}{z_{hub}}\right)^{\alpha} \tag{B.1}$$

where $V_{wind}(z)$ is the wind speed at height z measured in m/s. z_{hub} and V_{hub} are the hub height (in m) and the wind speed at that hub height, respectively; I use wind speed measurements at 100m hub heights. I assume rigid body motion, steady-state conditions, and an α equal to 0.14 [42]. I consider the changing diameter of the tower and blades when those have been specified in the technical data; otherwise, a constant cross-section is assumed. Similar to the Blade Element Method [43], I integrate over each component accounting for these functions:

$$F_{wind,component} = \int_z \frac{1}{2}\rho_{air}\, V_{wind}^2(z)\; D(z)\; C_d(z)\; dz \tag{B.2}$$

where ρ_{air} is the air density, $D(z)$ is the changing diameter of the component with height, and $C_d(z)$ is the changing drag coefficient with height. The cross-sectional dimensions also change along each blade. The force on the rotor is highly dependent on whether the turbine blades are arrested or spinning. When the blades are stationary, they are feathered, and I calculate their contribution using equation (B.2). For spinning blades, I use the reported rotor thrust force for the turbine [235], [236], [237], [238]. These thrust forces have been empirically or experimentally attained. In some cases, the coefficient of thrust data were provided at each wind speed, in which case I use the following equation to directly compute the force [43]:

$$F_{rotor}(V_{wind}) = \frac{1}{2}\rho_{air}V_{wind}^2 A_{rotor} C_T(V_{wind}) \tag{B.3}$$

where A_{rotor} is the rotor swept area and $C_T(V_{wind})$ is the coefficient of thrust of the turbine at a particular wind speed.

For current forces, the following equation (based on the drag force on a solid body caused by a constant flow [41], [42]) is used:

$$F_{current,component} = \frac{1}{2}\rho_{water}V_{current}^2 A_{eff}C_d \tag{B.4}$$

where ρ_{water} is the water density, $V_{current}$ is the current speed, A_{eff} is the effective surface area subjected to the moving current, and C_d is the drag coefficient, which varies between 0 and 1. Equation (B.4) can be applied individually to all of the submerged portions of the substructure (three floaters and one support beneath the turbine tower) and then summed.

For wave forces, I use the Morison equation to estimate the mean wind force on cylindrical bodies [48]:

$$F_{wave,component} = \int_{-z_D}^{0} \frac{1}{2} C_D D \rho_{water} v|v| \, dz + \int_{-z_D}^{0} \frac{\pi}{4} C_M D^2 \rho_{water} \dot{v} \, dz \tag{B.5}$$

The total wave force on the body is the integral of the two terms in equation (B.5) from the substructure depth ($z = z_D$) to the still water level ($z = 0$), where C_D and C_M are the wave drag and inertia coefficients, respectively, which are assumed to be 1.0 and 2.0 for cylindrical bodies, respectively, based on [239]. D corresponds to the body's diameter. Assuming linear wave theory with deep waves/swell, the horizontal particle velocity, v, and the acceleration, $\dot{v}$, are [240]:

$$v(x,z,t) = \frac{\pi H}{T} e^{kz} \cos(kx - \sigma t) \tag{B.6}$$

$$\dot{v}(x,z,t) = \frac{\partial v}{\partial t} = \frac{2\pi^2 H}{T^2} e^{kz} \sin(kx - \sigma t) \tag{B.7}$$

where x and z are cartesian coordinates of a cross-section of the water column (with the positive z-direction vertically upwards, $z = 0$ at the still water level, and the positive x-direction in the horizontal direction of wave propagation). t is time, H is the wave height (m), k is the wave number $2\pi/L$, with L as the wavelength (m), and σ is the wave frequency $2\pi/T$, with T as the period (s) [240].

The total wave force can be calculated for a single cylindrical body, knowing the wave height, H, and period, T, at a fixed position, x, at a given time, t. In the direction of wave propagation, a submerged body is subjected to a force that oscillates in direction and magnitude over time. Given that there are several submerged components in this substructure, their orientation matters in calculating the total force on the entire substructure as some components may be subjected to opposing forces. I thus consider the range of angular orientations of the substructure with respect to the wave direction.

B.3 Expected Energy Consumption, Generation, and LCOE Calculations

The expected thruster consumption, $\mathbb{E}_{TC}$, from the system over a typical year (8,760 hours) can be calculated from:

$$\mathbb{E}_{TC} = 8760 \times \left[\int_{V_{hub}} f(V_{hub}) \times P_{system,n}(F_{appl}(V_{wind}), n)\, dV_{hub} \right] \tag{B.8}$$

where $f(V_{hub})$ is a probability density function of wind speeds (at hub height). In a similar fashion, I compute the expected gross energy generation:

$$\mathbb{E}_{GEN} = 8760 \times \left[\int_{V_{hub}} f(V_{hub}) \times P_{turbine}(V_{hub})\, dV_{hub} \right] \tag{B.9}$$

where $P_{turbine}(V_{hub})$ is the gross power generation of the turbine as given by the turbine technical specifications.

The LCOE is calculated using the NREL Annual Technology Baseline (ATB) method [12][12]:

$$LCOE = ((CRF * PFF * CFF * netOCC) + FOM) * 1000/(netCF * 8760) \tag{B.10}$$

where the following assumptions from the NREL ATB are used [12][12]:

$CRF: Capital\ Recovery\ Factor = 4.9\%$

$PFF: Production\ Finance\ Factor = 1.045$

$CFF: Construction\ Finance\ Factor = 1.075$

$$baseOCC[\text{USD}/kW]: Base\ Overnight\ Capital\ Cost = \begin{cases} [3630, 3969], if\ WSC\ 08 \\ [4314, 4717], if\ WSC\ 14 \end{cases}$$

$$FOM\left[\frac{\text{USD}}{kW-yr}\right]: Fixed\ Operations\ \&\ Maintenance\ = \begin{cases}[80, 88], if\ WSC\ 08\\ [90, 98], if\ WSC\ 14\end{cases}$$

In addition to the FOM costs provided by the NREL ATB above the station keeping systems incur FOM specific to each type. The cost for mooring chain maintenance also includes some inspections of varying degrees of intensity (visual radar inspections or physical inspections of chain and anchor may be needed) which can be accomplished by service operations vessels (SOV) as studied in [61]. These vessels may be used for various operations and maintenance operations for a plant (and therefore, the amount attributable to mooring chain maintenance from such vessels is unclear). Therefore, I estimate maintenance cost as the 'failure rate' times the cost of a single mooring chain [61]:

- Mooring chain failure rate = 0.0025 – 0.00378/km (failures per component per year)
- Cost = 520,000 GBP (per component)

Avanessova and colleagues did not consider DP station-keeping in their study, and thus, it is unclear if the same SOV can accomplish the monitoring needed for DP thrusters as it is a novel application [61]. To remain conservative, I consider the annual monitoring and consumables cost as completely separate from those already included in the NREL ATB estimates, and increase the FOM estimates for the DP system per thruster given the following data from the manufacturer of the thrusters used in this study [241]:

- Monitoring of thruster condition = 20,000 EUR/year
- Consumables = 3,000 EUR/year
- Major Maintenance (after 15 years of service) = 600,000 EUR

The resulting increase in FOM for mooring chains ranges from 0.3 - 8.3 USD/kW-year depending on the water depth (m), weight of the chain (ton/m), and length of chains (km).

By comparison, the resulting increase in FOM for DP thrusters ranges from 3.1 - 9.4 USD/kW-year per thruster on a single platform.

B.4 Turbine and Thruster Specifications

The turbine specifications used in the analysis are given in Table B.1. The DP configuration (thruster size and number) that minimizes the LCOE in each WSC is also given. The resulting energy needed to power the thrusters during "Wind Droughts"—described later in this document—is also given. At low wind speeds, the environmental forces on the turbines are primarily the wave and current forces acting on the substructure. As I employed the same substructure for all turbines, at low wind speeds, the turbine thrust forces are similar for all turbines—mainly a result of wave and current forces on the substructure. Therefore, note that the energy requirement during wind droughts is primarily a function of DP system configuration. When a system has more DP thrusters, less energy is required to station-keep during wind droughts.

The floater specifications used are those for the NREL 15MW reference turbine semi-submersible floater (and are thus oversized for smaller turbines). Each turbine in this analysis has an associated power and rotor thrust curve. The results of the computed design load under operational conditions, and the LCOE-minimizing configuration for the turbine are also given in Figure B.1. The thruster specifications that are used in the analysis are seen in Table B.2.

Table B.1: Technical specifications and dimensions of the reference turbines considered in this analysis. Data come from publicly available sources [234], [235], [236], [237], [238].

Turbine Rated Power [MW]	5	8	10	15
Tower Height [m]	90	110	119	150
Tower Base Diameter [m]	6	7.7	8.3	10
Blade Length [m]	61.5	82	97	117
Floater Diameter [m]	12.5			
Floater Length [m]	35			
Cut-in Wind Speed [m/s]	3	4	4	3
Rated Wind Speed [m/s]	11.4	12.5	10.5	10.6
Cut-out Wind Speed [m/s]	25	25	25	25
Computed Design Load [kN]	1500	1930	2690	4810
LCOE minimizing configuration [# of thrusters, thruster type (**Table B.2**), Wind Speed Class 08	4H	4H	5H	13H
LCOE minimizing configuration [# of thrusters, thruster type (**Table B.2**), Wind Speed Class 14	6H	5H	7H	16H
Energy needed to power DP thrusters during longest wind-drought period [MWh]	1.9	2.8	2.9	1.3

Table B.2: DP thrusters considered in the analysis [57]. Thruster names are not commercial names and are only used to refer to each thruster in this analysis.

Thruster Name	Nominal Input Power (kW)	Propeller Size (m)	Nominal Delivered Thrust (kN)	Computed Delivered Thrust (kN)	Unit Price (USD) [a]
A	3200	3.2	598	589	995,100
B	4000	3.5	737	726	1,070,000
C	4800	3.8	881	866	1,230,500
D	5500	4.1	1018	998	1,534,380
E	6500	4.5	1,214	1,187	2,210,620
F	3200	4.1	707	695	1,177,000
G	3800	4.5	853	830	1,444,500
H	4500	5	1,026	996	1,765,500
I	5500	5.5	1,254	1,214	2,461,000

[a] Unit price includes acquisition, transportation, and commissioning.

The parameter, "Computed Delivered Thrust" in Table B.2 was computed using the relationship given by the ABS [42], [58]:

$$T_0 = K \times (P \times D)^{\frac{2}{3}}$$

where T_0 is the bollard pull force in newtons, K is a constant equal to 1,250, P is propeller power in kW, and D is propeller diameter in meters [58]. This was used to see how the functional relationship between thrust, power, and diameter compares with real-world product offerings. The computed thrust is always less than that advertised by the manufacturer as seen in the table above, and thus, using this functional relationship underestimates the capabilities of the thrusters, providing a conservative estimate of the power needed to supply a given thrust force.

B.5 Mean Wave Force Validation with Ashes

Ashes simulation software [242] was used to cross-validate the results obtained through Morison's equation. The substructure used was that designed for the 5MW NREL reference floating turbine [243]. The results obtained here are thus compared with those obtained by using Morison's equation. The validation method using Ashes simulation software [242] only considered the substructure, with only wave forces input into the simulation (no wind or current forces are added). The procedure is as follows:

1. The substructure for the 5MW turbine is used [243] as provided in the software, which includes three mooring chains, oriented with 120° angular separation as seen in Figure B.2 below.

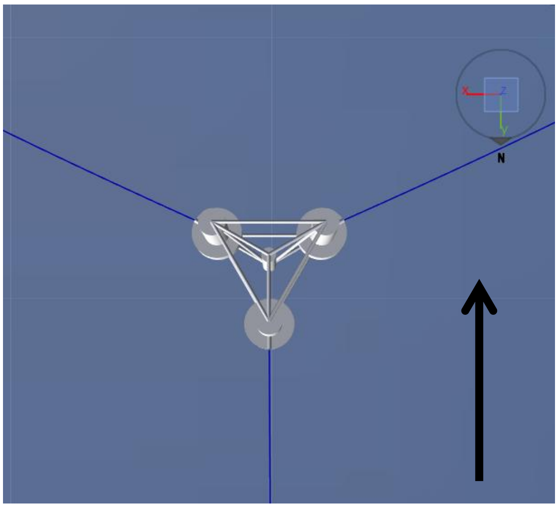

Figure B.2: Semisubmersible substructure with three mooring chains used in the simulation with Ashes simulation software. The incoming wave direction is denoted by the black arrow.

2. The wave height and period are input into the system oriented in the direction shown in Figure B.2.
3. The horizontal tension in each of the mooring chains is calculated by the simulation software and the simulation is allowed to proceed for 500s. After this amount of time, the

mean horizontal tension force on the platform calculated by the system stabilizes and reaches a steady state.

4. Using a free-body diagram, I can calculate the persistent mean wave force on the platform as shown in Figure B.3 below (assuming a static condition after the 500s simulation execution).

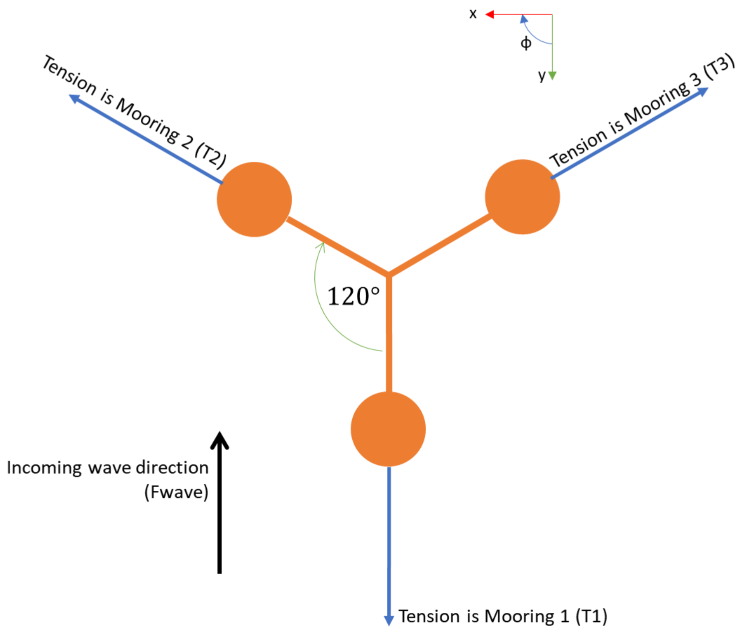

Figure B.3: The orientation of the forces exerted on the semisubmersible.

5. The resulting wave drifting force is the result of the solving the free body diagram in Figure B.3 for a static condition:

Forces in the y direction must sum to zero in a static condition,

$$
\begin{aligned}
F_y &= 0 = T1 + T2\,cos(120) + T3\,cos(240) + F_{wave}\,cos(180) \\
F_y &= 0 = T1 + T2(-0.5) + T3(-0.5) + F_{wave}(-1) \\
F_y &= 0 = T1 - 0.5T2 - 0.5T3 - F_{wave} \\
F_{wave} &= T1 - 0.5T2 - 0.5T3
\end{aligned}
\quad \text{(B.11)}
$$

This allows us to solve for the wave drift force given the horizontal tension forces from each of the mooring chains on the platform.

Using this procedure, I carry out the simulation considering a wave height of 1.8m and a period of 11s and yield the following simulation results from the software for each mooring line:

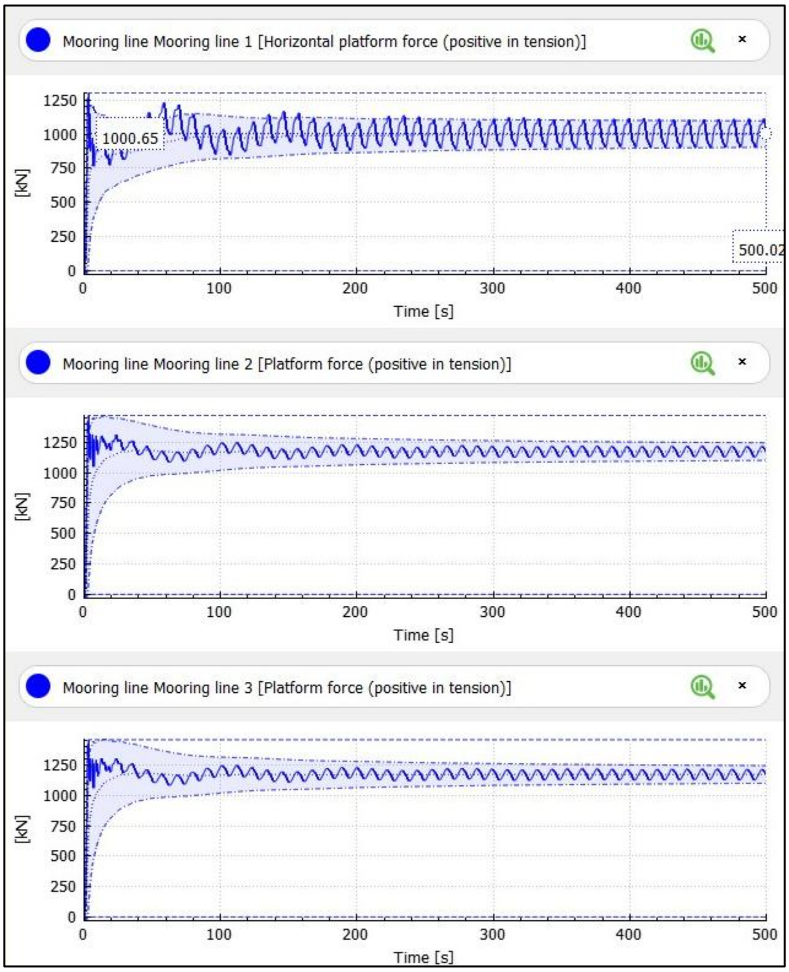

Figure B.4: Simulation results from Ashes simulation software with wave height = 1.8m and wave period = 11s.

The resulting mean forces in each of the mooring chains are as follows:

- Mooring Line 1 = 1,001 kN
- Mooring Line 2 = 983 kN
- Mooring Line 3 = 983 kN

Using these results and equation (B.11), the wave drift force can be computed as:

$$F_{wave} = 1001 - 0.5(983) - 0.5(983) = 18 \text{ kN}$$

Note that the tension force is always positive, as shown in Figure B.4, because even when the resulting force on the body that the mooring chain is connected to is in the direction of the anchor (which would typically result in a compressive force), the weight of the chain is constant, and therefore, even when no external force is applied to the body, the horizontal force on the body would result in a positive tensile force on the mooring chain, as the weight of the chain is constantly pulling on the substructure. Therefore, while the horizontal tensile force fluctuates, it never crosses the x-axis.

We carry out this process for all the wave conditions considered in this analysis and attain the results in Table B.3, which is compared to the same calculation using Morison's equation on the same substructure:

Table B.3: Results of the wave force simulation versus using Morison's equation on the 5MW floating turbine substructure described in [243].

Height (m)	Period (s)	Resultant Force – Simulation [kN]	Resultant Force – Morison's Equation [kN]	Squared Error
Portugal Operating Conditions				
1.2	11	6	11	25
1.2	14	16	5	121
1.8	11	18	16	4
1.8	14	45	7	1444
California Operating Conditions				
1.1	8.6	-1	12	169
1.1	10.9	4	10	36
1.4	8.6	-1	16	289
1.4	10.9	8	13	25
Portugal Extreme Conditions				
3.2	18.2	84	4	6400
3.5	18.3	102	5	9409
4.5	15.7	66	12	2916
4.1	18.4	147	6	19881
California Extreme Conditions				
7	8.8	86	81	25
9	12.2	- [b]	25	
11.2	17.3	- [b]	18	
9	21.1	- [b]	2	

[b] Simulation could not be completed due to simulation tolerance errors (the error messages read: "Displacement and load residual tolerances were not reached").

From the results in Table B.3, I see that choice of method has a large effect on the resultant wave force, and that Morison's equation tends to underestimate the wave heights in extreme conditions. Some simulations resulted in a negative mean force (opposite the direction of wave propagation) which Longuet-Higgins also found to be possible in experimental results [244]. For a few of the simulations (with wave heights greater than 9 m), the simulation could not complete, and could therefore not produce a resultant force for comparison. Without experimental data, I cannot confirm which method is more accurate, however, the maximum value across both methods (147 kN) is a fraction of the design load for the 5MW turbine (1,500 kN, see Table B.1); the proportion is even smaller for the remaining turbines considered.

Therefore, while there is a lot of uncertainty in the magnitude of the wave drift force, at the top of the range of values, it does not outweigh the contribution from the other environmental forces. I recommend further modeling efforts to compute the wave force more-accurately, but for this study, I proceed by calculating the wave force using Morison’s equation across all the wave parameter conditions considered, and I proceed with the maximum value attained applied as a uniform force contribution to the turbine thrust force in all conditions in an effort to use the most stringent condition possible. Table B.4 provides the results of the wave force calculation on the substructure used in this analysis.

Furthermore, Roald and colleagues calculated the mean wave drift force on the NREL 5MW turbine with a spar-type substructure across 12 different environmental conditions [47]. They find that the mean wave drift force never surpasses 10kN and during operation (less than 1% of the rotor thrust force); during idling of the turbine, the mean wave drift force reaches 10-15% of the rotor thrust force as the latter decreases significantly during idling—low enough to neglect this force.

Table B.4: Wave force results using Morison's equation on the 15MW turbine.

Height (m)	Period (s)	Resultant Force – Morison's Equation [kN]
Portugal Operating Conditions		
1.2	11	2
1.2	14.2	0.3
1.8	11	3
1.8	14.2	1
California Operating Conditions		
1.1	8.6	9
1.1	10.9	2
1.4	8.6	11
1.4	10.9	2
Portugal Extreme Conditions		
3.2	18.2	0.4
3.5	18.3	0.4
4.5	15.7	1
4.1	18.4	2
California Extreme Conditions		
7	8.8	48
9	12.2	9
11.2	17.3	4
9	21.1	2

B.6 R Model Validation with Orcaflex

OrcaFlex simulation software was used to validate the accuracy of the outputs from the R code on the 5MW NREL reference turbine. OrcaFlex is a simulation software developed by Orcina Ltd that is used for marine engineering of mooring systems, vessels, and OSW turbines [56]. The validation procedure is as follows:

1. The 5MW turbine is configured such that two downwind moorings are connected to two of the floaters, and an upwind mooring (in the direction of the incoming wind) is substituted for a 'link' component which acts similarly to a spring. One end of the link was fixed to the floating turbine at the water surface, and the distal end of the link was fixed at a point upwind such that there was no tension in the link under no applied forces (it was in a neutral position). This is illustrated in Figure B.5.

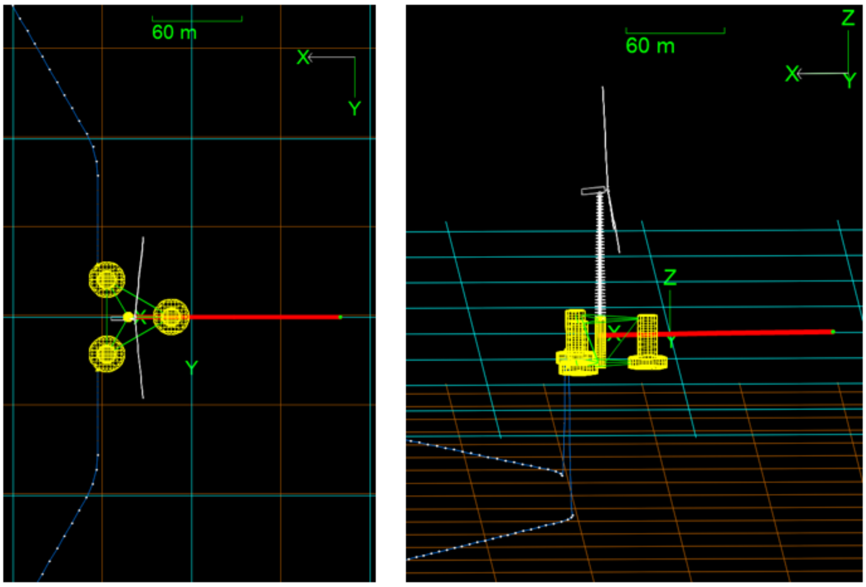

Figure B.5: Configuration of the starting position for the validation done with simulations in OrcaFlex. The red line shows the link component, while the thinner blue lines illustrate mooring lines.

2. The wave height and period, current speed, and wind speeds were entered into the software, starting with 0.5 m/s wind speed. The orientations of each are the same as the operational conditions described in Section 2.2 and provided in Figure B.6 below for reference.

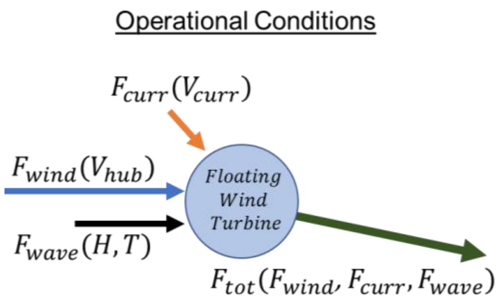

Figure B.6: Orientations of the wind, current, and wave environmental forces under A) operational conditions. The resultant vector F_{tot} is the vector combination of the three environmental force vectors. Note: the magnitude and direction of the vectors are not to scale in this figure.

3. The simulation was run until the oscillations in the forces registered in the link reached a steady state. Since the link is the only upwind station-keeping component, all the displacement forces should be felt by the link and, therefore, the steady state force in the link was then recorded as the reaction force on the turbine resulting from the wind speeds.
4. This process was repeated for every wind speed, increasing in 0.5 m/s intervals until a maximum of 40 m/s was reached. Figure B.7 illustrates the steady state conditions from

the simulations for each wind speed, along with some information on the steady state parameters of the simulations.

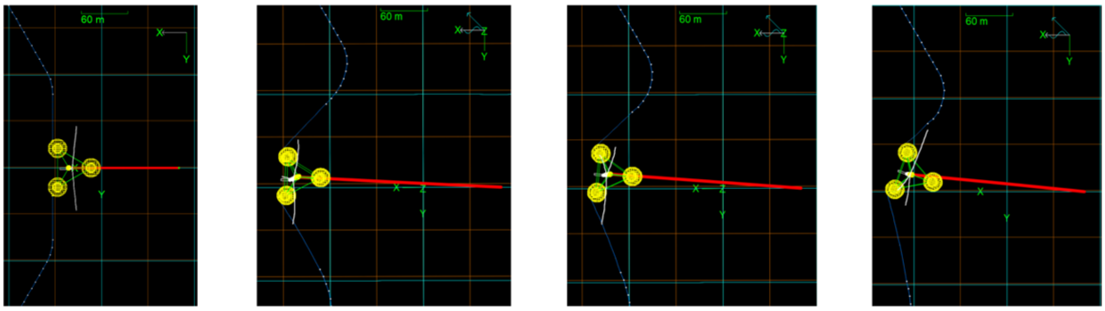

Figure B.7: Terminal state of the simulations after reaching steady state for selected wind speeds.

5. Below the cut-in wind speed and above the cut-out wind speed, the blade pitch angle was manually set to 90 degrees.

Once all the steady-state reaction forces were collected, they were compared with the reaction forces calculated using the R analytical model that I developed, given the same turbine size and assumptions for drag coefficients. This comparison is shown in Figure B.8.

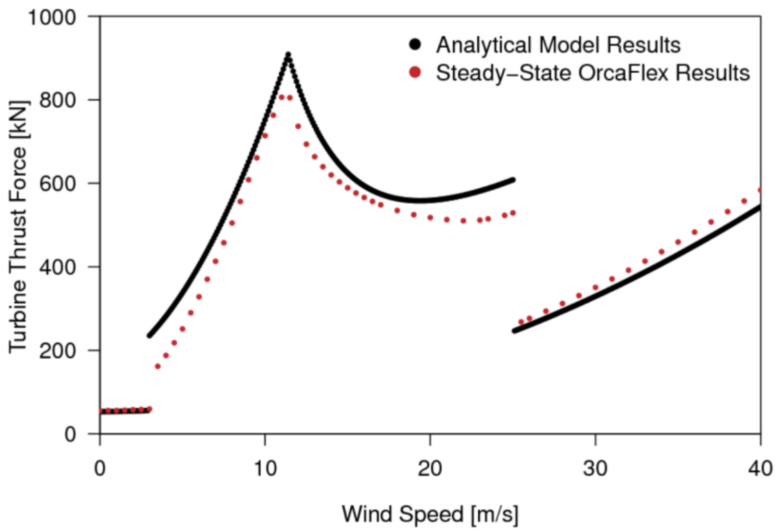

Figure B.8: R model thrust force vs. wind speed results and OrcaFlex model results for the 5MW turbine.

The R model slightly overestimates the horizontal thrust forces at windspeeds below the cut-out wind speed (Figure B.8). Beyond the cut-out wind speed, the OrcaFlex model estimates that the forces are slightly greater than those estimated by the R model.

Furthermore, Roald and colleagues estimates the overall turbine thrust force on the NREL 5MW turbine with a spar-type substructure, and although they only consider the wind force on the rotor (which is the largest component of the overall thrust force) and the mean wave drift force, their estimate never surpasses 140kN [47], but exhibits the same shape as that shown in Figure B.8 (see Figure B.9 below). While there are indeed differences between their analysis and ours (mainly in the substructure type, and which components were considered), the peak force was several factors greater than their calculation. This combined with the validation done with OrcaFlex indicate that while simplifications were made in this model, I can be confident that the turbine thrust force functions used are at or near the top of the range and are therefore conservative to use to estimate the expected power consumption needed by the DP to offset this force.

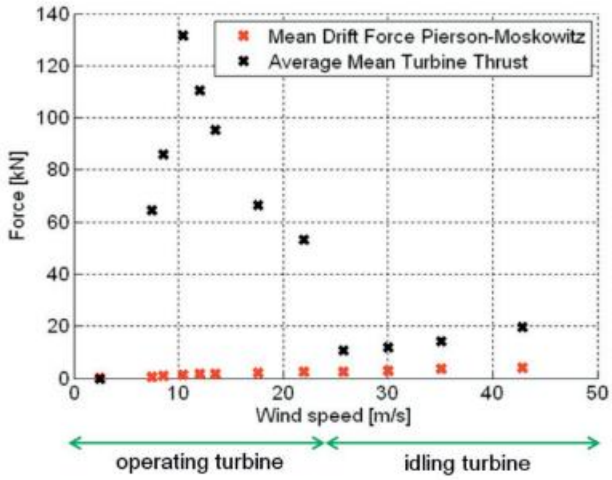

Figure B.9: NREL 5MW turbine with spar-type substructure estimates of mean wave forces and rotor thrust force from wind illustrated without changes from [47, Fig. 4].

B.7 Array Net Capacity Factors

The following net capacity factors are given in the NREL ATB for 1,000MW arrays considering turbines of the given sizes by 2030 [60], and calculated using the NREL flow redirection and induction in steady state (FLORIS) model [245]:

Table B.5: Array net capacity factors given turbine sizes used to deploy a 1,000MW array using data points from the NREL ATB [60], and NREL FLORIS models [245].

Turbine Size [MW]	Wind Speed Class 08 Net Capacity Factor	Wind Speed Class 14 Net Capacity Factor	Source Model
12	53%	31%	ATB
15	56%	34%	ATB
18	57%	35%	ATB
5	50%	28%	FLORIS
10	57%	35%	FLORIS
15	59%	37%	FLORIS

Given these data, I estimate the array net capacity factors for the turbines in the study by developing linear models as shown in Figure B.10 below:

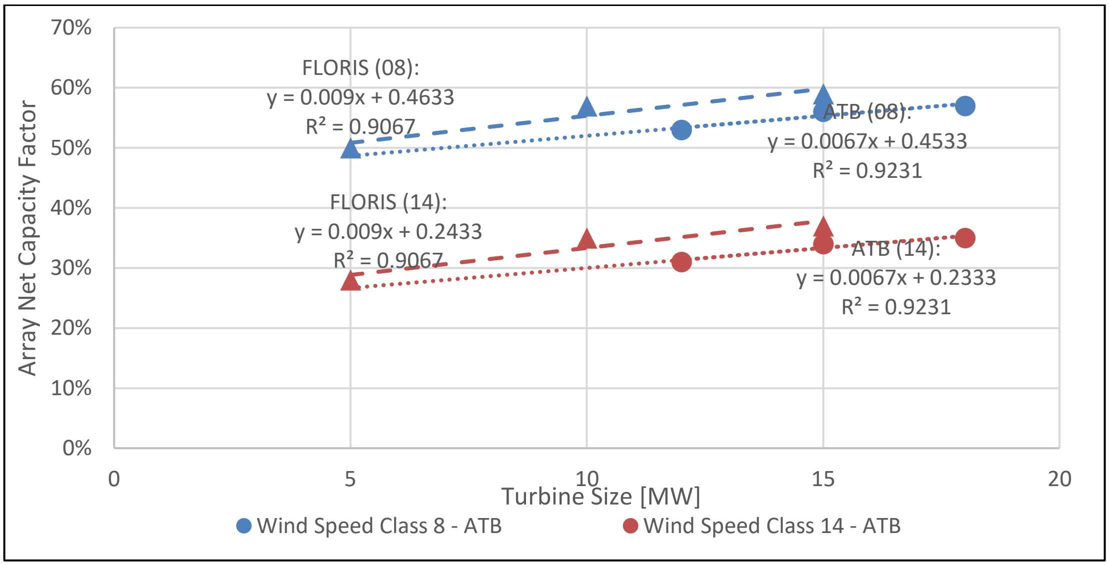

Figure B.10: Linear model developed from net capacity factor data in **Table B.5**.

The resulting baseline net capacity factors used in the study for the 1,000MW arrays of various turbine sizes are seen in Table B.6 below.

Table B.6: Array net capacity factor estimate given turbine sizes used to deploy a 1,000MW array calculated using linear models generated using the data from ATB and FLORIS models.

Turbine Size [MW]	Wind Speed Class 08 Net Capacity Factor		Wind Speed Class 14 Net Capacity Factor	
	ATB	FLORIS	ATB	FLORIS
5	49%	51%	27%	29%
8	51%	53%	29%	31%
10	52%	55%	30%	33%
15	55%	60%	33%	38%

As demonstrated, the slopes of the two linear models are similar. The FLORIS model predicts higher array net capacity factors than the ATB model, with the highest—in the range of turbine sizes I am considering—equal to 60% for the 15MW turbine. While simulated results from [4] indicate that OSW may be able to surpass 60% capacity factors in certain jurisdictions (the results indicate that 80% capacity factors are possible), the greatest country weighted average capacity factor for OSW plants in 2021 was 50% (Denmark) [246]. Therefore, I use the array net capacity factors estimated using the ATB model (the lower end of the predicted values) for the analysis.

B.8 Thruster System Power Function

Figure B.11 shows how the deployment of additional thrusters reduces the power needed to deliver a fixed level of thrust. While a one-thruster configuration would likely not be deployed in a real-life installation, the function for one thruster compared with the manufacturer's technical data is shown to verify the accuracy of the continuous functional relationship used.

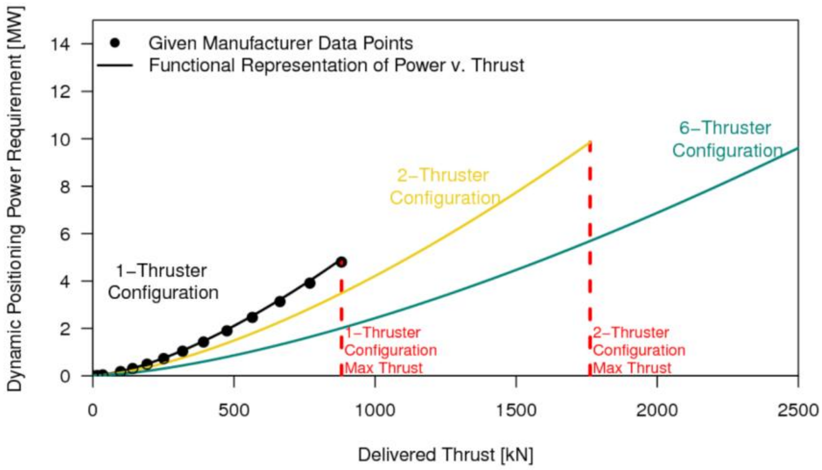

Figure B.11: Comparison of data from a DP thruster manufacturer [57]. Black dots illustrate given manufacturer performance data; solid black line illustrates the functional representation of power requirement *versus* applied force for one thruster, as described in equation (2.7) to illustrate the accuracy of the function used. This functional representation accurately represents observed manufacturer data. The other solid lines illustrate the functional representation of power requirement *versus* applied force for multi-thruster systems, as described in equation (2.8) of Section 2.2.3. The vertical, red, dashed lines illustrate the maximum applied force that one-thruster and two-thruster systems can provide.

B.9 Wind Probability Density Function

To calculate the expected thruster consumption, I apply the probability density functions in Figure B.12 of one potential Portuguese site [59] and two characteristic US sites taken from the NREL ATB [60].

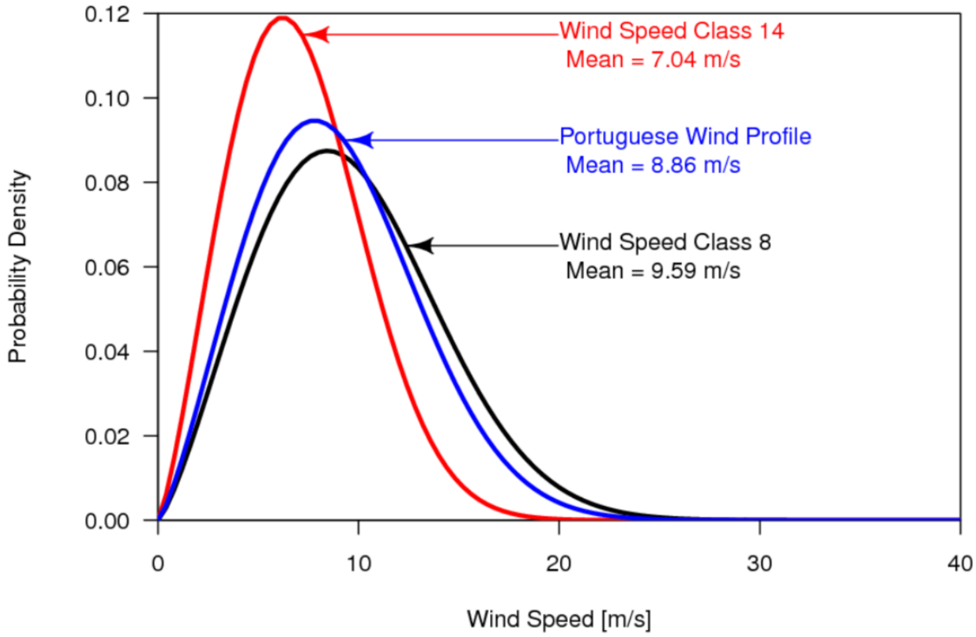

Figure B.12: Weibull wind speed probability distributions corresponding to US Wind Speed Classes 8 and 14, and Northern Portugal. NREL's Wind Speed Class 8 has the most favorable site characteristics for potential floating OSW candidate sites in the US, while Wind Speed Class 14 represents the least favorable sites. The ATB's classes are based on parameters like mean wind speed, vicinity to shore, and water depth.

B.10 Thrust Coefficient and Axial Induction Factor

There is a relationship between a wind turbine's coefficient of power (Cp) and the coefficient of thrust (Ct) with the axial induction factor. The axial induction factor is the change in wind speed that the rotor causes as a ratio of the upstream windspeed; more simply, it is a quantity that gives the rotor's interaction with the free-flowing wind. Reducing the axial induction factor is thus achieved by feathering the blades (so that the wind speed changes less as it crosses the rotor).

Typically, as a wind turbine is ramping up (before it achieves its rated wind speed), the blades are positioned to maximize Cp, which dictates the proportion of power available in the wind that the turbine 'captures'. As the wind increases beyond a certain point, the blades must be pitched to reduce Cp, since there is a limit to the generator's capacity; the blades cannot be designed to achieve maximum Cp at high wind speeds, since the resulting power would be too great for the generator. Thus, the blades must be pitched to reduce the Cp, and this reduces the axial induction factor. From the maximum Cp point (achieved at an axial induction factor of about 0.3), reducing the axial induction factor reduces the Ct faster than it reduces the Cp.

Thus, feathering the blades to reduce the Cp makes the Ct fall much more than the Cp, and thus, while power production may stay constant for the turbine, thrust forces will decrease.

This is demonstrated mathematically as follows [247]:

$$C_P = 4a(1-a)^2 \tag{B.12}$$
$$C_T = 4a(1-a) \tag{B.13}$$

where a is the axial induction factor that measures the fractional decrease in velocity about a wind turbine rotor, and 0.5 is the theoretical maximum value for a. At $a = 1/3$, the theoretical maximum value of Cp is reached (approximately 0.59, called the 'Betz limit'). Starting from a value of $a = 1/3$ (where Cp = 0.59 and Ct = 0.88), by decreasing a (by feathering the blades), Ct decreases faster than Cp. For example, calculating the coefficients at $a = 1/4$ gives Cp = 0.56 (a decrease of 0.03) and Ct = 0.75 (a decrease of 0.13). Therefore, the thrust force decreases much faster than the power generated and keeping a constant power level as wind speeds increase involves feathering the blades, decreasing a, and consequently, the thrust force on the rotor decreases. Visualizing these functions further illustrates this behavior as is done in [247].

For a complete physical model and mathematical representation of these interactions, see [247].

B.11 Design Load Cases

Figure B.13 illustrates the component environmental forces on a 15MW turbine under station-keeping design load case (DLC) described by Operational Conditions (DLC 1.3) and Extreme Weather Conditions (DLC 6.1) [58]. The design level for operational conditions is the maximum turbine thrust forces during operational wind speeds (above the cut-in and below the cut-out wind speed), and the design level for extreme weather conditions is the maximum turbine thrust forces during extreme winds (above the cut-out wind speed of the turbine) [58].

We use an estimate of currents dependent on wind speeds at 10m height according to Weber [27] which finds that the total current velocity (Ekman current plus wave-induced current) can be estimated as between 3 and 3.4% of the wind speed at 10m height [55]. Therefore, I estimate the current speed using 3.4% of the wind speed at 10m height,

$$V_{curr} = V_{wind}(z = 10) * 0.034 \tag{B.14}$$

where $V_{wind}(z)$ is calculated in equation (B.1). Considering a wind speed of 10 m/s (as near the mean wind speed according to WSC 8) and 40 m/s (for extreme conditions), the results of current speed using equation (B.14) are 0.25 m/s and 0.99 m/s, respectively. Data observations estimate surface currents are about 0.2 m/s, while in extreme conditions, surface currents can reach 0.9 m/s in coastal Portugal [41], [248]. Therefore, this function is able to estimate near those values, and is suitable to estimate surface current speeds.

In extreme conditions, I consider that the angle of incoming wave forces can vary across 180º. I therefore compute the total environmental load given the range of mean wave forces computed at each angle (at 10º intervals) and report its lower and upper bounds.

For operating conditions off the Portuguese coast, the wave period and wave heights range from 11s to 14.2s and 1.2m to 1.8m, respectively (taken as the inter quartile range of a week of observed wave heights and periods over one week in 2021) [249]. The interquartile range of values for a site off the California coast are 8.6s – 10.9s and 1.1m – 1.4m, respectively [250].

For extreme conditions, Oliveira and colleagues measured peak wave period and height during hurricanes that hit the Northern Portuguese coast finding heights ranging from 3.2m – 4.5m and periods of 15.7s – 18.4s [251]. For the California coast, Berg provides estimates for extreme 100-year parameters for wave heights and periods that range from 5m – 11.22m and 5.6s – 31.7s [32]. For both regions, specific combinations of wave heights and periods are given, and these parameter combinations are used to quantify the mean wave force [251], [252]. Figure B.13 illustrates the resulting forces from the Portuguese coastal area parameters.

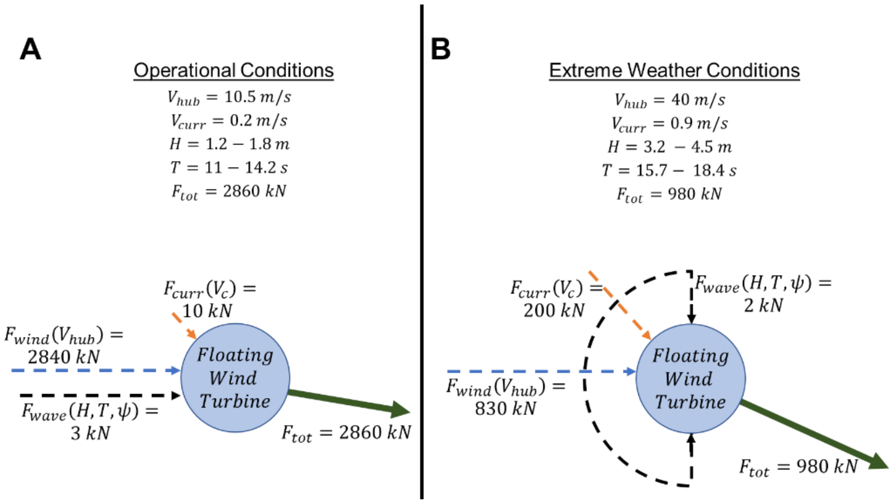

Figure B.13: Assumed parameters from a Portuguese offshore site [7], [9], resulting environmental loads, horizontal load, and design load accounting for factors of safety under A) operational conditions and B) extreme weather conditions. The results shown are for a 15MW turbine.

I find that the maximum environmental load is achieved under operating conditions (at or near the rated wind speed).

B.12 Wind Droughts

The distribution of wind drought lengths (consecutive hours where the wind speed in a specific area is below a turbine's cut-in wind speed, or above a turbine's cut-out wind speed) over a 10-year period (2011 to 2020) for two potential US OSW sites and one Portuguese site at 100m hub heights are shown in Figure B.14. A summary of the wind droughts for each area is shown in Table B.7. Hourly wind speed data come from [253].

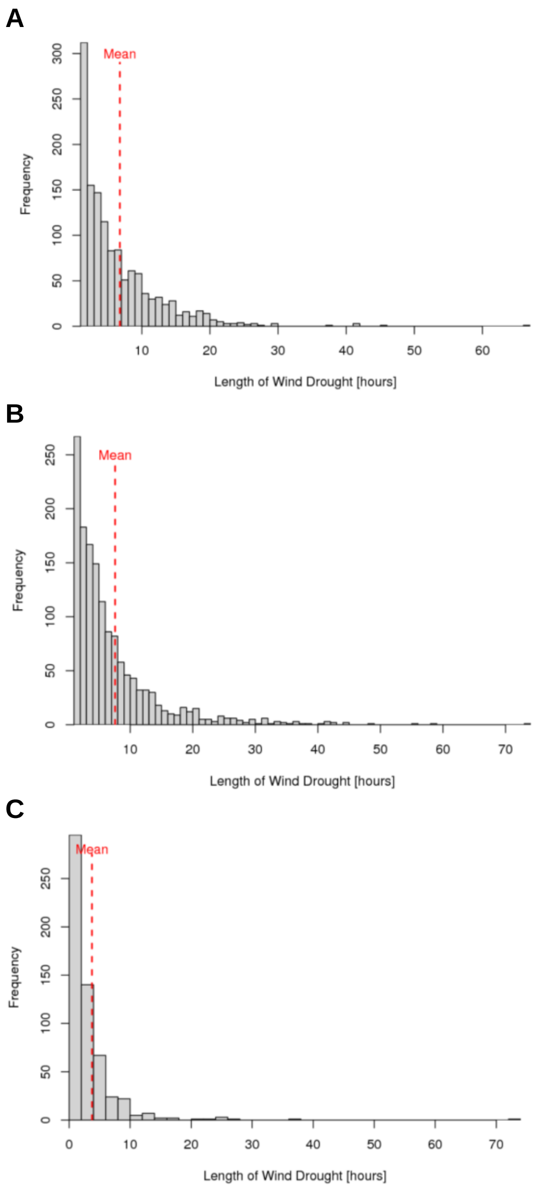

Figure B.14: The wind droughts (assuming a cut-in windspeed of 3 m/s and a cut-out windspeed of 25 m/s) over a 10-year period for the A) Humboldt call area. Mean value of 6.8 hours shown in red. B) Wind droughts for the Morro Bay call area. Mean value of 7.5 hours shown in red. C) Wind droughts for Portuguese wind development area. Mean value of 3.7 hours is shown in red.

Table B.7: Wind drought calculation summary.

Area	Coordinates	Median Wind Drought Duration (hours)	Mean Wind Drought Duration (hours)	Max Wind Drought Duration (hours)
Humboldt	40.95, -124.66	5	6.8	67
Morro Bay	35.56, -121.83	5	7.6	74
Viana do Castelo	41.70, -9.07	2	3.7	74

B.13 Making Use of the Generated Electricity

While the analysis demonstrates the likely viability of DP OSW platforms, it has not explored the issue of how to make use of the electricity that is generated. Several strategies deserve careful consideration. These include:

- An HVDC cable to shore along the seafloor from a single platform.
- Collection of power from several DP platforms (perhaps via cable suspended by floats add an intermediate depth) to a central floating substation and then HVDC cable to shore. Note that a number of very long oceanic HVDC cables exist (e.g in the North Sea) or are planned (e.g. from Morocco to the UK) [254], [255].
- Synthesis of a liquid or gaseous fuel, such as hydrogen from seawater, on each platform [256], [257], [258].
- Collection of power from several DP platforms (as above) with synthesis of a liquid or gaseous fuel from seawater at a central floating platform.

The fuel produced would be stored on site and periodically collected, either to be taken to shore or used by other facilities at sea.

B.14 Fixed DP System Configurations on LCOE

In the study, the results are provided for the DP system configuration that minimizes LCOE across the domain of configurations (thruster sizes and numbers). However, if the DP thruster configuration is fixed, the resulting turbine platform LCOE is shown in the following figure. As can be seen, when the same DP thruster configuration is used across all turbine sizes, the LCOE is still minimized for the intermediate thruster sizes.

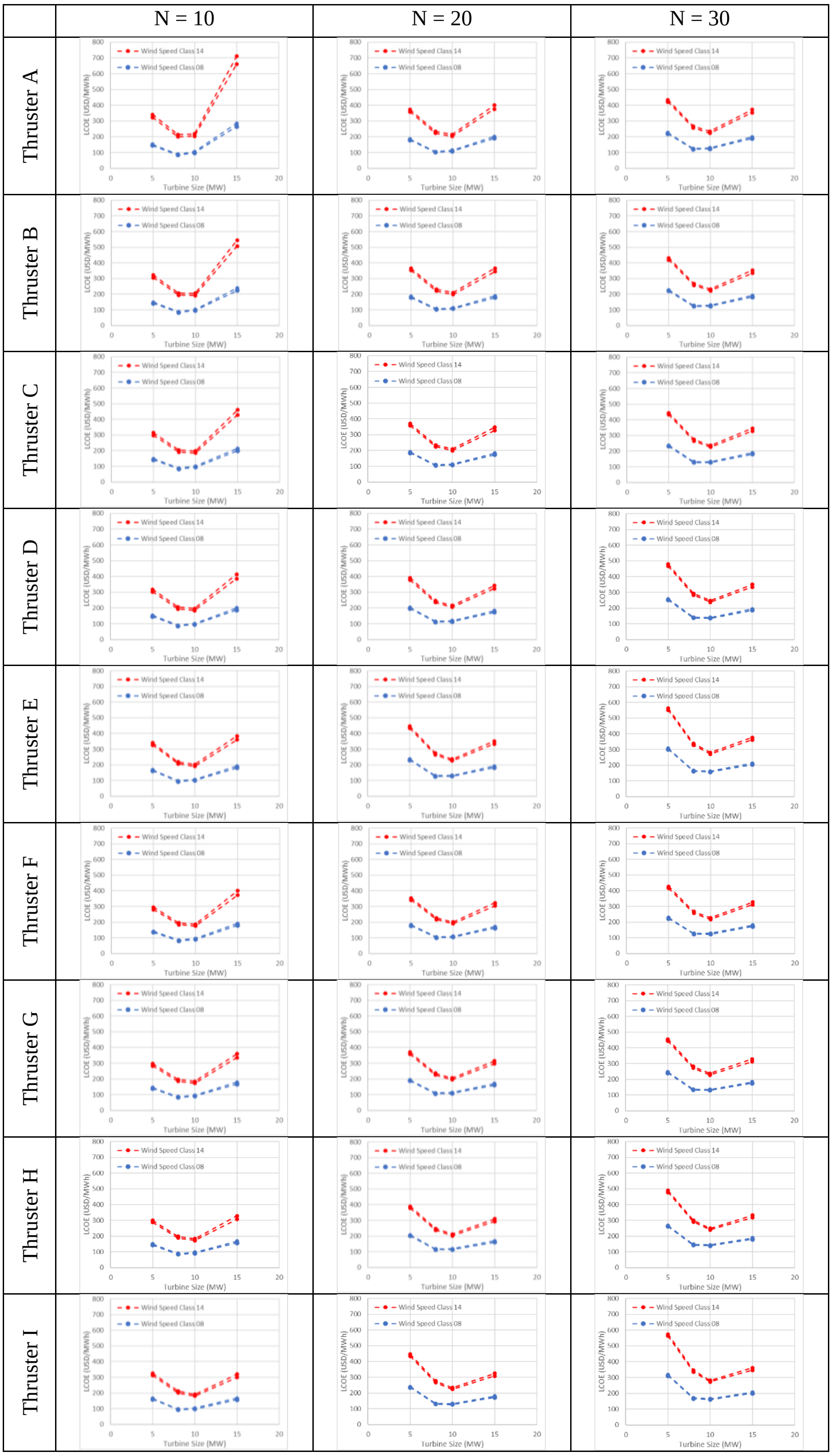

Figure B.15: Results of different DP system configurations. Rows correspond to thruster types, and columns correspond to number of replicates of the thruster.

B.15 Results of Each Thruster System Configuration

The analysis was done for each type and number of DP thrusters. The following tables report the TCP (expected DP system energy consumption divided by the expected gross turbine production) and the computed LCOE for each configuration. The lowest value is highlighted by a yellow box in the tables below, and for the LCOE values, those that are within 2.5% of the minimum value are highlighted with a yellow box to illustrate the configurations that may achieve close to the computed minimum LCOE. In the following tables, one can see that the TCP, which only considers energy efficiency, monotonically decreases with increasing numbers of thrusters, while the LCOE, which considers cost and energy efficiency, does not.

Table B.8: 5MW Turbine in Wind Speed Class 08.

# Thrusters	Thruster Consumption Percent										LCOE, High (USD/MWh, 30 years, 5.2%)										LCOE, Low (USD/MWh, 30 years, 5.2%)									
	A	B	C	D	E	F	G	H	I		A	B	C	D	E	F	G	H	I		A	B	C	D	E	F	G	H	I	
1	#N/A	#N/A	#N/A	#N/A	#N/A	#N/A	#N/A	#N/A	#N/A		#N/A	#N/A	#N/A	#N/A	#N/A	#N/A	#N/A	#N/A	#N/A		#N/A	#N/A	#N/A	#N/A	#N/A	#N/A	#N/A	#N/A	#N/A	
2	#N/A	#N/A	66%	62%	56%	#N/A	56%	50%	46%		#N/A	#N/A	202	180	164	#N/A	156	141	135		#N/A	#N/A	187	166	152	#N/A	144	131	126	
3	64%	59%	54%	50%	46%	50%	46%	41%	37%		199	173	158	149	145	144	136	**129**	**128**		184	161	147	139	136	134	126	**120**	**120**	
4	56%	51%	47%	43%	40%	43%	40%	36%	32%		169	154	145	141	142	135	130	**127**	130	8	157	143	135	132	133	126	122	**119**	122	8
5	50%	46%	42%	39%	35%	39%	35%	32%	29%		157	146	140	139	143	132	**130**	**128**	134		147	137	131	130	135	124	**122**	**121**	127	
6	45%	42%	38%	36%	32%	36%	32%	29%	26%		152	143	139	139	147	132	131	131	139		142	135	131	132	139	124	124	124	132	
7	42%	39%	35%	33%	30%	33%	30%	27%	25%		150	143	140	142	151	133	134	135	145		141	135	132	134	144	126	127	128	139	
8	39%	36%	33%	31%	28%	31%	28%	25%	23%		150	144	142	145	157	136	137	140	152		141	136	135	138	150	128	130	133	145	
9	37%	34%	31%	29%	26%	29%	26%	24%	22%		151	146	145	149	162	139	141	145	159		143	138	138	142	156	132	134	138	152	
10	35%	32%	30%	28%	25%	28%	25%	23%	21%		153	148	148	153	169	142	145	150	166		145	141	141	146	162	135	139	144	160	
11	34%	31%	28%	26%	24%	26%	24%	22%	20%		155	151	152	158	175	146	150	155	173		147	144	145	151	168	139	143	149	167	
12	32%	29%	27%	25%	23%	25%	23%	21%	19%		158	154	155	162	181	149	154	161	180		150	147	148	156	175	143	148	155	174	
13	31%	28%	26%	24%	22%	24%	22%	20%	18%		161	158	159	167	188	153	159	167	188		153	151	153	160	182	147	153	160	182	
14	30%	27%	25%	23%	21%	23%	21%	19%	17%		164	161	164	172	195	157	164	172	195		157	154	157	166	188	151	158	166	189	
15	29%	26%	24%	22%	20%	22%	20%	18%	17%		167	165	168	177	202	162	169	178	203		160	158	161	171	195	155	163	172	197	
16	28%	25%	23%	22%	20%	22%	20%	18%	16%		171	169	172	182	208	166	174	184	210		164	162	165	176	202	159	168	178	204	
17	27%	25%	23%	21%	19%	21%	19%	17%	16%		174	173	176	188	215	170	179	190	218		167	166	170	181	209	164	173	183	212	
18	26%	24%	22%	21%	19%	21%	19%	17%	15%		178	177	181	193	222	174	184	195	225		171	170	174	186	216	168	178	189	219	
19	26%	23%	22%	20%	18%	20%	18%	16%	15%		182	181	185	198	229	179	189	201	233		175	174	179	192	223	172	183	195	227	
20	25%	23%	21%	19%	18%	19%	18%	16%	14%		186	185	190	203	236	183	194	207	241		179	178	183	197	230	177	188	201	235	
21	24%	22%	20%	19%	17%	19%	17%	16%	14%		190	189	194	209	243	188	199	213	248		183	183	188	202	237	181	193	207	242	
22	24%	22%	20%	19%	17%	19%	17%	15%	14%		194	193	199	214	250	192	204	219	256		187	187	193	208	244	186	198	213	250	
23	23%	21%	20%	18%	17%	18%	17%	15%	14%		197	197	204	219	257	197	210	225	263		191	191	197	213	251	191	203	219	258	
24	23%	21%	19%	18%	16%	18%	16%	15%	13%		201	202	208	225	264	201	215	231	271		195	195	202	219	258	195	209	225	265	
25	22%	20%	19%	17%	16%	17%	16%	14%	13%		206	206	213	230	271	206	220	237	279		199	200	207	224	265	200	214	231	273	
26	22%	20%	18%	17%	16%	17%	16%	14%	13%		210	210	218	236	279	210	225	243	286		203	204	211	230	273	204	219	237	281	
27	21%	20%	18%	17%	15%	17%	15%	14%	12%		214	214	222	241	286	215	230	249	294		207	208	216	235	280	209	224	243	288	
28	21%	19%	18%	16%	15%	16%	15%	13%	12%		218	219	227	247	293	219	236	255	302		211	212	221	240	287	213	230	249	296	
29	21%	19%	17%	16%	15%	16%	15%	13%	12%		222	223	232	252	300	224	241	261	309		215	217	226	246	294	218	235	255	304	
30	20%	19%	17%	16%	14%	16%	14%	13%	**12%**	9	226	227	236	257	307	229	246	267	317		220	221	230	251	301	223	240	261	311	
BEST	**12%**										**127**										**119**									
Thruster Configuration	**30**	**I**		**5.5 m**		**5500 kW**					**4**	**H**		**5.0 m**		**4500 kW**					**4**	**H**		**5.0 m**		**4500 kW**				

Table B.9: 5MW Turbine in Wind Speed Class 14.

# Thrusters	Thruster Consumption Percent									
	A	B	C	D	E	F	G	H	I	
1	#N/A	#N/A	#N/A	#N/A	#N/A	#N/A	#N/A	#N/A	#N/A	
2	#N/A	#N/A	88%	81%	74%	#N/A	74%	67%	61%	
3	85%	78%	72%	67%	61%	67%	61%	55%	50%	
4	74%	67%	62%	58%	52%	58%	52%	47%	43%	
5	66%	60%	56%	52%	47%	52%	47%	42%	38%	
6	60%	55%	51%	47%	43%	47%	43%	39%	35%	
7	56%	51%	47%	44%	40%	44%	40%	36%	32%	
8	52%	48%	44%	41%	37%	41%	37%	33%	30%	
9	49%	45%	41%	38%	35%	38%	35%	31%	29%	
10	47%	43%	39%	36%	33%	36%	33%	30%	27%	
11	45%	41%	37%	35%	32%	35%	32%	28%	26%	
12	43%	39%	36%	33%	30%	33%	30%	27%	25%	
13	41%	37%	34%	32%	29%	32%	29%	26%	24%	
14	39%	36%	33%	31%	28%	31%	28%	25%	23%	
15	38%	35%	32%	30%	27%	30%	27%	24%	22%	
16	37%	34%	31%	29%	26%	29%	26%	24%	21%	
17	36%	33%	30%	28%	25%	28%	25%	23%	21%	
18	35%	32%	29%	27%	25%	27%	25%	22%	20%	
19	34%	31%	29%	26%	24%	26%	24%	22%	20%	
20	33%	30%	28%	26%	23%	26%	23%	21%	19%	
21	32%	29%	27%	25%	23%	25%	23%	21%	19%	
22	31%	29%	26%	25%	22%	25%	22%	20%	18%	
23	31%	28%	26%	24%	22%	24%	22%	20%	18%	
24	30%	28%	25%	24%	21%	24%	21%	19%	18%	
25	30%	27%	25%	23%	21%	23%	21%	19%	17%	
26	29%	26%	24%	23%	21%	23%	21%	19%	17%	
27	28%	26%	24%	22%	20%	22%	20%	18%	17%	
28	28%	26%	23%	22%	20%	22%	20%	18%	16%	
29	27%	25%	23%	21%	19%	21%	19%	18%	16%	
30	27%	25%	23%	21%	19%	21%	19%	17%	**16%**	9
BEST	16%									
Thruster Configuration	30	I		5.5 m		5500 kW				

# Thrusters	LCOE, High (USD/MWh, 30 years, 5.2%)									
	A	B	C	D	E	F	G	H	I	
1	#N/A	#N/A	#N/A	#N/A	#N/A	#N/A	#N/A	#N/A	#N/A	
2	#N/A	#N/A	1,109	724	536	#N/A	513	404	354	
3	935	621	489	421	377	409	355	315	299	
4	544	440	383	353	336	340	311	289	**286**	
5	437	378	343	326	322	312	294	**281**	**285**	
6	390	349	325	315	319	299	288	**280**	289	8
7	366	334	316	311	321	294	287	**282**	296	
8	352	326	313	311	325	293	289	287	305	
9	345	323	312	313	332	294	292	293	314	
10	341	322	314	318	340	296	297	300	325	
11	340	323	317	323	349	300	303	308	336	
12	340	325	321	329	359	304	309	316	347	
13	342	329	326	335	369	310	316	325	359	
14	345	333	331	343	379	315	323	333	371	
15	348	337	337	350	390	321	330	342	383	
16	352	342	343	358	401	327	338	352	396	
17	357	347	349	366	412	334	346	361	408	
18	362	353	356	374	423	340	354	370	420	
19	367	359	363	382	434	347	362	380	433	
20	372	365	370	391	446	354	370	390	445	
21	378	371	377	399	457	361	378	399	458	
22	384	378	384	408	469	368	387	409	471	
23	390	384	391	416	480	375	395	419	483	
24	396	391	399	425	492	383	403	429	496	
25	402	398	406	434	504	390	412	439	509	
26	408	404	414	443	515	398	421	449	522	
27	415	411	422	452	527	405	429	459	535	
28	421	418	429	461	539	412	438	469	547	
29	428	425	437	470	551	420	446	479	560	
30	434	432	445	479	563	427	455	489	573	
BEST	280									
Thruster Configuration	6	H		5.0 m		4500 kW				

# Thrusters	LCOE, Low (USD/MWh, 30 years, 5.2%)									
	A	B	C	D	E	F	G	H	I	
1	#N/A	#N/A	#N/A	#N/A	#N/A	#N/A	#N/A	#N/A	#N/A	
2	#N/A	#N/A	1,027	671	498	#N/A	475	375	329	
3	868	577	455	393	352	380	330	294	280	
4	507	410	358	330	316	317	291	271	**269**	
5	409	353	322	306	304	292	276	**264**	**269**	
6	366	327	305	297	302	281	271	**264**	274	8
7	344	314	298	294	305	277	271	**267**	282	
8	332	308	295	295	310	277	273	273	291	
9	326	305	296	298	318	278	277	279	301	
10	323	305	298	303	326	281	283	286	312	
11	322	307	302	308	335	285	289	294	323	
12	324	310	306	315	345	290	295	303	335	
13	326	313	311	321	355	296	302	312	347	
14	329	318	317	329	366	301	310	321	359	
15	333	322	323	336	377	307	317	330	371	
16	337	328	329	344	388	314	325	339	383	
17	342	333	336	352	399	321	333	349	396	
18	347	339	342	361	410	327	341	358	408	
19	352	345	349	369	422	334	349	368	421	
20	358	351	357	378	433	341	357	378	434	
21	364	358	364	386	445	348	366	387	446	
22	370	364	371	395	456	356	374	397	459	
23	376	371	379	404	468	363	383	407	472	
24	382	378	386	413	480	370	391	417	485	
25	388	384	394	422	492	378	400	427	497	
26	395	391	401	431	503	385	409	437	510	
27	401	398	409	440	515	393	417	447	523	
28	408	405	417	449	527	400	426	457	536	
29	414	412	424	458	539	408	435	467	549	
30	421	419	432	467	551	415	443	477	562	
BEST	264									
Thruster Configuration	6	H		5.0 m		4500 kW				

Table B.10: 8MW Turbine in Wind Speed Class 08.

# Thrusters	Thruster Consumption Percent									
	A	B	C	D	E	F	G	H	I	
1	#N/A	#N/A	#N/A	#N/A	#N/A	#N/A	#N/A	#N/A	#N/A	
2	#N/A	#N/A	#N/A	45%	41%	#N/A	#N/A	37%	33%	
3	#N/A	43%	39%	37%	33%	37%	33%	30%	27%	
4	41%	37%	34%	32%	29%	32%	29%	26%	24%	
5	36%	33%	31%	28%	26%	28%	26%	23%	21%	
6	33%	30%	28%	26%	24%	26%	24%	21%	19%	
7	31%	28%	26%	24%	22%	24%	22%	20%	18%	
8	29%	26%	24%	22%	20%	22%	20%	18%	17%	
9	27%	25%	23%	21%	19%	21%	19%	17%	16%	
10	26%	23%	22%	20%	18%	20%	18%	16%	15%	
11	24%	22%	21%	19%	17%	19%	17%	16%	14%	
12	23%	21%	20%	18%	17%	18%	17%	15%	14%	
13	22%	21%	19%	18%	16%	18%	16%	14%	13%	
14	22%	20%	18%	17%	15%	17%	15%	14%	13%	
15	21%	19%	18%	16%	15%	16%	15%	13%	12%	
16	20%	19%	17%	16%	14%	16%	14%	13%	12%	
17	20%	18%	17%	15%	14%	15%	14%	13%	11%	
18	19%	17%	16%	15%	14%	15%	14%	12%	11%	
19	19%	17%	16%	15%	13%	15%	13%	12%	11%	
20	18%	17%	15%	14%	13%	14%	13%	12%	11%	
21	18%	16%	15%	14%	13%	14%	13%	11%	10%	
22	17%	16%	15%	13%	12%	13%	12%	11%	10%	
23	17%	15%	14%	13%	12%	13%	12%	11%	10%	
24	17%	15%	14%	13%	12%	13%	12%	11%	10%	
25	16%	15%	14%	13%	12%	13%	12%	10%	9%	
26	16%	15%	13%	12%	11%	12%	11%	10%	9%	
27	16%	14%	13%	12%	11%	12%	11%	10%	9%	
28	15%	14%	13%	12%	11%	12%	11%	10%	9%	
29	15%	14%	13%	12%	11%	12%	11%	10%	9%	
30	15%	14%	12%	12%	11%	12%	11%	9%	**9%**	9
BEST	9%									
Thruster Configuration	30	I		5.5 m		5500 kW				

# Thrusters	LCOE, High (USD/MWh, 30 years, 5.2%)									
	A	B	C	D	E	F	G	H	I	
1	#N/A	#N/A	#N/A	#N/A	#N/A	#N/A	#N/A	#N/A	#N/A	
2	#N/A	#N/A	#N/A	94	90	#N/A	#N/A	83	81	
3	#N/A	92	88	86	85	84	81	**79**	**79**	
4	92	87	85	83	84	81	**80**	**78**	**80**	8
5	89	85	83	83	86	80	**80**	**79**	82	
6	88	85	84	84	88	81	81	81	85	
7	88	85	84	85	90	82	82	83	88	
8	88	86	86	87	93	83	84	85	91	
9	89	87	87	89	96	84	86	88	95	
10	90	88	89	91	99	86	88	90	98	
11	91	90	90	93	102	88	90	93	102	
12	93	91	92	96	105	90	92	96	105	
13	94	93	94	98	108	92	95	98	109	
14	96	95	96	100	111	94	97	101	112	
15	97	97	98	103	115	96	99	104	116	
16	99	99	100	105	118	98	102	107	120	
17	101	101	103	108	121	100	104	110	123	
18	103	102	105	111	125	102	107	113	127	
19	105	104	107	113	128	104	109	115	131	
20	106	106	109	116	132	106	112	118	135	
21	108	108	111	118	135	108	114	121	138	
22	110	111	114	121	138	111	117	124	142	
23	112	113	116	124	142	113	119	127	146	
24	114	115	118	126	145	115	122	130	149	
25	116	117	120	129	149	117	124	133	153	
26	118	119	123	132	152	120	127	136	157	
27	120	121	125	134	156	122	129	139	161	
28	122	123	127	137	159	124	132	142	165	
29	124	125	130	140	163	126	135	145	168	
30	126	127	132	142	166	128	137	148	172	
BEST	78									
Thruster Configuration	4	H		5.0 m		4500 kW				

# Thrusters	LCOE, Low (USD/MWh, 30 years, 5.2%)									
	A	B	C	D	E	F	G	H	I	
1	#N/A	#N/A	#N/A	#N/A	#N/A	#N/A	#N/A	#N/A	#N/A	
2	#N/A	#N/A	#N/A	86	83	#N/A	#N/A	76	**75**	
3	#N/A	85	81	79	79	77	75	**73**	**74**	
4	85	81	78	78	79	75	**74**	**73**	75	8
5	83	79	78	78	80	**75**	**74**	**74**	77	
6	82	79	78	79	82	75	75	76	80	
7	82	80	79	80	85	76	77	78	83	
8	82	80	80	82	88	78	79	80	86	
9	83	82	82	84	91	79	81	83	90	
10	84	83	83	86	94	81	83	86	93	
11	86	85	85	88	97	83	85	88	97	
12	87	86	87	91	100	85	87	91	100	
13	89	88	89	93	103	87	90	94	104	
14	90	90	91	96	107	89	92	96	108	
15	92	92	93	98	110	91	95	99	111	
16	94	94	96	101	113	93	97	102	115	
17	96	96	98	103	117	95	100	105	119	
18	98	98	100	106	120	97	102	108	123	
19	100	100	102	108	124	99	105	111	126	
20	101	102	104	111	127	102	107	114	130	
21	103	104	107	114	130	104	110	117	134	
22	105	106	109	116	134	106	112	120	137	
23	107	108	111	119	137	108	115	122	141	
24	109	110	113	122	141	110	117	125	145	
25	111	112	116	124	144	113	120	128	149	
26	113	114	118	127	148	115	122	131	153	
27	115	116	120	130	151	117	125	134	156	
28	117	118	123	132	155	119	127	137	160	
29	119	120	125	135	158	122	130	140	164	
30	121	123	127	138	162	124	133	143	168	
BEST	73									
Thruster Configuration	4	H		5.0 m		4500 kW				

Table B.11: 8MW Turbine in Wind Speed Class 14.

# Thrusters	Thruster Consumption Percent A	B	C	D	E	F	G	H	I	
1	#N/A	#N/A	#N/A	#N/A	#N/A	#N/A	#N/A	#N/A	#N/A	
2	#N/A	#N/A	#N/A	62%	57%	#N/A	#N/A	51%	46%	
3	#N/A	60%	55%	51%	46%	51%	46%	42%	38%	
4	56%	52%	48%	44%	40%	44%	40%	36%	33%	
5	50%	46%	42%	39%	36%	39%	36%	32%	29%	
6	46%	42%	39%	36%	33%	36%	33%	29%	27%	
7	43%	39%	36%	33%	30%	33%	30%	27%	25%	
8	40%	36%	34%	31%	28%	31%	28%	26%	23%	
9	38%	34%	32%	29%	27%	29%	27%	24%	22%	
10	36%	33%	30%	28%	25%	28%	25%	23%	21%	
11	34%	31%	29%	27%	24%	27%	24%	22%	20%	
12	33%	30%	27%	25%	23%	25%	23%	21%	19%	
13	31%	29%	26%	24%	22%	24%	22%	20%	18%	
14	30%	28%	25%	24%	21%	24%	21%	19%	18%	
15	29%	27%	25%	23%	21%	23%	21%	19%	17%	
16	28%	26%	24%	22%	20%	22%	20%	18%	16%	
17	27%	25%	23%	21%	19%	21%	19%	18%	16%	
18	27%	24%	22%	21%	19%	21%	19%	17%	15%	
19	26%	24%	22%	20%	18%	20%	18%	17%	15%	
20	25%	23%	21%	20%	18%	20%	18%	16%	15%	
21	25%	23%	21%	19%	18%	19%	18%	16%	14%	
22	24%	22%	20%	19%	17%	19%	17%	15%	14%	
23	24%	22%	20%	18%	17%	18%	17%	15%	14%	
24	23%	21%	19%	18%	16%	18%	16%	15%	13%	
25	23%	21%	19%	18%	16%	18%	16%	14%	13%	
26	22%	20%	19%	17%	16%	17%	16%	14%	13%	
27	22%	20%	18%	17%	15%	17%	15%	14%	13%	
28	21%	19%	18%	17%	15%	17%	15%	14%	12%	
29	21%	19%	18%	16%	15%	16%	15%	13%	12%	
30	21%	19%	17%	16%	15%	16%	15%	13%	**12%**	9
BEST	12%									
Thruster Configuration	30	I		5.5 m		5500 kW				

# Thrusters	LCOE, High (USD/MWh, 30 years, 5.2%) A	B	C	D	E	F	G	H	I	
1	#N/A	#N/A	#N/A	#N/A	#N/A	#N/A	#N/A	#N/A	#N/A	
2	#N/A	#N/A	#N/A	291	260	#N/A	#N/A	226	212	
3	#N/A	276	250	233	222	229	213	199	194	
4	264	239	223	214	209	208	198	**190**	**189**	
5	240	222	211	205	205	199	193	**187**	**190**	8
6	227	213	205	202	205	195	**191**	**187**	193	
7	220	209	202	201	207	193	**191**	**189**	197	
8	216	207	202	202	210	193	192	**192**	201	
9	214	206	202	204	214	194	194	195	207	
10	214	206	204	206	218	196	197	199	212	
11	214	208	206	209	223	198	200	203	218	
12	215	209	208	213	228	201	203	208	224	
13	217	211	211	216	234	203	207	212	231	
14	218	214	214	220	239	206	211	217	237	
15	221	216	217	224	245	210	215	222	244	
16	223	219	220	228	251	213	219	227	250	
17	226	222	224	233	257	217	223	232	257	
18	228	225	227	237	263	220	228	237	264	
19	231	228	231	242	269	224	232	242	270	
20	234	232	235	246	275	227	236	247	277	
21	237	235	239	251	281	231	241	252	284	
22	240	238	243	255	288	235	245	258	291	
23	244	242	246	260	294	239	250	263	298	
24	247	246	250	265	300	243	254	268	304	
25	250	249	255	269	307	247	259	274	311	
26	254	253	259	274	313	251	263	279	318	
27	257	256	263	279	319	255	268	284	325	
28	261	260	267	284	326	259	273	290	332	
29	264	264	271	289	332	263	277	295	339	
30	268	268	275	294	338	267	282	301	346	
BEST	187									
Thruster Configuration	5	H		5.0 m		4500 kW				

# Thrusters	LCOE, Low (USD/MWh, 30 years, 5.2%) A	B	C	D	E	F	G	H	I	
1	#N/A	#N/A	#N/A	#N/A	#N/A	#N/A	#N/A	#N/A	#N/A	
2	#N/A	#N/A	#N/A	269	241	#N/A	#N/A	209	196	
3	#N/A	256	231	216	206	212	197	185	180	
4	245	221	207	199	195	193	184	**177**	**177**	
5	223	206	196	191	192	185	179	**175**	**178**	8
6	212	199	191	189	192	182	**178**	**176**	181	
7	205	195	189	188	195	181	**179**	**178**	185	
8	202	193	189	190	198	181	180	181	190	
9	201	193	190	192	202	182	183	184	196	
10	201	194	192	195	207	184	186	188	202	
11	201	195	194	198	212	187	189	192	208	
12	203	197	196	201	217	189	192	197	214	
13	204	199	199	205	223	192	196	202	220	
14	206	202	202	209	229	195	200	207	227	
15	209	205	206	213	235	199	204	211	233	
16	211	208	209	218	241	202	208	216	240	
17	214	211	213	222	247	206	213	222	247	
18	217	214	216	226	253	209	217	227	254	
19	220	217	220	231	259	213	222	232	260	
20	223	221	224	236	265	217	226	237	267	
21	226	224	228	240	271	221	230	242	274	
22	229	228	232	245	278	225	235	248	281	
23	233	231	236	250	284	229	240	253	288	
24	236	235	240	254	290	233	244	258	295	
25	239	239	244	259	297	237	249	264	302	
26	243	242	248	264	303	241	253	269	309	
27	246	246	252	269	309	245	258	275	316	
28	250	250	256	274	316	249	263	280	322	
29	254	254	261	279	322	253	268	285	329	
30	257	257	265	284	329	257	272	291	336	
BEST	175									
Thruster Configuration	5	H		5.0 m		4500 kW				

Table B.12: 10MW Turbine in Wind Speed Class 08.

# Thrusters	Thruster Consumption Percent									
	A	B	C	D	E	F	G	H	I	
1	#N/A	#N/A	#N/A	#N/A	#N/A	#N/A	#N/A	#N/A	#N/A	
2	#N/A	#N/A	#N/A	#N/A	#N/A	#N/A	#N/A	#N/A	#N/A	
3	#N/A	#N/A	#N/A	51%	47%	#N/A	#N/A	42%	38%	
4	#N/A	52%	48%	44%	40%	44%	40%	36%	33%	
5	51%	46%	43%	40%	36%	40%	36%	33%	30%	
6	46%	42%	39%	36%	33%	36%	33%	30%	27%	
7	43%	39%	36%	33%	31%	33%	31%	27%	25%	
8	40%	37%	34%	31%	29%	31%	29%	26%	23%	
9	38%	35%	32%	30%	27%	30%	27%	24%	22%	
10	36%	33%	30%	28%	26%	28%	26%	23%	21%	
11	34%	31%	29%	27%	24%	27%	24%	22%	20%	
12	33%	30%	28%	26%	23%	26%	23%	21%	19%	
13	31%	29%	27%	25%	22%	25%	22%	20%	18%	
14	30%	28%	26%	24%	22%	24%	22%	19%	18%	
15	29%	27%	25%	23%	21%	23%	21%	19%	17%	
16	28%	26%	24%	22%	20%	22%	20%	18%	17%	
17	28%	25%	23%	21%	20%	21%	20%	18%	16%	
18	27%	24%	23%	21%	19%	21%	19%	17%	16%	
19	26%	24%	22%	20%	19%	20%	19%	17%	15%	
20	25%	23%	21%	20%	18%	20%	18%	16%	15%	
21	25%	23%	21%	19%	18%	19%	18%	16%	14%	
22	24%	22%	20%	19%	17%	19%	17%	15%	14%	
23	24%	22%	20%	18%	17%	18%	17%	15%	14%	
24	23%	21%	20%	18%	16%	18%	16%	15%	13%	
25	23%	21%	19%	18%	16%	18%	16%	15%	13%	
26	22%	20%	19%	17%	16%	17%	16%	14%	13%	
27	22%	20%	18%	17%	16%	17%	16%	14%	13%	
28	21%	20%	18%	17%	15%	17%	15%	14%	12%	
29	21%	19%	18%	16%	15%	16%	15%	13%	12%	
30	21%	19%	17%	16%	15%	16%	15%	13%	**12%**	9
BEST	**12%**									
Thruster Configuration	**30**	**I**		**5.5 m**		**5500 kW**				

# Thrusters	LCOE, High (USD/MWh, 30 years, 5.2%)									
	A	B	C	D	E	F	G	H	I	
1	#N/A	#N/A	#N/A	#N/A	#N/A	#N/A	#N/A	#N/A	#N/A	
2	#N/A	#N/A	#N/A	#N/A	#N/A	#N/A	#N/A	#N/A	#N/A	
3	#N/A	#N/A	#N/A	117	111	#N/A	#N/A	99	97	
4	#N/A	120	111	107	104	104	99	**94**	**94**	
5	120	111	105	102	101	99	96	**93**	**94**	
6	113	106	102	100	101	97	**94**	**93**	**95**	8
7	109	104	100	99	102	96	**94**	**93**	96	
8	107	102	100	99	103	95	**95**	**94**	98	
9	106	102	100	100	105	96	95	96	101	
10	106	102	100	101	107	96	97	97	103	
11	106	102	101	102	109	97	98	99	106	
12	106	103	102	104	111	98	99	101	109	
13	106	104	103	106	114	100	101	103	112	
14	107	105	104	107	116	101	103	106	115	
15	108	106	106	109	119	102	105	108	118	
16	109	107	107	111	122	104	107	110	121	
17	110	108	109	113	124	105	108	112	124	
18	111	110	111	115	127	107	110	115	127	
19	113	111	112	117	130	109	112	117	130	
20	114	113	114	119	133	110	114	119	133	
21	115	114	116	121	136	112	116	122	136	
22	117	116	118	123	138	114	119	124	140	
23	118	117	119	126	141	116	121	127	143	
24	120	119	121	128	144	118	123	129	146	
25	121	121	123	130	147	119	125	132	149	
26	123	122	125	132	150	121	127	134	152	
27	124	124	127	134	153	123	129	137	156	
28	126	126	129	137	156	125	131	139	159	
29	128	127	131	139	159	127	133	142	162	
30	129	129	133	141	162	129	136	144	165	
BEST	**93**									
Thruster Configuration	**6**	**H**		**5.0 m**		**4500 kW**				

# Thrusters	LCOE, Low (USD/MWh, 30 years, 5.2%)									
	A	B	C	D	E	F	G	H	I	
1	#N/A	#N/A	#N/A	#N/A	#N/A	#N/A	#N/A	#N/A	#N/A	
2	#N/A	#N/A	#N/A	#N/A	#N/A	#N/A	#N/A	#N/A	#N/A	
3	#N/A	#N/A	#N/A	108	102	#N/A	#N/A	92	89	
4	#N/A	111	103	99	97	96	92	**88**	**87**	
5	111	103	97	95	95	92	89	**86**	**87**	8
6	105	99	95	93	95	90	**88**	**86**	89	
7	102	96	93	93	95	89	**88**	**87**	91	
8	100	95	93	93	97	89	88	**88**	93	
9	99	95	93	94	99	90	89	90	95	
10	99	95	94	95	101	90	91	92	98	
11	99	96	95	97	103	91	92	94	101	
12	99	97	96	98	106	92	94	96	104	
13	100	98	97	100	108	94	96	98	106	
14	101	99	99	102	111	95	97	100	109	
15	102	100	100	104	113	97	99	102	113	
16	103	101	102	105	116	98	101	105	116	
17	104	103	103	107	119	100	103	107	119	
18	105	104	105	110	122	102	105	109	122	
19	107	105	107	112	124	103	107	112	125	
20	108	107	108	114	127	105	109	114	128	
21	110	109	110	116	130	107	111	117	131	
22	111	110	112	118	133	109	113	119	134	
23	113	112	114	120	136	110	115	122	138	
24	114	113	116	122	139	112	118	124	141	
25	116	115	118	125	142	114	120	127	144	
26	117	117	120	127	145	116	122	129	147	
27	119	119	121	129	148	118	124	132	151	
28	121	120	123	131	151	120	126	134	154	
29	122	122	125	134	154	122	128	137	157	
30	124	124	127	136	157	123	130	139	160	
BEST	**86**									
Thruster Configuration	**5**	**H**		**5.0 m**		**4500 kW**				

Table B.13: 10MW Turbine in Wind Speed Class 14.

# Thrusters	Thruster Consumption Percent									
	A	B	C	D	E	F	G	H	I	
1	#N/A	#N/A	#N/A	#N/A	#N/A	#N/A	#N/A	#N/A	#N/A	
2	#N/A	#N/A	#N/A	#N/A	#N/A	#N/A	#N/A	#N/A	#N/A	
3	#N/A	#N/A	#N/A	65%	59%	#N/A	#N/A	53%	49%	
4	#N/A	66%	61%	56%	51%	56%	51%	46%	42%	
5	65%	59%	54%	50%	46%	50%	46%	41%	38%	
6	59%	54%	50%	46%	42%	46%	42%	38%	34%	
7	55%	50%	46%	43%	39%	43%	39%	35%	32%	
8	51%	47%	43%	40%	36%	40%	36%	33%	30%	
9	48%	44%	41%	38%	34%	38%	34%	31%	28%	
10	46%	42%	38%	36%	32%	36%	32%	29%	27%	
11	44%	40%	37%	34%	31%	34%	31%	28%	25%	
12	42%	38%	35%	33%	30%	33%	30%	27%	24%	
13	40%	37%	34%	31%	29%	31%	29%	26%	23%	
14	39%	35%	33%	30%	27%	30%	27%	25%	22%	
15	37%	34%	31%	29%	27%	29%	27%	24%	22%	
16	36%	33%	30%	28%	26%	28%	26%	23%	21%	
17	35%	32%	30%	27%	25%	27%	25%	22%	20%	
18	34%	31%	29%	27%	24%	27%	24%	22%	20%	
19	33%	30%	28%	26%	24%	26%	24%	21%	19%	
20	32%	30%	27%	25%	23%	25%	23%	21%	19%	
21	32%	29%	27%	25%	22%	25%	22%	20%	18%	
22	31%	28%	26%	24%	22%	24%	22%	20%	18%	
23	30%	28%	25%	24%	21%	24%	21%	19%	18%	
24	29%	27%	25%	23%	21%	23%	21%	19%	17%	
25	29%	26%	24%	23%	21%	23%	21%	18%	17%	
26	28%	26%	24%	22%	20%	22%	20%	18%	16%	
27	28%	25%	23%	22%	20%	22%	20%	18%	16%	
28	27%	25%	23%	21%	19%	21%	19%	17%	16%	
29	27%	25%	23%	21%	19%	21%	19%	17%	16%	
30	26%	24%	22%	21%	19%	21%	19%	17%	**15%**	9
BEST	15%									
Thruster Configuration	30	I		5.5 m		5500 kW				

# Thrusters	LCOE, High (USD/MWh, 30 years, 5.2%)									
	A	B	C	D	E	F	G	H	I	
1	#N/A	#N/A	#N/A	#N/A	#N/A	#N/A	#N/A	#N/A	#N/A	
2	#N/A	#N/A	#N/A	#N/A	#N/A	#N/A	#N/A	#N/A	#N/A	
3	#N/A	#N/A	#N/A	293	259	#N/A	#N/A	221	206	
4	#N/A	304	265	242	225	237	216	198	191	
5	298	258	234	220	211	214	200	188	**185**	
6	263	235	218	208	204	202	192	**184**	**183**	
7	243	222	209	202	201	195	188	**182**	**184**	
8	231	214	203	198	200	191	**185**	**181**	**185**	8
9	223	208	200	197	201	189	**185**	**182**	188	
10	218	205	198	196	202	188	**185**	**183**	191	
11	214	203	197	197	204	188	186	**185**	194	
12	212	202	197	198	207	188	187	187	198	
13	211	202	198	199	210	189	189	190	202	
14	210	202	198	201	213	190	191	193	206	
15	210	202	200	203	217	191	193	196	210	
16	210	203	201	205	220	193	195	199	215	
17	211	205	203	208	224	195	198	202	219	
18	212	206	205	210	228	197	200	205	224	
19	213	208	207	213	232	199	203	209	229	
20	215	209	209	216	236	201	206	212	233	
21	216	211	212	219	240	204	209	216	238	
22	218	213	214	222	245	206	212	219	243	
23	220	215	216	225	249	209	215	223	248	
24	221	217	219	228	253	211	218	227	253	
25	223	220	222	231	258	214	221	230	257	
26	225	222	224	235	262	216	224	234	262	
27	227	224	227	238	267	219	227	238	267	
28	230	227	230	241	271	222	231	242	272	
29	232	229	232	244	276	225	234	245	277	
30	234	232	235	248	280	227	237	249	282	
BEST	181									
Thruster Configuration	8	H		5.0 m		4500 kW				

# Thrusters	LCOE, Low (USD/MWh, 30 years, 5.2%)									
	A	B	C	D	E	F	G	H	I	
1	#N/A	#N/A	#N/A	#N/A	#N/A	#N/A	#N/A	#N/A	#N/A	
2	#N/A	#N/A	#N/A	#N/A	#N/A	#N/A	#N/A	#N/A	#N/A	
3	#N/A	#N/A	#N/A	271	240	#N/A	#N/A	204	191	
4	#N/A	281	246	224	209	219	200	184	178	
5	276	239	217	204	197	199	186	175	**173**	
6	244	218	203	194	191	188	179	**171**	**172**	
7	226	206	194	188	188	182	175	**170**	**173**	8
8	215	199	190	186	188	178	**173**	**170**	175	
9	208	195	187	184	189	177	**173**	**171**	177	
10	204	192	185	184	191	176	**174**	**172**	181	
11	201	190	185	185	193	176	175	175	184	
12	199	190	185	186	196	177	176	177	188	
13	198	190	186	188	199	178	178	180	192	
14	198	190	187	190	203	179	180	183	196	
15	198	191	189	192	206	181	183	186	201	
16	198	192	190	195	210	183	185	189	205	
17	199	193	192	197	214	185	188	192	210	
18	200	195	194	200	218	187	190	196	214	
19	202	197	196	203	222	189	193	199	219	
20	203	198	199	206	226	191	196	203	224	
21	205	200	201	209	231	194	199	206	229	
22	207	203	204	212	235	196	202	210	234	
23	209	205	206	215	239	199	205	214	238	
24	211	207	209	218	244	201	208	217	243	
25	213	209	211	221	248	204	212	221	248	
26	215	212	214	225	253	207	215	225	253	
27	217	214	217	228	257	209	218	229	258	
28	219	216	220	231	262	212	221	232	263	
29	221	219	223	235	266	215	224	236	268	
30	224	222	225	238	271	218	228	240	273	
BEST	170									
Thruster Configuration	7	H		5.0 m		4500 kW				

Table B.14: 15MW Turbine in Wind Speed Class 08.

# Thrusters	Thruster Consumption Percent								
	A	B	C	D	E	F	G	H	I
1	#N/A	#N/A	#N/A	#N/A	#N/A	#N/A	#N/A	#N/A	#N/A
2	#N/A	#N/A	#N/A	#N/A	#N/A	#N/A	#N/A	#N/A	#N/A
3	#N/A	#N/A	#N/A	#N/A	#N/A	#N/A	#N/A	#N/A	#N/A
4	#N/A	#N/A	#N/A	#N/A	#N/A	#N/A	#N/A	#N/A	68%
5	#N/A	#N/A	#N/A	81%	74%	#N/A	#N/A	67%	61%
6	#N/A	#N/A	80%	74%	68%	#N/A	68%	61%	55%
7	#N/A	81%	74%	69%	63%	69%	63%	56%	51%
8	#N/A	75%	69%	64%	59%	64%	59%	53%	48%
9	78%	71%	65%	61%	55%	61%	55%	50%	45%
10	74%	67%	62%	58%	52%	58%	52%	47%	43%
11	70%	64%	59%	55%	50%	55%	50%	45%	41%
12	67%	62%	57%	53%	48%	53%	48%	43%	39%
13	65%	59%	54%	50%	46%	50%	46%	41%	38%
14	62%	57%	52%	49%	44%	49%	44%	40%	36%
15	60%	55%	51%	47%	43%	47%	43%	39%	35%
16	58%	53%	49%	45%	41%	45%	41%	37%	34%
17	57%	52%	48%	44%	40%	44%	40%	36%	33%
18	55%	50%	46%	43%	39%	43%	39%	35%	32%
19	53%	49%	45%	42%	38%	42%	38%	34%	31%
20	52%	48%	44%	41%	37%	41%	37%	33%	30%
21	51%	47%	43%	40%	36%	40%	36%	33%	30%
22	50%	45%	42%	39%	35%	39%	35%	32%	29%
23	49%	44%	41%	38%	35%	38%	35%	31%	28%
24	48%	44%	40%	37%	34%	37%	34%	30%	28%
25	47%	43%	39%	36%	33%	36%	33%	30%	27%
26	46%	42%	38%	36%	33%	36%	33%	29%	27%
27	45%	41%	38%	35%	32%	35%	32%	29%	26%
28	44%	40%	37%	34%	31%	34%	31%	28%	26%
29	43%	40%	36%	34%	31%	34%	31%	28%	25%
30	43%	39%	36%	33%	30%	33%	30%	27%	**25%**
BEST	**25%**								
Thruster Configuration	**30**	**I**		**5.5 m**		**5500 kW**			

# Thrusters	LCOE, High (USD/MWh, 30 years, 5.2%)								
	A	B	C	D	E	F	G	H	I
1	#N/A	#N/A	#N/A	#N/A	#N/A	#N/A	#N/A	#N/A	#N/A
2	#N/A	#N/A	#N/A	#N/A	#N/A	#N/A	#N/A	#N/A	#N/A
3	#N/A	#N/A	#N/A	#N/A	#N/A	#N/A	#N/A	#N/A	#N/A
4	#N/A	#N/A	#N/A	#N/A	#N/A	#N/A	#N/A	#N/A	228
5	#N/A	#N/A	#N/A	350	280	#N/A	#N/A	221	199
6	#N/A	#N/A	335	278	240	#N/A	228	198	184
7	#N/A	344	278	242	219	236	207	185	176
8	#N/A	291	246	222	206	215	193	177	171
9	319	260	227	209	198	202	185	172	**169**
10	285	240	214	200	193	193	179	**168**	**167**
11	262	226	205	194	190	186	175	**166**	**167**
12	246	216	198	189	188	182	172	**165**	**167**
13	235	209	194	186	187	178	171	**165**	**168**
14	226	203	190	184	186	176	169	**165**	169
15	219	199	187	183	186	174	169	**165**	171
16	214	196	185	182	187	173	**169**	**166**	173
17	210	193	184	182	188	172	**169**	**166**	175
18	207	191	183	182	189	172	169	**168**	177
19	204	190	183	182	190	172	170	169	179
20	202	189	183	182	192	172	170	170	181
21	201	188	183	183	193	172	171	172	183
22	200	188	183	184	195	173	172	173	186
23	199	188	183	185	197	173	173	175	188
24	198	188	184	186	199	174	175	177	191
25	198	188	184	187	201	175	176	178	194
26	198	189	185	189	204	176	177	180	196
27	198	189	186	190	206	177	179	182	199
28	198	190	187	191	208	178	180	184	202
29	198	190	188	193	210	179	182	186	204
30	199	191	189	195	213	180	184	188	207
BEST	**165**								
Thruster Configuration	**14**	**H**		**5.0 m**		**4500 kW**			

# Thrusters	LCOE, Low (USD/MWh, 30 years, 5.2%)								
	A	B	C	D	E	F	G	H	I
1	#N/A	#N/A	#N/A	#N/A	#N/A	#N/A	#N/A	#N/A	#N/A
2	#N/A	#N/A	#N/A	#N/A	#N/A	#N/A	#N/A	#N/A	#N/A
3	#N/A	#N/A	#N/A	#N/A	#N/A	#N/A	#N/A	#N/A	#N/A
4	#N/A	#N/A	#N/A	#N/A	#N/A	#N/A	#N/A	#N/A	211
5	#N/A	#N/A	#N/A	323	259	#N/A	#N/A	205	184
6	#N/A	#N/A	310	257	223	#N/A	211	184	171
7	#N/A	318	257	225	204	219	192	172	164
8	#N/A	270	229	206	192	200	180	165	160
9	296	241	211	194	185	188	172	160	**158**
10	265	223	199	186	181	179	167	**157**	**157**
11	244	210	191	181	178	174	164	**156**	**157**
12	229	201	185	177	176	170	161	**155**	**158**
13	219	195	181	175	176	167	160	**155**	159
14	211	190	178	173	176	165	159	**155**	160
15	205	186	176	172	176	163	159	**155**	162
16	200	183	174	171	177	162	159	**156**	164
17	197	181	173	171	178	162	159	**157**	166
18	194	180	172	172	179	162	159	**158**	168
19	192	179	172	172	181	162	160	160	170
20	190	178	172	173	182	162	161	161	172
21	189	178	172	173	184	163	162	163	175
22	188	177	173	174	186	163	163	165	177
23	187	177	173	176	188	164	164	166	180
24	187	178	174	177	190	165	166	168	183
25	187	178	175	178	192	166	167	170	185
26	187	179	176	179	195	167	169	172	188
27	187	179	177	181	197	168	170	174	191
28	188	180	178	182	199	169	172	176	194
29	188	181	179	184	202	170	173	178	196
30	189	182	180	186	204	172	175	180	199
BEST	**155**								
Thruster Configuration	**13**	**H**		**5.0 m**		**4500 kW**			

Table B.15: 15MW Turbine in Wind Speed Class 14.

# Thrusters	Thruster Consumption Percent								
	A	B	C	D	E	F	G	H	I
1	#N/A	#N/A	#N/A	#N/A	#N/A	#N/A	#N/A	#N/A	#N/A
2	#N/A	#N/A	#N/A	#N/A	#N/A	#N/A	#N/A	#N/A	#N/A
3	#N/A	#N/A	#N/A	#N/A	#N/A	#N/A	#N/A	#N/A	#N/A
4	#N/A	#N/A	#N/A	#N/A	#N/A	#N/A	#N/A	#N/A	80%
5	#N/A	#N/A	#N/A	96%	88%	#N/A	#N/A	79%	72%
6	#N/A	#N/A	95%	88%	80%	#N/A	80%	72%	66%
7	#N/A	96%	88%	82%	74%	82%	74%	67%	61%
8	#N/A	89%	82%	76%	70%	76%	70%	63%	57%
9	92%	84%	78%	72%	66%	72%	66%	59%	54%
10	87%	80%	74%	68%	62%	68%	62%	56%	51%
11	83%	76%	70%	65%	59%	65%	59%	53%	48%
12	80%	73%	67%	62%	57%	62%	57%	51%	46%
13	77%	70%	65%	60%	55%	60%	55%	49%	45%
14	74%	68%	62%	58%	53%	58%	53%	47%	43%
15	71%	65%	60%	56%	51%	56%	51%	46%	42%
16	69%	63%	58%	54%	49%	54%	49%	44%	40%
17	67%	61%	56%	52%	48%	52%	48%	43%	39%
18	65%	60%	55%	51%	46%	51%	46%	42%	38%
19	63%	58%	53%	49%	45%	49%	45%	41%	37%
20	62%	57%	52%	48%	44%	48%	44%	40%	36%
21	60%	55%	51%	47%	43%	47%	43%	39%	35%
22	59%	54%	50%	46%	42%	46%	42%	38%	34%
23	58%	53%	49%	45%	41%	45%	41%	37%	34%
24	56%	52%	48%	44%	40%	44%	40%	36%	33%
25	55%	51%	47%	43%	39%	43%	39%	35%	32%
26	54%	50%	46%	42%	39%	42%	39%	35%	32%
27	53%	49%	45%	42%	38%	42%	38%	34%	31%
28	52%	48%	44%	41%	37%	41%	37%	33%	30%
29	51%	47%	43%	40%	37%	40%	37%	33%	30%
30	50%	46%	43%	39%	36%	39%	36%	32%	**29%**
BEST	29%								
Thruster Configuration	30	I		5.5 m	5500 kW				

# Thrusters	LCOE, High (USD/MWh, 30 years, 5.2%)								
	A	B	C	D	E	F	G	H	I
1	#N/A	#N/A	#N/A	#N/A	#N/A	#N/A	#N/A	#N/A	#N/A
2	#N/A	#N/A	#N/A	#N/A	#N/A	#N/A	#N/A	#N/A	#N/A
3	#N/A	#N/A	#N/A	#N/A	#N/A	#N/A	#N/A	#N/A	#N/A
4	#N/A	#N/A	#N/A	#N/A	#N/A	#N/A	#N/A	#N/A	525
5	#N/A	#N/A	#N/A	1,077	706	#N/A	#N/A	502	425
6	#N/A	#N/A	986	704	547	#N/A	524	424	378
7	#N/A	1,026	702	562	472	549	449	382	351
8	#N/A	752	576	488	429	475	406	357	336
9	870	621	505	443	402	430	379	340	326
10	710	545	460	414	385	401	360	329	319
11	617	495	430	394	372	380	347	321	315
12	557	461	408	379	364	365	337	316	**313**
13	515	436	392	368	358	354	330	**312**	**313**
14	484	418	380	360	354	345	325	**310**	**313**
15	461	403	370	354	351	339	321	**308**	**313**
16	443	392	363	349	350	334	319	**308**	**315**
17	428	383	357	346	349	330	317	**308**	317
18	417	376	353	344	349	327	316	**308**	319
19	408	371	350	342	350	325	315	**309**	322
20	400	366	347	341	351	323	315	**310**	324
21	394	362	345	341	353	322	316	**312**	328
22	389	360	344	341	355	322	316	**313**	331
23	385	357	343	341	357	322	317	315	334
24	382	356	342	342	359	322	318	317	338
25	379	354	342	343	362	322	320	320	341
26	377	353	342	344	364	323	321	322	345
27	375	353	343	345	367	324	323	325	349
28	374	353	344	347	370	325	325	327	353
29	373	353	344	349	373	326	327	330	357
30	372	353	345	350	377	327	329	333	361
BEST	308								
Thruster Configuration	17	H		5.0 m	4500 kW				

# Thrusters	LCOE, Low (USD/MWh, 30 years, 5.2%)								
	A	B	C	D	E	F	G	H	I
1	#N/A	#N/A	#N/A	#N/A	#N/A	#N/A	#N/A	#N/A	#N/A
2	#N/A	#N/A	#N/A	#N/A	#N/A	#N/A	#N/A	#N/A	#N/A
3	#N/A	#N/A	#N/A	#N/A	#N/A	#N/A	#N/A	#N/A	#N/A
4	#N/A	#N/A	#N/A	#N/A	#N/A	#N/A	#N/A	#N/A	486
5	#N/A	#N/A	#N/A	997	655	#N/A	#N/A	465	394
6	#N/A	#N/A	913	653	509	#N/A	485	394	351
7	#N/A	951	651	522	440	509	417	355	328
8	#N/A	697	535	454	401	441	378	332	314
9	808	577	470	413	376	400	353	317	305
10	660	507	429	386	360	373	336	307	300
11	575	461	401	368	349	354	324	300	**296**
12	519	430	381	354	342	341	315	**296**	**295**
13	480	407	366	345	337	331	309	**293**	**295**
14	452	390	355	338	334	323	305	**291**	**295**
15	431	377	347	332	332	317	302	**290**	**296**
16	414	367	341	329	331	313	300	**290**	298
17	401	359	336	326	331	310	298	**290**	300
18	391	353	332	324	331	307	298	**291**	303
19	383	348	329	323	332	306	297	**292**	306
20	376	344	327	322	334	304	298	**294**	309
21	371	341	325	322	335	304	298	**295**	312
22	366	339	324	323	337	304	299	297	315
23	363	337	324	323	340	304	300	299	319
24	360	336	324	324	342	304	302	302	323
25	358	335	324	325	345	305	303	304	326
26	356	334	324	327	348	305	305	307	330
27	355	334	325	328	351	306	307	309	334
28	354	334	326	330	354	308	309	312	338
29	353	334	327	332	357	309	311	315	342
30	353	335	328	334	361	310	313	318	347
BEST	290								
Thruster Configuration	16	H		5.0 m	4500 kW				

Appendix C

Supplementary Material for Chapter III

C.1 Summary of US Offshore Wind Capacity Development

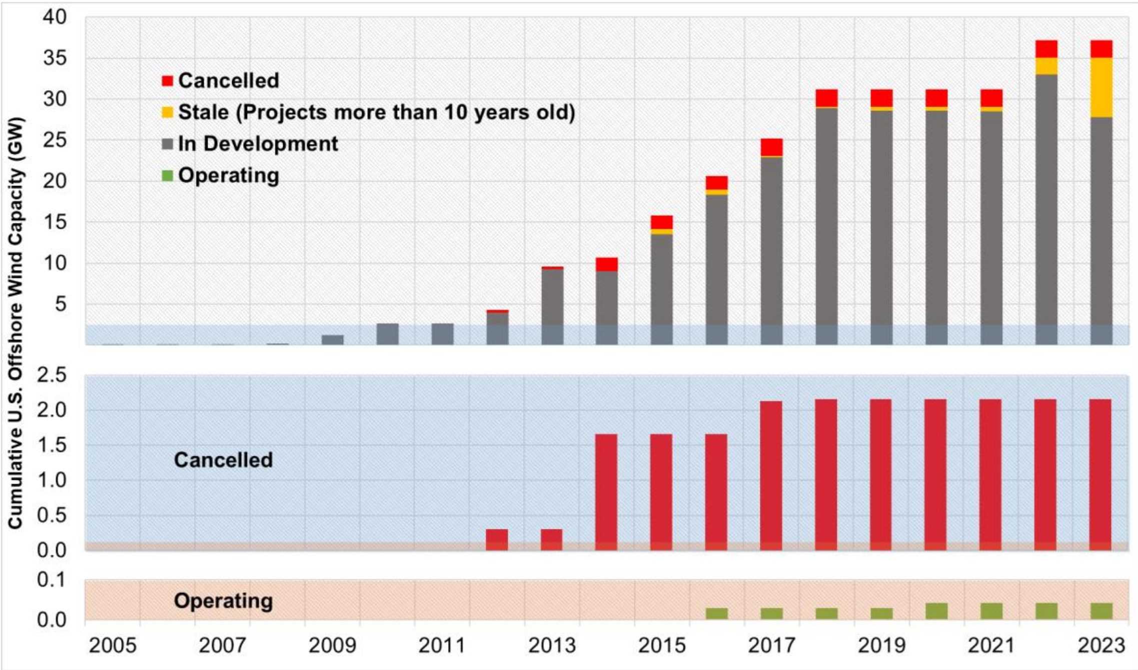

Figure C.1: US leased OSW capacity potentials based on status [7], [80], [259], [260], [261], [262], [263], [264], [265].

C.2 Value Chain Technology Descriptions

C.2.1 Turbine and Plant Sizes

Four turbine types are considered as options in this analysis as described in Table C.1. These are reference turbine specifications and represent a range of commercial or next-generation turbine capacities.

Table C.1: Turbine specifications and dimensions

Turbine Rated Power [MW]	5	8	10	15
Hub Height [m]	90	110	119	150
Tower Base Diameter [m]	6	7.7	8.3	10
Blade Length [m]	61.5	82	96	117
2km spacing in rotor diameters [-]	16.3D	12.2D	10.4D	8.5D
Cut-in Wind Speed [m/s]	3	4	4	3
Rated Wind Speed [m/s]	11.4	12.5	10.5	10.6
Cut-out Wind Speed [m/s]	25	25	25	25
Source	[38]	[39]	[40]	[37]

These turbine sizes are deployed in plants of various sizes ranging from 200MW to 1,400MW in this study. A discrete number of turbines is deployed for the plant, therefore, in certain instances, the plant nameplate capacity with some turbine sizes may be more than the nameplate capacity of others as shown in Table C.2.

Table C.2: Actual nameplate capacity for some turbine and plant size combinations in this analysis. Number of turbines required is given in parentheses.

<table>
<tr><th></th><th></th><th>200</th><th>600</th><th>1000</th><th>1400</th></tr>
<tr><td rowspan="4">Turbine Size (MW)</td><td>5</td><td>200 (40)</td><td>600 (120)</td><td>1000 (200)</td><td>1400 (280)</td></tr>
<tr><td>8</td><td>200 (25)</td><td>600 (75)</td><td>1000 (125)</td><td>1400 (175)</td></tr>
<tr><td>10</td><td>200 (20)</td><td>600 (60)</td><td>1000 (100)</td><td>1400 (140)</td></tr>
<tr><td>15</td><td>210 (14)</td><td>600 (40)</td><td>1005 (67)</td><td>1410 (94)</td></tr>
</table>

C.2.2 Station-keeping Types

Three station-keeping types are considered. A monopile foundation is the only fixed foundation type in this analysis in which a cylindrical substructure that is embedded in the seabed supports the wind turbine above the water surface. Monopiles are considered for depths up to 60m [18]. Two types of station-keeping are considered for floating foundations—moored and dynamic positioning (DP). A floating semisubmersible platform as described in Allen et al. (2020) is used for all floating turbines [36]. A schematic and the dimensions of the floating semisubmersible are given in Figure C.2.

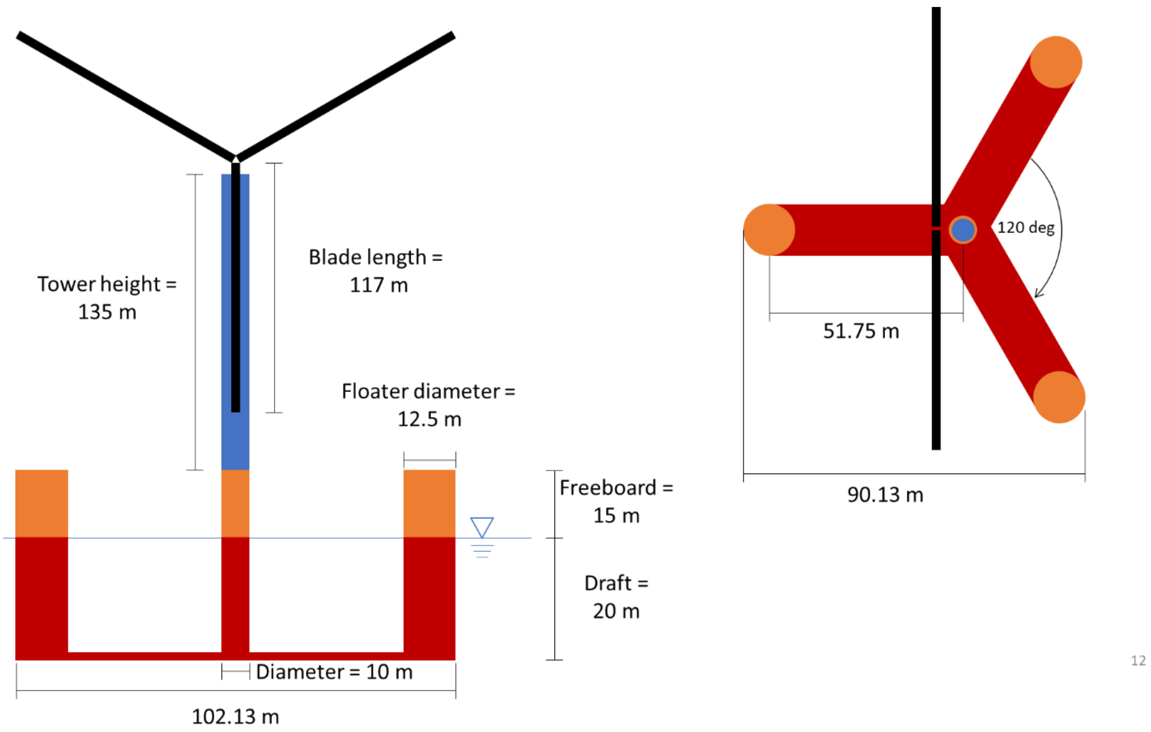

Figure C.2: Dimensions of floating substructure used, adapted from [36, Fig. 3].

A mooring system uses catenary mooring chains and drag embedment anchors to keep a floating turbine in position. A DP system uses thrusters mounted on the underside of the floating platform to counteract the environmental forces from wind, wave, and currents to keep the turbine in position [31], [32]. The DP system consumes some of the energy output from the generating turbine, and therefore the net energy generation from the turbine is decreased when deployed with DP.

C.2.3 Transmission Types

Two transmission types are considered in this analysis. A HVDC transmission system is considered as the most likely candidate for high-capacity transmission for OSW plants in the near term. In a HVDC transmission system, the energy generated at the turbines is collected at a single collector platform using inter-array cables between turbines and the platform, where an offshore substation is located. At the offshore substation (OfSS) a step-up transformer increases the voltage of the system. At the OfSS, the electricity is also converted from alternating current to direct current. Subsea high voltage transmission cables then transport the electricity from the OfSS to shore. The cables are typically buried in the seabed and require some area of buffer around the cable during service to prevent damage to cables and potential harm to flora and fauna in the vicinity of the cable. The cables then make landfall on the coast where they arrive at an onshore substation (OnSS). At the OnSS, the electricity is converted back to alternating current, and the voltage may be reduced. From the OnSS, the electricity is distributed through the existing transmission system. Specifics on the cables considered in the analysis to compute transmission losses for HVAC and HVDC systems are provided in the Table C.3 and Table C.4 below, taken from Xiang and colleagues [141]:

Table C.3: HVAC cable parameters considered in the analysis [141].

Voltage (kV)	Size (mm^2)	Resistance (Ω/km)	Nominal Current (A)	Capacitance (F/km)	Cost (GBP/km)
132	500	4.93E-02	739	1.92E-07	6.35E+05
132	630	3.95E-02	818	2.09E-07	6.85E+05
132	800	3.24E-02	888	2.17E-07	7.95E+05
132	1000	2.75E-02	949	2.38E-07	8.60E+05
220	500	4.89E-02	732	1.39E-07	8.15E+05
220	630	3.91E-02	808	1.51E-07	8.50E+05
220	800	3.19E-02	879	1.63E-07	9.75E+05
220	1000	2.70E-02	942	1.77E-07	1.00E+06
400	800	3.14E-02	870	1.30E-07	1.40E+06
400	1000	2.65E-02	932	1.40E-07	1.55E+06
400	1200	2.21E-02	986	1.70E-07	1.70E+06
400	1400	1.89E-02	1015	1.80E-07	1.85E+06
400	1600	1.66E-02	1036	1.90E-07	2.00E+06
400	2000	1.32E-02	1078	2.00E-07	2.15E+06

Table C.4: HVDC cable parameters considered in the analysis[141].

Voltage (kV)	Size (mm^2)	Resistance (Ω/km)	Current (A)	Cost (GBP/km)
150	1000	2.24E-02	1644	6.70E+05
150	1200	1.92E-02	1791	7.30E+05
150	1400	1.65E-02	1962	7.85E+05
150	1600	1.44E-02	2123	8.40E+05
150	2000	1.15E-02	2407	9.00E+05
220	1000	2.24E-02	1644	8.55E+05
220	1200	1.92E-02	1791	9.40E+05
220	1400	1.65E-02	1962	1.02E+06
220	1600	1.44E-02	2123	1.09E+06
220	2000	1.15E-02	2407	1.18E+06

A power-to-hydrogen (PtH) system is considered as a potential candidate to forgo cables, the installation time and effort, the area requirement, fixed infrastructure (and accompanying concerns), regulatory requirements associated with leasing, installing, and permitting associated with cable transmission systems. In this system, the electricity generated at the turbines is collected at a single collector platform using inter-array cables between turbines and the platform where an OfSS is located, similar to the HVDC system. At the OfSS the electricity is used in an electrolyzer in which desalinized water is electrolyzed into hydrogen and compressed for shipping to shore. A hydrogen tanker as described in [188], [219] is used to periodically collect the hydrogen generated and stored at the collector site to a storage facility on shore. One potential benefit of this system is the flexibility in delivery that it can accommodate. A single hydrogen ship may collect hydrogen from several locations (OSW plants) and deliver the hydrogen to several locations on shore (different storage facilities).

C.3 Distribution of Normalized Metrics

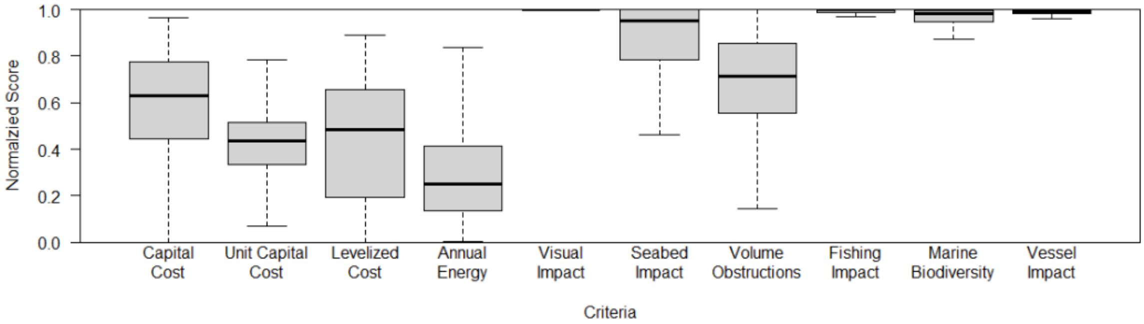

Figure C.3: Distribution of normalized metrics across the entire alternatives space.

C.4 Thruster Consumption

We compute the thruster consumption in a three-step process:

1. Estimate the environmental thrust forces under a range of conditions for each turbine size.
2. Considering several DP Thruster configurations (numbers of thrusters on the turbine), calculate the expected annual thruster consumption.
3. Calculate the LCOE from the thruster investment for each of the DP thruster configurations.
4. The minimum LCOE configuration is optimal for the turbine, and the resulting consumption from the configuration is used.
5. Extrapolate the results across several mean wind speeds.

Step 1: Environmental thrust forces

Wind, wave, and current forces are considered using a design load case (DLC) by the American Bureau of Shipping (ABS) for station-keeping design for floating OSW turbines [266]. The parameters used are shown in Table C.5.

Table C.5: Environmental loading conditions, parameters used, and orientations to compute the total environmental thrust force on the turbines.

Parameter	**Conditions Used**
Design Load Case [266]	DLC 1.3
Wind Speed (at hub height), V_{hub}	$V_{cut-in} < V_{hub} < V_{cut-out}$
Surface Current Speed, V_{curr}	The wind-generated currents, $V_{curr} = \mathbb{E}[V_{curr} \mid \mu(V_{hub})]$
Wave Height, H	Normal Sea State, $H = \mathbb{E}[H \mid V_{hub}]$
Wave Period, T	(Not defined)
Wind and Wave Directionality	Unidirectional wind and wave directions

The total thrust force, $\vec{F}_{tot}$, is the vector combination of the wind, wave, and current force vectors,

$$\vec{F}_{tot}(V_{hub}) = \vec{F}_{wind}(V_{hub}) + \vec{F}_{curr}(V_{curr}(V_{hub})) + \max_{H,T}\left(\vec{F}_{wave}(\widehat{H}, \widehat{T})\right) \tag{C.1}$$

Step 2: Expected annual thruster consumption

ABS provides a generalized relationship between input power and applied force for the DP thrusters in equation (C.2) [266], [267]. Equation (C.3) gives the power as a function of applied force for a single thruster. I assume the force is applied equally across all thrusters and each consumes an equivalent amount of power. The power consumption of a system consisting of n thrusters is estimated using equation (C.4).

$$F_1 = K \times (P_1 \times D)^{\frac{2}{3}} \tag{C.2}$$

$$P_1 = \left(\frac{F_1}{K}\right)^{\frac{3}{2}} \times \frac{1}{D} \tag{C.3}$$

$$P_{DP}(F_{tot}, n) = \frac{n}{D} \times \left(\frac{F_{tot}}{n\,K}\right)^{\frac{3}{2}} \tag{C.4}$$

where F_1 is the bollard pull force (N), P_1 is the power required (kW) for a single thruster, K is a constant equal to 1,250, and D is propeller diameter (m) [267]. F_{tot} is the needed station-keeping force (equation (C.1)), and P_{DP} is the DP system power requirement (kW).

The annual expected thruster energy consumption, $\mathbb{E}_{TC}$, is computed as an expectation of the power consumption of the DP system considering a probability density function of wind speeds at hub height, $f(V_{hub})$—for which I consider a Weibull distribution.

$$\mathbb{E}_{TC} = 8760 \times \left[\int_{V_{hub}} f(V_{hub}) \times P_{DP}(F_{tot}(V_{hub}), n) \, dV_{hub} \right] \tag{C.5}$$

The expected wind turbine generation, $\mathbb{E}_{GEN}$, is computed similarly, with the wind power curve in place of the thruster power consumption function in equation (C.5).

We compute this expected energy consumption under two WSCs adopted from the National Renewable Energy Laboratory (NREL) Annual Technology Baseline (ATB) for OSW [142]. Along with different wind speed probability distributions, the WSCs are also characterized by different plant deployment, operation, financing, and operations & maintenance costs that I use to calculate the cost effectiveness of the systems in the next step.

Step 3: Compute LCOE for the DP turbine configurations

The calculation method employed by the NREL ATB to calculate the LCOE of the turbine is used [142]:

$$LCOE = ((CRF * PFF * CFF * netOCC) + FOM) * 1000/(netCF * 8760)$$

where CRF, PFF, and CFF are the capital recovery, production finance, and construction finance factors, respectively. The net CF for the turbine is calculated as,

$$netCF_{turbine} = \frac{\mathbb{E}_{GEN} - \mathbb{E}_{TC}}{8760 \times turbine\ size}$$

The net overnight capital cost, $netOCC$, for DP is adjusted from the NREL base overnight capital cost (OCC) by reducing it by the proportion estimated for mooring and increasing it by the DP system cost (USD/kW).

Step 4: Identify the LCOE-minimizing configuration

Once the LCOE is computed for all the configurations of DP thruster systems, and for each turbine, the configuration that minimizes the LCOE is the configuration required for the turbine. The results are reported in Table C.6. The TCP is also reported under the three wind speed distributions (described by their annual mean wind speed). The TCP is computed as,

$$TCP = \frac{\mathbb{E}_{TC}}{\mathbb{E}_{GEN}}$$

and this parameter gives the percent of annual generation that is consumed by the thrusters. In areas where the annual mean wind speed is different, the TCP may be different, as evidenced by the differences in the TCP when computed for different WSCs.

Table C.6: Number of thrusters for the LCOE-minimizing DP configuration, and the TCP under different wind profiles, with different wind probability distribution functions (defined using only the mean).

Turbine Rated Power [MW]	5	8	10	15
LCOE minimizing configuration (number of 5m thrusters)	4	4	5	13
TCP (annual mean of the wind profile = 7.1 m/s)	39%	30%	38%	72%
TCP (annual mean of the wind profile = 8.9 m/s)	32%	23%	32%	64%
TCP (annual mean of the wind profile = 9.6 m/s)	30%	21%	30%	61%

Step 5: Extrapolate the results across different annual mean wind speeds

Using the results of TCP given wind speed profiles in Table C.6, a linear model for each turbine size that relates mean windspeed to the TCP is calculated (see Figure C.4). The TCP gives the expected proportion of annual generated energy that is consumed by the thrusters, and therefore, turbines that employ DP have an annual electricity output that is reduced by the TCP.

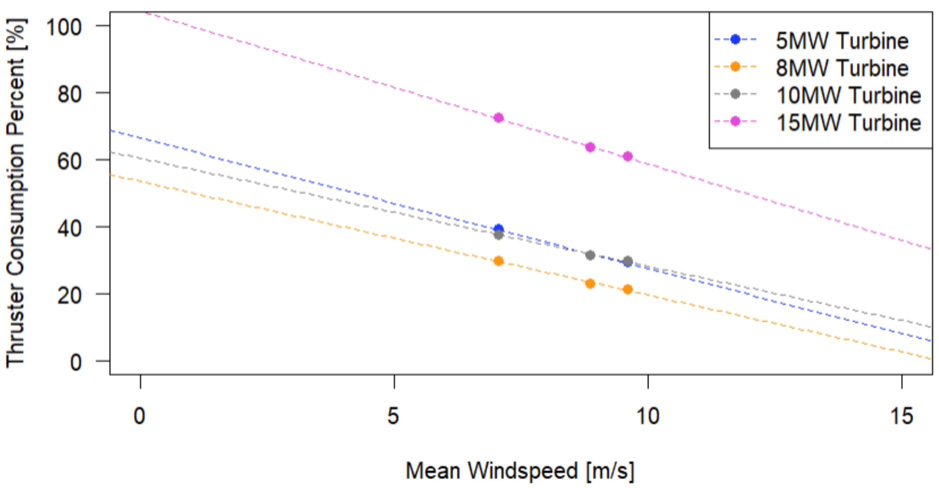

Figure C.4: Linear models to compute TCP for each turbine size at various annual mean wind speeds.

Using this linear model, given a turbine size and a mean wind speed for a given grid square, the TCP is calculated and the expected net energy generation by a turbine in the grid square is calculated as,

$$E_{DP\ turbine}\left[\frac{MWh}{year}\right] = E_{turbine}\ \times \left(1 - TCP(V_{wind}, T)\right)$$

where the expected annual energy generation of a DP turbine, $E_{DP\ turbine}$, is the equal to that of a non-DP turbine, $E_{turbine}$, reduced by the TCP.

C.5 Turbine Asset Cost and Efficiency Computations

The cost of the system is quantified as the OCC of the system which considers the procurement cost of the turbine, substructure (monopiles are considered for fixed-bottom, and semisubmersibles are considered for floating foundations), inter-array cables, onshore spur line to interconnect to the existing transmission system, station-keeping system, and the export system. Turbine costs come from [117] and vary with turbine rated capacity, monopile costs come from [268] and vary with water depth, semisubmersible costs come from [36] (sized for a 15MW turbine, the same is used for all turbines).

Mooring costs come from [269] assuming three catenary mooring chains. DP costs are computed considering the number of thrusters needed (see Table C.6). Inter-array cable costs use unit costs from [270], and assume the grid spacing of 2km. Onshore spur line cost is estimated assuming 2 million USD/mile of distance from landfall to a point of interconnection [271].

A description of the cost assumptions used for the components of each value chain is given in Table C.7. The costs of are calculated given the physical parameters (distance, depth, wind speed, etc.) and components of the value chain.

Table C.7: Cost assumptions and sources for value chain components.

Parameter	Value	Source
TURBINES		
Turbine cost	1,300 USD/kW	Beiter et al. (2020) [117]
Turbine annual O&M	2% of CAPEX/year	Van Wingerden et al. (2023) [210]
SUBSTRUCTURES		
Steel cost	1,000 USD/ton	Myhr et al. (2014) [268]
Monopile steel consumption	40 ton/m of water depth	Myhr et al. (2014) [268]
Semisubmersible steel consumption	3,900 ton/substructure	Allen et al. (2020) [36]
Monopile annual O&M	2% of CAPEX/year [b]	Van Wingerden et al. (2023) [210]
Semisubmersible annual O&M	2% of CAPEX/year [b]	Van Wingerden et al. (2023) [210]
STATION KEEPING		
Mooring chain breaking load (MBL)	4500 kN	[135]
Mooring chain cost	0.0591*MBL-87.6 USD/m	Beiter et al. (2016) [269]
Mooring annual O&M	1% of CAPEX/year [c]	Avanessova et al. (2022) [272]
Drag embedment anchor cost	10.198*MBL USD/anchor	Beiter et al. (2016) [269]
DP thruster cost	1,700,000 USD/thruster	[273]
DP annual O&M	4% of CAPEX/year	[274]
ARRAY CABLES		
Cable cost	45,000 USD/km	Jung et al. (2018) [270]
Array cable annual O&M	3% of CAPEX/year	Van Wingerden et al. (2023) [210]
Array cable length	2 km/turbine	US Coast Guard (2020), spacing between turbines [120]
EXPORT SYSTEM		
Collector platform cost	6,710,000 USD/platform	Xiang et al. (2016) [275]
HVDC terminal fixed cost [a]	30,750,000 USD	Xiang et al. (2021) [141]
HVDC terminal variable cost [a]	134,070 USD/MVA	Xiang et al. (2021) [141]
HVDC export cable cost	(**Table C.4**) [a]	Xiang et al. (2021) [141]
HVDC system annual O&M	3% of CAPEX/year	Van Wingerden et al. (2023) [210]
HVAC terminal fixed cost	6,150,000 USD	Xiang et al. (2021) [141]
HVAC terminal variable cost	55,350 USD/MVA	Van Wingerden et al. (2023) [210]
HVAC export cable cost	(see **Table C.3**)	Van Wingerden et al. (2023) [210]
HVAC system annual O&M	2.5 % of CAPEx/year	Van Wingerden et al. (2023) [210]
Electrolyzer cost	900 USD/kW	Saba et al. (2018), median for projection years beyond 2010 [276];
Electrolyzer annual O&M	1.5% of CAPEX/year	Van Wingerden et al. (2023) [210]
Transformer cost	1,300,000 USD/MW	Xiang et al. (2016) [275]
Transformer annual O&M	2.3% of CAPEX/year	Van Wingerden et al. (2023) [210]
Hydrogen shipping vessel cost	440,000,000 USD/ship	Alkhaledi et al. (2022) [219]
Hydrogen ship annual O&M	4% of CAPEX/year	Alkhaledi et al. (2022) [219]
Hydrogen production rate	67 kWh/kgH_2	IRENA (2020) [277]
Hydrogen loss in liquefication	15%	Popov & Baldynov (2019) [278]
ONSHORE CABLE		
Onshore spur line	2,000,000 USD/mile	Saadi et al. (2018) [271]
Onshore cable annual O&M	3% of CAPEX/year	Van Wingerden et al. (2023) [210]

[a] The number of cables needed for the export cable system considers the physical capabilities of the cable options, and therefore is calculated for a set of cables and functions from [141], [275].
[b] Assumed to be the same as the turbine annual O&M percent.
[c] The failure rate of a single chain times number of chains.

C.5.1 Comparing Cost Model

We compare the cost model developed in this analysis to an analysis of OSW sites done by NREL [117]. Three OSW sites are assessed for their costs, potential energy generation, and LCOE. Table C.8 summarizes the results from the NREL model and the results attained from this analysis for each of the three sites.

Table C.8: Comparative costs calculated using NREL models [117] and the model used in this analysis. Major differences in the costs computed are highlighted.

	Morro Bay		**Diablo Canyon**		**Humboldt**	
	NREL	**Our Model**	**NREL**	**Our Model**	**NREL**	**Our Model**
Turbine (USD/kW)	1,297	1,300	1,297	1,300	1,297	1,300
Substructure (USD/kW)	1,235	1,170	1,235	1,170	1,235	1,170
Array Cables	291	90	258	90	275	90
Export Cables	454	498	487	484	447	410
Onshore spur line	78	65	78	17	78	13
Total Electric System (USD/kW)	823	653	823	591	800	513
Installation Cost (USD/kW)	333	0	306	0	269	0
Development	142	0	141	0	139	0
Lease Price	88	0	88	0	88	0
Project Management	74	0	73	0	72	0
Insurance	46	0	46	0	45	0
Project Completion	46	0	46	0	45	0
Decommissioning	50	0	45	0	39	0
Procurement Contingency	213	0	213	0	211	0
Install Contingency	100	0	90	0	78	0
Construction Financing	191	0	189	0	186	0
"Soft" CAPEX (USD/kW)	950	0	931	0	903	0
Total CAPEX (USD/kW)	4,638	[redacted]	4,592	[redacted]	4,504	[redacted]
Total CAPEX of Included Items (USD/kW)	3,355	3,123	3,355	3,061	3,332	2,983
Plant Characteristics						
LCOE (USD/MWh)	90	100	92	102	81	80
Capacity Factor	49%	38%	48%	39%	53%	45%
Site Characteristics						
Average Shore Distance (km)	43-53		43-67		36-46	
Average Water Depth (m)	830-1067		495-840		608-890	
Average Port Distance (km)	192-235		206-232		253-292	

As Table C.8 demonstrates, the main differences between the costs calculated in this model compared with the more detailed NREL model are the inclusion of installation costs and project execution costs in the latter. The costs for plant components are closely represented aside from the array cable costs, which the model in this analysis underestimates compared to the NREL calculations. Furthermore, the capacity factor for the plant sites is underestimated by the model in this analysis, and as a result, the LCOE is overestimated by this model—both conservative estimates for these parameters, and thus this model is conservative in its outputs.

As there is discrepancy between the sophisticated NREL model and this analysis, I compare the relative differences of capital costs and LCOE (two of the criteria in the MCDM) in Table C.9. The MCDM in this analysis compares relative, normalized values (as opposed to absolute values), and Table C.9 shows that these relative differences of these criteria calculated using the NREL model are closely captured with the model in this analysis.

Table C.9: Indexed values for capital costs and LCOE between an NREL model [117] and the models used in this analysis illustrating how the relative differences compare between the models.

Relative Differences (Indexed to Diablo Canyon)	Morro Bay	Diablo Canyon	Humboldt
CAPEX Overall – NREL	101	100	98
CAPEX – This R Model	102	100	97
LCOE – NREL	98	100	88
LCOE – This R Model	98	100	78

C.6 Novel Deployment Options

Table C.10: A description of the novel deployment options and the benefits and costs realized by these options.

Deployment Option	Description	Benefits	Costs
Baseline Facility	10MW Turbine Moored Foundations HV Cable Transmission 1,000 MW Plant	Accepted method for next generation deep water deployment	Cost sensitive to water depth Depth is a limitation Cost sensitive to shore distance
Novel Deployment Facility	10MW Turbine DP Foundations PtH Transmission Pathway 1,000 MW Plant	Eliminate cost sensitivity to shore distance Eliminate depth limit (more area is available for deployment) Eliminate disrupted seabed from cables Eliminate ocean obstructions from mooring chains	Highest capital cost deployment option Reduced energy output (DP consumption) Reduced energy efficiency (Hydrogen conversion efficiency)

C.7 Distribution of Normalized Scores based on Plant Scale

Figure C.5 illustrates the distribution of each normalized metric that contributes to the suitability scores for the smallest (200MW) and largest (1,400MW) plant scales considered in this analysis.

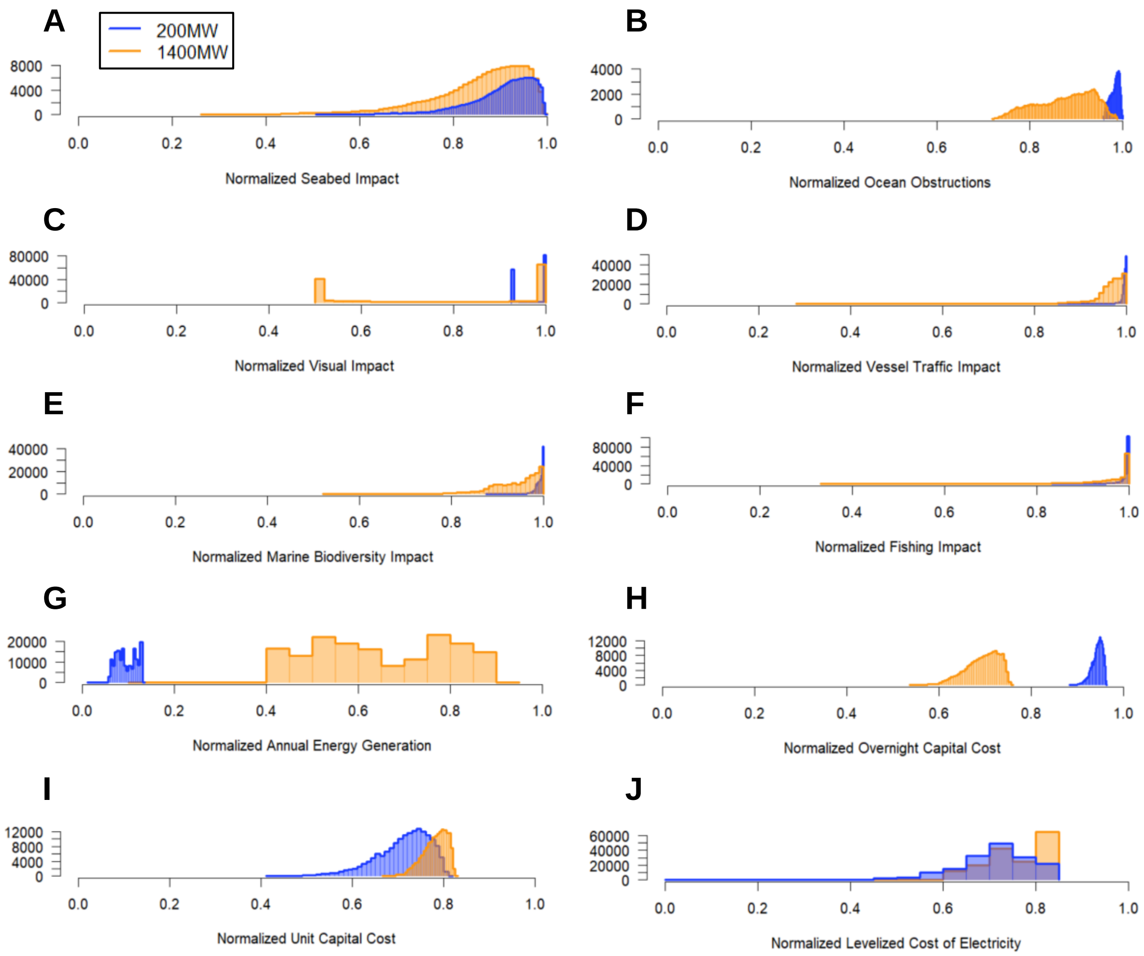

Figure C.5: A) – J) Distribution of all 10 normalized metrics for the smallest and largest plant sizes considered in this study; each observation in the histograms are site locations for the plant. Normalized values reflect whether the metric is a cost or benefit already, therefore, a value of one indicates the preferred outcome in each.

The stakeholder suitability score is defined by the scores in Figure C.5A to Figure C.5G. The implication of this is that small capacity plants have less variance in stakeholder perspectives across potential sites. While the outlay of energy output from larger plants dominates that of smaller plants (Figure C.5G), a smaller physical presence results in a tight distribution of normalized scores for the physical impact metrics of the plant (Figure C.5A to Figure C.5F).

The developer suitability score is defined by the scores in Figure C.5G to Figure C.5J. The smaller plant realizes a wider distribution of unit capital cost and LCOE, while a tighter distribution of overall capital cost is seen.

C.8 Other Weight Profiles

Figure C.6 illustrates the suitability score maps of the baseline value chains under uniform-weighting. These results can be compared to the stakeholder and developer weighting maps in Figure 3.5 of Section 3.3. The stakeholder-weighted and uniform-weighted maps appear very similar. As Dawes has noted, uniformly weighting criteria is good policy, as it requires fewer assumptions, and can suitably represent expert judgements [148], [172]. This suggests that stakeholder-weighted maps should be used to a greater extent in matters regarding OSW project decision-making.

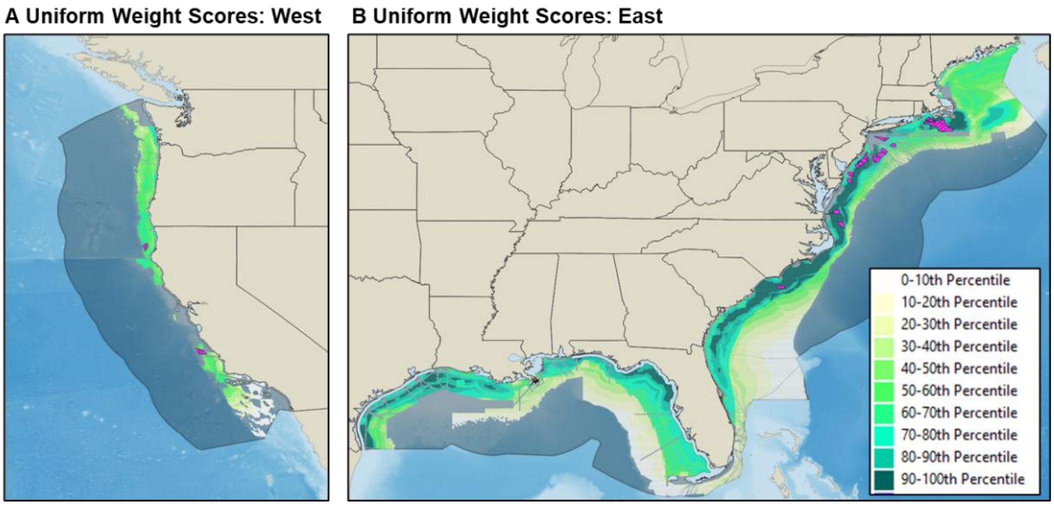

Figure C.6: Maps of the baseline value chain scores under uniform weighting.

Figure C.7 illustrates the distribution of scores with varying plant scale of all the weight profiles. These are demonstrated for the baseline facility with different plant capacities.

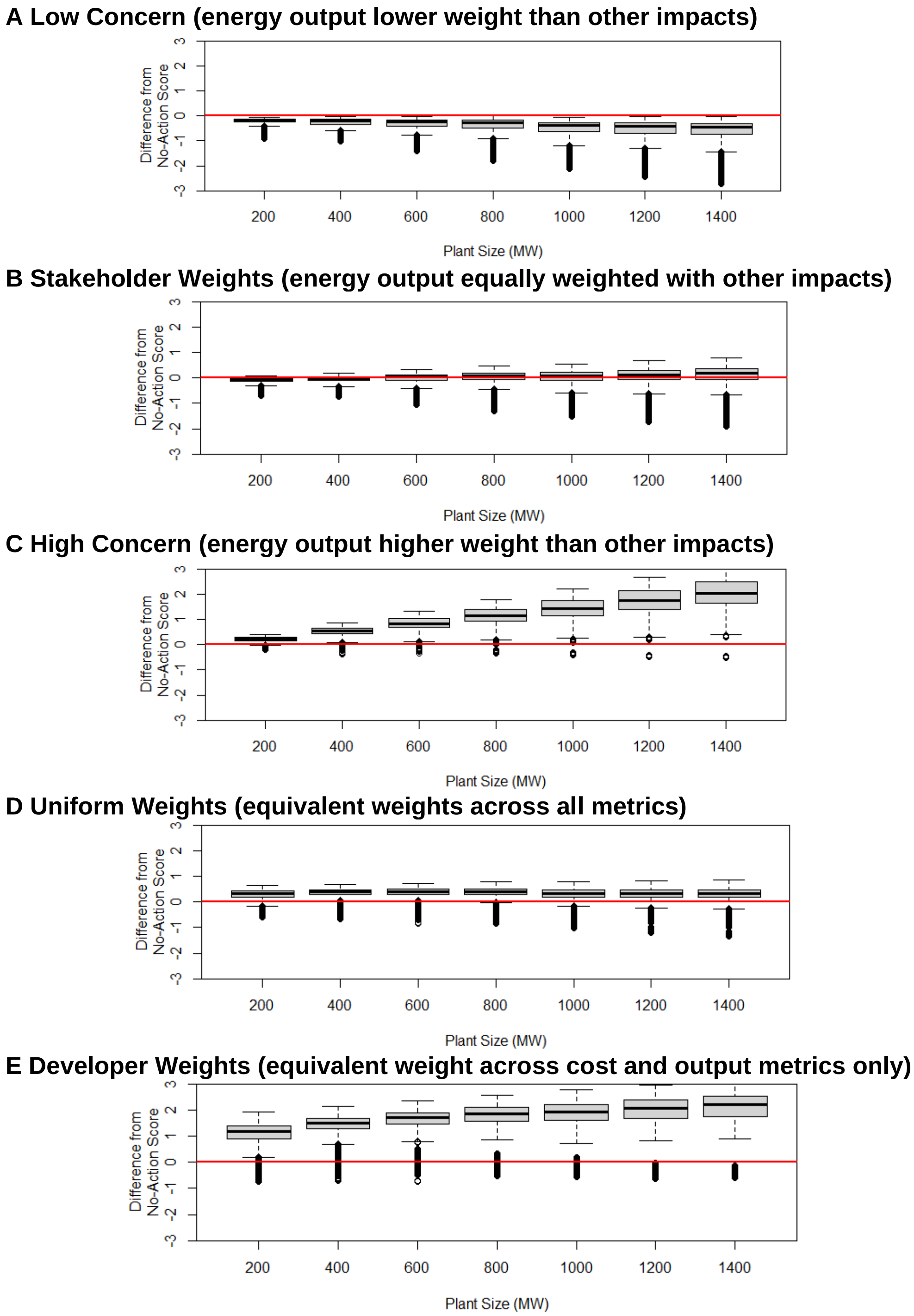

Figure C.7: The distribution of suitability scores by plant size considering 10MW fixed foundation turbines, and DC cable transmission under the weight profiles given in Table 3.7 of the Section 3.2.4.

As concern for deploying more clean energy increases relative to other impacts, the suitability of all plants increases, but larger plants increase by even more. When there is high concern for deploying clean energy (Figure C.7C) nearly all site alternatives for the largest plant dominate all the small plant site alternatives. When concerns for deploying more clean energy are low, small are preferred to large plants. Smaller plants are tightly distributed, and achieve similar scores regardless of the level of concern for energy output (Figure C.7A to Figure C.7C), and therefore, smaller plants are more robust to the institutional context if there is considerable uncertainty of the context the plant is being deployed in.

The context in which a renewable energy plant is deployed will play a role in the potential success of the plant. Furthermore, while I have reported on a national-scale model, perspectives may change at more granular scales, from community to community. As demonstrated here, there are certain options that are more robust (scores do not vary greatly) to different institutional contexts (represented by different weight profiles).

C.9 Robustness Checks

Table C.11 provides a qualitative analysis of the categories of metrics that may be included in the developer and stakeholder weight profiles. In the first column, whether the metric is a benefit or a cost is described. Given that the No-Action choice realizes a metric of zero—as the plant alternative is not built—when it is normalized (see equation (3.2) in Section 3.2.4), the No-Action score would not change if the metric is a benefit, and the No-Action score would increase by one if the metric is a cost when the metric is part of the weight profile.

For each metric type (benefit or costs) there are four combinations of inclusion or exclusion in the stakeholder and developer weight profiles, and the impact for each category of metrics on the stakeholder and developer score difference to the No-Action score (which is the primary reported result of this framework) is then reported in Table C.11. For example, taking the first row of the table, including a benefit metric that will end up being part of both the stakeholder and developer weight profiles will not change the No-Action score, but plant alternatives will have a metric value for the metric that is greater than or equal to zero. After normalizing the metric, it would elevate the stakeholder and developer scores for plant alternatives by a value between zero and one times the applied weight on this metric. An example of a metric that fits this category is job creation—it is likely seen as a benefit for both developers and external stakeholders. No-Action creates no jobs, and therefore does not change the No-Action score, while plant alternatives would create jobs and therefore increase the difference between plant alternative scores and the No-Action score by a value between one and zero times the applied weight on the criterion, depending on the number of jobs created relative to the maximum. Examples of metrics are provided in Table C.11, including how these metrics might already be related to the datasets included in the study.

Table C.11: Categories of metrics and how their inclusion might impact the main results of the study.

Type of metric (Change to No-Action Score if included)	Stakeholder weight profile inclusion	Developer Weight Profile inclusion	Impact on Stakeholder Score Difference	Impact on Developer Score Difference	Examples	Impacts on Main Numerical Suitability Score Results
Benefit (+ 0)	Yes	Yes	+ [0, w]	+ [0, w]	• Job creation (likely related to plant size) • Pollution reduction (likely related to annual energy output)	Elevate all scores, decrease estimate of “at-risk” plant proposals, increase amount of consensus areas
Benefit (+ 0)	Yes	No	+ [0, w]	0		Elevate Stakeholder scores, decrease estimate of “at-risk” plant proposals, increase amount of consensus areas
Benefit (+ 0)	No	Yes	0	+ [0, w]		Elevate Developer scores
Benefit (+ 0)	No	No	0	0		No effect
Cost (+ w)	Yes	Yes	- [0, w]	- [0, w]	• Construction impacts (likely related to plant size) • Habitat loss (likely related to biodiversity dataset) • Noise (likely related to plant size and type of substructure) • Military operations (related to vessel presence dataset)	Depress all scores, increase estimate of “at-risk” plant proposals, decrease amount of consensus areas
Cost (+ w)	Yes	No	- [0, w]	0		Depress Stakeholder scores, increase estimate of “at-risk” plant proposals, decrease amount of consensus areas
Cost (+ w)	No	Yes	0	- [0, w]		Depress Developer scores
Cost (+ w)	No	No	0	0		No effect

There are three main numerical results given in the study: the distribution of stakeholder and developer scores for the entire alternatives space, the scores of US plant proposals (and “at-risk” proposals), and the amount of consensus areas on each coast. The final column of Table C.11 provides a qualitative description of how each category of metrics might impact these main results. Among potential metrics, there are likely more costs than benefits that are missing from the analysis as certain environmental and industry impacts can be further disaggregated—this is demonstrated by the number of possible examples of missing metrics in the table for which there are more possible cost metrics missing than benefit metrics. The result of including more cost metrics (or adding more cost metrics than benefit metrics in a future iteration of this work) would be that the estimate of 'at-risk' capacity increases, and the amount of consensus areas decreases. Therefore, the study presented here may give a more optimistic view of suitability of plant alternatives.

There are two more qualitative or conceptual results from this study: the spatial distribution and behaviors of the weight profiles, and the variance of small plant scores vs large plant scores. Both of these conceptual results should not be fundamentally changed by the inclusion of other metrics. Regarding the impact of plant scale on the variance of suitability scores, the inclusion of any missing metrics should not affect the main outcome—that smaller plants are more robust (with a tighter variance of scores) than larger plants. Any of the missing metrics included in the table above should have a variance that is nearly equal across all plant sizes, or varies more with larger plants as with most of the included metrics in the existing study (see Figure C.5 in Appendix C.7). Regarding the behavior with distance to shore, none of the missing metrics should counteract the outcome that stakeholder scores tend to be higher away from shore while developer scores tend to be higher closer to shore. Either the metrics would be distributed independent of distance to shore (as with job creation or pollution reduction which likely is more related to plant size and output), or the main effects realized from the current study would be enhanced. For example, habitat loss and military operations are likely related to the biodiversity and vessel presence datasets already included in the analysis, and these would disfavor nearshore alternatives. As these two cost metrics would likely be part of the stakeholder weight profile, the effect realized in the current study—that near shore alternatives score lower from a stakeholder perspective—would therefore be enhanced. Therefore, these results are robust to missing metrics.

Because many of the identified missing metrics are likely related to existing metrics in the current study, I conduct a more comprehensive sensitivity analysis on each metric. As some metrics may be derived from the existing datasets, including them in the study would be operationally similar to having an increased weight on the metrics they are related to. I therefore conduct a sensitivity analysis where each of the 10 metrics are included but provide a disproportionately large weight on one of the metrics, resulting in 10 new weight profiles. For each of the 10 additional weight profiles, one metric is given a weight that is more than 10 times larger than the others, while the remaining nine metrics have an equivalent weight. These additional weight profiles are given in Table C.12.

Table C.12: Additional 10 single-metric-skewed weight profiles considered.

Metric	$Z_{NA,j}$ [a]	**Weight profiles skewed toward one metric**									
OCC	1	**5.5**	0.5	0.5	0.5	0.5	0.5	0.5	0.5	0.5	0.5
Unit OCC	1	0.5	**5.5**	0.5	0.5	0.5	0.5	0.5	0.5	0.5	0.5
Annual Energy/H_2 Output	0	0.5	0.5	**5.5**	0.5	0.5	0.5	0.5	0.5	0.5	0.5
LCOE/LCOH	0	0.5	0.5	0.5	**5.5**	0.5	0.5	0.5	0.5	0.5	0.5
Visual Impact	1	0.5	0.5	0.5	0.5	**5.5**	0.5	0.5	0.5	0.5	0.5
Impact on Fishing	1	0.5	0.5	0.5	0.5	0.5	**5.5**	0.5	0.5	0.5	0.5
Impact on Marine Life	1	0.5	0.5	0.5	0.5	0.5	0.5	**5.5**	0.5	0.5	0.5
Impact on Vessel Traffic	1	0.5	0.5	0.5	0.5	0.5	0.5	0.5	**5.5**	0.5	0.5
Disrupted Seabed	1	0.5	0.5	0.5	0.5	0.5	0.5	0.5	0.5	**5.5**	0.5
Obstructions	1	0.5	0.5	0.5	0.5	0.5	0.5	0.5	0.5	0.5	**5.5**
No-Action Score [b]	–	**9.0**	**9.0**	**4.0**	**4.0**	**9.0**	**9.0**	**9.0**	**9.0**	**9.0**	**9.0**

[a] The normalized No-Action metrics computed as defined in equation (3.2), see Table 3.7 of Section 3.2.4.
[b] Maximum of 10 possible, computed as described in equation (3.6) of Section 3.2.4.

The results of the sensitivity analysis are shown in Figure C.8. As seen with the results, the variance of the smaller plants (provided in the figure) is smaller than that of large plants for each of the weight profiles except the unit OCC skewed, cost of energy skewed, and the disrupted seabed skewed weight profiles. If weight profiles were heavily skewed toward these three metrics, we might see the opposite effect than what was found in the main results and see that small plants have greater variance of scores than large plants. This might occur for a heavily techno-economic optimizing decision-maker, for example. The remaining single-metric-skewed weight profiles exhibit a tighter variance for smaller plants than larger ones as found with the main results, and therefore, that result would hold when a disproportionate amount of weight is placed on these metrics.

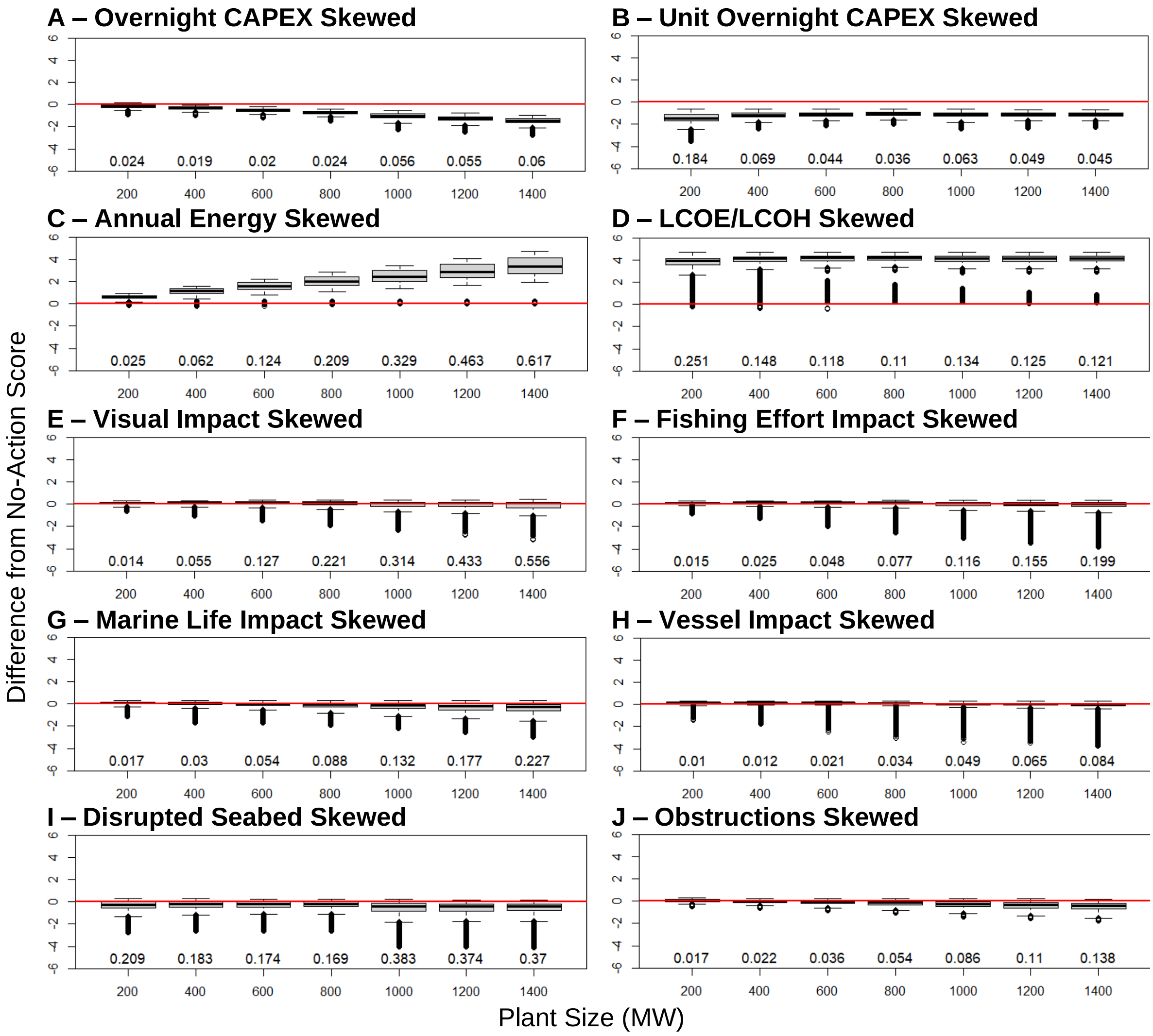

Figure C.8: Effect of single-metric-skewed weights on suitability scores of alternatives. Shown by plant size as the difference from the No-Action score of that weight profile. Numbers below each boxplot give the variance of the suitability scores for alternatives of that plant size.

Appendix D

Supplementary Material for Chapter IV

D.1 Sensitivity analysis results

The baseline outcomes from the model are provided in Table D.1. The three outcomes considered are: the LCOE of Topology A in EUR/MJ, the difference between the LCOE of Topology C and Topology A in EUR/MJ, and the difference between the LCOE of Topology B and Topology A in EUR/MJ.

Table D.1: Baseline outcome for the sensitivity analysis.

Baseline Outcome A: Topology A [EUR/MJ]	0.0164
Baseline Outcome B: Topology C Difference [EUR/MJ]	0.0247
Baseline Outcome C: Topology B Difference [EUR/MJ]	0.0126

The detailed sensitivity analysis results of the low input values is given in Table D.2, and the detailed sensitivity analysis results of the high input values is given in Table D.3 below.

Table D.2: Results of the low inputs of the sensitivity analysis.

Parameter	**Baseline Value of Input**	**Low value of input (%)**	**Outcome A [EUR/MJ] (%)**	**Outcome B [EUR/MJ] (%)**	**Outcome C [EUR/MJ] (%)**
Discount Rate [%]	**5.2%**	2.0% (-61.5%)	0.0148 (-10%)	0.0207 (-16%)	0.0103 (-18%)
Years of lag [Years]	**10**	3 (-70%)	0.0164 (0%)	0.0248 (0%)	0.0126 (0%)
Distance to shore [km]	**20**	5 (-75%)	0.0162 (-1%)	0.0249 (+1%)	0.0127 (+1%)
Electricity cost [EUR/MWh]	**33**	29 (-12%)	0.0152 (-7%)	0.0235 (-5%)	0.0121 (-4%)
Topology A Curtailment [%]	**5%**	2% (-60%)	0.0159 (-3%)	0.0253 (+2%)	0.0131 (+4%)
Electrolyzer efficiency [%]	**64.20%**	62% (-3.4%)	0.0164 (0%)	0.0262 (+6%)	0.0137 (+9%)
Pipe cost [EUR/MW]	**615**	500 (-18.7%)	0.0164 (0%)	0.0248 (0%)	0.0126 (0%)
Electrolyzer cost [EUR/MW]	**1519000**	1198000 (-21.1%)	0.0164 (0%)	0.0205 (-17%)	0.00963 (-24%)
Project Size [MW]	**1000**	100 (-90%)	0.0166 (1%)	0.0308 (+25%)	0.0138 (+10%)
Ship cost [EUR]	**43000000**	25000000 (-42%)	0.0164 (0%)	0.0245 (-1%)	0.0126 (0%)

Table D.3: Results of the high inputs of the sensitivity analysis.

Parameter	Baseline Value of Input	High value of input	Outcome A [EUR/MJ] (%)	Outcome B [EUR/MJ] (%)	Outcome C [EUR/MJ] (%)
Discount Rate [%]	**5.2%**	10% (+92%)	0.0195 (+19%)	0.0327 (+32%)	0.0172 (+37%)
Years of lag [Years]	**10**	18 (+80%)	0.0189 (+15%)	0.0312 (+26%)	0.0164 (+30%)
Distance to shore [km]	**20**	200 (+900%)	0.0181 (+10%)	0.0231 (-6%)	0.0119 (-6%)
Electricity cost [EUR/MWh]	**33**	35 (+6%)	0.017 (+4%)	0.0254 (+3%)	0.0129 (+2%)
Topology A Curtailment [%]	**5%**	30% (+500%)	0.0222 (+35%)	0.01894 (-23%)	0.00678 (-46%)
Electrolyzer efficiency [%]	**64.20%**	70% (+9%)	0.0164 (0%)	0.0214 (-13%)	0.0102 (-19%)
Pipe cost [EUR/MW]	**615**	700 (+14%)	0.0164 (0%)	0.0248 (0%)	0.0127 (+1%)
Electrolyzer cost [EUR/MW]	**1519000**	1926000 (+27%)	0.0164 (0%)	0.0301 (+22%)	0.0165 (+31%)
Project Size [MW]	**1000**	2000 (+100%)	0.0164 (0%)	0.0245 (-1%)	0.0126 (0%)
Ship cost [EUR]	**43000000**	80000000 (+86%)	0.0164 (0%)	0.0253 (+2%)	0.0126 (0%)

The spider plot of the results provided in the above tables in depicted in Figure D.1 below for Topology A vs C and Figure D.2 below for Topology A vs B.

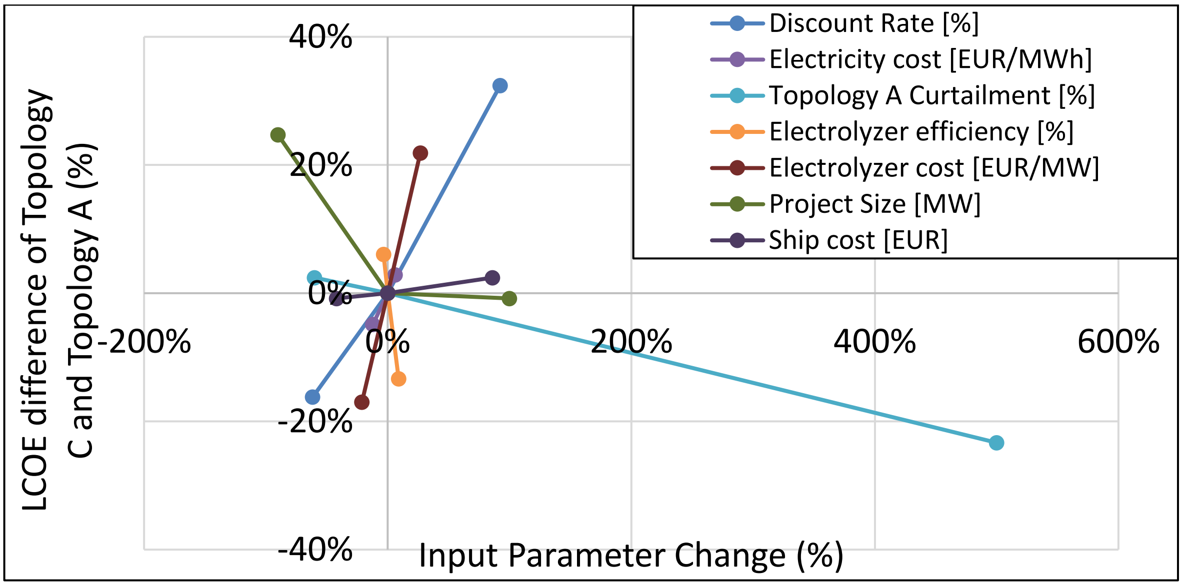

Figure D.1: Spider plot of sensitivity of LCOE difference between Topology A and Topology C to various parameters.

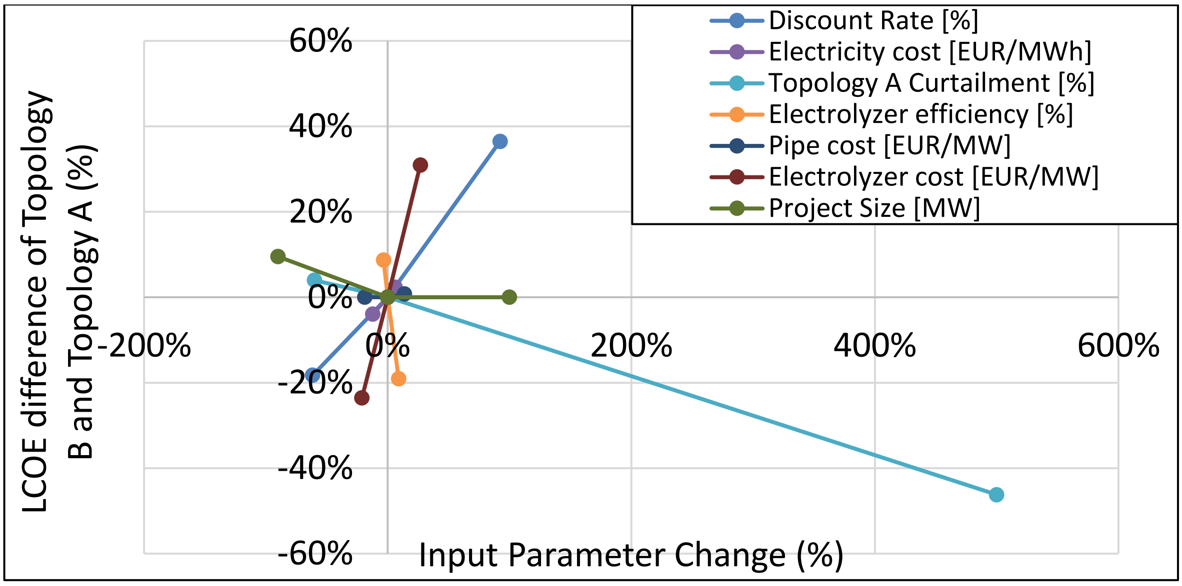

Figure D.2: Spider plot of sensitivity of LCOE difference between Topology A and Topology B to various parameters.

Bibliography

[1] World Meteorological Organization, *The Global Climate 2011-2020: A Decade of Accelerating Climate Change*. 2023.

[2] United Nations Environment Programme, *Emissions Gap Report 2023: Broken Record – Temperatures hit new highs, yet world fails to cut emissions (again)*. United Nations Environment Programme, 2023. doi: 10.59117/20.500.11822/43922.

[3] IEA, "Tracking Clean Energy Progress," Jul. 2023. Accessed: May 16, 2023. [Online]. Available: https://www.iea.org/reports/tracking-clean-energy-progress-2023#whats-on-track

[4] IEA, "Offshore Wind Outlook 2019," Paris, 2019.

[5] W. Musial *et al.*, "Offshore Wind Market Report: 2021 Edition," 2021.

[6] GWEC, "Global Wind Report: Annual market update 2010," Apr. 2011.

[7] Navigant Consulting Inc., "Offshore Wind Market and Economic Analysis Annual Market Assessment," Feb. 2013. Accessed: May 12, 2023. [Online]. Available: www.navigant.com

[8] IRENA, "Renewable Capacity Statistics 2023," Abu Dhabi, 2023. Accessed: Mar. 05, 2024. [Online]. Available: www.irena.org

[9] A. Odenweller, F. Ueckerdt, G. F. Nemet, M. Jensterle, and G. Luderer, "Probabilistic feasibility space of scaling up green hydrogen supply," *Nature Energy 2022 7:9*, vol. 7, no. 9, pp. 854–865, Sep. 2022, doi: 10.1038/s41560-022-01097-4.

[10] GWEC, "Global Wind Report 2023," Brussels, Mar. 2023.

[11] IRENA, *Renewable Power Generation Costs in 2021*. 2022. [Online]. Available: https://www.irena.org/-/media/Files/IRENA/Agency/Publication/2018/Jan/IRENA_2017_Power_Costs_2018.pdf

[12] I. Mignon and A. Bergek, "System- and actor-level challenges for diffusion of renewable electricity technologies: an international comparison," *J Clean Prod*, vol. 128, pp. 105–115, Aug. 2016, doi: 10.1016/J.JCLEPRO.2015.09.048.

[13] D. Toke, S. Breukers, and M. Wolsink, "Wind power deployment outcomes: How can we account for the differences?," *Renewable and Sustainable Energy Reviews*, vol. 12, no. 4, pp. 1129–1147, May 2008, doi: 10.1016/J.RSER.2006.10.021.

[14] A. Gumber, R. Zana, and B. Steffen, "A global analysis of renewable energy project commissioning timelines," *Appl Energy*, vol. 358, p. 122563, Mar. 2024, doi: 10.1016/J.APENERGY.2023.122563.

[15] R. Wüstenhagen, M. Wolsink, and M. J. Bürer, "Social acceptance of renewable energy innovation: An introduction to the concept," *Energy Policy*, vol. 35, no. 5, pp. 2683–2691, May 2007, doi: 10.1016/J.ENPOL.2006.12.001.

[16] U.S. DOE, "Offshore Wind Energy Strategies Regional and national strategies to accelerate and maximize the effectiveness, reliability, and sustainability of U.S. offshore wind energy deployment and operation," Washington D.C., Jan. 2022.

[17] R. Fairgrieve, K. Wellard, and C. Trigg, "Floating Offshore Wind Development and Consenting Process: Risks and Opportunities," Jul. 2021.

[18] IEA, "Offshore Wind Outlook 2019," Paris, 2019. [Online]. Available: https://www.iea.org/reports/offshore-wind-outlook-2019

[19] U.S. DOE, "2018 Offshore Wind Technologies Market Report," Oak Ridge, TN, 2018.

[20] P. Beiter *et al.*, "The Cost of Floating Offshore Wind Energy in California Between 2019 and 2032," Golden, CO (United States), 2020. doi: NREL/TP-5000-77384.

[21] W. Musial, D. Heimiller, P. Beiter, G. Scott, and C. Draxl, "2016 Offshore Wind Energy Resource Assessment for the United States," Sep. 2016.

[22] European Marine Observation and Data Network, "EMODnet Human Activities." Accessed: Dec. 02, 2020. [Online]. Available: https://www.emodnet-humanactivities.eu/view-data.php

[23] M. Chen *et al.*, "Study on Mooring Design of 15 MW Floating Wind Turbines in South China Sea," *J Mar Sci Eng*, vol. 12, no. 1, p. 33, Dec. 2023, doi: 10.3390/jmse12010033.

[24] Y. Jiang, Y. Duan, J. Li, M. Chen, and X. Zhang, "Optimization of mooring systems for a 10MW semisubmersible offshore wind turbines based on neural network," *Ocean Engineering*, vol. 296, p. 117020, Mar. 2024, doi: 10.1016/J.OCEANENG.2024.117020.

[25] M. Chen, C. B. Li, Z. Han, and J. bin Lee, "A simulation technique for monitoring the real-time stress responses of various mooring configurations for offshore floating wind turbines," *Ocean Engineering*, vol. 278, p. 114366, Jun. 2023, doi: 10.1016/J.OCEANENG.2023.114366.

[26] V. Harnois, H. C. M. Smith, S. Benjamins, and L. Johanning, "Assessment of entanglement risk to marine megafauna due to offshore renewable energy mooring systems," *International Journal of Marine Energy*, vol. 11, pp. 27–49, 2015, doi: 10.1016/J.IJOME.2015.04.001.

[27] S. Benjamins *et al.*, "Understanding the potential for marine megafauna entanglement risk from renewable marine energy developments," 2014.

[28] A. Broad, M. J. Rees, and A. R. Davis, "Anchor and chain scour as disturbance agents in benthic environments: trends in the literature and charting a course to more sustainable boating and shipping," *Mar Pollut Bull*, vol. 161, no. August, p. 111683, 2020, doi: 10.1016/j.marpolbul.2020.111683.

[29] H. Farr, B. Ruttenberg, R. K. Walter, Y. H. Wang, and C. White, "Potential environmental effects of deepwater floating offshore wind energy facilities," *Ocean Coast Manag*, vol. 207, no. February, p. 105611, 2021, doi: 10.1016/j.ocecoaman.2021.105611.

[30] Offshore Engineering, "Introduction to DP Systems - What is a Dynamic Positioning." Accessed: Nov. 24, 2020. [Online]. Available: https://www.offshoreengineering.com/education/dynamic-positioning-dp/what-is-dynamic-positioning

[31] S. Xu, M. Murai, X. Wang, and K. Takahashi, "A novel conceptual design of a dynamically positioned floating wind turbine," *Ocean Engineering*, vol. 221, no. December 2020, p. 108528, 2021, doi: 10.1016/j.oceaneng.2020.108528.

[32] P. Connolly and C. Crawford, "Analytical modelling of power production from Unmoored Floating Offshore Wind Turbines," *Ocean Engineering*, vol. 259, p. 111794, Sep. 2022, doi: 10.1016/J.OCEANENG.2022.111794.

[33] M. Ikhennicheu *et al.*, "Corewind Review of the state of the art of mooring and anchoring designs 2," Feb. 2020.

[34] R. Alwan, A. Babarit, and J. C. Gilloteaux, "Investigation of a dynamically positioned floating offshore wind turbine concept," in *Journal of Physics: Conference Series*, IOP Publishing Ltd, Sep. 2021. doi: 10.1088/1742-6596/2018/1/012001.

[35] P. Connolly and C. Crawford, "Comparison of optimal power production and operation of unmoored floating offshore wind turbines and energy ships," *Wind Energ. Sci*, vol. 8, pp. 725–746, 2023, doi: 10.5194/wes-8-725-2023.

[36] C. Allen *et al.*, "Definition of the UMaine Volturn US-S Reference Platform Developed for the IEA Wind 15-Megawatt Offshore Reference Wind Turbine," 2020.

[37] E. Gaertner *et al.*, "Definition of the IEA Wind 15-Megawatt Offshore Reference Wind Turbine Technical Report," 2020. Accessed: Jul. 24, 2020. [Online]. Available: www.nrel.gov/publications.

[38] J. Jonkman, S. Butterfield, W. Musial, and G. Scott, "Definition of a 5-MW reference wind turbine for offshore system development," 2009. [Online]. Available: http://tethys-development.pnnl.gov/sites/default/files/publications/Jonkman_et_al_2009.pdf

[39] C. Desmond, J. Murphy, L. Blonk, and W. Haans, "Description of an 8 MW reference wind turbine," *J Phys Conf Ser*, vol. 753, no. 9, 2016, doi: 10.1088/1742-6596/753/9/092013.

[40] P. Bortolotti *et al.*, "IEA Wind Task 37 on Systems Engineering in Wind Energy - WP2.1 Reference Wind Turbines: Technical Report," 2019. doi: https://doi.org/10.2172/1529216.

[41] DNV GL, "DNVGL-ST-0119 Floating wind turbine structures," Jul. 2018.

[42] ABS, "Guide for Building and Classifying Floating Offshore Wind Turbine Installations," Jan. 2013.

[43] F. D. Bianchi, H. De Battista, and R. J. Mantz, *Wind Turbine Control Systems - Principles, Modelling and Gain Scheduling Design*, vol. 53, no. 9. London: Springer-Verlag, 2007.

[44] M. S. Longuet-Higgins, "The Mean Forces Exerted by Waves on Floating or Submerged Bodies with Applications to Sand Bars and Wave Power Machines," *Proc R Soc Lond A Math Phys Sci*, vol. 352, no. 1671, pp. 463–480, 1977.

[45] S. Xu, B. Li, X. Wang, and L. Wang, "A novel real-time estimate method of wave drift force for wave feed-forward in dynamic positioning system," *Ships and Offshore Structures*, vol. 11, no. 7, pp. 747–756, Oct. 2016, doi: 10.1080/17445302.2015.1062334.

[46] E. Konstantinidis and D. Bouris, "Drag and inertia coefficients for a circular cylinder in steady plus low-amplitude oscillatory flows," *Applied Ocean Research*, vol. 65, pp. 219–228, Apr. 2017, doi: 10.1016/J.APOR.2017.04.010.

[47] J. Roald, A. Robertson, and N. Chokani, “The effect of second-order hydrodynamics on floating offshore wind turbines Conference Paper,” *Energy Procedia*, vol. 35, pp. 253–264, 2013, doi: 10.3929/ethz-b-000072587.

[48] B. Y. Dagli, I. Tuskan, and U. GökkusGökkus, “Evaluation of Offshore Wind Turbine Tower Dynamics with Numerical Analysis,” *Advances in Civil Engineering*, vol. 2018, 2018, doi: 10.1155/2018/3054851.

[49] J. Bosboom and M. Stive, *Coastal Dynamics*. TU Delft Open, 2021. doi: 10.5074/T.2021.001.

[50] myweather2.com, “Marine weather forecast for Off Figueira Da Foz | Marine | Portugal, Coastal Areas.” Accessed: Mar. 02, 2021. [Online]. Available: https://www.myweather2.com/Marine/Coastal-Areas/Portugal/Off-Figueira-Da-Foz.aspx?sday=0&eday=7

[51] myweather2.com, “Marine weather forecast for Morro Bay | Marine | United States of America, Global Ports.” Accessed: Jun. 21, 2022. [Online]. Available: https://www.myweather2.com/Marine/Global-Ports/United-States-of-America/Morro-Bay.aspx?sday=0&eday=7#

[52] T. C.A. Oliveira, E. Cagnin, and P. A. Silva, “Wind-waves in the coast of mainland Portugal induced by post-tropical storms,” *Ocean Engineering*, vol. 217, no. January, p. 108020, 2020, doi: 10.1016/j.oceaneng.2020.108020.

[53] J. C. Berg, “Extreme Ocean Wave Conditions for Northern California Wave Energy Conversion Device,” *Sandia National Laboratories*, 2011.

[54] Simis.io, “Ashes.” [Online]. Available: https://www.simis.io/

[55] J. E. Weber, “Steady Wind- and Wave-Induced Currents in the Open Ocean,” *J Phys Oceanogr*, vol. 13, pp. 524–530, 1982.

[56] Orcina, “OrcaFlex - dynamic analysis software for offshore marine systems.” Accessed: Nov. 22, 2021. [Online]. Available: https://www.orcina.com/orcaflex/

[57] Vice President (Personal Communication), “Kongsberg Thruster Specifications.” 2021.

[58] ABS, “Guide for Dynamic Positioning Systems,” Spring, TX, 2020.

[59] R. M. Campos and C. Guedes Soares, “Spatial distribution of offshore wind statistics on the coast of Portugal using Regional Frequency Analysis,” *Renew Energy*, vol. 123, pp. 806–816, 2018, doi: 10.1016/j.renene.2018.02.051.

[60] NREL, “Offshore Wind Annual Technology Baseline,” Annual Technology Baseline: Offshore Wind. Accessed: Nov. 05, 2021. [Online]. Available: https://atb.nrel.gov/electricity/2021/offshore_wind

[61] N. Avanessova, A. Gray, I. Lazakis, R. C. Thomson, and G. Rinaldi, “Analysing the effectiveness of different offshore maintenance base options for floating wind farms,” *Wind Energy Science*, vol. 7, no. 2, pp. 887–901, 2022, doi: 10.5194/wes-7-887-2022.

[62] R. James and M. C. Ros, “Floating Offshore Wind: Market and Technology Review Important notice and disclaimer,” London, Jun. 2015.

[63] S. F. Rodrigues, R. Teixeira Pinto, M. Soleimanzadeh, P. A. N. Bosman, and P. Bauer, “Wake losses optimization of offshore wind farms with moveable floating wind

turbines," *Energy Convers Manag*, vol. 89, pp. 933–941, Jan. 2015, doi: 10.1016/J.ENCONMAN.2014.11.005.

[64] W. H. Huang and R. Y. Yang, "Water depth variation influence on the mooring line design for fowt within shallow water region," *J Mar Sci Eng*, vol. 9, no. 4, 2021, doi: 10.3390/jmse9040409.

[65] Daihan Anchor Chain Mfg. Co. Ltd., "Proof & Breaking Loads for Studless Link Mooring Chain (I)." Accessed: Nov. 11, 2020. [Online]. Available: http://www.dhac.co.kr/m32.php?pn=3&sn=2&sn2=1

[66] B. Saunders and R. Nagamune, "Fatigue Load Minimization for a Position-Controlled Floating Offshore Wind Turbine," *Journal of Marine Science and Engineering 2023, Vol. 11, Page 2274*, vol. 11, no. 12, p. 2274, Nov. 2023, doi: 10.3390/JMSE11122274.

[67] M. Shields, P. Beiter, J. Nunemaker, A. Cooperman, and P. Duffy, "Impacts of turbine and plant upsizing on the levelized cost of energy for offshore wind," *Appl Energy*, vol. 298, p. 117189, Sep. 2021, doi: 10.1016/J.APENERGY.2021.117189.

[68] U.S. DOE, "Offshore Wind Technologies Market Report," 2018.

[69] B. Sweerts, R. J. Detz, and B. van der Zwaan, "Evaluating the Role of Unit Size in Learning-by-Doing of Energy Technologies," *Joule*, vol. 4, no. 5, pp. 967–970, 2020, doi: 10.1016/j.joule.2020.03.010.

[70] C. Wilson, A. Grubler, N. Bento, S. Healey, S. De Stercke, and C. Zimm, "Granular technologies to accelerate decarbonization," *Science (1979)*, vol. 368, no. 6486, pp. 36–39, 2020, doi: 10.1126/science.aaz8060.

[71] D. Morrisey, M. Cameron, E. Newcombe, and C. Cornelisen, "Effects of Moorings on Different Types of Marine Habitat," Jan. 2018.

[72] ICF, "Comparison of Environmental Effects from Different Offshore Wind Turbine Foundations," Sterling, VA, 2020. [Online]. Available: https://www.boem.gov/sites/default/files/documents/environment/Wind-Turbine-Foundations-White Paper-Final-White-Paper.pdf

[73] R. P. Schoeman, C. Patterson-Abrolat, and S. Plön, "A Global Review of Vessel Collisions With Marine Animals," *Front Mar Sci*, vol. 7, p. 292, May 2020, doi: 10.3389/FMARS.2020.00292/BIBTEX.

[74] C. M. Duarte *et al.*, "The soundscape of the Anthropocene ocean," *Science* , vol. 371, no. 6529, Feb. 2021, doi: 10.1126/science.aba4658.

[75] MIT Lincoln Laboratory, "Innovation Highlight: Toroidal Propeller," 2022.

[76] White & Case, "Offshore wind projects: Assessing the environmental impact," 2019.

[77] J. L. Rebecca Williams, Feng Zhao, "Global Offshore Wind Report 2022," *Global Wind Energy Council*, pp. 86–88, 2022, [Online]. Available: https://gwec.net/wp-content/uploads/2021/03/GWEC-Global-Wind-Report-2021.pdf

[78] European Commission, "Communication from the Commission to the European Parliament, the Council, the European Economic and Social Committee and the Committee of the Regions - An EU Strategy to Harness the Potential of Offshore Renewable Energy for a Climate Neutral Future," Brussels, Nov. 2020. [Online]. Available: https://ec.europa.eu/energy/topics/energy-system-integration/eu-strategy-energy-system-integration_en

[79] Biden Administration, “Fact Sheet: Biden Administration Jumpstarts Offshore Wind Energy Projects to Create Jobs,” The White House, Mar. 2021. Accessed: Nov. 21, 2021. [Online]. Available: https://www.whitehouse.gov/briefing-room/statements-releases/2021/03/29/fact-sheet-biden-administration-jumpstarts-offshore-wind-energy-projects-to-create-jobs/

[80] W. Musial *et al.*, “Offshore Wind Market Report: 2022 Edition,” 2022. Accessed: Apr. 13, 2023. [Online]. Available: https://www.energy.gov/eere/wind/articles/offshore-wind-market-report-2022-edition

[81] BOEM, “Cape Wind.” Accessed: Feb. 15, 2023. [Online]. Available: https://www.boem.gov/renewable-energy/studies/cape-wind

[82] M. Froese, “Lessons learned from Cape Wind.” Accessed: Nov. 05, 2020. [Online]. Available: https://www.windpowerengineering.com/lessons-learned-from-cape-wind/

[83] BOEM, “Delaware Activities.” Accessed: Feb. 15, 2023. [Online]. Available: https://www.boem.gov/renewable-energy/state-activities/delaware-activities

[84] J. Quilter, “NRG halts Bluewater Wind Delaware offshore project | Windpower Monthly.” Accessed: Feb. 15, 2023. [Online]. Available: https://www.windpowermonthly.com/article/1108978/nrg-halts-bluewater-wind-delaware-offshore-project

[85] K. Leslie, “Navy concerned about offshore wind turbines in Morro Bay, CA,” *San Luis Obispo Tribune*, Mar. 21, 2019. Accessed: Jun. 14, 2022. [Online]. Available: https://www.sanluisobispo.com/news/local/article228249684.html

[86] *United States District Court for the District of Columbia (Case No. 22-237)*. 2022. Accessed: Feb. 14, 2023. [Online]. Available: https://www.boem.gov/sites/default/files/documents/renewable-energy/state-activities/USACE-

[87] B. Crowley, “Avangrid Cancels Park City Wind Contract, Pays State $16m Penalty - CT Examiner,” CT Examiner. Accessed: Jan. 16, 2024. [Online]. Available: https://ctexaminer.com/2023/10/03/avangrid-cancels-park-city-wind-contract-pays-state-16m-penalty/

[88] S. Wolfe, “SouthCoast Wind agrees to pay $60M to scrap power purchase agreements,” Renewable Energy World. Accessed: Jan. 16, 2024. [Online]. Available: https://www.renewableenergyworld.com/wind-power/offshore/southcoast-wind-agrees-to-pay-60m-to-scrap-power-purchase-agreements/#gref

[89] E. W. Merrow, “Understanding the Outcomes of Megaprojects,” Santa Monica, CA, 1988.

[90] A. M. O’Hagan, “2020 State of the Science Report, Chapter 11: Marine Spatial Planning and Marine Renewable Energy,” Richland, WA (United States), Sep. 2020. doi: 10.2172/1633204.

[91] G. Paolinelli, L. Fortuna, L. Marinaro, and A. Valentini, “On marine wind power expressiveness: Not just an issue of visual impact,” *Front Energy Res*, vol. 10, Sep. 2022, doi: 10.3389/fenrg.2022.937828.

[92] J. Ladenburg and S. Lutzeyer, “The economics of visual disamenity reductions of offshore wind farms—Review and suggestions from an emerging field,” *Renewable*

and Sustainable Energy Reviews, vol. 16, no. 9, pp. 6793–6802, Dec. 2012, doi: 10.1016/J.RSER.2012.08.017.

[93] A. Cranmer, A. E. Broughel, J. Ericson, M. Goldberg, and K. Dharni, “Getting to 30 GW by 2030: Visual preferences of coastal residents for offshore wind farms on the US East Coast,” *Energy Policy*, vol. 173, p. 113366, Feb. 2023, doi: 10.1016/J.ENPOL.2022.113366.

[94] J. Ladenburg and A. Dubgaard, “Willingness to pay for reduced visual disamenities from offshore wind farms in Denmark,” *Energy Policy*, vol. 35, no. 8, pp. 4059–4071, Aug. 2007, doi: 10.1016/J.ENPOL.2007.01.023.

[95] K. Ek and L. Persson, “Wind farms - Where and how to place them? A choice experiment approach to measure consumer preferences for characteristics of wind farm establishments in Sweden,” *Ecological Economics*, vol. 105, pp. 193–203, 2014, doi: 10.1016/j.ecolecon.2014.06.001.

[96] A. D. Krueger, G. R. Parsons, and J. Firestone, “Valuing the Visual Disamenity of Offshore Wind Power Projects at Varying Distances from the Shore: An Application on the Delaware Shoreline,” 2011.

[97] A. Carr-Harris and C. Lang, “Sustainability and tourism: the effect of the United States’ first offshore wind farm on the vacation rental market,” *Resour Energy Econ*, vol. 57, pp. 51–67, Aug. 2019, doi: 10.1016/J.RESENEECO.2019.04.003.

[98] M. F. Teisl, C. L. Noblet, R. R. Corey, and N. A. Giudice, “Seeing clearly in a virtual reality: Tourist reactions to an offshore wind project,” *Energy Policy*, vol. 122, pp. 601–611, Nov. 2018, doi: 10.1016/J.ENPOL.2018.08.018.

[99] S. Lutzeyer, D. J. Phaneuf, and L. O. Taylor, “The amenity costs of offshore wind farms: Evidence from a choice experiment,” *Energy Econ*, vol. 72, pp. 621–639, May 2018, doi: 10.1016/J.ENECO.2018.03.020.

[100] C. E. Landry, T. Allen, T. Cherry, and J. C. Whitehead, “Wind turbines and coastal recreation demand,” *Resour Energy Econ*, vol. 34, no. 1, pp. 93–111, Jan. 2012, doi: 10.1016/J.RESENEECO.2011.10.001.

[101] G. Parsons, J. Firestone, L. Yan, and J. Toussaint, “The effect of offshore wind power projects on recreational beach use on the east coast of the United States: Evidence from contingent-behavior data,” *Energy Policy*, vol. 144, p. 111659, Sep. 2020, doi: 10.1016/J.ENPOL.2020.111659.

[102] T. Börger, T. L. Hooper, and M. C. Austen, “Valuation of ecological and amenity impacts of an offshore windfarm as a factor in marine planning,” *Environ Sci Policy*, vol. 54, pp. 126–133, Dec. 2015, doi: 10.1016/j.envsci.2015.05.018.

[103] K. Samoteskul, J. Firestone, J. Corbett, and J. Callahan, “Changing vessel routes could significantly reduce the cost of future offshore wind projects,” *J Environ Manage*, vol. 141, pp. 146–154, 2014, doi: 10.1016/j.jenvman.2014.03.026.

[104] P. Hoagland, T. M. Dalton, D. Jin, and J. B. Dwyer, “An approach for analyzing the spatial welfare and distributional effects of ocean wind power siting: The Rhode Island/Massachusetts area of mutual interest,” *Mar Policy*, vol. 58, pp. 51–59, Aug. 2015, doi: 10.1016/J.MARPOL.2015.04.010.

[105] L. C. Stokes, E. I. Franzblau, J. R. Lovering ID, and C. Miljanich, “Prevalence and predictors of wind energy opposition in North America,” 2023, doi: 10.1073/pnas.

[106] S. Fast *et al.*, “Lessons learned from Ontario wind energy disputes,” *Nat Energy*, vol. 1, no. 2, pp. 1–7, Feb. 2016, doi: 10.1038/nenergy.2015.28.

[107] C. Emery, T. Garcia, and C. Ortega, “Social Impacts to Other Communities that Experienced Offshore Wind,” Humboldt, CA, Sep. 2020. Accessed: Jan. 20, 2024. [Online]. Available: schatzcenter.org/pubs/2020-OSW-R20.pdf

[108] M. Deveci, E. Özcan, R. John, C.-F. Covrig, and D. Pamucar, “A study on offshore wind farm siting criteria using a novel interval-valued fuzzy-rough based Delphi method,” *J Environ Manage*, vol. 270, no. May, p. 110916, Sep. 2020, doi: 10.1016/j.jenvman.2020.110916.

[109] S. J. W. Klein and S. Whalley, “Comparing the sustainability of U.S. electricity options through multi-criteria decision analysis,” *Energy Policy*, vol. 79, pp. 127–149, 2015, doi: 10.1016/j.enpol.2015.01.007.

[110] M. Deveci, E. Özcan, R. John, D. Pamucar, and H. Karaman, “Offshore wind farm site selection using interval rough numbers based Best-Worst Method and MARCOS,” *Appl Soft Comput*, vol. 109, p. 107532, 2021, doi: 10.1016/j.asoc.2021.107532.

[111] M. Deveci, N. Erdogan, U. Cali, J. Stekli, and S. Zhong, “Type-2 neutrosophic number based multi-attributive border approximation area comparison (MABAC) approach for offshore wind farm site selection in USA,” *Eng Appl Artif Intell*, vol. 103, no. October 2020, p. 104311, 2021, doi: 10.1016/j.engappai.2021.104311.

[112] A. Fetanat and E. Khorasaninejad, “A novel hybrid MCDM approach for offshore wind farm site selection: A case study of Iran,” *Ocean Coast Manag*, vol. 109, pp. 17–28, 2015, doi: 10.1016/j.ocecoaman.2015.02.005.

[113] A. D. Mekonnen and P. V. Gorsevski, “A web-based participatory GIS (PGIS) for offshore wind farm suitability within Lake Erie, Ohio,” *Renewable and Sustainable Energy Reviews*, vol. 41, pp. 162–177, 2015, doi: 10.1016/J.RSER.2014.08.030.

[114] Z. Li, G. Tian, and A. S. El-Shafay, “Statistical-analytical study on world development trend in offshore wind energy production capacity focusing on Great Britain with the aim of MCDA based offshore wind farm siting,” *J Clean Prod*, vol. 363, no. March, p. 132326, 2022, doi: 10.1016/j.jclepro.2022.132326.

[115] M. S. Genç, F. Karipoğlu, K. Koca, and Ş. T. Azgın, “Suitable site selection for offshore wind farms in Turkey’s seas: GIS-MCDM based approach,” *Earth Sci Inform*, vol. 14, no. 3, pp. 1213–1225, 2021, doi: 10.1007/s12145-021-00632-3.

[116] M. Shao, Z. Han, J. Sun, C. Xiao, S. Zhang, and Y. Zhao, “A review of multi-criteria decision making applications for renewable energy site selection,” *Renew Energy*, vol. 157, pp. 377–403, 2020, doi: 10.1016/j.renene.2020.04.137.

[117] P. Beiter *et al.*, “The Cost of Floating Offshore Wind Energy in California Between 2019 and 2032,” Golden, CO (United States), 2020. doi: NREL/TP-5000-77384.

[118] N. Maslov, C. Claramunt, T. Wang, and T. Tang, “Method to estimate the visual impact of an offshore wind farm,” *Appl Energy*, vol. 204, pp. 1422–1430, 2017, doi: 10.1016/j.apenergy.2017.05.053.

[119] *Submerged Lands Act*. 2002.

[120] Unites States Coast Guard, “The Areas Offshore of Massachusetts and Rhode Island Port Access Route Study,” 2020. [Online]. Available:

https://www.federalregister.gov/documents/2020/05/27/2020-11262/port-access-route-study-the-areas-offshore-of-massachusetts-and-rhode-island

[121] GEBCO Bathymetric Compilation Group 2020, "The GEBCO_2020 Grid - a continuous terrain model of the global oceans and land."

[122] Data.gov, "Submarine Cable Lines (USACE IENC) - Catalog." Accessed: May 22, 2023. [Online]. Available: https://catalog.data.gov/dataset/submarine-cable-lines-usace-ienc

[123] NOAA National Marine Protected Areas Center, "The MPA Inventory." Accessed: Sep. 30, 2022. [Online]. Available: https://marineprotectedareas.noaa.gov/dataanalysis/mpainventory/

[124] *Shipping safety fairways and anchorage areas, Gulf of Mexico*. Accessed: Jan. 19, 2024. [Online]. Available: https://www.ecfr.gov/current/title-33/chapter-I/subchapter-P/part-166/subpart-B/section-166.200

[125] *Areas along the coast of California*. Accessed: Jan. 19, 2024. [Online]. Available: https://www.ecfr.gov/current/title-33/chapter-I/subchapter-P/part-166/subpart-B/section-166.300

[126] *Areas along the coast of Alaska*. Accessed: Jan. 19, 2024. [Online]. Available: https://www.ecfr.gov/current/title-33/chapter-I/subchapter-P/part-166/subpart-B/section-166.400

[127] *Areas along the Atlantic Coast*. Accessed: Jan. 19, 2024. [Online]. Available: https://www.ecfr.gov/current/title-33/chapter-I/subchapter-P/part-166/subpart-B/section-166.500

[128] N. O. and A. A. US Department of Commerce, "De Facto Marine Protected Areas," National Marine Protected Areas Center. Accessed: Jan. 24, 2024. [Online]. Available: https://marineprotectedareas.noaa.gov/dataanalysis/defacto/

[129] Global Fishing Watch, "Data download portal." Accessed: Jun. 13, 2022. [Online]. Available: https://globalfishingwatch.org/data-download/

[130] NREL, "The Wind Prospector." Accessed: Dec. 11, 2020. [Online]. Available: https://maps.nrel.gov/?da=wind-prospector

[131] MarineCadastre.gov, "Data Registry." Accessed: May 22, 2023. [Online]. Available: https://marinecadastre.gov/data/

[132] OBIS, "Ocean Biodiversity Information System - Data Access." Accessed: Jan. 10, 2023. [Online]. Available: https://obis.org/data/access/#

[133] P. Provoost, "Diversity indicators using OBIS data." Accessed: Dec. 22, 2022. [Online]. Available: https://iobis.github.io/notebook-diversity-indicators/

[134] W. H. Huang and R. Y. Yang, "Water depth variation influence on the mooring line design for fowt within shallow water region," *J Mar Sci Eng*, vol. 9, no. 4, 2021, doi: 10.3390/jmse9040409.

[135] Daihan Anchor Chain Mfg. Co. Ltd., "Proof & Breaking Loads for Studless Link Mooring Chain (I)." Accessed: Nov. 11, 2020. [Online]. Available: http://www.dhac.co.kr/m32.php?pn=3&sn=2&sn2=1

[136] V. Harnois, H. C. M. Smith, S. Benjamins, and L. Johanning, "Assessment of entanglement risk to marine megafauna due to offshore renewable energy mooring

systems," *International Journal of Marine Energy*, vol. 11, pp. 27–49, 2015, doi: 10.1016/J.IJOME.2015.04.001.

[137] Q. Pan, M. Y. Mahfouz, and F. Lemmer, "Assessment of mooring configurations for the IEA 15MW floating offshore wind turbine," *J Phys Conf Ser*, p. 12030, 2018, doi: 10.1088/1742-6596/2018/1/012030.

[138] US DOI - Bureau of Safety and Environmental Enforcement, "Offshore Wind Submarine Cable Spacing Guidance," Dec. 2014.

[139] D. Engberg, J. Cohon, and C. ReVelle, "Multiobjective modeling for OCS Pipeline Systems," in *The Second Symposium on Management, Conservation and Utilization of the Coastal Zone*, Hollywood, FL, 1980.

[140] D. Engberg, E. Linke, J. Cohon, and C. ReVelle, "Siting an Offshore Natural Gas Pipeline Using a Mathematical Model," *National Development*, 1982.

[141] X. Xiang *et al.*, "Comparison of cost-effective distances for LFAC with HVAC and HVDC in their connections for offshore and remote onshore wind energy," *CSEE Journal of Power and Energy Systems*, vol. 7, no. 5, pp. 954–975, Sep. 2021, doi: 10.17775/CSEEJPES.2020.07000.

[142] NREL, "Offshore Wind Annual Technology Baseline," Annual Technology Baseline: Offshore Wind. Accessed: Nov. 05, 2021. [Online]. Available: https://atb.nrel.gov/electricity/2021/offshore_wind

[143] Lazard, "Levelized Cost of Energy+," 2023.

[144] A. Aytekin, "Comparative Analysis of the Normalization Techniques in the Context of MCDM Problems," *Decision Making: Applications in Management and Engineering*, vol. 4, no. 2, pp. 1–25, Mar. 2021, doi: 10.31181/dmame210402001a.

[145] A. R. Krishnan, "Past efforts in determining suitable normalization methods for multi-criteria decision-making: A short survey," *Front Big Data*, vol. 5, Aug. 2022, doi: 10.3389/fdata.2022.990699.

[146] B. Wu, T. L. Yip, L. Xie, and Y. Wang, "A fuzzy-MADM based approach for site selection of offshore wind farm in busy waterways in China," *Ocean Engineering*, vol. 168, pp. 121–132, Nov. 2018, doi: 10.1016/J.OCEANENG.2018.08.065.

[147] National Academies of Sciences Engineering and Medicine, "Laying the Foundation for New and Advanced Nuclear Reactors in the United States," in *Laying the Foundation for New and Advanced Nuclear Reactors in the United States*, 2023, pp. 155–177. doi: 10.17226/26630.

[148] R. M. Dawes and B. Corrigan, "Linear Models in Decision Making," 1974.

[149] T. Kim, J. Il Park, and J. Maeng, "Offshore wind farm site selection study around Jeju Island, South Korea," *Renew Energy*, vol. 94, pp. 619–628, Aug. 2016, doi: 10.1016/J.RENENE.2016.03.083.

[150] P. Beiter, W. Musial, L. Kilcher, M. Maness, and A. Smith, "An Assessment of the Economic Potential of Offshore Wind in the United States from 2015 to 2030," Mar. 2015. Accessed: Oct. 13, 2023. [Online]. Available: www.nrel.gov/publications.

[151] M. Serreze, "Commercial fisheries sue Biden administration over Vineyard Wind I," Providence Business First. Accessed: Jul. 10, 2022. [Online]. Available: https://www.bizjournals.com/rhodeisland/news/2022/02/01/roda-sues-feds-over-vineyard-wind.html

[152] US Wind, “Construction and Operations Plan: Maryland Offshore Wind Project,” Jul. 2023.

[153] Ocean Wind LLC, “Construction & Operations Plan Ocean Wind Offshore Wind Farm,” May 2023.

[154] Atlantic Shores Offshore Wind, “Atlantic Shores [South] Offshore Wind - Construction and Operations Plan,” May 2023.

[155] Revolution Wind, “Construction & Operations Plan Revolution Wind Farm Volume I,” Mar. 2023.

[156] Equinor, “Empire Wind Project (EW 1 and EW 2) Construction and Operations Plan Volume 1: Project Information,” Jun. 2022.

[157] South Fork Wind, “South Fork Construction and Operations Plan,” May 2021.

[158] Vineyard Wind, “Draft Construction and Operations Plan Volume I,” Sep. 2020.

[159] Sunrise Wind, “Sunrise Wind Farm Project Construction and Operations Plan,” Aug. 2022.

[160] Dominion Energy, “Construction and Operations Plan: Coastal Virginia Offshore Wind Commercial Project,” Feb. 2023. Accessed: May 23, 2023. [Online]. Available: https://www.boem.gov/sites/default/files/documents/renewable-energy/state-activities/Public%20Sec%201-3.pdf

[161] Kitty Hawk Wind LLC, “Construction and Operations Plan - Executive Summary,” Sep. 2022. Accessed: May 23, 2023. [Online]. Available: https://www.whitehouse.gov/briefing-room/statements-releases/2021/03/29/fact-sheet-biden-administration-jumpstarts-offshore-

[162] Park City Wind LLC, “New England Wind Construction and Operations Plan for Lease Area OCS-A 0534 Volume I Text,” Jun. 2022.

[163] Beacon Wind LLC, “Beacon Wind Project: Beacon Wind 1 and Beacon Wind 2 Construction and Operations Plan,” Jun. 2023.

[164] Mayflower Wind, “Construction and Operations Plan Volume 1,” Dec. 2022.

[165] Orsted, “Orsted Ceases Development of Ocean Wind 1 and Ocean Wind 2.” Accessed: Jan. 16, 2024. [Online]. Available: https://oceanwindone.com/news-archive/2023/11/orsted

[166] W. Musial, D. Heimiller, P. Beiter, G. Scott, and C. Draxl, “2016 Offshore Wind Energy Resource Assessment for the United States,” Sep. 2016. Accessed: Oct. 22, 2021. [Online]. Available: www.nrel.gov/publications.

[167] M. J. Costello and C. Chaudhary, “Marine Biodiversity, Biogeography, Deep-Sea Gradients, and Conservation,” *Current Biology*, vol. 27, no. 11, pp. R511–R527, Jun. 2017, doi: 10.1016/J.CUB.2017.04.060.

[168] M. Bolinger, J. Seel, J. M. Kemp, C. Warner, A. Katta, and D. Robson, “Utility-Scale Solar, 2023 Edition,” Oct. 2023. Accessed: Oct. 13, 2023. [Online]. Available: http://utilityscalesolar.lbl.gov

[169] R. Santarromana, A. Abdulla, J. Mendonça, M. Granger Morgan, M. Russo, and R. Haakonsen, “Assessing the costs and benefits of dynamically positioned floating wind turbines to enable expanded deployment,” *Energy Convers Manag*, vol. 306, p. 118301, Apr. 2024, doi: 10.1016/j.enconman.2024.118301.

[170] O. S. Ibrahim, A. Singlitico, R. Proskovics, S. McDonagh, C. Desmond, and J. D. Murphy, "Dedicated large-scale floating offshore wind to hydrogen: Assessing design variables in proposed typologies," *Renewable and Sustainable Energy Reviews*, vol. 160, p. 112310, May 2022, doi: 10.1016/J.RSER.2022.112310.

[171] Congress.gov, *Text - H.R.5376 - 117th Congress (2021-2022): Inflation Reduction Act of 2022*. Washington D.C.: United States House of Representatives, 2022, pp. 1818–2090.

[172] R. M. Dawes, "The robust beauty of improper linear models in decision making," *American Psychologist*, vol. 34, no. 7, pp. 571–582, 1979, doi: 10.1037/0003-066X.34.7.571.

[173] European Commission, "Commission Recommendation of 18.5.2022 on speeding up permit-granting procedures for renewable energy projects and facilitating Power Purchase Agreements," Brussels, May 2022.

[174] A. Malhotra and T. S. Schmidt, "Accelerating Low-Carbon Innovation," *Joule*, vol. 4, no. 11, pp. 2259–2267, 2020, doi: 10.1016/j.joule.2020.09.004.

[175] D. Caporale and C. De Lucia, "Social acceptance of on-shore wind energy in Apulia Region (Southern Italy)," *Renewable and Sustainable Energy Reviews*, vol. 52, pp. 1378–1390, Dec. 2015, doi: 10.1016/J.RSER.2015.07.183.

[176] J. Meyerhoff, "Do turbines in the vicinity of respondents' residences influence choices among programmes for future wind power generation?," *Journal of Choice Modelling*, vol. 7, pp. 58–71, Jun. 2013, doi: 10.1016/j.jocm.2013.04.010.

[177] R. Lacal-Arántegui, J. M. Yusta, and J. A. Domínguez-Navarro, "Offshore wind installation: Analysing the evidence behind improvements in installation time," *Renewable and Sustainable Energy Reviews*, vol. 92. Elsevier Ltd, pp. 133–145, Sep. 01, 2018. doi: 10.1016/j.rser.2018.04.044.

[178] BVG Associates, "Guide to an offshore wind farm," Jan. 2019. Accessed: Feb. 27, 2024. [Online]. Available: www.thecrownestate.co.uk

[179] Iberdrola, "Construction of an offshore wind plant." Accessed: Feb. 27, 2024. [Online]. Available: https://www.iberdrola.com/about-us/our-activity/offshore-wind-energy/offshore-wind-park-construction

[180] Permitting Dashboard, "Federal Environmental Review and Authorization Inventory." Accessed: Jan. 30, 2024. [Online]. Available: https://www.permits.performance.gov/tools/federal-environmental-review-and-authorization-inventory

[181] R. Sud and S. Patnaik, "How does permitting for clean energy infrastructure work?," Brookings Institution. Accessed: Jan. 30, 2024. [Online]. Available: https://www.brookings.edu/articles/how-does-permitting-for-clean-energy-infrastructure-work/

[182] Congressional Research Service, "Wind Energy: Offshore Permitting," 2021.

[183] US DOE, "Queued Up … But in Need of Transmission," 2022.

[184] J. D. Jenkins, J. Farbes, R. Jones, N. Patankar, and G. Schivley, "Electricity Transmission is Key to Unlock the Full Potential of the Inflation Reduction Act repeatproject.org," Princeton, NJ, Sep. 2022. doi: 10.5281/zenodo.7106176.

[185] S. P. Vajjhala and P. S. Fischbeck, “Quantifying siting difficulty: A case study of US transmission line siting,” *Energy Policy*, vol. 35, no. 1, pp. 650–671, Jan. 2007, doi: 10.1016/J.ENPOL.2005.12.026.

[186] W. J. Peplinski *et al.*, “Marine energy environmental permitting and compliance costs,” *Energies (Basel)*, vol. 14, no. 16, Aug. 2021, doi: 10.3390/en14164719.

[187] J. McDermott, M. Daly, M. Hill, and M. Catalini, “Offshore wind project cancellations jeopardize Biden’s clean energy goals,” *PBS News Hour*, Nov. 04, 2023. Accessed: Nov. 29, 2023. [Online]. Available: https://www.pbs.org/newshour/nation/offshore-wind-project-cancellations-jeopardize-bidens-clean-energy-goals

[188] A. N. Alkhaledi, S. Sampath, and P. Pilidis, “Economic analysis of a zero-carbon liquefied hydrogen tanker ship,” *Int J Hydrogen Energy*, 2022, doi: 10.1016/J.IJHYDENE.2022.06.168.

[189] P. ; Corey, M. ; Weber, Hale, and Zack, “Separate Senate deal aims to shorten timelines for US energy project permitting,” 2022. [Online]. Available: https://www.proquest.com/trade-journals/separate-senate-deal-aims-shorten-

[190] Federal Energy Regulatory Commission, “Explainer on the Interconnection Final Rule.” Accessed: Dec. 10, 2023. [Online]. Available: https://www.ferc.gov/explainer-interconnection-final-rule

[191] J. J. Häußermann, M. J. Maier, T. C. Kirsch, S. Kaiser, and M. Schraudner, “Social acceptance of green hydrogen in Germany: building trust through responsible innovation,” *Energy Sustain Soc*, vol. 13, no. 1, pp. 1–19, Dec. 2023, doi: 10.1186/S13705-023-00394-4/TABLES/1.

[192] A. L. Schönauer and S. Glanz, “Hydrogen in future energy systems: Social acceptance of the technology and its large-scale infrastructure,” *Int J Hydrogen Energy*, vol. 47, no. 24, pp. 12251–12263, Mar. 2022, doi: 10.1016/J.IJHYDENE.2021.05.160.

[193] P. Scherhaufer, S. Höltinger, B. Salak, T. Schauppenlehner, and J. Schmidt, “Patterns of acceptance and non-acceptance within energy landscapes: A case study on wind energy expansion in Austria,” *Energy Policy*, vol. 109, pp. 863–870, Oct. 2017, doi: 10.1016/J.ENPOL.2017.05.057.

[194] M. Ali, M. Irfan, I. Ozturk, and A. Rauf, “Modeling public acceptance of renewable energy deployment: a pathway towards green revolution,” *Economic Research-Ekonomska Istraživanja*, vol. 36, no. 3, Dec. 2023, doi: 10.1080/1331677X.2022.2159849.

[195] J. Firestone, B. Hoen, J. Rand, D. Elliott, G. Hübner, and J. Pohl, “Reconsidering barriers to wind power projects: community engagement, developer transparency and place,” *Journal of Environmental Policy & Planning*, vol. 20, no. 3, pp. 370–386, 2018, doi: 10.1080/1523908X.2017.1418656.

[196] S. Reddy and J. P. Painuly, “Diffusion of renewable energy technologies—barriers and stakeholders’ perspectives,” *Renew Energy*, vol. 29, no. 9, pp. 1431–1447, Jul. 2004, doi: 10.1016/J.RENENE.2003.12.003.

[197] K. Johansen and J. Emborg, “Wind farm acceptance for sale? Evidence from the Danish wind farm co-ownership scheme,” *Energy Policy*, vol. 117, pp. 413–422, Jun. 2018, doi: 10.1016/J.ENPOL.2018.01.038.

[198] K. Langer, T. Decker, and K. Menrad, "Public participation in wind energy projects located in Germany: Which form of participation is the key to acceptance?," *Renew Energy*, vol. 112, pp. 63–73, Nov. 2017, doi: 10.1016/J.RENENE.2017.05.021.

[199] P. del Río and G. Unruh, "Overcoming the lock-out of renewable energy technologies in Spain: The cases of wind and solar electricity," *Renewable and Sustainable Energy Reviews*, vol. 11, no. 7, pp. 1498–1513, Sep. 2007, doi: 10.1016/J.RSER.2005.12.003.

[200] A. Grubler, C. Wilson, and G. Nemet, "Apples, oranges, and consistent comparisons of the temporal dynamics of energy transitions," *Energy Res Soc Sci*, vol. 22, pp. 18–25, Dec. 2016, doi: 10.1016/J.ERSS.2016.08.015.

[201] P. Bergquist, S. Ansolabehere, S. Carley, and D. Konisky, "Backyard voices: How sense of place shapes views of large-scale energy transmission infrastructure," *Energy Res Soc Sci*, vol. 63, no. December 2019, p. 101396, 2020, doi: 10.1016/j.erss.2019.101396.

[202] E. O'Shaughnessy *et al.*, "Effects of local permitting and interconnection requirements on solar PV installation durations," *Energy Policy*, vol. 161, no. December 2021, p. 112734, 2022, doi: 10.1016/j.enpol.2021.112734.

[203] F. W. Geels, B. K. Sovacool, T. Schwanen, and S. Sorrell, "Sociotechnical transitions for deep decarbonization," *Science*, Sep. 22, 2017. Accessed: Jun. 03, 2021. [Online]. Available: https://science-sciencemag-org.cmu.idm.oclc.org/content/sci/357/6357/1242.full.pdf

[204] W. Peng *et al.*, "Climate policy models need to get real about people-here's how," *Nature*, vol. 594, Jun. 2021.

[205] F. C. Moore, K. Lacasse, K. J. Mach, Y. A. Shin, L. J. Gross, and B. Beckage, "Determinants of emissions pathways in the coupled climate–social system," *Nature*, vol. 603, no. 7899, pp. 103–111, Mar. 2022, doi: 10.1038/s41586-022-04423-8.

[206] B. Noll, B. Steffen, and T. S. Schmidt, "The effects of local interventions on global technological change through spillovers: A modeling framework and application to the road-freight sector," *Proceedings of the National Academy of Sciences*, vol. 120, no. 42, p. e2215684120, Oct. 2023, doi: 10.1073/PNAS.2215684120.

[207] J. D. Hunt *et al.*, "Using the jet stream for sustainable airship and balloon transportation of cargo and hydrogen," *Energy Conversion and Management: X*, vol. 3, no. July, p. 100016, 2019, doi: 10.1016/j.ecmx.2019.100016.

[208] B. Li and J. Li, "Deploy Mobile Hydrogen Trucks to Improve Energy Supply System Resilience," in *2021 IEEE 5th Conference on Energy Internet and Energy System Integration (EI2)*, IEEE, Oct. 2021, pp. 2258–2263. doi: 10.1109/EI252483.2021.9713160.

[209] M. Ban *et al.*, "Optimal Scheduling for Integrated Energy-Mobility Systems Based on Renewable-to-Hydrogen Stations and Tank Truck Fleets," *IEEE Trans Ind Appl*, vol. 58, no. 2, pp. 2666–2676, Mar. 2022, doi: 10.1109/TIA.2021.3116117.

[210] T. Van Wingerden, D. Geerdink, C. Taylor, and C. F. Hülsen, "Specification of a European Offshore Hydrogen Backbone," Feb. 2023.

[211] A. Nuñez-Jimenez and N. De Blasio, "The Future of Renewable Hydrogen in the European Union Market and Geopolitical Implications," Mar. 2022. Accessed: Nov. 09, 2023. [Online]. Available: www.belfercenter.org/ENRP

[212] IEA, “Technology Roadmap Hydrogen and Fuel Cells,” Paris, France, 2015. Accessed: Oct. 10, 2023. [Online]. Available: www.iea.org/t&c/

[213] IEA, “The Future of Hydrogen,” Jun. 2019.

[214] F. Egli, B. Steffen, and T. S. Schmidt, “Bias in energy system models with uniform cost of capital assumption,” *Nature Communications 2019 10:1*, vol. 10, no. 1, pp. 1–3, Oct. 2019, doi: 10.1038/s41467-019-12468-z.

[215] M. Đukan, A. Gumber, F. Egli, and B. Steffen, “The role of policies in reducing the cost of capital for offshore wind,” *iScience*, vol. 26, no. 6, Jun. 2023, doi: 10.1016/j.isci.2023.106945.

[216] H. Díaz and C. Guedes Soares, “Review of the current status, technology and future trends of offshore wind farms,” *Ocean Engineering*, vol. 209, p. 107381, Aug. 2020, doi: 10.1016/J.OCEANENG.2020.107381.

[217] I. Daminov, A. Blavette, S. Bourguet, H. Ben Ahmed, T. Soulard, and P. Warlop, “Economic performance of an overplanted offshore wind farm under several commitment strategies and dynamic thermal ratings of submarine export cable,” *Appl Energy*, vol. 346, p. 121326, Sep. 2023, doi: 10.1016/J.APENERGY.2023.121326.

[218] M. Putnam and M. Perez, “Solar Potential Analysis Report,” 2018. Accessed: Feb. 28, 2024. [Online]. Available: https://energy.gov/solar-office.

[219] A. N. Alkhaledi, S. Sampath, and P. Pilidis, “Propulsion of a hydrogen-fuelled LH2 tanker ship,” *Int J Hydrogen Energy*, vol. 47, no. 39, pp. 17407–17422, May 2022, doi: 10.1016/J.IJHYDENE.2022.03.224.

[220] Hydrogen and Fuel Cell Technologies Office, “Technical Targets for Proton Exchange Membrane Electrolysis.” Accessed: Apr. 26, 2024. [Online]. Available: https://www.energy.gov/eere/fuelcells/technical-targets-proton-exchange-membrane-electrolysis

[221] M. Serreze, “Rhode Island commercial fishers join anti-Vineyard Wind lawsuit,” Providence Business First. Accessed: Jul. 10, 2022. [Online]. Available: https://www.bizjournals.com/rhodeisland/news/2021/12/23/ri-commercial-fishers-join-vineyard-wind-lawsuit.html

[222] D. Choi and Y. J. Kim, “Local and global experience curves for lumpy and granular energy technologies,” *Energy Policy*, vol. 174, p. 113426, Mar. 2023, doi: 10.1016/J.ENPOL.2023.113426.

[223] M. Beuse, B. Steffen, and T. S. Schmidt, “Projecting the Competition between Energy-Storage Technologies in the Electricity Sector,” *Joule*, vol. 4, no. 10, pp. 2162–2184, Oct. 2020, doi: 10.1016/j.joule.2020.07.017.

[224] B. Battke and T. S. Schmidt, “Cost-efficient demand-pull policies for multi-purpose technologies - The case of stationary electricity storage,” *Appl Energy*, vol. 155, pp. 334–348, Oct. 2015, doi: 10.1016/j.apenergy.2015.06.010.

[225] T. S. Schmidt, B. Battke, D. Grosspietsch, and V. H. Hoffmann, “Do deployment policies pick technologies by (not) picking applications?—A simulation of investment decisions in technologies with multiple applications,” *Res Policy*, vol. 45, no. 10, pp. 1965–1983, Dec. 2016, doi: 10.1016/J.RESPOL.2016.07.001.

[226] L. Haelg, M. Waelchli, and T. S. Schmidt, “Supporting energy technology deployment while avoiding unintended technological lock-in: a policy design perspective,”

Environmental Research Letters, vol. 13, no. 10, p. 104011, Oct. 2018, doi: 10.1088/1748-9326/AAE161.

[227] M. Liebreich, “Clean Hydrogen Ladder,” Oct. 2023.

[228] B. K. Sovacool, “How long will it take? Conceptualizing the temporal dynamics of energy transitions,” *Energy Res Soc Sci*, vol. 13, pp. 202–215, 2016, doi: 10.1016/j.erss.2015.12.020.

[229] S. Griffiths, B. K. Sovacool, J. Kim, M. Bazilian, and J. M. Uratani, “Industrial decarbonization via hydrogen: A critical and systematic review of developments, socio-technical systems and policy options,” *Energy Res Soc Sci*, vol. 80, no. August, p. 102208, 2021, doi: 10.1016/j.erss.2021.102208.

[230] Hydrogen Council, “Path to hydrogen competitiveness A cost perspective,” Jan. 2020. Accessed: Apr. 08, 2021. [Online]. Available: www.hydrogencouncil.com.

[231] D. Ferrero, M. Gamba, A. Lanzini, and M. Santarelli, “Power-to-Gas Hydrogen: Techno-economic Assessment of Processes towards a Multi-purpose Energy Carrier,” *Energy Procedia*, vol. 101, no. September, pp. 50–57, 2016, doi: 10.1016/j.egypro.2016.11.007.

[232] J. C. Stephens, E. J. Wilson, and T. R. Peterson, “Socio-Political Evaluation of Energy Deployment (SPEED): An integrated research framework analyzing energy technology deployment,” *Technol Forecast Soc Change*, vol. 75, no. 8, pp. 1224–1246, Oct. 2008, doi: 10.1016/J.TECHFORE.2007.12.003.

[233] L. R. Brown, “Supporting Data for Chapter 9 - Wind,” in *World on the Edge: How to Prevent Environmental and Economic Collapse*, New York: W.W. Norton & Company, 2010. Accessed: Feb. 28, 2024. [Online]. Available: http://www.earth-policy.org/books/wote/wote_datawww.earth-policy.org.

[234] C. Allen *et al.*, “Definition of the UMaine Volturn US-S Reference Platform Developed for the IEA Wind 15-Megawatt Offshore Reference Wind Turbine,” 2020.

[235] E. Gaertner *et al.*, “Definition of the IEA Wind 15-Megawatt Offshore Reference Wind Turbine Technical Report,” 2020.

[236] P. Bortolotti *et al.*, “IEA Wind Task 37 on Systems Engineering in Wind Energy - WP2.1 Reference Wind Turbines: Technical Report,” 2019.

[237] C. Desmond, J. Murphy, L. Blonk, and W. Haans, “Description of an 8 MW reference wind turbine,” *J Phys Conf Ser*, vol. 753, no. 9, 2016, doi: 10.1088/1742-6596/753/9/092013.

[238] J. Jonkman, S. Butterfield, W. Musial, and G. Scott, “Definition of a 5-MW reference wind turbine for offshore system development,” 2009.

[239] H. A. Agerschou and J. J. Edens, “Fifth and first order wave-force coefficients for cylindrical piles,” *ASCE*, 1965.

[240] P. Holmes, “Professional Development Programme: Coastal Infrastructure Design, Construction and Maintenance - A Course in Coastal Defense Systems I Coastal Processes: Waves.” 2001.

[241] Director (Personal Communication), “Kongsberg O&M Estimates.” Houston, TX, 2022.

[242] Simis.io, “Ashes.” [Online]. Available: https://www.simis.io/

[243] A. Robertson *et al.*, "Definition of the Semisubersible Floating System for Phase II of OC4," 2014.

[244] M. S. Longuet-Higgins, "The Mean Forces Exerted by Waves on Floating or Submerged Bodies with Applications to Sand Bars and Wave Power Machines," *Proc R Soc Lond A Math Phys Sci*, vol. 352, no. 1671, pp. 463–480, 1977.

[245] NREL, "FLORIS v3.3," *GitHub repository*, 2022.

[246] IRENA, *Renewable Power Generation Costs in 2021*. 2022.

[247] A. M. Biadgo and G. Aynekulu, "Aerodynamic Design of Horizontal Axis Wind Turbine Blades," *FME Transactions*, vol. 45, pp. 647–640, May 2017, doi: 10.5937/fmet1704647M.

[248] European Space Agency, "Surface current speed." Accessed: Oct. 20, 2020. [Online]. Available: https://www.esa.int/ESA_Multimedia/Images/2012/05/Surface_current_speed

[249] myweather2.com, "Marine weather forecast for Off Figueira Da Foz | Marine | Portugal, Coastal Areas." Accessed: Mar. 02, 2021. [Online]. Available: https://www.myweather2.com/Marine/Coastal-Areas/Portugal/Off-Figueira-Da-Foz.aspx?sday=0&eday=7

[250] myweather2.com, "Marine weather forecast for Morro Bay | Marine | United States of America, Global Ports." Accessed: Jun. 21, 2022. [Online]. Available: https://www.myweather2.com/Marine/Global-Ports/United-States-of-America/Morro-Bay.aspx?sday=0&eday=7#

[251] T. C.A. Oliveira, E. Cagnin, and P. A. Silva, "Wind-waves in the coast of mainland Portugal induced by post-tropical storms," *Ocean Engineering*, vol. 217, no. January, p. 108020, 2020, doi: 10.1016/j.oceaneng.2020.108020.

[252] J. C. Berg, "Extreme Ocean Wave Conditions for Northern California Wave Energy Conversion Device," *Sandia National Laboratories*, 2011.

[253] Renewables.ninja, "Renewables.ninja." Accessed: Jun. 09, 2022. [Online]. Available: https://www.renewables.ninja/

[254] S. Patel, "The Vital Link: How HVDC Is Modernizing the Grid," Power Magazine. Accessed: Jul. 06, 2022. [Online]. Available: https://www.powermag.com/the-vital-link-how-hvdc-is-modernizing-the-grid/

[255] D. Proctor, "Morocco Project Could Support UK's Renewable Goals, Hydrogen Economy," Power Magazine. Accessed: Jul. 06, 2022. [Online]. Available: https://www.powermag.com/morocco-project-could-support-uks-renewable-goals-hydrogen-economy/

[256] IRENA, "Green Hydrogen: A guide to policy making," Abu Dhabi, 2020.

[257] IRENA, "Green Hydrogen Cost Reduction: Scaling Up Electrolysers to meet the 1.5C Climate Goal," 2020.

[258] Burges Salmon, "Offshore Wind – Exploring the advent of Green Hydrogen Power." Accessed: Feb. 17, 2022. [Online]. Available: https://www.burges-salmon.com/news-and-insight/legal-updates/energy-power-utilities/offshore-wind-exploring-the-advent-of-green-hydrogen-power

[259] Navigant Consulting Inc., “Offshore Wind Market and Economic Analysis 2014 Annual Market Assessment,” Sep. 2014. Accessed: May 12, 2023. [Online]. Available: www.navigant.com

[260] Navigant Consulting Inc., “Offshore Wind Market and Economic Analysis Annual Market Assessment,” Oct. 2013. Accessed: May 12, 2023. [Online]. Available: www.navigant.com

[261] W. Musial, P. Beiter, P. Schwabe, T. Tian, T. Stehly, and P. Spitsen, “2016 Offshore Wind Technologies Market Report,” 2016. Accessed: Apr. 21, 2023. [Online]. Available: http:/www.osti.gov/scitech

[262] P. Beiter *et al.*, “2017 Offshore Wind Technologies Market Update,” Sep. 2018. Accessed: May 12, 2023. [Online]. Available: https://www.energy.gov/eere/wind/downloads/2017-offshore-wind-

[263] U.S. DOE, “2018 Offshore Wind Technologies Market Report - Executive Summary,” 2018.

[264] W. Musial *et al.*, “Offshore Wind Market Report: 2021 Edition,” 2021.

[265] 4COffshore, “Global Offshore Wind Farms Database | 4C Offshore.” Accessed: May 12, 2023. [Online]. Available: https://www.4coffshore.com/windfarms/

[266] ABS, “Guide for Building and Classifying Floating Offshore Wind Turbine Installations,” Jan. 2013. Accessed: Sep. 21, 2020. [Online]. Available: www.eagle.org

[267] ABS, “Guide for Dynamic Positioning Systems,” Spring, TX, 2020. Accessed: Aug. 04, 2020. [Online]. Available: www.eagle.org

[268] A. Myhr, C. Bjerkseter, A. Ågotnes, and T. A. Nygaard, “Levelised cost of energy for offshore floating wind turbines in a lifecycle perspective,” *Renew Energy*, vol. 66, no. November, pp. 714–728, 2014, doi: 10.1016/j.renene.2014.01.017.

[269] P. Beiter *et al.*, “A Spatial-Economic Cost-Reduction Pathway Analysis for U.S. Offshore Wind Energy Development from 2015–2030,” Golden, CO (United States), Sep. 2016. doi: 10.2172/1324526.

[270] G. E. Jung, M. C. Dinh, H. J. Sung, M. Park, and I. K. Yu, “Economic analysis of a 22.9 kv hts power cable and conventional ac power cable for an offshore wind farm connections,” *Progress in Superconductivity and Cryogenics (PSAC)*, vol. 20, no. 4, pp. 60–64, 2018, doi: 10.9714/psac.2018.20.4.060.

[271] F. H. Saadi, N. S. Lewis, and E. W. McFarland, “Relative costs of transporting electrical and chemical energy,” *Energy Environ Sci*, vol. 11, no. 3, pp. 469–475, 2018, doi: 10.1039/c7ee01987d.

[272] N. Avanessova, A. Gray, I. Lazakis, R. C. Thomson, and G. Rinaldi, “Analysing the effectiveness of different offshore maintenance base options for floating wind farms,” *Wind Energy Science*, vol. 7, no. 2, pp. 887–901, 2022, doi: 10.5194/wes-7-887-2022.

[273] Vice President (Personal Communication), “Kongsberg Thruster Specifications.” 2021.

[274] Director (Personal Communication), “Kongsberg O&M Estimates.” Houston, TX, 2022.

[275] X. Xiang, M. M. C. Merlin, and T. C. Green, "Cost analysis and comparison of HVAC, LFAC and HVDC for offshore wind power connection," *IET Conference Publications*, vol. 2016, no. CP696, 2016, doi: 10.1049/cp.2016.0386.

[276] S. M. Saba, M. Müller, M. Robinius, and D. Stolten, "The investment costs of electrolysis – A comparison of cost studies from the past 30 years," *Int J Hydrogen Energy*, vol. 43, no. 3, pp. 1209–1223, Jan. 2018, doi: 10.1016/J.IJHYDENE.2017.11.115.

[277] IRENA, "Green Hydrogen Cost Reduction: Scaling Up Electrolysers to meet the 1.5C Climate Goal," 2020. [Online]. Available: /publications/2020/Dec/Green-hydrogen-cost-reduction%0Ahttps://www.irena.org/-/media/Files/IRENA/Agency/Publication/2020/Dec/IRENA_Green_hydrogen_cost_2020.pdf

[278] S. P. Popov and O. A. Baldynov, "Evaluation of energy efficiency of the long distance energy transport systems for renewable energy," *Energy Systems Research*, 2019, doi: 10.1051/e3sconf/20191140.

[279] P. Sherman, X. Chen, and M. McElroy, "Offshore wind: An opportunity for cost-competitive decarbonization of China's energy economy," *Sci Adv*, vol. 6, no. 8, pp. 1–9, 2020, doi: 10.1126/sciadv.aax9571.

[280] L. Bird *et al.*, "Wind and solar energy curtailment: A review of international experience," *Renewable and Sustainable Energy Reviews*, vol. 65, pp. 577–586, 2016, doi: 10.1016/j.rser.2016.06.082.